Title
CYCLING ZONE ADSORPTION. SEPARATION OF GAS MIXTURES

Author
Blum, Dwain E.

Publication Date
1971-09-01

LBL-247
c.1

CYCLING ZONE ADSORPTION

Separation of Gas Mixtures

Dwain E. Blum
(Ph. D. Thesis)

September 1971

AEC Contract No. W-7405-eng-48

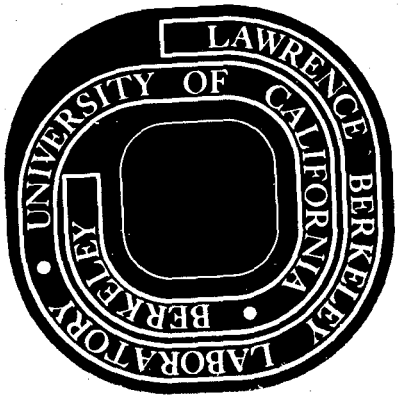

LBL-247
c.1

DISCLAIMER

CYCLING ZONE ADSORPTION

Separation of Gas Mixtures

Dwain E. Blum

Department of Chemical Engineering
and Lawrence Berkeley Laboratory
University of California
Berkeley, California 94720

ABSTRACT

A theoretical explanation is presented for cycling zone adsorption, a wave-propagating separation process utilized to effect separations of gaseous mixtures. Experimental results confirming the theoretical predictions are also included. The minor effect of finite mass transfer rates on the separative power was also investigated.

The addition of an isothermal adsorbent bed to a cycling zone adsorption process being fed a dilute mixture of adsorbing components is suggested to enhance the separation further. Elimination of the carrier gas was found not to alter the separative power of the process significantly.

A frequency response method was used for determination of equilibrium distribution coefficients for the fluid-solid adsorbing systems investigated.

TABLE OF CONTENTS

LIST OF FIGURES

Page

Page

LIST OF TABLES

INTRODUCTION AND BACKGROUND

Development of continuous countercurrent processes for the separation of fluid mixtures by adsorption has had only partial success owing to the mechanical difficulties involved in the movement of the solid adsorbent particles. Kehde (1948) discussed such problems in the hypersorption process. Fixed-bed operation has had to be intermittent because of the required regeneration of the adsorbent after it had become saturated with the feed mixture. Generally, four types of reverse-flow regenerative cycles have been employed: thermal (Weiss, 1965), pressure (Skarstrom, 1959)(Alexis, 1967), purge-gas stripping (Wunder, 1962), and displacement (Bohrer, 1965).

In recent times, scaled-up, continuously intermittent chromatographic processes have been employed and described by Timmins et al. (1968),(1969). Production-scale chromatographic processes depend upon overcoming large losses in resolution accompanied by column diameter scale-up. Baffles have been developed to improve radial mixing without causing significant axial dispersion (Baddour, 1966).

Recently, attention has turned to cyclic operation of fixed beds, as presented in papers by Wilhelm and his co-workers (Wilhelm et al., 1966, 1968, 1969a, 1969b), where "parametric pumping" has been described and shown to lead to large separation factors. Extensions and ramifications of this process have been explored by Jencewski and Myers (1968), Pigford et al. (1969a), Aris (1969), Horn and Lin (1969), and Hyun-Kee and Amundson (1970). In these processes there is a periodic reversal of the fluid velocity synchronous with imposed changes in a thermodynamic gradient, usually owing to temperature or pressure. Wilhelm et al. (1968) suggested that the separation results from a coupling of the variations

in flow and temperature in the transport equations to produce large changes in fluid composition.

On the other hand, Pigford et al. (1969b, 1970) have pointed out that flow reversal is not necessary to produce a separation, and have termed their continuous flow scheme "cycling zone" adsorption. Indeed, flow reversal may be a disadvantage because of the limitation on production rates it imposes. Introduction of pressure or temperature cycles into a fixed bed without simultaneous flow reversals will lead to cycling changes in the fluid composition inside and leaving the bed. The cycling changes are propagated through the adsorbent bed as waves and, by setting cycle times at optimum values, the amplitude of the concentration wave can be made large. Baker and Pigford (1971) have described both "standing-wave" and "traveling-wave" temperature modes of operation and have called attention to the increased separative power obtainable by staging of cycling zones.

Because of the wide range of solid adsorbents and ion-exchange resins, many applications of such cyclic processing methods suggest themselves. In the cycling zone adsorption process, no batch-type regeneration of the adsorbent is required, and indeed, in many cases the sweep fluid may be eliminated completely. The main disadvantage of this process is that, similar to other adsorption processes, the mass transfer rates are usually low, restricting throughput rates. Also, nearly complete separations will be more difficult to obtain than by elution chromatography.

This dissertation will investigate methods of operating cycling-zone adsorption units to effect separations of gas mixtures. A linearized equilibrium theory will be used to determine optimum operating conditions.

A qualitative discussion of the cycling zone adsorption process is given in Chapter 1. In Chapter 2 a mathematical description of the process and solutions under special restrictions are presented. Chapter 3 contains the linearized equilibrium theory results. The experimental system and apparatus are discussed in Chapter 4. Chapters 5 and 6 report the experimental aspects and results of this study. Following the conclusion section, Appendices A and B include some additional aspects of the process. Sample calculations are presented in Appendix C.

CHAPTER 1

A QUALITATIVE DESCRIPTION OF THE CYCLING ZONE ADSORPTION PROCESS

In a recent publication by Pigford, Baker, and Blum (1969b), a qualitative description of a new separation process, termed cycling zone adsorption was presented. Baker and Pigford (1971) described the "standing-wave" and "traveling-wave" temperature modes of operation with a quantitive theory and experimental results for the acetic acid-water-activated carbon system.

Consider the process scheme shown in Figure 1-1, in which a fluid having a constant solute concentration, y_f, is passed into a bed of solid particles. The bed temperature is being altered cyclically by heating and cooling the column walls (standing-wave operation). As pointed out in the earlier articles, periodic changes in the effluent concentration are obtained; these changes can be amplified by using a series of such cycling beds, the temperature in each being out of phase with those in the adjacent beds.

A shift in some thermodynamic potential, such as temperature, pressure, concentration of a third species, electric or magnetic fields, may be used to produce a change in the equilibrium distribution relationship. In this thesis only temperature changes are considered, as exemplified in Figure 1-2.

The system is oscillated between a cold temperature, T_C, and a hot temperature, T_H, periodically. The solute, which was previously stored on the solid during the cold portion of the cycle, is expelled into the fluid during the hot portion of the cycle. The effluent composition, y, depends upon the relative capacity ratios of the fluid and solid and on the equilibrium distribution coefficient, K.

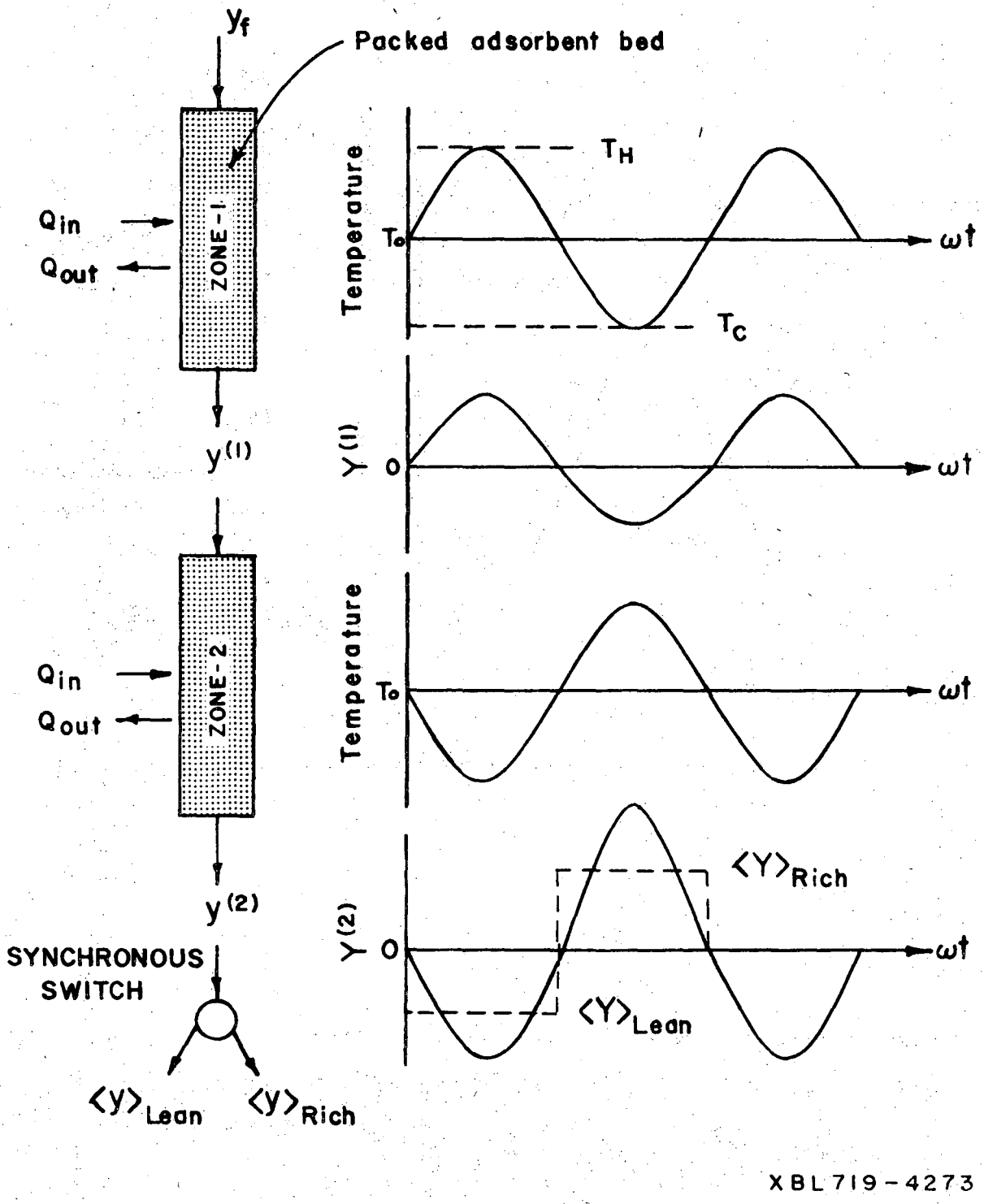

Figure 1-1. Cycling Zone Adsorption Process Scheme: Dual Zone.

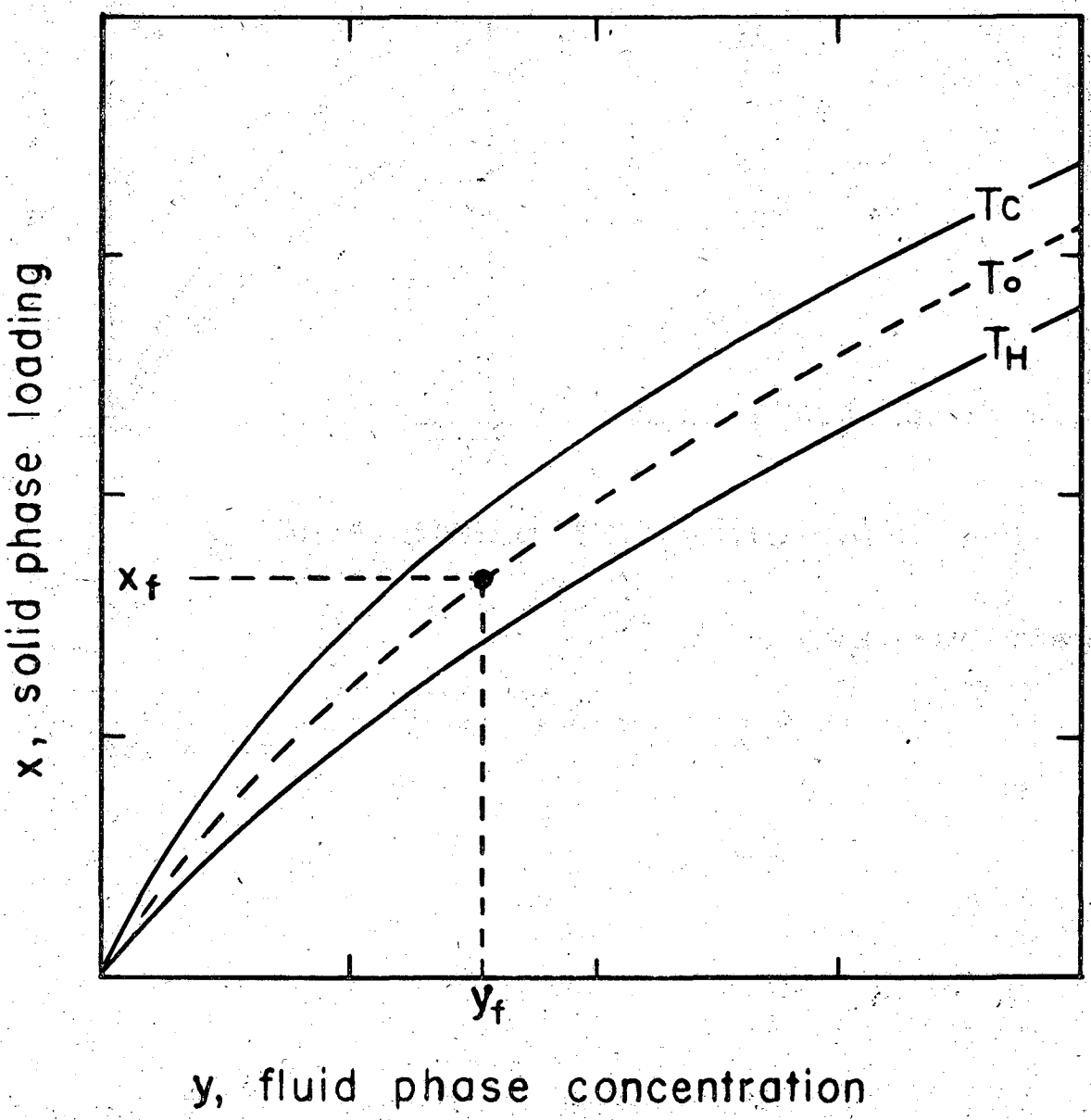

Figure 1-2. Temperature Effect on Solid-Fluid Equilibrium Distribution.

It can be shown that the process has an optimum cycle time which depends on time of passage of the concentration wave thru the bed. This is analogous to the optimum flow-temperature phase relationship of parametric pumping as discussed by Wilhelm et al. (1968b).

If parallel columns are used as shown in Figure 1-3, each one-half cycle out of phase with the other, a separation can be achieved by periodically switching the output of each column. The result is continuous production of two streams of different composition, one richer and one leaner than the feed.

The separation can be improved considerably, however, by operating two or more zones in series, the temperature change in each zone being a half-cycle out of phase with that in the previous zone. The increase in separation factors have been shown to be comparable to those obtained in the direct mode of parametric pumping by Pigford et al. (1969b). Indeed, the number of zones, N, is analogous to the number of batch cycles in the direct mode of parametric pumping. The advantage of the cycling zone adsorption process is that it operates without flow reversal and therefore produces enriched and depleted streams continuously. Theory indicates that operation of a parametric pump with positive feed and continuous withdrawal of tops and bottoms streams requires considerable recycle, in multiple-stage operation, to obtain large separation factors. Baker (1969) has shown that multiple-zone cycling zone adsorption is an approximation to applying a thermal velocity to an adsorption column (traveling-wave mode of operation).

Previously, only single adsorbing specie systems have been considered. Two cases of dual adsorbing species appear to warrant investigation in order to gain insight into multi-component separations. These

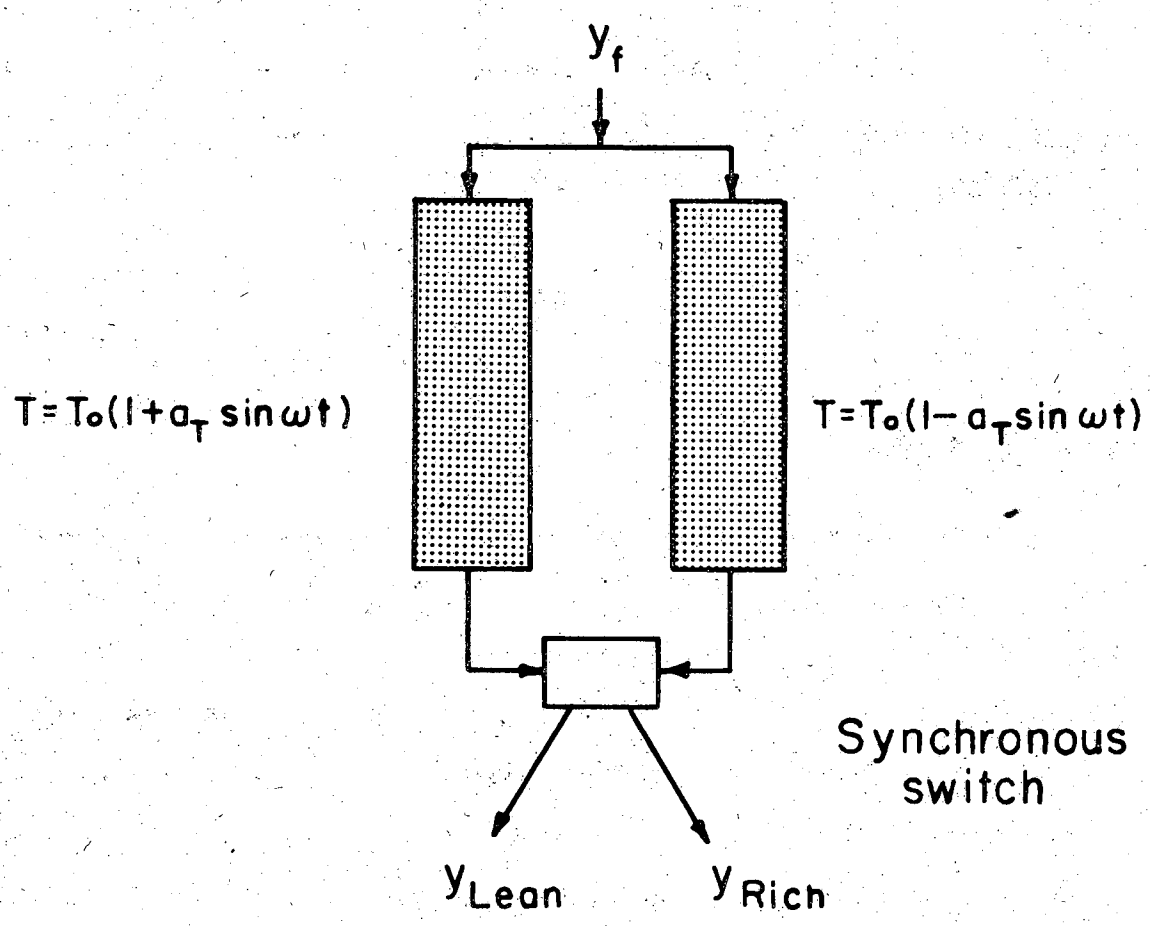

Figure 1-3. Parallel-Zone System for Continuous Production.

are: 1) two adsorbing species diluted with a non-adsorbing carrier gas, and 2) binary gas mixtures of two adsorbing species.

In the first case, the two adsorbing species can be considered non-interacting when at "trace conditions" where $\sum_i (y_i)_a < 0.1$. The adsorption characteristics of each component depends on its respective isotherm , as in Figure 1-4. Each species, now, possesses its own independent wave velocity, thus the optimum cycle time-concentration wave residence time relationship for each component will be different. A typical effluent composition-time response of a cycling zone adsorption unit, utilizing a trace feed containing two adsorbing species, is presented in Figure 1-5. The best separation that can be obtained for this set of response waves depends upon how this cyclic effluent is split into enriched and depleted half-cycle portions.

The use of additional zones then requires making the splitting decision after the last zone. In addition, a compromise will be required in selecting the best temperature phase relationship between adjacent zones. It will be shown that employment of an isothermal adsorbent bed, before splitting, designed to produce a set of output concentration waves that are 180° out of phase, greatly improves the separation, as illustrated in Figure 1-6.

For a binary mixture of two adsorbing species, the effective isotherm controls the overall optimum separative power. Since the species now compete with each other for the adsorption sites, the effective individual distribution coefficients will be changed from those that would exist if each was present in a non-adsorbing carrier. This in turn alters the concentration wave velocities. The concentration output waves are exactly 180° out of phase, as implied by a gas-phase mass

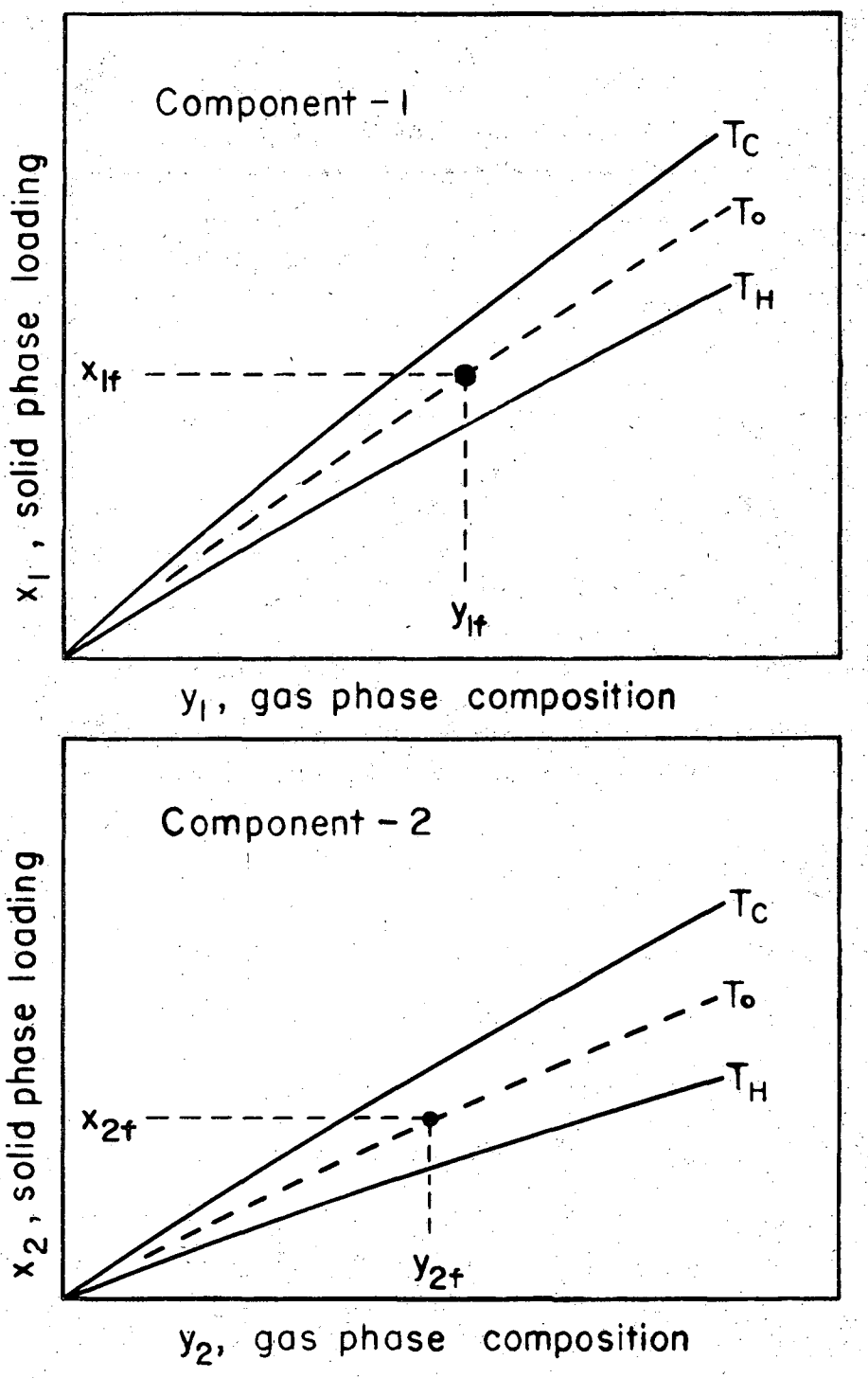

Figure 1-4. Individual Component Isotherms in a Trace System.

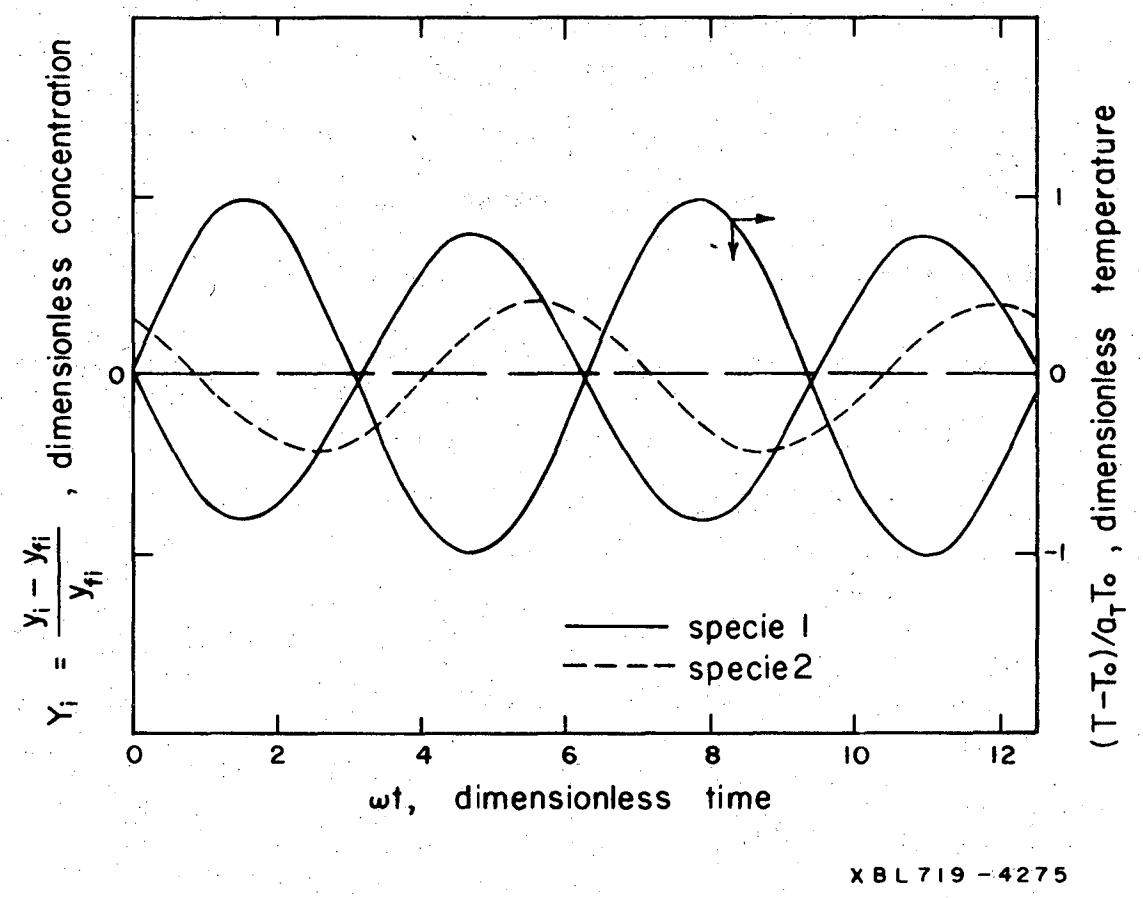

Figure 1-5. Input and Response Waves For Cycling Zone Adsorption Utilizing a Trace Feed.

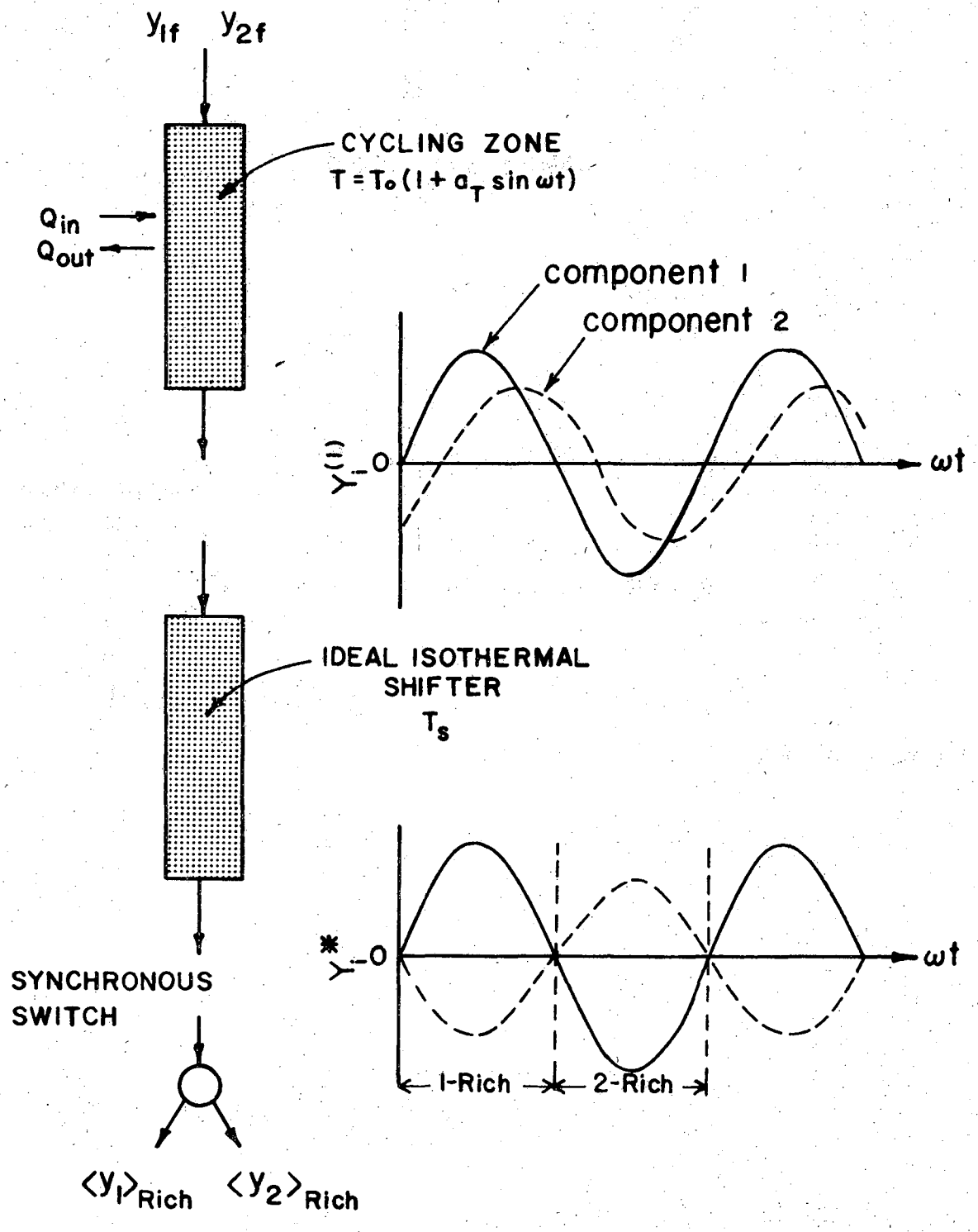

Figure 1-6. Employment of Isothermal Shifter Bed to Improve Separation of Trace System.

balance. Thus, the mathematical analysis of the carrier-free binary system is similar in form to that for a single adsorbing specie within a carrier.

It is evident that as the number of zones of a processing scheme is increased, the concentration gradients in the final zone become larger since the effluent concentration waves are amplified in each additional zone but oscillate about the initial feed compositions. Thus, mass transfer losses owing to longitudinal mixing are greatly enhanced. In order to reduce the concentration gradients and to reduce mass transfer losses, a splitting and recycle scheme, such as that shown in Figure 1-7, may be employed to establish enriched and depleted streams each of which may be processed further by a train of cycling zone adsorption units.

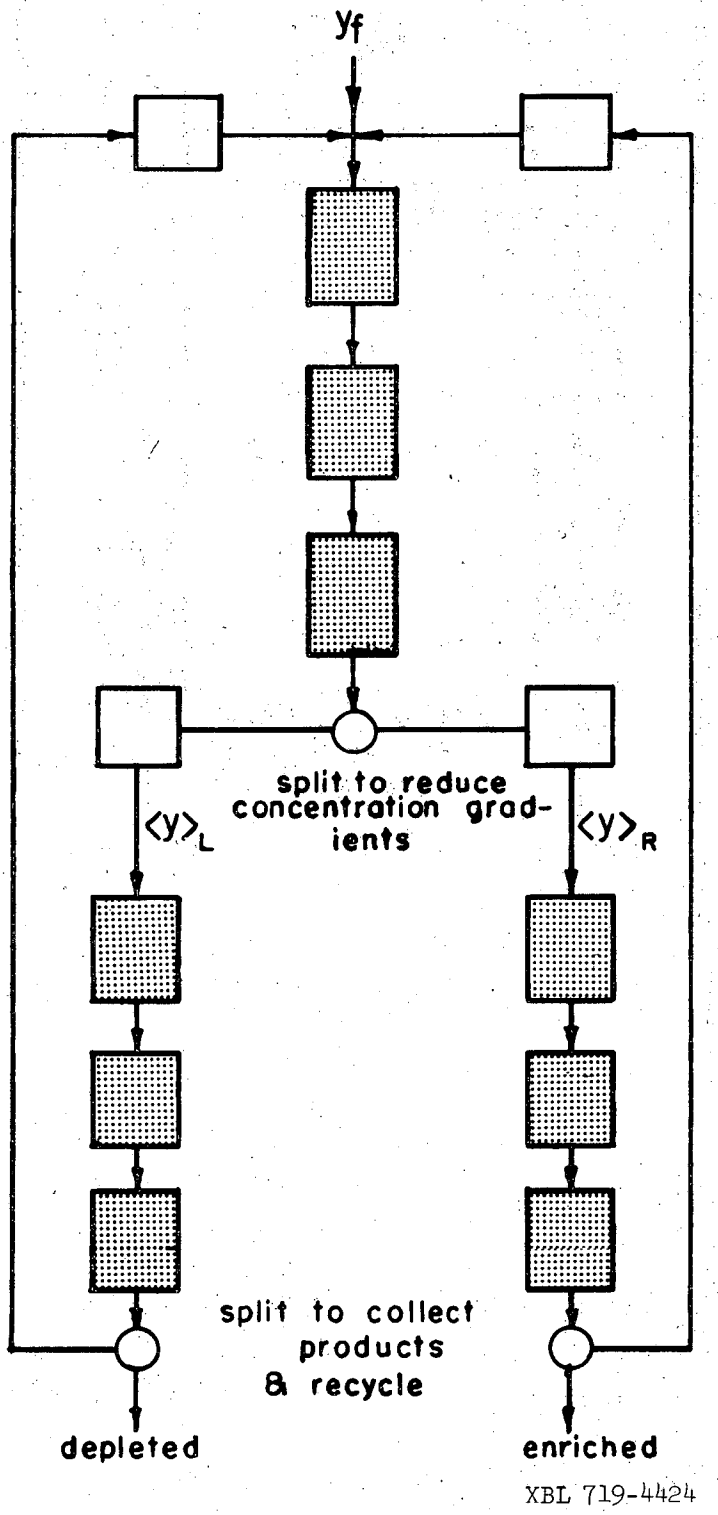

Figure 1-7. Splitting and Recycle Scheme for Multiple-Zone Operation.

CHAPTER 2

MATHEMATICAL DESCRIPTION OF CYCLING ZONE ADSORPTION PROCESS

The governing equations for a non-isothermal fixed bed system are derived from mass and energy balances over each phase in the system. The assumption that the rates of exchange between the fluid phase and the solid adsorbent particles are very large, yields the local equilibrium theory.

GENERAL EQUATIONS

Disregarding any radial gradients in velocity, concentration, or temperature, the balances over an axial differential section of the packed bed thru which a fluid containing a single adsorbate is flowing are as previously derived by Baker (1969):

$$\frac{\partial y}{\partial t} + \frac{(1-\varepsilon)\chi}{\varepsilon}\frac{\partial y^*}{\partial t} + \frac{(1-\varepsilon)\rho_s}{\rho_f}\frac{\partial x}{\partial t} + v\frac{\partial y}{\partial z} - (E_D + D_M)\frac{\partial^2 y}{\partial z^2} = 0 \qquad (2\text{-}1)$$

$$\frac{\partial T}{\partial t} + \left[\frac{\rho_s C_s + \rho_f C_f}{\rho_f C_f \varepsilon}(1-\varepsilon)\chi\right]\frac{\partial T_s}{\partial t} + v\frac{\partial T}{\partial z} - (E_D + D_T)\frac{\partial^2 T}{\partial z^2} = \frac{h'_w a'_w}{\rho_f C_f \varepsilon}(T_w - T) \qquad (2\text{-}2)$$

$$\frac{\partial x}{\partial t} + \frac{\chi \rho_f}{\rho_s}\frac{\partial y^*}{\partial t} = -\frac{k_m a'_p}{\rho_s(1-\varepsilon)}(y^* - y) \qquad (2\text{-}3)$$

$$\frac{\partial T_s}{\partial t} = - \frac{h'_p a'_p}{[\rho_s C_s + \chi \rho_f C_f] (1 - \varepsilon)} (T_s - T)$$

$$+ \frac{\rho_s \Delta H_{ads}}{[\rho_s C_s + \rho_f C_f \chi]} \frac{\partial x}{\partial t} \qquad (2\text{-}4)$$

where ε = volume fraction of the packed bed outside the adsorbent particles and χ = volume fraction of immobile fluid inside the particle. The immobile fluid and the particles are assumed to be in thermal equilibrium.

Radial particle temperature and concentration gradients have been neglected by assuming that the interface between the solid surface and the immobile fluid inside the particle are considered to be at equilibrium and represented by the function:

$$x = x(T_s, y^*) \qquad (2\text{-}5)$$

Any effects of concentration or temperature on the parameters have been neglected except in the equilibrium relationship. Since most adsorption and ion-exchange processes are particle-diffusion controlled, the assumption of an over-all linear driving force mass transfer mechanism is then only approximate (Sweed and Wilhelm, 1969). Thus radial particle profiles should be included for a complete process description. For slow mass transfer processes, the simpler expressions are sufficient (Vermeulen, 1966).

In a multi-adsorbing specie system, mass balances for each component, restricted by the overall balance, are required.

Three main types of equilibrium distribution relationships for fluid-solid systems are described by Adamson (1967) are

$$x = Ky^* \qquad \text{(Linear)} \qquad (2\text{-}6)$$

$$x = K(y^*)^{\beta'}, \ \beta' < 1 \qquad \text{(Freundlich)} \qquad (2\text{-}7)$$

$$x = \frac{Ky^*}{1 + Ky^*} \qquad \text{(Langmuir)} \qquad (2\text{-}8)$$

where K and β' are functions of the solid-phase temperature, T_s. Other multi-parameter equilibrium distribution relationships have been listed by Vermeulen (1970).

Analytical solutions of this set of general equations are not known, but numerical computations have been reported by Wilhelm et al. (1968), Sweed and Wilhelm (1969), and Rolke and Wilhelm (1969) for the parametric pumping process.

LOCAL EQUILIBRIUM THEORY

Since the separation effect in the cycling zone adsorption process depends on a periodic alteration of the phase equilibrium rather than on any rate differences, the approach in this study is to evaluate the qualitative and semi-quantitative aspects of the process based upon the equilibrium theory. This assumes that the rates of exchange between the fluid phase and the solid particles are very high. The design based upon an equilibrium process would then be modified by mass and heat transfer relationships when the exchange rates become limited. An analogy is the example of frontal adsorption, in which the design is first made on the assumption of height of a theoretical plate (HETP) and then modified by the incorporation of a number of transfer units based on the selected mass transfer mechanism.

If it is assumed that at any point in the column the solid and fluid phases are in local equilibrium (i.e. $y = y^*$ and $T_s = T$), and that

axial dispersion and diffusion and heat of adsorption effects may be neglected, analytical solutions to the simplified equations can be obtained, as shown by Lapidus and Amundson (1952).

One may approach the equilibrium condition by decreasing the flow rate through the column. This in turn increases the axial dispersion and axial diffusion effects. These effects may be reduced by the proper selection of the ratio of particle size to column diameter. However, it is common in ion-exchange and chromatographic analyses to neglect those effects as a first approximation, leading to an adequate description of these processes, as described by DeVault (1943) and Glueckauf (1955).

For the "standing wave" mode of operation, to which this discussion is limited, no longitudinal temperature gradients exist. Thus we arrive at the following set of equations:

$$\left[1 + \frac{(1-\varepsilon)\chi}{\varepsilon}\right] \frac{\partial y}{\partial t} + \frac{\rho_s}{\rho_f} \frac{(1-\varepsilon)}{\varepsilon} \frac{\partial x}{\partial t} + v \frac{\partial y}{\partial z} = 0 \qquad (2\text{-}9)$$

$$x = x(T, y) \qquad (2\text{-}10)$$

Differentiating equation (2-10) and substituting into equation (2-9) gives

$$\left[1 + \frac{(1-\varepsilon)\chi}{\varepsilon} + \frac{(1-\varepsilon)\rho_s}{\varepsilon\ \rho_f} \left(\frac{\partial x}{\partial y}\right)\right] \frac{\partial y}{\partial t} + v \frac{\partial y}{\partial z} =$$

$$- \frac{(1-\varepsilon)}{\varepsilon} \frac{\rho_s}{\rho_f} \left(\frac{\partial x}{\partial T}\right) \left(\frac{dT}{dt}\right) \qquad (2\text{-}11)$$

In general, for gaseous systems at low pressures and dilute liguid systems, $\rho_f \ll \rho_s$. Therefore equation (2-11) can be approximated extremely well by:

$$\left[1 + \frac{\rho_s(1-\varepsilon)}{\rho_f \varepsilon}\left(\frac{\partial x}{\partial y}\right)\right]\frac{\partial y}{\partial t} + v\frac{\partial y}{\partial z} = -\frac{\rho_s(1-\varepsilon)}{\rho_f \varepsilon}\left(\frac{\partial x}{\partial T}\right)\left(\frac{dT}{dt}\right) \qquad (2\text{-}12)$$

when one neglects the amount of solute contained in the pores of the solid particles. That is

$$\rho_s(1-\varepsilon)\tilde{x} = \chi\,\rho_f\,y^* + \rho_s(1-\varepsilon)x$$

$$\cong \rho_s(1-\varepsilon)x \qquad (2\text{-}13)$$

Generalized Method of Solution

Assuming the column temperature is changed by passing heat through its walls ("standing wave" mode of operation), the boundary condition is

$$y = y_f, \quad z = 0, \quad t > 0$$

and the temperature forcing function is

$$T = T_o(1 + a_T e^{i\omega t}), \qquad t > 0 \qquad (2\text{-}14)$$

where

$$a_T = \frac{T_H - T_o}{T_o} \qquad (2\text{-}15)$$

The equilibrium relationship is written in terms of an equilibrium distribution coefficient, K(T, y) as

$$x = K(T, y)y \qquad (2\text{-}16)$$

Differentiating equation (2-16) and substituting into equation (2-12) yields the combined mass balance equation:

$$\left[1 + \frac{\rho_s(1-\varepsilon)}{\rho_f \varepsilon} \left.\frac{\partial K}{\partial y}\right|_T \cdot y + \frac{\rho_s(1-\varepsilon)}{\rho_f \varepsilon} K\right] \frac{\partial y}{\partial t} + v \frac{\partial y}{\partial z}$$

$$= - \frac{\rho_s(1-\varepsilon)}{\rho_f \varepsilon} \left.\frac{\partial K}{\partial T}\right|_y \left(\frac{dT}{dt}\right) \cdot y \qquad (2\text{-}17)$$

Following the approach for the solution of distributed parameter systems first suggested by Acrivos (1956), application of the method of characteristics to reduce a partial differential equation into two characteristic ordinary differential equations yields

$$\frac{dt}{1 + \frac{\rho_s(1-\varepsilon)}{\rho_f \varepsilon} \left[y \left.\frac{\partial K}{\partial y}\right|_T + K\right]} = \frac{dz}{v} = \frac{-dy}{\frac{\rho_s(1-\varepsilon)}{\rho_f \varepsilon} \left[\left.\frac{\partial K}{\partial T}\right|_y \left(\frac{dT}{dt}\right) \cdot y\right]} \qquad (2\text{-}18)$$

Defining the following dimensionless variables:

$$Y = (y - y_f)/y_f$$

$$Z = \omega(L/v)(z/L) = \omega(z/v)$$

$$\theta = \omega t$$

and

$$M(\theta, Y) = \frac{\rho_s(1-\varepsilon)}{\rho_f \varepsilon} K(T, y) \qquad (2\text{-}19)$$

equation (2-18) can be split into two equations

$$\frac{d\theta}{dZ} = 1 + (Y + 1) \left.\frac{\partial M}{\partial Y}\right|_{\theta} + M(\theta, Y) \qquad (2\text{-}20)$$

$$\frac{dY}{dZ} = - (Y + 1) \left.\frac{\partial M}{\partial \theta}\right|_{Y} \qquad (2\text{-}21)$$

with the forcing function:

$$T = T_o(1 + a_T e^{i\theta})$$

and boundary condition:

$$Y = 0, \qquad \text{at } Z = 0, \qquad \theta > 0$$

For a given forcing function and distribution function, $K(T, y)$, equations (2-20) and (2-21) may be solved simultaneously by the fourth-order Runge-Kutta-Gill numerical method, involving considerable computational time, yielding $Y(\theta, Z)$. This procedure may be extended to multiple-zone description by setting the boundary condition of each subsequent zone, N, such that

$$Y_N = Y_{N-1}(Z_{N-1}, \theta_{N-1}) \qquad \text{at } Z_N = 0, \qquad \theta_N > 0 \qquad (2\text{-}22)$$

and repeating the calculational scheme, now with a time-dependent boundary condition.

Equilibrium Limit of Cycling Zone Adsorption

Alternatively, we may look at the change in y related to the change in t in equation (2-18)

$$\frac{d\ln y}{dt} = \frac{- \dfrac{\rho_s(1 - \varepsilon)}{\rho_f \varepsilon} \left.\dfrac{\partial K}{\partial T}\right|_y}{1 + \dfrac{\rho_s(1 - \varepsilon)}{\rho_f \varepsilon} \left[\left.\dfrac{\partial K}{\partial \ln y}\right|_T + K\right]} \qquad (2\text{-}23)$$

The total derivative of K is

$$dK = \frac{\partial K}{\partial \ln y}\Big|_T \; d\ln y + \frac{\partial K}{\partial T}\Big|_y \; dT \qquad (2\text{-}24)$$

Combining equation (2-24) and equation (2-23) we have

$$d\ln y = \frac{-\dfrac{\rho_s(1-\varepsilon)}{\rho_f \varepsilon}\, dK}{\left[1 + \dfrac{\rho_s(1-\varepsilon)}{\rho_f \varepsilon}\, K\right]} = -d\ln\left[1 + \frac{\rho_s(1-\varepsilon)}{\rho_f \varepsilon}\, K\right] \qquad (2\text{-}25)$$

Integration of the above equation gives

$$y(1 + \psi) = C \quad \text{(constant)} \qquad (2\text{-}26)$$

where the solids-fluid capacity ratio is

$$\psi = \frac{\rho_s(1-\varepsilon)\, K}{\rho_f \varepsilon}$$

Therefore

$$x = Ky = \frac{C - y}{\dfrac{\rho_s(1-\varepsilon)}{\rho_f \varepsilon}} \qquad (2\text{-}27)$$

can be represented as straight lines on an x-y diagram with slope $= -\dfrac{\rho_f \varepsilon}{\rho_s(1-\varepsilon)}$ and intercept of $C/\left[\dfrac{\rho_s(1-\varepsilon)}{\rho_f \varepsilon}\right]$, as illustrated in Figure 2-1. The characteristic line which passes thru (y_f, T_o), the bed average conditions, represents the equilibrium limit of the cycling operation. In addition, we can conclude from the arrowed line that the equilibrium limit occurs when the temperature input and the concentration

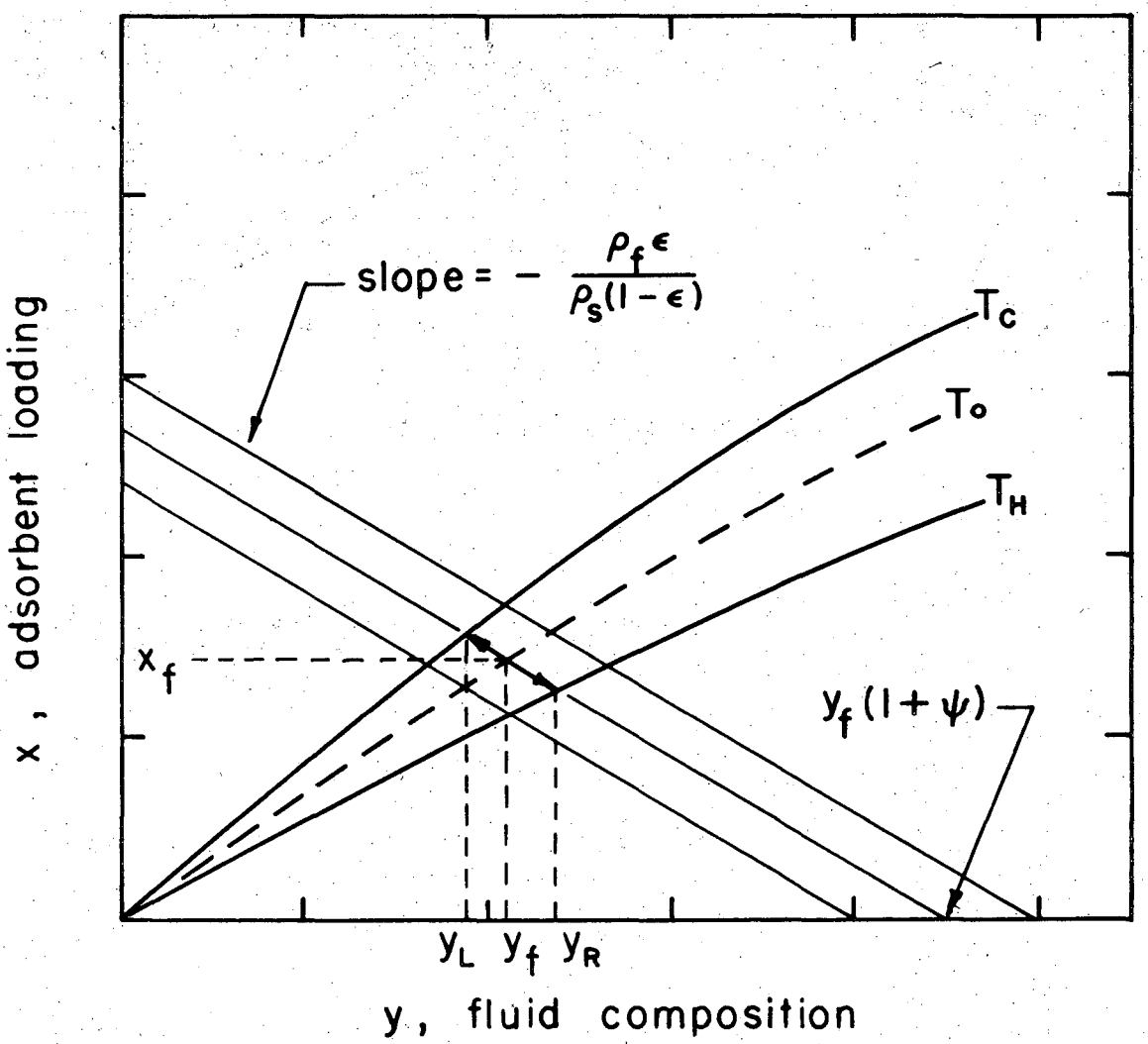

Figure 2-1. Equilibrium Limit of a Single Cycling Zone Unit: Single Solute Feed.

response are exactly in phase. The conditions under which this situation occurs will be explored in the following chapter.

Linear Systems Behavior

A restrictive but useful approximation with which first to examine the cycling zone adsorption process is to consider that the system responds linearily. This is valid for small changes in composition, for linear isotherms, and for distribution functions which are linear functions of temperature. By imposing small temperature changes upon the adsorption zone, which result in small concentration changes, one can closely approximate linear behavior in most adsorption systems. For a linear isotherm, the equilibrium relationship is

$$x = K(T)y$$

The variation of the distribution coefficient, K, with temperature, over moderate temperature ranges, may be represented by

$$K(T) = A_o \exp(-\Delta H_a/RT) \tag{2-28}$$

For a sinusoidal temperature input

$$T = T_o(1 + a_T \sin\omega t) \tag{2-29}$$

and a linear response in the distribution function, K(T), about T_o

$$K(\theta) = K_o(1 + a \sin\theta) \tag{2-30}$$

where

$$a = a_T(\Delta H_a/RT_o) \text{ and } K_o = A_o \exp(-\Delta H_a/RT_o)$$

Equations (2-19) and (2-20) become:

$$\frac{d\theta}{dZ} = 1 + \psi(1 + a \sin\theta) \tag{2-31}$$

$$\frac{dY}{dZ} = -(Y + 1)\, \psi\, a \cos\theta \tag{2-32}$$

where the solids-fluid capacity ratio, ψ, is

$$\psi = \frac{\rho_s (1 - \varepsilon) K_o}{\rho_f \varepsilon}$$

The characteristics represented by equation (2-31) are independent of Y and may be located on θ,Z coordinates without regard to equation (2-32). Their slopes are determined by the temperature which exists at time θ.

Assuming that $a \ll \psi$, we obtain

$$\frac{dZ}{d\theta} \cong \frac{1}{1 + \psi} \left[1 - \frac{a\, \psi}{1 + \psi} \sin\theta\right] \tag{2-33}$$

and integration gives

$$Z = \frac{\theta}{1 + \psi} + \frac{a\, \psi}{(1 + \psi)^2} \cos\theta + \text{constant} \tag{2-34}$$

The characteristics, given by equation (2-34), for the cycling zone process are shown in Figure 2-2 for the special case where the cycle time is set equal to twice the time of passage of the concentration wave at the bed average temperature, T_o, implying

$$\pi/\omega = L/v^* \tag{2-35}$$

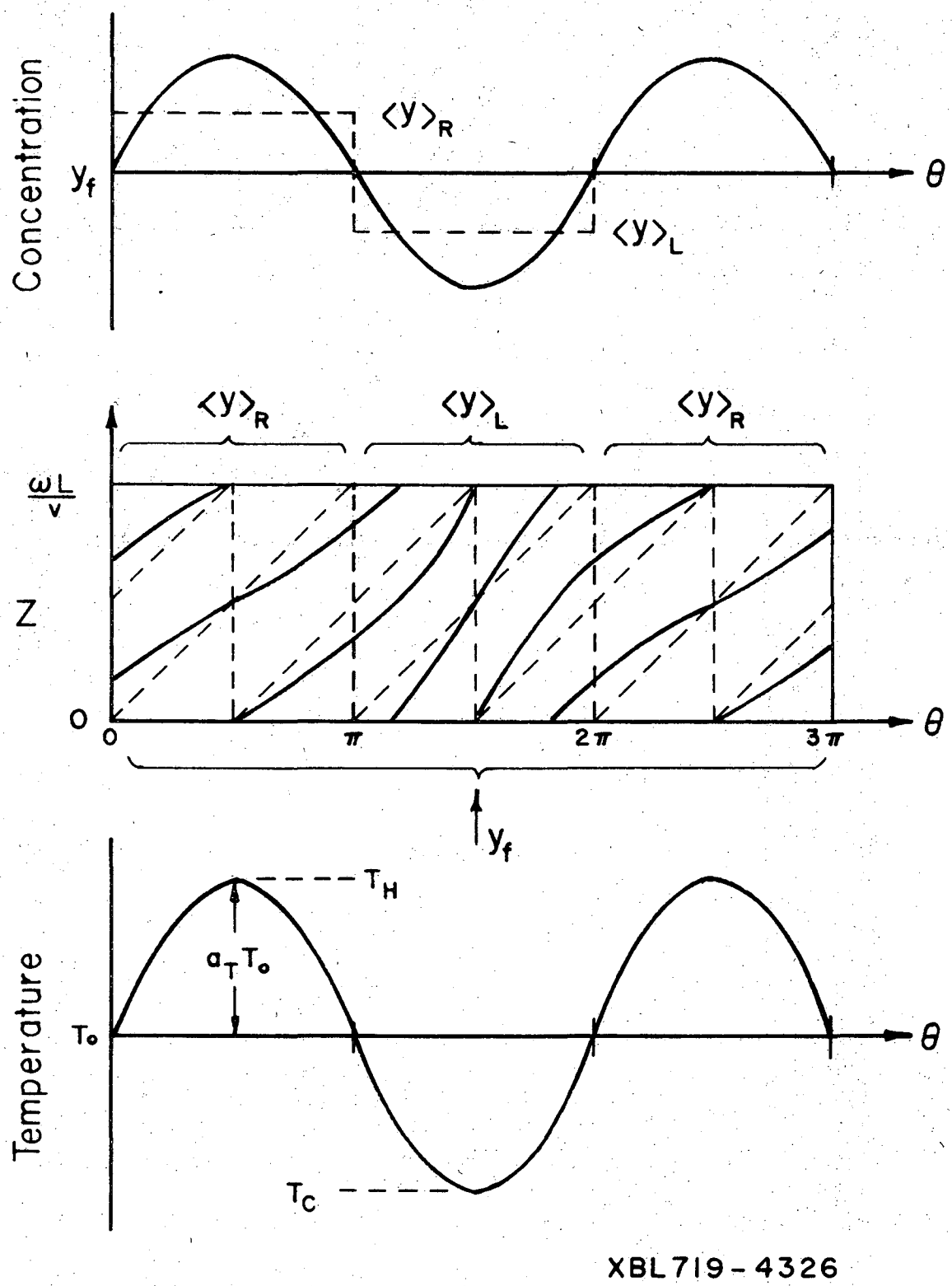

Figure 2-2. Characteristic Lines for Equilibrium Linear Behavior of Single Cycling Zone.

where the concentration wave velocity is

$$v^* = \frac{v}{1 + \psi} \tag{2-36}$$

A sinusoidal response in effluent composition results from a set of simple wave regions. The characteristic representation for square wave forcing has been discussed in detail by Baker (1969). Aris and Amundson (1965) have presented an interesting discussion of simple wave regions.

CHAPTER 3

LINEAR BEHAVIOR OF CYCLING ZONE ADSORPTION

Because of the computational time and difficulties encountered when employing numerical solution techniques, a first-order approximation method is utilized, which in the limit is exact for small variations in temperature and concentration. We shall refer to this approach as the First Perturbation Solution Method. Results, based upon linear behavior, will lead to generalizations about the relationships between operating variables. These generalizations may hold approximately in practice for large variations in composition.

SINGLE ADSORBING SPECIE SYSTEM

In a single adsorbing specie system, a solute in a non-adsorbing carrier gas is passed thru a packed bed of adsorbent particles which are heated and cooled thru the column wall. The maximum separation conditions for both single and dual cycling zone schemes were determined. The effect of periodic velocity fluctuations on the process's performance is also investigated. For a single zone process, the effect of solid-phase mass transfer resistance is discussed.

Single Zone

For small changes in composition, the equilibrium relationship may be approximated by

$$x = K(t)\, y$$

Employing the temperature forcing relationship

$$T = T_o(1 + a_T e^{i\omega t})$$

and for small changes in temperature, linearization of the Arrhenius expression gives the form:

$$K(t) = K_o(1 + a\, e^{i\omega t}) \tag{3-1}$$

where $a = a_T(\Delta H_a/RT_o)$.

For a first perturbation result we assume the solution form:

$$y(z,t) = y_f + ae^{i\omega t}\, Y_1(z) \tag{3-2}$$

A constant composition feed input requires $Y_1(0) = 0$. Substituting equations (3-1) and (3-2) into equation (2-12) and collecting coefficients of $ae^{i\omega t}$, solving the resulting ordinary differential equation for $Y_1(z)$, and applying the inlet boundary condition, we obtain

$$Y(z,t) = \frac{y(z,t) - y_f}{y_f} = -\frac{a\,\psi}{1 + \psi}\left[1 - \exp\{-i\omega\tfrac{z}{v}(1 + \psi)\}\right]e^{i\omega t} \tag{3-3}$$

where $Y(z,t)$ = dimensionless concentration; the solids-fluid capacity ratio, ψ, is defined as

$$\psi = \frac{\rho_s(1 - \varepsilon)\, K_o}{\rho_f\, \varepsilon}$$

For a sine wave temperature input, the concentration response is the imaginary part of equation (3-3), i.e.

$$\frac{Y(z,t)}{a\,\psi/(1 + \psi)} = -\left[\sin(\omega t) - \sin(\omega t - [1 + \psi]\underline{\omega})\right] \tag{3-4}$$

where the dimensionless frequency $\underline{\omega} = \omega(z/v)$. The dimensionless amplitude of the output wave is the magnitude of equation (3-3)

$$\mathcal{A} = \left|\frac{Y(z,t)}{a\ \psi/(1+\psi)}\right| = \sqrt{2}\ \left[1 - \cos\{(1+\psi)\underline{\omega}\}\right]^{1/2} \qquad (3\text{-}5)$$

The maximum amplitude achievable is 2, and exists at the condition:

$$\underline{\omega}_{max} = \frac{n\,\pi}{1+\psi}\ ,\quad n = 1,3,5\ \text{-----}$$

For n = 1, this requires that at the column exit of length L

$$(1+\psi)(L/v) = \pi/\omega \qquad (3\text{-}6)$$

We note that: L/v = fluid residence time

and

$$v^* = \frac{v}{1+\psi} = \text{concentration wave velocity at the bed average temperature.}$$

Therefore, maximum amplification requires that the time of passage of a concentration wave be equal to one-half the cycle time, that is

$$L/v^* = \pi/\omega \qquad (3\text{-}7)$$

For n = 2, no useful output occurs, Y(L,t) = 0. We therefore define a dimensionless frequency factor which is equal to unity at this condition, that is

$$\mathcal{F} = \frac{(1+\psi)\ \omega(L/v)}{2\pi} \qquad (3\text{-}8)$$

At the maximum amplification condition, $\mathcal{J} = 0.5$. In general, one would operate in the vicinity of the first maximum (n = 1) because of greater thru-puts and lower frequency requirements. It will be shown in a subsequent section that attenuations due to mass transfer resistance are smaller at low frequencies.

The phase difference between the dimensionless concentration response wave and the dimensionless input temperature wave, $(T - T_o)/T_o = a_T e^{i\omega t}$, is

$$\phi = \phi_{Rp} - \phi_I$$

where

$$\tan \phi_I = (Im/Re)_I = \sin(\omega t)/\cos(\omega t) \tag{3-9}$$

and

$$\tan \phi_{Rp} = (Im/Re)_R = \frac{\sin(\omega t) - \sin(\omega t - 2\pi\mathcal{J})}{\cos(\omega t) - \cos(\omega t - 2\pi\mathcal{J})} \tag{3-10}$$

Since

$$\tan \phi = \tan(\phi_{Rp} - \phi_I) = \frac{\tan \phi_{Rp} - \tan \phi_I}{1 + \tan \phi_{Rp} \tan \phi_I}$$

and upon substituting equations (3-9) and (3-10) into the above expression, the result is

$$\tan \phi = \tan(\pi/2 - \pi\mathcal{J})$$

or

$$\phi = \pi/2 - \pi\mathcal{J} \tag{3-11}$$

Therefore, at the maximum amplification condition ($\mathcal{J} = 0.5$), the phase difference is zero. Thus, the temperature input and the output concentration response are exactly in phase. This corresponds to the equilibrium limit situation for a linearily behaving system. It is valid also for non-linear systems as indicated in Figure 2-1.

The average separation factor, $\langle \alpha \rangle$, is defined as the ratio of the average concentration in the rich half-cycle divided by the average concentration in the lean half-cycle.

$$\langle \alpha \rangle = \langle y \rangle_R / \langle y \rangle_L \tag{3-12}$$

The average compositions, $\langle y \rangle_R$ and $\langle y \rangle_L$, are illustrated in Figure 2-2 Since the average dimensionless concentrations are

$$\left\langle \frac{y_R - y_f}{y_f} \right\rangle = - \left\langle \frac{y_L - y_f}{y_f} \right\rangle = \frac{\mathcal{A}}{\pi} \cdot \frac{a\,\psi}{(1+\psi)} \int_0^{\pi} \sin(\omega t)\, d(\omega t)$$

$$= \frac{2\sqrt{2}}{\pi} \frac{a\,\psi}{1+\psi} \left[1 - \cos(2\pi\mathcal{J})\right]^{1/2}, \tag{3-13}$$

equation (3-12) may be put in terms of dimensionless concentrations

$$\langle \alpha \rangle = \frac{\langle y \rangle_R}{\langle y \rangle_L} = \frac{1 + \left\langle \frac{y_R - y_f}{y_f} \right\rangle}{1 + \left\langle \frac{y_L - y_f}{y_f} \right\rangle} = \frac{1 + \left\langle \frac{y_R - y_f}{y_f} \right\rangle}{1 - \left\langle \frac{y_R - y_f}{y_f} \right\rangle} \tag{3-14}$$

For small concentration deviations, $\left\langle \frac{y_R - y_f}{y_f} \right\rangle \ll 1$, and therefore

$$\ln\langle\alpha\rangle \cong 2\left\langle\frac{y_R - y_f}{y_f}\right\rangle$$

$$= \frac{4}{\pi}\,\frac{a\,\psi}{1+\psi}\,\sqrt{2}\,\left[1 - \cos(2\pi\mathcal{J})\right]^{1/2}$$

We now define a dimensionless separation factor as

$$\mathcal{S} = \frac{\ln\langle\alpha\rangle\cdot(\pi/4)}{a\,\psi/(1+\psi)} = \sqrt{2}\,\left[1 - \cos(2\pi\mathcal{J})\right]^{1/2} \qquad (3\text{-}15)$$

Equation (3-15) shows that the maximum separation corresponds to the maximum amplification condition of $\mathcal{J} = 0.5$. The significance of this result is that the average concentration wave velocity, which depends upon the solids-fluid capacity ratio of a particular system, establishes the proper relationship between operating variables for maximum separation.

Dual Zone

In order to further increase the amplification of the concentration wave, it is fed into a subsequent cycling zone adsorber being cycled at an identical frequency, ω. The input to the second zone is

$$y^{(2)}(0,t) = y_f - y_f\,\frac{a\,\psi}{1+\psi}\,\left[1 - e^{-i2\pi\mathcal{J}^{(1)}}\right]e^{i\omega t} \qquad (3\text{-}16)$$

where $\mathcal{J}^{(1)}$ = dimensionless frequency factor for the first zone. The assumed solution form is

$$y^{(2)}(z,t) = y_f + ae^{i(\omega t + \phi_T)}\,Y_2(z) \qquad (3\text{-}17)$$

where ϕ_T = the phase between the second zone and the first zone's temperature inputs. Substituting equation (3-17) into equation (2-12),

collecting coefficients of $ae^{i(\omega t+\phi_T)}$ and solving the resulting differential equation for $Y_2(z)$, and applying the boundary condition at the inlet,

$$Y_2(0) = - y_f \frac{\psi}{1 + \psi} \left[1 - e^{-i2\pi \mathcal{J}^{(1)}}\right]e^{-i\phi_T} \tag{3-18}$$

yields

$$\frac{Y^{(2)}(z,t)}{a\ \psi/(1 + \psi)} = - \left[1 + \{-1 + (1 - e^{-i2\pi \mathcal{J}^{(1)}})e^{-i\phi_T}\}e^{-i2\pi \mathcal{J}^{(2)}}\right]e^{i(\omega t + \phi_T)} \tag{3-19}$$

where $\mathcal{J}^{(2)}$ = the dimensionless frequency factor for the second zone. The dimensionless amplitude of the response is:

$$\mathcal{A}^{(2)} = \left|\frac{Y^{(2)}(z,t)}{a\ \psi/(1 + \psi)}\right| = \sqrt{2}\ \left[2 - \cos(2\pi \mathcal{J}^{(2)}) - \cos(2\pi \mathcal{J}^{(1)}) + \cos(2\pi \mathcal{J}^{(2)} + \phi_T) + \cos(2\pi \mathcal{J}^{(1)} + \phi_T) - \cos(2\pi\{\mathcal{J}^{(1)} + \mathcal{J}^{(2)}\} + \phi_T) - \cos(\phi_T)\right]^{1/2} \tag{3-20}$$

For non-identical zone operation, $\mathcal{J}^{(1)} \neq \mathcal{J}^{(2)}$, and if the first zone is operated at its maximum amplification ($\mathcal{J}^{(1)} = 0.5$), the maximum amplitude of zone two, as described by equation (3-20) occurs when

$$\phi_T = \pm (\pi/2 + \pi \mathcal{J}^{(2)}) \tag{3-21}$$

When $\mathcal{J}^{(1)} = \mathcal{J}^{(2)}$ (identical zone operation) the amplitude of the second zone's effluent is:

$$\mathcal{A}^{(2)} = \sqrt{2}\ [2 - 2\cos(2\pi\mathcal{T}) + 2\cos(2\pi\mathcal{T} + \phi_T) - \cos(4\pi\mathcal{T} + \phi_T) - \cos(\phi_T)]^{1/2} \tag{3-22}$$

The maximum amplitude that exists at

$$\phi_T = \pm 2\pi\mathcal{T} \tag{3-23}$$

is

$$\mathcal{A}^{(2)} = 2\sqrt{2}\ [1 - \cos(2\pi\mathcal{T})]^{1/2}$$

$$= 2 \cdot \mathcal{A} \tag{3-24}$$

For $\mathcal{T} = 0.5$, the maximum amplification condition for a single zone, then

$$\mathcal{A}^{(2)} = 4 \quad \text{and} \quad \phi_T = \pm \pi$$

Therefore, the absolute maximum amplification for the dual zone system occurs when the system's dimensionless frequency factor, $\mathcal{T}$, is selected for the maximum amplification for a single zone and the phase between the temperature forcing functions is 180°. The resulting amplitude is twice that of a single zone. Figure 3-1 shows that the 180° temperature phase operation does not produce the maximum amplification when the dual zone system is operated at other than $\mathcal{T} = 0.5$.

For a multiple-zone system of N identically operated zones in which each zone's temperature is 180° out of phase with the previous zone's temperature input and $\mathcal{T} = 0.5$, the amplitude of the N-th zone effluent is

$$\mathcal{A}^{(N)} = 2^N \tag{3-25}$$

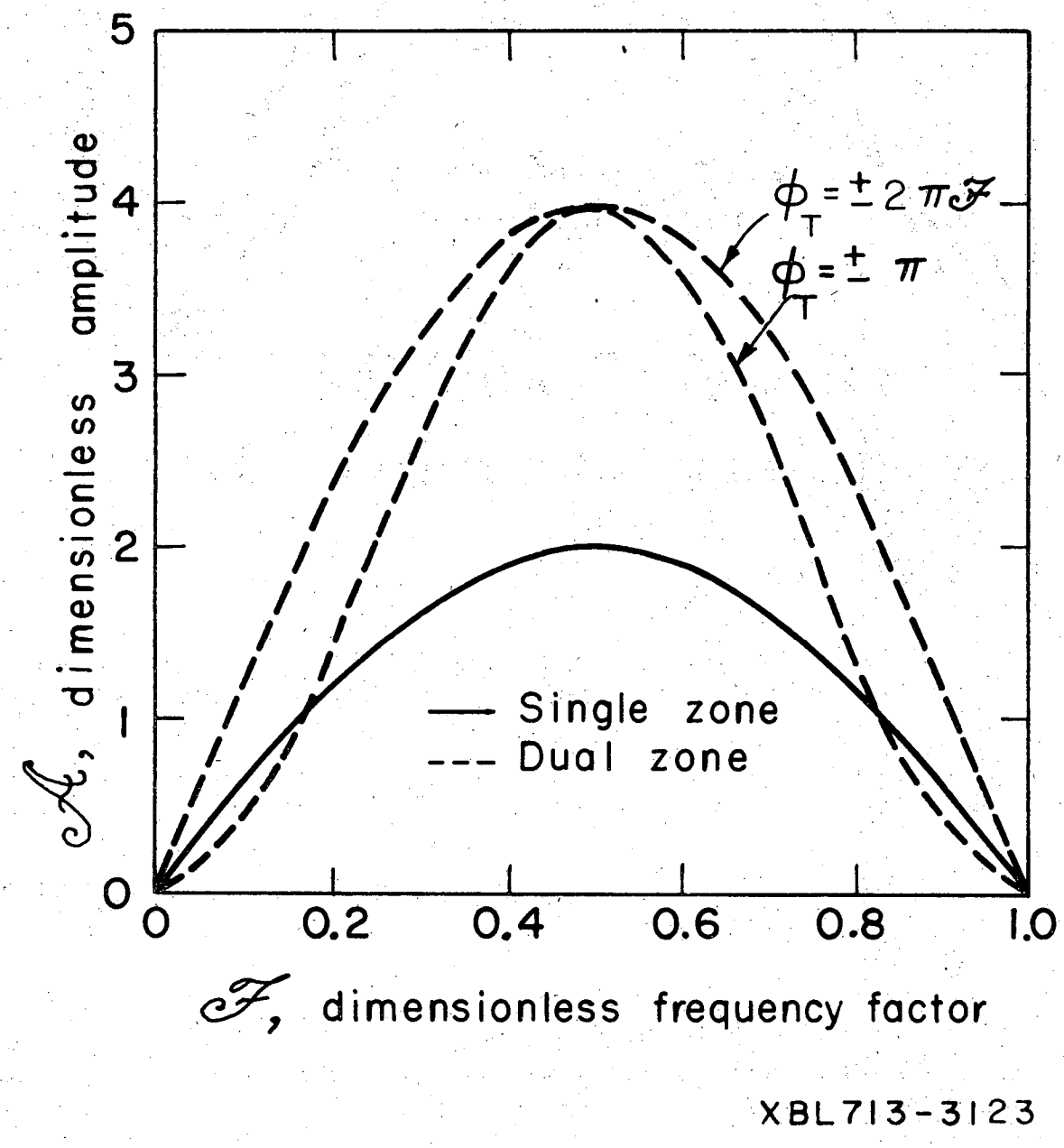

Figure 3-1. Dimensionless Amplitude of Effluent Wave: Single and Dual (identical) Zone Systems-Single Adsorbing Specie Feed.

In this study we have limited ourselves to the situation in which all zones are identical and $\mathcal{T}^{(1)} = \mathcal{T}^{(2)} = \mathcal{T}$. The concentration-time response of the second zone is the imaginary part of equation (3-19)

$$\frac{Y^{(2)}(z,t)}{a\,\psi/(1+\psi)} = -\left[\sin(2\pi\mathcal{T}) - \sin(2\pi\mathcal{T} + \phi_T) + \sin(4\pi\mathcal{T} + \phi_T)\right]\cos(\omega t + \phi_T)$$

$$-\left[1 - \cos(2\pi\mathcal{T}) + \cos(2\pi\mathcal{T} + \phi_T) - \cos(4\pi\mathcal{T} + \phi_T)\right]\sin(\omega t + \phi_T)$$

$$= -A\cos(\omega t + \phi_T) - B\sin(\omega t + \phi_T) \qquad (3\text{-}26)$$

The average dimensionless composition over a half-cycle is then

$$\langle Y^{(2)}(z,t)\rangle = -\frac{a\,\psi}{1+\psi}\left\{A\,\overline{\cos(\omega t + \phi_T)} + B\,\overline{\sin(\omega t + \phi_T)}\right\}$$

where

$$\overline{\sin(\omega t + \phi_T)} = \frac{1}{\pi}\int_{\beta}^{\beta+\pi}\sin(\omega t + \phi_T)\,d(\omega t)$$

$$= \frac{2}{\pi}\cos(\beta + \phi_T)$$

and

$$\overline{\cos(\omega t + \phi_T)} = -\frac{2}{\pi}\sin(\beta + \phi_T)$$

Here β, defined as the switching location in the dimensionless time space, is chosen to correspond to $Y^{(2)}(z,\beta/\omega) = 0$; increasing ωt yields $Y^{(2)}(z,t) > 0$. Thus the average dimensionless concentration (rich portion) is:

$$\langle Y^{(2)}(z,t) \rangle = \frac{2\sqrt{2}}{\pi} \frac{a\psi}{1+\psi} [2 - 2\cos(2\pi\mathcal{J}) + 2\cos(2\pi\mathcal{J} + \phi_T) - \cos(4\pi\mathcal{J} + \phi_T) - \cos(\phi_T)]^{1/2} \quad (3\text{-}27)$$

Substituting equation (3-27) into equation (3-14) yields the dimensionless separation factor expression:

$$\mathcal{S}^{(2)} = \sqrt{2} [2 - 2\cos(2\pi\mathcal{J}) + 2\cos(2\pi\mathcal{J} + \phi_T) - \cos(4\pi\mathcal{J} + \phi_T) - \cos(\phi_T)]^{1/2} \quad (3\text{-}28)$$

For the case when the temperature phase is given by

$$\phi_T = \pm 2\pi\mathcal{J}$$

the dual zone separation factor is

$$\mathcal{S}^{(2)} = 2\sqrt{2} [1 - \cos(2\pi\mathcal{J})]^{1/2} = 2 \cdot \mathcal{S} \quad (3\text{-}29)$$

Thus, for N identical zones:

$$\mathcal{S}^{(N)} = 2^{N-1}\mathcal{S} \quad (3\text{-}30)$$

The dimensionless separation factor when

$$\phi_T = \pm \pi$$

is

$$\mathcal{S}^{(2)} = \sqrt{2} [3 - 4\cos(2\pi\mathcal{J}) + \cos(4\pi\mathcal{J})]^{1/2} \quad (3\text{-}31)$$

and the dual zone optimum is

$$\mathcal{S}_{opt}^{(2)} = 4 \quad \text{at} \quad \mathcal{I} = 0.5$$

The use of multiple, identical CZA units in series leads to 2^{N-1} magnification of the first zone's effluent wave when the temperature change within a zone is 180° out of phase of those in adjacent zones and the optimum operating variables' relationship has been selected. The theoretical upper limit of the separation is approached when no solute exists in the lean half-cycle portion and the solute concentration in the enriched half-cycle portion is equal to twice the feed concentration. Deviations from the theoretically derived temperature phase value of π would be expected when finite mass transfer rates and/or non-linear isotherms are encountered.

The Effect of Velocity Fluctuations Upon Cycling Zone Adsorption

The first-order effect of imposing a velocity oscillation upon a single cycling zone adsorption (CZA) system is presented for a linear behaving zone. The velocity forcing function is

$$v = v_o(1 + b'e^{i(\omega t + \phi)}), \quad |b'| < 1 \tag{3-32}$$

where ϕ = phase between temperature and velocity forcing functions.

Since $|b'| < 1$, flow reversal does not occur. The assumed solution form is

$$y(z,t) = y_f + ae^{i\omega t} Y_1(z) + b'e^{i(\omega t + \phi)} Y_2(z) + ab'e^{i(2\omega t + \phi)} Y_3(z) \tag{3-33}$$

Substituting equations (3-1), (3-32), and (3-33) into equation (2-12), collecting coefficients of $ae^{i\omega t}$, $b'e^{i(\omega t + \phi)}$, and $ab'e^{i(2\omega t + \phi)}$, and

solving the resulting set of differential equations for $Y_1(z)$, $Y_2(z)$, and $Y_3(z)$ with the boundary condition of constant feed composition which implies:

$$Y_1(0) = Y_2(0) = Y_3(0) = 0$$

yields:

$$Y_1(z) = - y_f \frac{\psi}{1 + \psi} \left[1 - e^{-i2\pi\mathcal{J}}\right] ,$$

$$Y_2(z) = 0$$

where

$$\mathcal{J} = \frac{(1 + \psi)\omega(z/v_o)}{2\pi}$$

and

$$Y_3(z) = y_f \frac{\psi}{1 + \psi} \left[e^{-i2\pi\mathcal{J}} - e^{-i4\pi\mathcal{J}}\right]$$

$$= - Y_1(z)\, e^{-i2\pi\mathcal{J}}$$

Substituting the above results into equation (3-33) and rearranging, the dimensionless concentration response is

$$\frac{Y(z,t)}{a\ \psi/(1 + \psi)} = \left[1 - e^{-i2\pi\mathcal{J}}\right] \left[-e^{i\omega t} + b' e^{-i2\pi\mathcal{J}}\ e^{i(2\omega t + \phi)}\right] \qquad (3\text{-}34)$$

Averaging over a temperature half-cycle yields

$$\left\langle \frac{Y(z,t)}{a\ \psi/(1+\psi)} \right\rangle = -i\ \frac{2}{\pi}\ [1 - e^{-i2\pi\mathcal{J}}] \qquad (3\text{-}35)$$

The magnitude of equation (3-35) gives the average dimensionless concentration

$$\left| \left\langle \frac{Y(z,t)}{a\ \psi/(1+\psi)} \right\rangle \right| = \frac{2\sqrt{2}}{\pi}\ [1 - \cos(2\pi\mathcal{J})]^{1/2} \qquad (3\text{-}13)$$

The result is identical to the single-zone result obtained in equation (3-13). Thus, flow oscillations do not benefit the separations achieved by the cycling zone adsorption process. In fact, on the temperature averaged cycle, they neither help nor hinder the separation.

Mass Transfer Aspects - Solid-Phase Resistance

In general, the mass transfer resistance in adsorption processes exists primarily in the particle phase. The two mechanisms which operate in the solid phase that can be considered to operate in series are; 1) particle-phase diffusion (adsorbed state) and 2) pore diffusion. Lumping the above two resistances into an overall resistance, the mass balances on the fluid and solid phases are

$$\rho_s(1-\varepsilon)\ \frac{\partial x}{\partial t} = \rho_s(1-\varepsilon)\ k_p a_p'\ (x^* - x) \qquad (3\text{-}36)$$

$$\rho_f \varepsilon\ \frac{\partial y}{\partial t} + \rho_f \varepsilon\ v\ \frac{\partial y}{\partial z} = \rho_s(1-\varepsilon)\ k_p a_p'\ (x^* - x) \qquad (3\text{-}37)$$

where

$k_p a_p'$ = overall particle-phase mass transfer coefficient, assumed to be independent of frequency.

The equilibrium relationship is

$$x^* = K\, y$$

The distribution coefficient is forced in the following manner

$$K(t) = K_o(1 + ae^{i\omega t})$$

The initial conditions of the bed are

$$y(z,0) = y_f$$

$$x(z,0) = x_f = K_o\, y_f$$

and the entrance conditions are

$$y(0,t) = y_f$$

$$x(0,t) = x_f$$

The solution is assumed to be of the form:

$$y(z,t) = y_f + ae^{i\omega t}\, Y_1(z) \tag{3-38}$$

$$x(z,t) = x_f + ae^{i\omega t}\, X_1(z) \tag{3-39}$$

Substituting the above relationships into equation (3-36), collecting coefficients of $ae^{i\omega t}$, and solving the resultant equation for $X_1(z)$, we obtain:

$$X_1(z) = \frac{k_p a'_p\, K_o [Y_1(z) - y_f]}{i\omega + k_p a'_p} \tag{3-40}$$

Substituting equation (3-40) and the above relationships into equation (3-37), collecting coefficients of $ae^{i\omega t}$, and solving the resultant differential equation for $Y_1(z)$, gives

$$Y_1(z) = \left[\frac{-i\omega k_p a_p' y_f \psi}{i\omega k_p a_p'(1+\psi) - \omega^2}\right]\left[1 - \exp\left\{-\frac{i\omega k_p a_p'(1+\psi) - \omega^2}{i\omega + k_p a_p'}\,\frac{(\omega z)}{v}\right\}\right] \tag{3-41}$$

We define the following dimensionless variables:

$$\psi = \frac{\rho_s(1-\varepsilon)K_o}{\rho_f \varepsilon} = \text{solids-fluid capacity ratio}$$

$$\mathcal{I} = \frac{(1+\psi)\,\omega(z/v)}{2\pi} = \text{dimensionless frequency factor}$$

$$Y(z,t) = \frac{y(z,t) - y_f}{y_f} = \text{dimensionless concentration}$$

$$\Gamma = \frac{\omega/k_p a_p'}{1+\psi} = \text{dimensionless mass transfer-capacity ratio}$$

$$\Omega = \frac{\omega}{k_p a_p'} = \text{dimensionless mass transfer resistance factor}$$

The amplitude of the response is then:

$$\mathcal{A} = \left|\frac{Y(z,t)}{a\,\psi/(1+\psi)}\right|$$

$$= \frac{1}{(\Gamma+1)^{1/2}}\left[1 - 2\exp\left(-\left\{\frac{\Omega}{\Omega^2+1}\right\}2\pi\mathcal{I}\right)\cos\left(\left\{\frac{\Omega\Gamma+1}{\Omega^2+1}\right\}2\pi\mathcal{I}\right)\right.$$

$$\left. + \exp\left(-\left\{\frac{4\Omega}{\Omega^2+1}\right\}\pi\mathcal{I}\right)\right]^{1/2} \tag{3-42}$$

The effects of particle-phase mass transfer resistance on the dimensionless amplitude are shown in Figure 3-2 for $\psi = 25$, and for various values of Ω. The abscissa is the dimensionless frequency factor, $\mathcal{J}$. The equilibrium case, as described earlier, corresponds to $\Omega = 0$. As expected, the amplitude reduction is greater at higher $\mathcal{J}$ values. This corresponds to low velocities, high frequencies, and long beds. In addition, we note that the optimum $\mathcal{J}$, which yields the maximum separation, is diminished as the mass transfer resistance is increased. Therefore, the separation is attenuated from that predicted from the equilibrium theory when the resistance to mass transfer in the particle-phase is significant. In addition, the optimum dimensionless frequency factor is reduced, requiring operation at higher velocities, low frequencies, or with short beds, all of which may enhance the less important fluid-phase mass transfer effects.

TWO ADSORBING SPECIES - TRACE SYSTEM

In this section, we consider two adsorbing species within a non-adsorbing carrier gas being fed to a temperature forced cycling zone unit. The adsorbing species will be considered to exist in "trace quantities", that is $\sum_i (y_i)_a < 0.1$. Adsorption of each species is assumed independent of the other. This implies that each species behaves according to its respective equilibrium distribution function.

The optimum separation is determined for both single and dual-zone, cycling adsorption systems. The use of an isothermal adsorbent bed to further enhance the separation is investigated.

Single Zone

Assuming linear behavior, the concentration time response as previously derived, may be written for each independently adsorbing

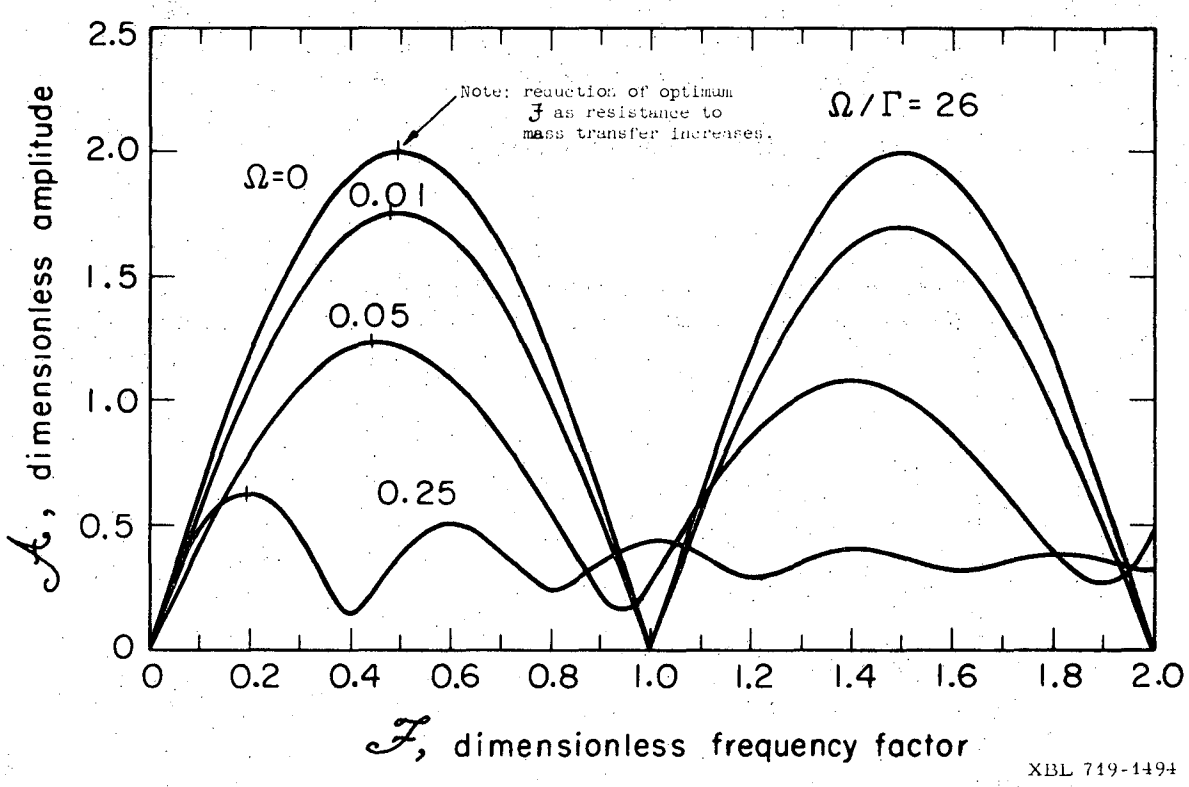

Figure 3-2. Effect of Particle-Phase Mass Transfer Resistance on Effluent Wave Amplitude; Single Zone-Single Adsorbing Specie Feed.

component as:

$$Y_1(z,t) = \frac{y_1(z,t) - y_{1f}}{y_{1f}} = - \frac{a_1 \psi_1}{1 + \psi_1} \left[\sin(\omega t) - \sin(\omega t - 2\pi \mathcal{J}_1)\right]$$

$$Y_2(z,t) = \frac{y_2(z,t) - y_{2f}}{y_{2f}} = - \frac{a_2 \psi_2}{1 + \psi_2} \left[\sin(\omega t) - \sin(\omega t - 2\pi \mathcal{J}_2)\right]$$

where

$\mathcal{J}_1$ = dimensionless frequency factor for component 1.

and

$\mathcal{J}_2$ = dimensionless frequency factor for component 2.

The following definition is made to relate the two species:

$$\Lambda = \frac{(1 + \psi_2)}{(1 + \psi_1)} = v_1^*/v_2^* = \text{concentration wave velocity ratio} \qquad (3\text{-}43)$$

therefore,

$$\mathcal{J}_2 = \Lambda \cdot \mathcal{J}_1 \qquad (3\text{-}44)$$

The average compositions over a half-cycle are determined by integration of the concentration-time responses, selecting a switching location, β, such that $\langle y_1 \rangle_R > y_{1f}$,

$$\langle Y_1(z,t) \rangle_R = - \frac{a_1 \psi_1}{1 + \psi_1} \frac{\omega}{\pi} \int_{\beta}^{\beta+\pi} Y_1(z,t)\, d(\omega t)$$

$$= \frac{a_1 \psi_1}{1 + \psi_1} \frac{2}{\pi} \left[\sin(\beta) - \sin(\beta - 2\pi \mathcal{J}_1)\right] \qquad (3\text{-}45)$$

and

$$\langle Y_2(z,t) \rangle_R = \frac{a_2 \psi_2}{1 + \psi_2} \cdot \frac{2}{\pi} \left[\sin(\beta) - \sin(\beta - 2\pi\Lambda\mathcal{T}_1)\right] \qquad (3\text{-}46)$$

The dimensionless amplitudes of each species are

$$\mathcal{A}_1 = \sqrt{2} \left[1 - \cos(2\pi\mathcal{T}_1)\right]^{1/2} \qquad (3\text{-}47)$$

$$\mathcal{A}_2 = \sqrt{2} \left[1 - \cos(2\pi\Lambda\mathcal{T}_1)\right]^{1/2} \qquad (3\text{-}48)$$

Figure 3-3 shows the dimensionless amplitudes for a system where $\Lambda = 2.2$.

The average separation factor for a two-adsorbing-specie system, or for the keys in a multicomponent adsorbing system, is defined as:

$$\langle \alpha_{12} \rangle = \frac{\langle y_1 \rangle_R}{\langle y_1 \rangle_L} \cdot \frac{\langle y_2 \rangle_L}{\langle y_2 \rangle_R} \qquad (3\text{-}49)$$

For small concentration deviations

$$\ln \langle \alpha_{12} \rangle \cong 2 \left[\langle Y_1 \rangle_R - \langle Y_2 \rangle_R \right] \qquad (3\text{-}50)$$

The dimensionless separation factor for the two adsorbing component system is found by substituting equations (3-45) and (3-46) into equation (3-50):

$$\mathcal{S}_{12} = \frac{\ln \langle \alpha_{12} \rangle (\pi/4)}{a_1 \psi_1/(1 + \psi_1)} = \sin(\beta) - \sin(\beta - 2\pi\mathcal{T}_1)$$

$$- \gamma[\sin(\beta) - \sin(\beta - 2\pi\Lambda\mathcal{T}_1)] \qquad (3\text{-}51)$$

where

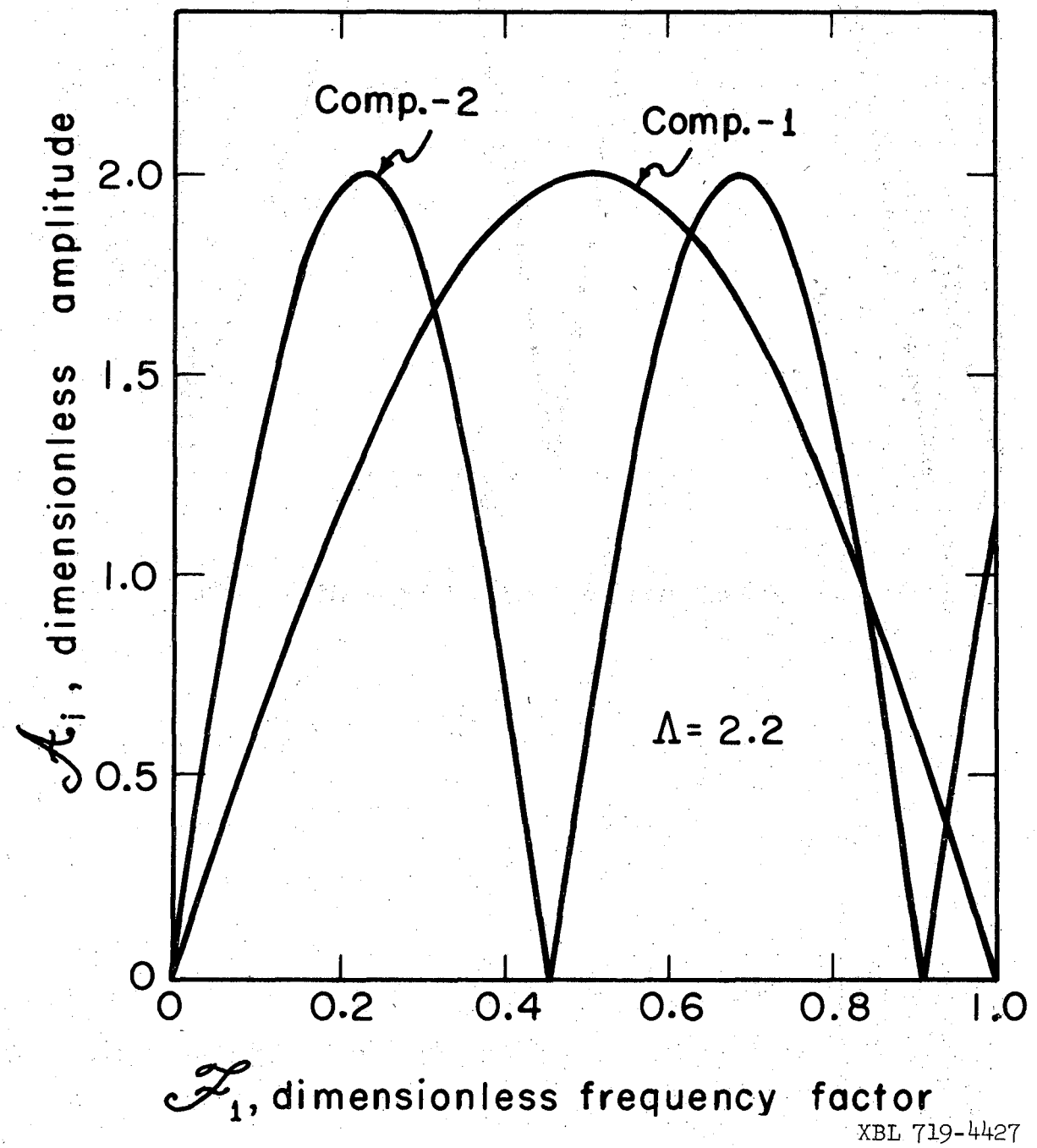

Figure 3-3. Dimensionless Amplitudes of Effluent Waves: Single Zone-Trace Feed.

$$\gamma = \left(\frac{a_2\,\psi_2}{a_1\,\psi_1}\right)\left(\frac{1+\psi_1}{1+\psi_2}\right) = \left(\frac{a_2\,\hat{\psi}_2}{a_1\,\psi_1}\right)\frac{1}{\Lambda} = \left(\frac{\Delta H a_2}{\Delta H a_1}\right)\left(\frac{K_{o_2}}{K_{o_1}}\right)\frac{1}{\Lambda} \quad ,$$

an equilibrium isotherm parameter. Thus $\mathcal{S}_{12} = \mathcal{S}_{12}(\Lambda, \gamma, \beta, \mathcal{I}_1)$ where Λ, γ are parameters dependent upon the individual equilibrium isotherms at the bed average conditions.

The problem of finding the best dimensionless separation factor, given a set of isotherm parameters (Λ, γ), can be reduced to a one-dimensional search to locate the value of $\mathcal{I}_1$ which yields the optimum $\mathcal{S}_{12}$. At the optimum

$$\frac{\partial \mathcal{S}_{12}}{\partial \beta} = 0$$

and solving for β:

$$\beta = \tan^{-1}\left[\frac{\sin(2\pi\mathcal{I}_1) - \gamma\sin(2\pi\Lambda\mathcal{I}_1)}{\gamma[1-\cos(2\pi\Lambda\mathcal{I}_1)] - [1-\cos(2\pi\mathcal{I}_1)]}\right] \qquad (3\text{-}52)$$

Equation (3-52) gives the switching location, β, which yields the maximum separation for a given $\mathcal{I}_1$. The steepest ascent numerical method was applied to equation (3-51) under the restriction stated in equation (3-52) to obtain the values of β and $\mathcal{I}_1$ which yield the optimum $\mathcal{S}_{12}$, that lies within the dimensionless frequency factor range $0 \leq \mathcal{I}_1 \leq 1$ and for various values of Λ and γ. These results are presented in Figure 3-4.

For the special case of $\gamma = 1$, as encountered in this study, the optimum $\mathcal{I}_1$ predicted, shown in Figure 3-4, is about 0.45. As shown in Figure 3-3, a value of $\mathcal{I}_1 = 0.45$ corresponds to the situation where the second component's amplitude is zero. This means that optimum separation occurs when only component-1 is amplified. Obviously, when $\gamma \neq 1$, both components are amplified at the optimum separation condition.

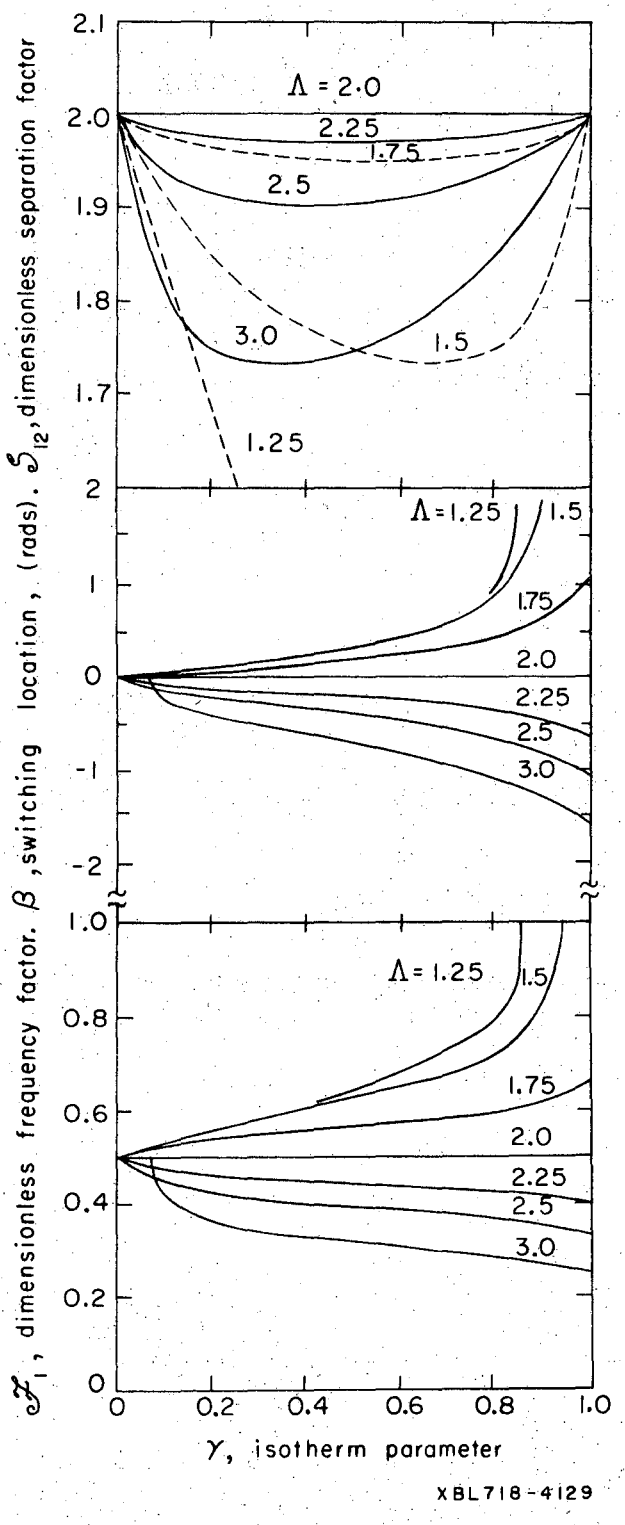

Figure 3-4. Optimum Separation Factor, Switching Location, and Dimensionless Frequency Factor: Single Zone-Trace Feed.

One may use Figure 3-4 to determine the theoretical equilibrium optimum separation and the corresponding dimensionless frequency factor for other solid-fluid adsorbing systems exhibiting linear behavior.

Dual Zone

The effluent of the first zone is fed to a second zone which is also operated at the dimensionless frequency factor $\mathcal{J}_1$. The following discussion will be limited to identical zones, their only difference being the phase of their temperature imputs. The dimensionless concentration-time response, previously stated in equation (3-26), can be written for both components. The dimensionless amplitudes of the components leaving the second zone are then:

$$\mathcal{A}_1^{(2)} = \sqrt{2}\,[2 - 2\cos(2\pi\mathcal{J}_1) + 2\cos(2\pi\mathcal{J}_1 + \phi_T) - \cos(4\pi\mathcal{J}_1 + \phi_T) - \cos(\phi_T)]^{1/2} \tag{3-53}$$

$$\mathcal{A}_2^{(2)} = \sqrt{2}\,[2 - 2\cos(2\pi\Lambda\mathcal{J}_1) + 2\cos(2\pi\Lambda\mathcal{J}_1 + \phi_T) - \cos(4\pi\Lambda\mathcal{J}_1 + \phi_T) - \cos(\phi_T)]^{1/2} \tag{3-54}$$

The dimensionless ampltiudes for the special case, $\phi_T = \pi$ and $\Lambda = 2.2$, are plotted in Figure 3-5.

The time-averaged concentrations may be determined by integration over a half-cycle, starting at an arbitrary switching location, β. Substituting the average concentration expressions into the expression for the separation factor, equation (3-50), rearranging terms we obtain

$$\mathcal{S}_{12}^{(2)} = \frac{\ln \langle \alpha_{12} \rangle (\pi/4)}{a_1 \psi_1/(1 + \psi_1)} = \mathcal{S}_{12}^{(2)}(\Lambda, \gamma, \beta, \mathcal{J}_1, \phi_T) \tag{3-55}$$

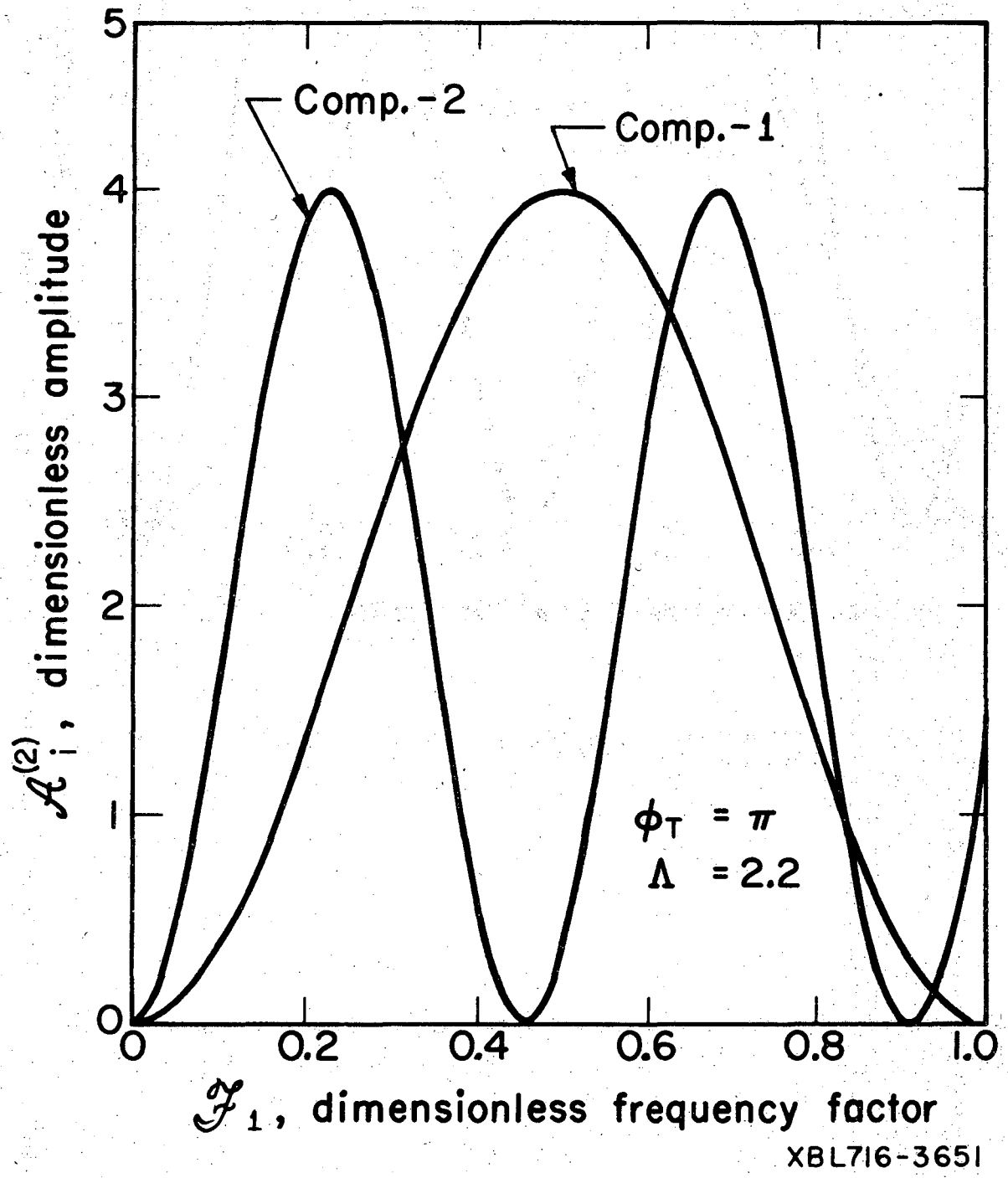

Figure 3-5. Dimensionless Amplitudes of Effluent Waves, Constant Temperature Phase: Dual (identical) Zone-Trace Feed.

$$= [\sin(2\pi\mathcal{J}_1) - \sin(2\pi\mathcal{J}_1 + \phi_T) + \sin(4\pi\mathcal{J}_1 + \phi_T) - \gamma\{\sin(2\pi\Lambda\mathcal{J}_1)$$

$$- \sin(2\pi\Lambda\mathcal{J}_1 + \phi_T) + \sin(4\pi\Lambda\mathcal{J}_1 + \phi_T)\}] \sin(\beta + \phi_T)$$

$$+ [-1 + \cos(2\pi\mathcal{J}_1) - \cos(2\pi\mathcal{J}_1 + \phi_T) + \cos(4\pi\mathcal{J}_1 + \phi_T) + \gamma\{1$$

$$- \cos(2\pi\Lambda\mathcal{J}_1) + \cos(2\pi\Lambda\mathcal{J}_1 + \phi_T) - \cos(4\pi\Lambda\mathcal{J}_1 + \phi_T)\}] \cos(\beta + \phi_T)$$

The optimum relationship between (β, ϕ_T) and $\mathcal{J}_1$ may be found by setting

$$\frac{\partial \mathcal{S}_{12}^{(2)}}{\partial \beta} = 0$$

Solving for $(\beta + \phi_T)$, we find

$$\tan(\beta + \phi_T) = \frac{A_1 - \gamma A_3}{\gamma A_4 - A_2} \tag{3-56}$$

where

$$A_1 = \sin(2\pi\mathcal{J}_1) - \sin(2\pi\mathcal{J}_1 + \phi_T) + \sin(4\pi\mathcal{J}_1 + \phi_T)$$

$$A_2 = -1 + \cos(2\pi\mathcal{J}_1) - \cos(2\pi\mathcal{J}_1 + \phi_T) + \cos(4\pi\mathcal{J}_1 + \phi_T)$$

$$A_3 = \sin(2\pi\Lambda\mathcal{J}_1) - \sin(2\pi\Lambda\mathcal{J}_1 + \phi_T) + \sin(4\pi\Lambda\mathcal{J}_1 + \phi_T)$$

$$A_4 = 1 - \cos(2\pi\Lambda\mathcal{J}_1) + \cos(2\pi\Lambda\mathcal{J}_1 + \phi_T) - \cos(4\pi\Lambda\mathcal{J}_1 + \phi_T)$$

Therefore, the computation of a best separation factor is reduced to a two-dimensional search of the function, $\mathcal{S}_{12}^{(2)} = \mathcal{S}_{12}^{(2)}(\mathcal{J}_1, \phi_T)$. A two-directional, steepest ascent vector may then be applied for the

optimization of $S_{12}^{(2)}$, given a set of Λ, γ. A typical search path is shown in Figure 3-6, for $\Lambda = 2.2$ and $\gamma = 1.0$. Two peaks are encountered, but the first peak is the global maximum. This is beneficial since its location corresponds to greater thru-puts than for the second peak. In addition, we note that the optimum phase difference of the temperature inputs for the dual zone system processing a trace feed does not equal π, as in the single adsorbing specie case. For the special case of $\gamma = 1$, the optimum $\mathcal{I}_1$ of 0.29 corresponds to amplification of both components, as indicated in Figure 3-5.

The optimum values of ϕ_T and $\mathcal{I}_1$ which yield optimum separation are presented in Figure 3-7 for various values of Λ and γ. This plot may be used to predict the optimum equilibrium separation and optimum operating conditions for other dual zone, solid-fluid adsorbing systems.

Utilization of an Isothermal Shifter

For a "trace component" system, the effluent of a series of cycling zones may be passed through an isothermal bed, equal in diameter to that of the zones and packed with the same adsorbent particles. The isothermal bed is designed, by selection of its length and/or temperature level, such that its output concentration waves are 180° out of phase. Then the stream is split into enriched and depleted portions to accomplish the separation. The shift in the concentration waves' phase toward 180° from the value entering the shifter bed is accomplished by the relative differences in the individual specie concentration wave velocities within the isothermal shifter.

For a linear behaving isothermal bed;

$$x = K_o\, y$$

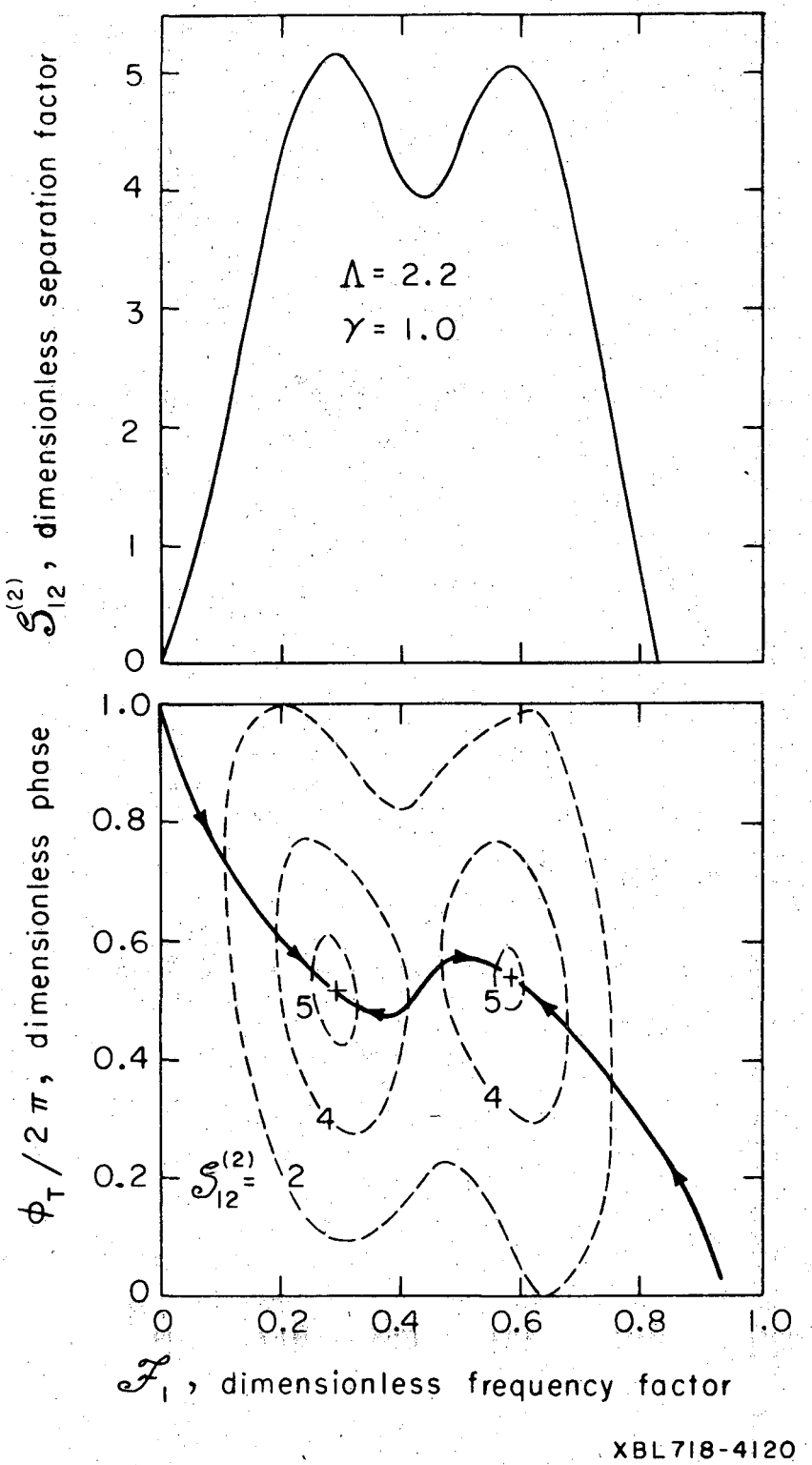

Figure 3-6. Search Path for Optimization of Separation Factor: Dual (identical) Zone-Trace Feed.

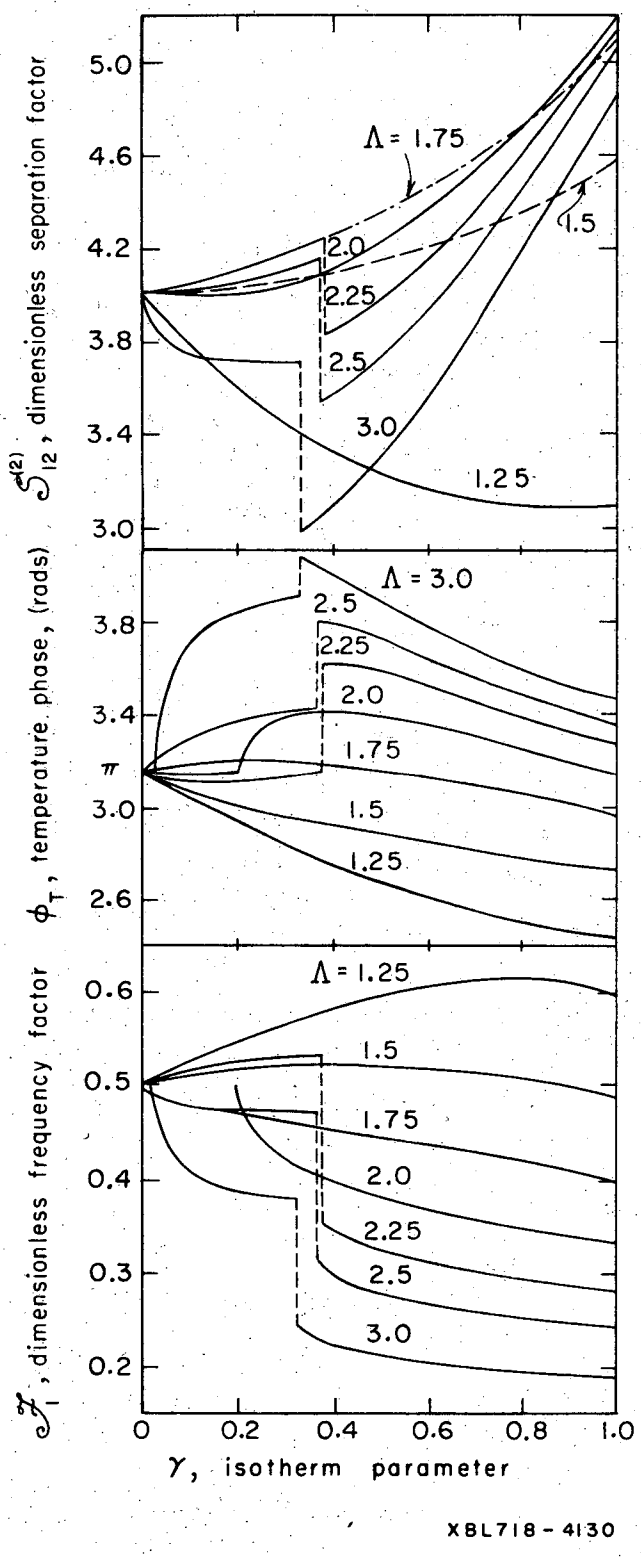

Figure 3-7. Optimum Separation Factor, Temperature Phase, and Dimensionless Frequency Factor: Dual (identical) Zone-Trace Feed.

to which a sinusoidal varying concentration wave is fed of the form

$$y(0,t) = y_f(1 + de^{i\omega t}), \quad |d| < 1 \tag{3-57}$$

the response is assumed to be of the form:

$$y(z,t) = y_f + de^{i\omega t}Z_1(z) \tag{3-58}$$

Substituting the above equations into the differential mass balance, equation (2-12), and solving the resulting differential equation for $Z_1(z)$, we obtain

$$Z_1(z) = y_f \exp(-i2\pi\mathcal{J}^*)$$

$$= y_f\, e^{-i\phi_s} \tag{3-59}$$

where

$$\mathcal{J}^* = \frac{(1 + \psi)\omega(L_s/v)}{2\pi} = \text{shifter dimensionless frequency factor.}$$

and

ϕ_s = phase lag of output concentration wave.

Thus

$$\phi_s = 2\pi\mathcal{J}^*. \tag{3-60}$$

For an isothermal shifter of length L_s, the net shift in the concentration waves, for two adsorbing species, resulting from passage thru the shifter, is

$$\phi_{NET} = \phi_{s_2} - \phi_{s_1} = 2\pi(\mathcal{T}_2^* - \mathcal{T}_1^*)$$

or

$$\phi_{NET}/2\pi = (\Lambda^* - 1)\mathcal{T}_1^* \tag{3-61}$$

where

$$\Lambda^* = \frac{1 + \psi_2}{1 + \psi_1} = \frac{v_1^*}{v_2^*} = \text{concentration wave velocity ratio in shifter.}$$

Adjustment in the shifter length, L_s and the shifter temperature, T_s, which influences Λ^* and $\mathcal{T}_1^*$, is made to produce an output phase difference of 180°. The phase relationship of the input concentration waves is required before the shifter length can be specified.

Assume that an ideal shifter can be selected to produce exactly 180° concentration phase differences and assume that it is applied at the end of a single cycling zone. The dimensionless amplitudes leaving the cycling zone for the individual species are given by equations (3-47) and (3-48). Since there is no amplitude loss in the ideal shifter, the average dimensionless concentrations leaving the shifter are

$$\frac{\langle Y_1^*(L_s,t)\rangle_R}{a_1\,\psi_1/(1+\psi_1)} = \frac{2}{\pi}\cdot\mathcal{A}_1 \tag{3-62}$$

$$\frac{\langle Y_2^*(L_s,t)\rangle_L}{a_2\,\psi_2/(1+\psi_2)} = \frac{2}{\pi}\cdot\mathcal{A}_2 \tag{3-63}$$

Substituting the above relationships into equation (3-50) and rearranging, we obtain

$$S_{12}^{*} = A_1 + \gamma A_2 = \sqrt{2}\,\{[1 - \cos(2\pi \mathcal{T}_1)]^{1/2} + \gamma[1 - \cos(2\pi\Lambda \mathcal{T}_1)]^{1/2}\} \tag{3-64}$$

The enhancement of the dimensionless separation factor by employing an ideal shifter after a single zone cycling unit, before the effluent is split into its enriched and depleted portions, is presented in Figure 3-8 for $\Lambda = 2.2$ and $\gamma = 1.0$.

Similarily, for a dual zone system in which $\phi_T = \pi$, followed by an ideal shifter, the separation factor is

$$S_{12}^{*} = A_1^{(2)} + \gamma\, A_2^{(2)}$$

where

$$A_1^{(2)} = \sqrt{2}\,[3 - 4\cos(2\pi \mathcal{T}_1) + \cos(4\pi \mathcal{T}_1)]^{1/2} \tag{3-65}$$

$$A_2^{(2)} = \sqrt{2}\,[3 - 4\cos(2\pi\Lambda \mathcal{T}_1) + \cos(4\pi\Lambda \mathcal{T}_1)]^{1/2} \tag{3-66}$$

Application of a shifter to the effluent of a dual zone system does not improve the separation factor as significantly as when it is applied to a single zone system. The improvement by application of a shifter to a dual zone system is shown in Figure 3-9. The improvement is less significant, because part of the necessary shifting takes place in the second cycling zone.

The use of an ideal shifter results in two peaks in the improved separation factor, the larger being at higher dimensionless frequency factors, $\mathcal{T}_1$. As discussed earlier, this region of operation is not favorable since significant attenuations occur in the CZA system and

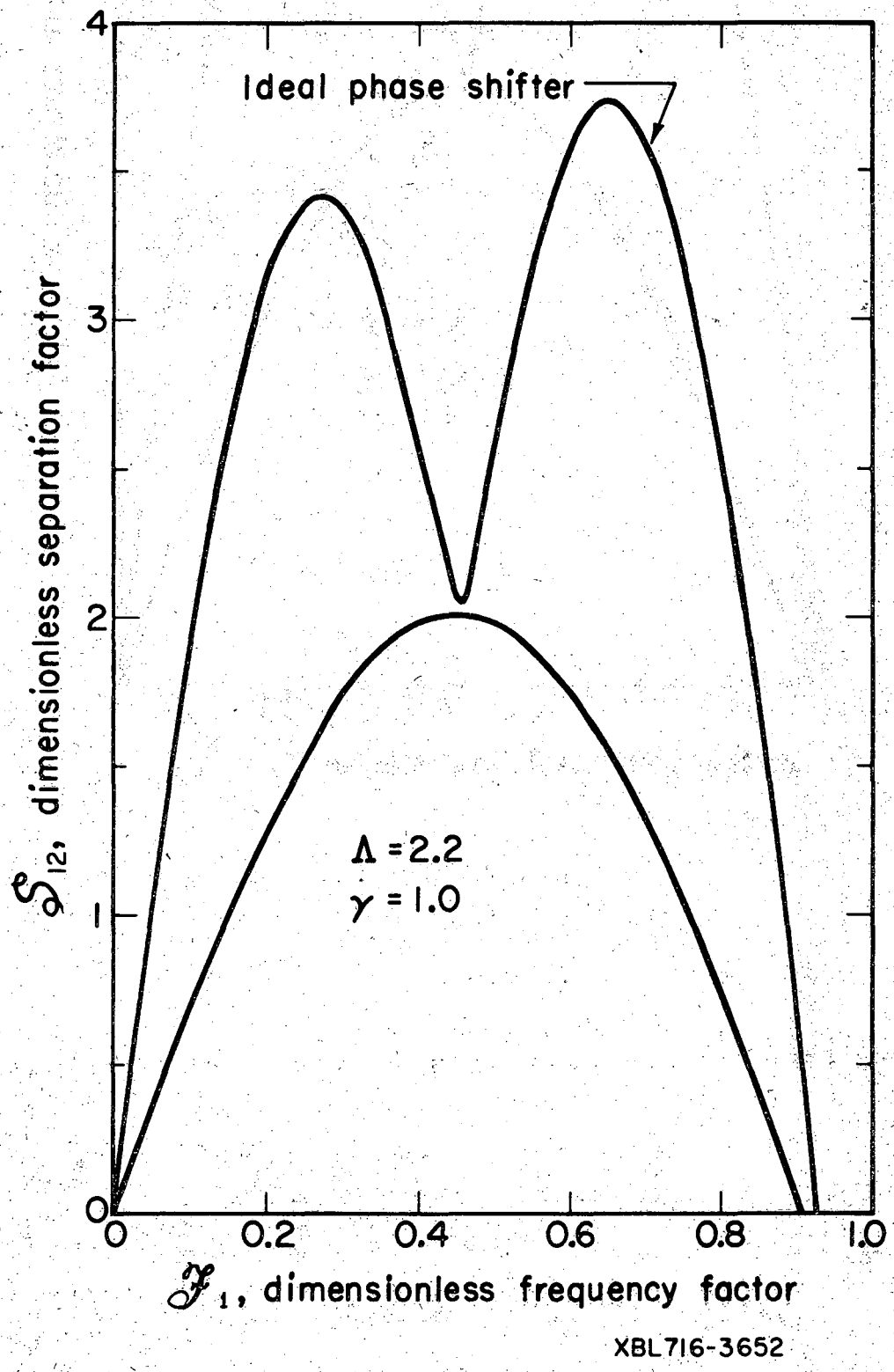

Figure 3-8. Improvement of Separation Factor by Addition of an Ideal Isothermal Shifter Bed: Single Zone System.

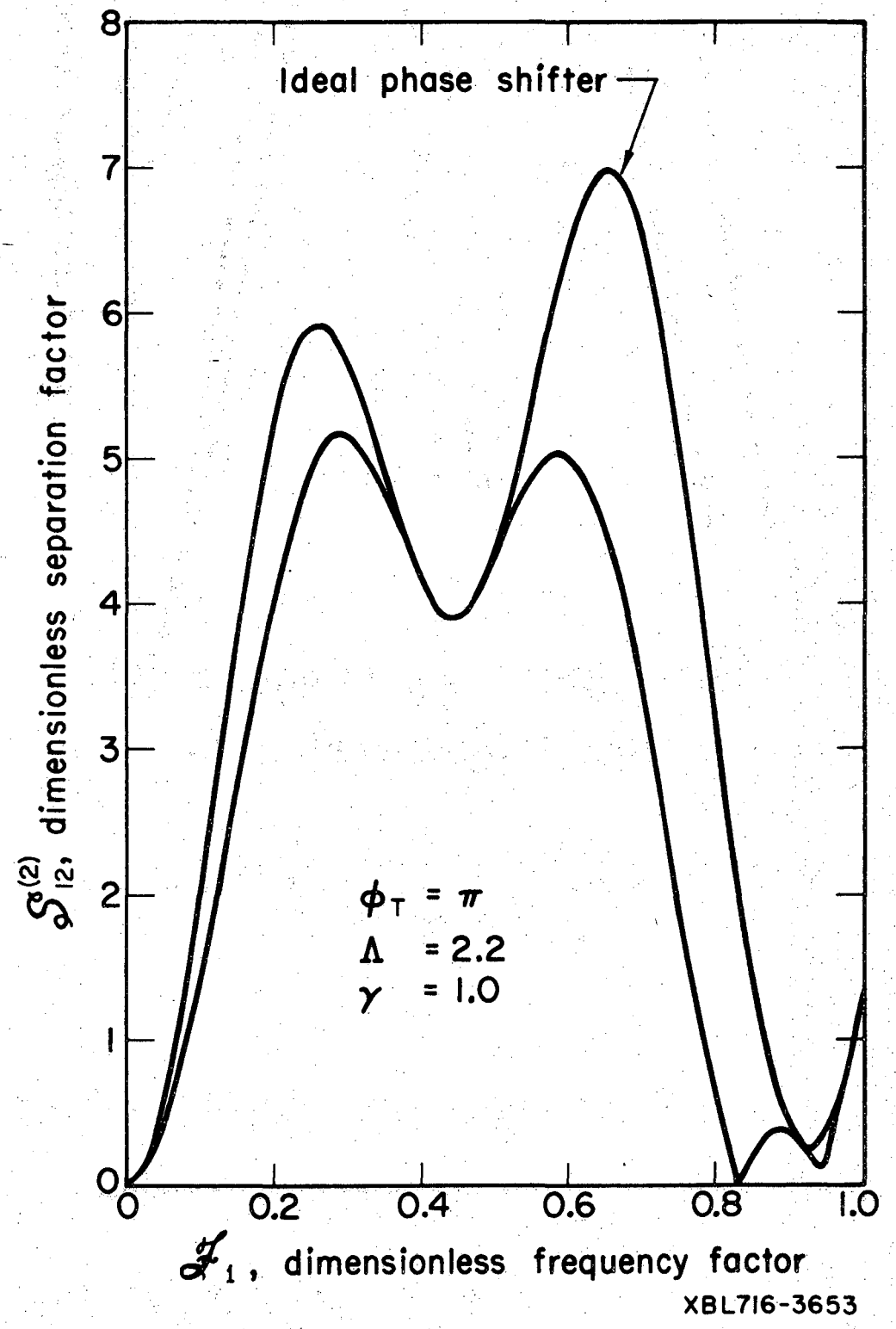

Figure 3-9. Improvement of Separation Factor by Addition of an Ideal Isothermal Shifter Bed: Dual (identical) Zone System.

within the shifter when resistance to mass transfer is present. In addition, it corresponds to lower thru-puts than that for the first peak. Therefore, in practice the region around the first peak is the more desirable operating region when employing an isothermal shifter bed.

We have avoided the problem of designing the shifter for the above results. An example of specifing the shifter design is given in a later chapter.

BINARY ADSORBING SYSTEMS

In the binary adsorbing system, a binary mixture of two adsorbing species is utilized as the feed to the cycling zone adsorber. In the fluid phase, a material balance requires that $y_1 + y_2 = 1$ is satisfied at all times. In the adsorbed state, interaction and competition for available adsorption sites alter the behavior of the individual adsorbing species from that which would exist in the presence of a non-adsorbing diluent.

Both single and dual zone schemes are investigated to determine the maximum separation conditions.

Single Zone

A constant composition mixture of components 1 and 2 is fed to a packed bed of adsorbent particles whose temperature is oscillated. The component material balances over a small section of the adsorbtive bed are

$$\frac{\partial y_1}{\partial t} + \frac{\rho_s(1-\varepsilon)}{\rho_f \varepsilon}\frac{\partial x_1}{\partial t} + \frac{\partial}{\partial z}(vy_1) = 0 \qquad (3\text{-}67)$$

$$\frac{\partial y_2}{\partial t} + \frac{\rho_s(1-\varepsilon)}{\rho_f \varepsilon}\frac{\partial x_2}{\partial t} + \frac{\partial}{\partial z}(vy_2) = 0 \qquad (3\text{-}68)$$

Adding equations (3-67) and (3-68), applying the gas-phase material balance, and substituting the result into equation (3-68), we obtain

$$\frac{\partial y_1}{\partial t} + \frac{\rho_s(1-\varepsilon)}{\rho_f \varepsilon}\left[y_2 \frac{\partial x_1}{\partial t} - y_1 \frac{\partial x_2}{\partial t}\right] + v \frac{\partial y_1}{\partial z} = 0 \qquad (3\text{-}69)$$

The boundary condition at the entrance is

$$y_1(0,t) = y_{1f}$$

Once equation (3-69) is solved for $y_1(z,t)$, then the component 2 solution is

$$y_2(z,t) = 1 - y_1(z,t)$$

The equilibrium relationships for the individual species in the binary mixture may be written as:

$$\begin{aligned} x_1 &= F_1(y_1, y_2, T) \\ x_2 &= F_2(y_1, y_2, T) \end{aligned} \qquad (3\text{-}70)$$

For the input temperature disturbance of

$$T = T_o(1 + a_T e^{i\omega t})$$

the assumed first-order solution forms are

$$y_1(z,t) = y_{1f} + a\, Y_o(z)\, e^{i\omega t}, \qquad |Y_o| \ll y_{1f} \qquad (3\text{-}71)$$

$$\begin{aligned} x_1(z,t) &= x_{1f} + a\, X_1(z)\, e^{i\omega t} \\ x_2(z,t) &= x_{2f} + a\, X_2(z)\, e^{i\omega t}, \end{aligned} \qquad |X_i| \ll x_{if} \qquad (3\text{-}72)$$

Since $y_1 + y_2 = 1$, then

$$y_2(z,t) = y_{2f} - a\, Y_o(z)\, e^{i\omega t} \tag{3-73}$$

Substituting the assumed response forms into equation (3-69), retaining only the first order terms, one arrives at:

$$Y_o + \frac{\rho_s(1-\varepsilon)}{\rho_f\,\varepsilon}\,[y_{2f}\,X_1 - y_{1f}\,X_2] + \frac{v}{i\omega}\,\frac{dY_o}{dz} = 0 \tag{3-74}$$

Linearization of the distribution functions about the feed condition (y_{1f}, y_{2f}, T_o) gives

$$x_1 - x_{1f} = \frac{\partial F_1}{\partial y_1}\Big|_f (y_1 - y_{1f}) + \frac{\partial F_1}{\partial y_2}\Big|_f (y_2 - y_{2f}) + \frac{\partial F_1}{\partial T}\Big|_f (T - T_o)$$

$$x_2 - x_{2f} = \frac{\partial F_2}{\partial y_1}\Big|_f (y_1 - y_{1f}) + \frac{\partial F_2}{\partial y_2}\Big|_f (y_2 - y_{2f}) + \frac{\partial F_2}{\partial T}\Big|_f (T - T_o)$$

Upon substitution of the input and response forms into the linearized equilibrium relationships, we obtain:

$$X_1(z) = (A_{11} - A_{12})\, Y_o(z) + A_1\,\frac{(a_T\, T_o)}{a} \tag{3-75}$$

$$X_2(z) = (A_{21} - A_{22})\, Y_o(z) + A_2\,\frac{(a_T\, T_o)}{a} \tag{3-76}$$

where

$$A_{11} = (\partial F_1/\partial y_1)_f$$

$$A_{12} = (\partial F_1/\partial y_2)_f$$

$$A_{21} = (\partial F_2/\partial y_1)_f \qquad (3\text{-}77)$$

$$A_{22} = (\partial F_2/\partial y_2)_f$$

$$A_1 = (\partial F_1/\partial T)_f$$

$$A_2 = (\partial F_2/\partial T)_f$$

The bracketed term in equation (3-74) may then be written as

$$y_{2f} X_1 - y_{1f} X_2 = M_o Y_o + [y_{2f} A_1 - y_{1f} A_2] (a_T T_o/a)$$

where the effective distribution coefficient for the binary mixture, M_o, is defined as:

$$M_o = y_{2f}(A_{11} - A_{12}) + y_{1f}(A_{22} - A_{21}) \qquad (3\text{-}78)$$

Equation (3-74) now becomes:

$$[1 + \psi_m] Y_o + \frac{v}{i\omega} \frac{dY_o}{dz} = - \psi_m C_1 y_{1f} \qquad (3\text{-}79)$$

where:

$$\psi_m = \frac{\rho_s(1 - \varepsilon)}{\rho_f \varepsilon} \cdot M_o \quad , \quad \text{solids-fluid capacity ratio at bed average conditions.}$$

and

$$C_1 = \text{constant} = \left(\frac{y_{2f} A_1 - y_{1f} A_2}{y_{1f}}\right)\left(\frac{a_T T_o}{a M_o}\right)$$

The solution of equation (3-79), applying the entrance condition, $Y_o(0) = 0$, is

$$Y_o(z) = - C_1 y_{1f} \left(\frac{\psi_m}{1 + \psi_m}\right)[1 - \exp(-i \{1 + \psi_m\} \frac{\omega z}{v})]$$

and the concentration-time response is

$$y_1(z,t) = y_{1f} - \frac{a_m \psi_m}{1 + \psi_m} \cdot y_{1f} [1 - \exp(-i \{1 + \psi_m\} \frac{\omega z}{v})] e^{i\omega t} \tag{3-80}$$

where

$$a_m = \left(\frac{y_{2f} A_1 - y_{1f} A_2}{y_{1f}}\right)\left(\frac{a_T T_o}{M_o}\right) = C_1 a \tag{3-81}$$

For a sine wave temperature input, the concentration response is the imaginary part of equation (3-80), which may be written in the following dimensionless form:

$$\frac{Y_1(L,t)}{a_m \psi_m/(1 + \psi_m)} = \frac{(y_1 - y_{1f})/y_{1f}}{a_m \psi_m/(1 + \psi_m)} = - [\sin(\omega t) - \sin(\omega t - 2\pi \mathcal{J}_m)] \tag{3-82}$$

where

$\mathcal{J}_m = \dfrac{(1 + \psi_m)}{2\pi} \cdot \omega(L/v)$, the dimensionless frequency factor for the mixture.

The dimensionless amplitude of the concentration response is the magnitude of equation (3-80):

$$\mathcal{A}_1 = \frac{(y_{1_{max}} - y_{1f})/y_{1f}}{a_m \psi_m/(1 + \psi_m)} = \sqrt{2}\,[1 - \cos(2\pi \mathcal{J}_m)]^{1/2} \qquad (3\text{-}83)$$

whose maximum exists at $\mathcal{J}_m = 0.5$.

The phase difference between the dimensionless concentration response of component 1 at the exit of the bed and the dimensionless input temperature wave can be shown to be:

$$\phi = \pi/2 - \pi \mathcal{J}_m \qquad (3\text{-}84)$$

The phase difference between component 1 and component 2 concentration waves, ϕ_c, for a binary system is always 180°.

We note that the above results are of identical form of those obtained for the single adsorbing specie case, (See equations (3-4) and (3-5)). The essential difference lies in the evaluation of the parameters a_m and ψ_m.

The average separation factor, as previously defined by equation (3-49), for small concentration deviations, becomes

$$\ln \langle \alpha_{12} \rangle \cong 2\,[\langle Y_1 \rangle_R - \langle Y_2 \rangle_R]$$

For a binary mixture

$$\langle y_2 \rangle_R = 1 - \langle y_1 \rangle_R$$

or

$$\langle Y_2 \rangle_R = -\frac{y_{1f}}{1 - y_{1f}} \langle Y_1 \rangle_R$$

Therefore, the average separation factor for the mixture is

$$\ln \langle \alpha_{12} \rangle_m \cong \left(\frac{2}{1 - y_{1f}} \right) \langle Y_1 \rangle_R \tag{3-85}$$

The average half-cycle dimensionless concentration may be evaluated by integration of the sinusoidal output wave, yielding

$$\frac{\langle Y_1 \rangle_R}{a_m \psi_m/(1 + \psi_m)} = \frac{1}{\pi} \int_0^{\pi} \mathcal{A}_1 \sin(\omega t)\, d(\omega t)$$

$$= \frac{2}{\pi} \cdot \mathcal{A}_1 \tag{3-86}$$

The dimensionless separation factor for the binary system is now defined as:

$$(\mathcal{S}_{12})_m = \frac{(1 - y_{1f}) \ln \langle \alpha_{12} \rangle_m \cdot (\pi/4)}{a_m \psi_m/(1 + \psi_m)} = \mathcal{A}_1$$

$$= \sqrt{2}\, [1 - \cos(2\pi \mathcal{T}_m)]^{1/2} \tag{3-87}$$

Equation (3-87) shows that the maximum separation condition corresponds to the maximum amplification condition of $\mathcal{T}_m = 0.5$.

Dual Zone

The cyclic effluent of the first zone is fed to a subsequent CZA unit, whose temperature input function is of the form:

$$T = T_o [1 + a_T e^{i(\omega t + \phi_T)}]$$

where ϕ_T is the phase difference between the second and first zones'

temperature inputs. This discussion will be restricted to the case of identical zone operation, that is

$$\mathcal{T}_m = \mathcal{T}_m^{(1)} = \mathcal{T}_m^{(2)}$$

Other special cases can be readily derived without the above restriction.

The input concentrations to the second zone are

$$y_1^{(2)}(0,t) = y_{1f} - \frac{a_m \psi_m}{1 + \psi_m} \cdot y_{1f} \left[1 - e^{-i2\pi\mathcal{T}_m}\right] e^{i\omega t}$$

$$y_2^{(2)}(0,t) = 1 - y_1^{(2)}(0,t) \tag{3-88}$$

The assumed solution forms are

$$y_1^{(2)}(z,t) = y_{1f} + a\, Y_o^{(2)}(z)\, e^{i(\omega t + \phi_T)}$$

$$y_2^{(2)}(z,t) = y_{2f} - a\, Y_o^{(2)}(z)\, e^{i(\omega t + \phi_T)}$$

$$x_1^{(2)}(z,t) = x_{1f} + a\, X_1^{(2)}(z)\, e^{i(\omega t + \phi_T)} \tag{3-89}$$

$$x_2^{(2)}(z,t) = x_{2f} + a\, X_2^{(2)}(z)\, e^{i(\omega t + \phi_T)}$$

Proceeding in the manner described in the previous sections, the following results may be derived. The dimensionless concentration of component 1 at the bed exit is

$$\frac{Y_1^{(2)}(L,t)}{a_m \psi_m/(1 + \psi_m)} = -\left[1 + \left\{-1 + \left(1 - e^{-i2\pi\mathcal{T}_m}\right) e^{-i\phi_T}\right\} e^{-i2\pi\mathcal{T}_m}\right] e^{i(\omega t + \phi_T)} \tag{3-90}$$

whose dimensionless amplitude is

$$\mathcal{A}_1^{(2)} = \sqrt{2}\,[2 - 2\cos(2\pi\mathcal{J}_m) + 2\cos(2\pi\mathcal{J}_m + \phi_T) - \cos(4\pi\mathcal{J}_m + \phi_T) - \cos(\phi_T)]^{1/2} \tag{3-91}$$

When the temperature phase is set as

$$\phi_T = \pm\, 2\pi\mathcal{J}_m \tag{3-92}$$

the dimensionless amplitude becomes

$$\mathcal{A}_1^{(2)} = 2\,\sqrt{2}\,[1 - \cos(2\pi\mathcal{J}_m)]^{1/2} = 2\,\mathcal{A}_1^{(1)} \tag{3-93}$$

For the special case of $\mathcal{J}_m = 0.5$, the optimum amplification condition for single zone operation, the dimensionless amplitude is;

$$\mathcal{A}_1^{(2)} = 2\,\sqrt{2}\,[1 - \cos(\phi_T)]^{1/2} \tag{3-94}$$

whose optimum value of 4 exists at $\phi_T = \pm\,\pi$. Therefore, the absolute maximum amplification for the dual, identically operated, zone system occurs when the system's dimensionless frequency factor, $\mathcal{J}_m$, is selected for maximum amplification in the first zone and when the phase between the input temperature forcing functions is 180°. The amplitudes versus the dimensionless frequency factor for the binary adsorbing system are shown in Figure 3-10. It is clear that the 180° temperature phase yields maximum amplification only when $\mathcal{J}_m$ is equal to 0.5. Here again, we note the similarity of the above results and those obtained for a single adsorbing specie system.

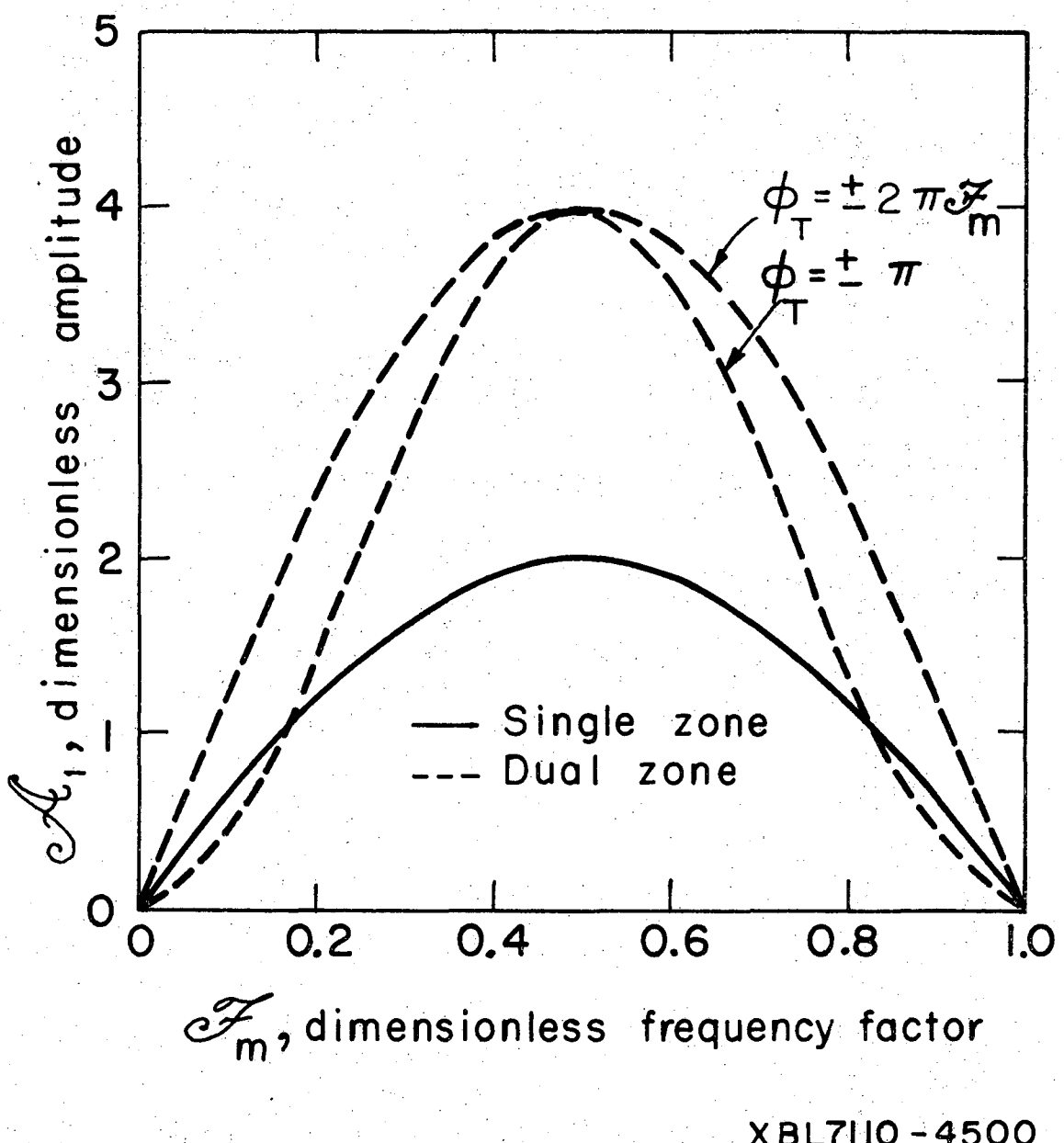

Figure 3-10. Dimensionless Amplitude of Effluent Wave: Single and Dual (identical) Zone Systems-Binary Feed.

The expressions for the average dimensionless separation factor may be derived in a manner analogous to that utilized for the single adsorbing specie system and are listed below.

$$(\mathcal{S}_{12})_m^{(2)} = \frac{(1 - y_{1f}) \ln \langle \alpha_{12} \rangle_m \cdot (\pi/4)}{a_m \psi_m/(1 + \psi_m)}$$

$$= \sqrt{2} \left[2 - 2\cos(2\pi \mathcal{J}_m) + 2\cos(2\pi \mathcal{J}_m + \phi_T) - \cos(4\pi \mathcal{J}_m + \phi_T) - \cos(\phi_T)\right]^{1/2} \quad (3\text{-}95)$$

For $\phi_T = \pm 2\pi \mathcal{J}_m$,

$$(\mathcal{S}_{12})_m^{(2)} = 2\sqrt{2} \left[1 - \cos(2\pi \mathcal{J}_m)\right]^{1/2} = 2(\mathcal{S}_{12})_m^{(1)} \quad (3\text{-}96)$$

For $\phi_T = \pm \pi$,

$$(\mathcal{S}_{12})_m^{(2)} = \sqrt{2} \left[3 - 4\cos(2\pi \mathcal{J}_m) + \cos(4\pi \mathcal{J}_m)\right]^{1/2} \quad (3\text{-}97)$$

The optimum separation factor exists at $\mathcal{J}_m = 0.5$ and $\phi_T = \pm \pi$ and is

$$(\mathcal{S}_{12})_{m\ opt}^{(2)} = 4$$

The theoretical results for linear behaving CZA systems are summarized in Table 3-1.

Table 3-1. Theoretical Results for Linear CZA Behavior.

Type of Feed	Dimensionless Separation Factor		Optimum Separation & Operating Conditions	
	Single Zone	Dual Zone*	Single Zone	Dual Zone*
Single Solute Feed	$S = \sqrt{2}\,[1 - \cos(2\pi\vartheta)]^{1/2}$	$S^{(2)} = \sqrt{2}\,[2 - 2\cos(2\pi\vartheta) + 2\cos(2\pi\vartheta + \phi_T) - \cos(4\pi\vartheta + \phi_T) - \cos(\phi_T)]^{1/2}$	$\vartheta = 0.5$ $S = 2$	$\vartheta = 0.5$ $\phi_T = \pi$ $S^{(2)} = 4$
Two Solute-Trace Feed	$S_{12} = \sin(\beta) - \sin(\beta - 2\pi\vartheta_1) - \gamma[\sin(\beta) - \sin(\beta - 2\pi A\vartheta_1)]$	$S_{12}^{(2)} = [\sin(2\pi\vartheta_1) - \sin(2\pi\vartheta_1 + \phi_T) + \sin(4\pi\vartheta_1 + \phi_T) - \gamma\{\sin(2\pi A\vartheta_1) - \sin(2\pi A\vartheta_1 + \phi_T) + \sin(4\pi A\vartheta_1 + \phi_T)\}] \times \sin(\beta + \phi_T) + [-1 + \cos(2\pi\vartheta_1) - \cos(2\pi\vartheta_1 + \phi_T) + \cos(4\pi\vartheta_1 + \phi_T) + \gamma\{1 - \cos(2\pi A\vartheta_1) + \cos(2\pi A\vartheta_1 + \phi_T) - \cos(4\pi A\vartheta_1 + \phi_T)\}] \cos(\beta + \phi_T)$	For $A = 2.2$ & $\gamma = 1$: $\vartheta_1 = 0.45$ $\beta = -0.5$ $S_{12} = 2$	For $A = 2.2$ & $\gamma = 1$: $\vartheta_1 = 0.29$ $\beta = \sim\pi$ $\phi_T = \sim\pi$ $S_{12}^{(2)} = 5.2$
Two Solute- Trace Feed + Ideal Isothermal Shifter Bed	$S_{12}^{\bullet} = \sqrt{2}\,\{[1 - \cos(2\pi\vartheta_1)]^{1/2} + \gamma[1 - \cos(2\pi A\vartheta_1)]^{1/2}\}$	$S_{12}^{\bullet} = \sqrt{2}\,\{[3 - 4\cos(2\pi\vartheta_1) + \cos(4\pi\vartheta_1)]^{1/2} + \gamma[3 - 4\cos(2\pi A\vartheta_1) + \cos(4\pi A\vartheta_1)]^{1/2}\}$	For $A = 2.2$ & $\gamma = 1$: $\vartheta_1 = 0.65$ $S_{12}^{\bullet} = 3.7$	For $A = 2.2$ & $\gamma = 1$: $\vartheta_1 = 0.65$ $\phi_T = \pi$ $S_{12}^{\bullet} = 6.9$
Binary Adsorbing Feed	$(S_{12})_m = \sqrt{2}\,[1 - \cos(2\pi\vartheta_m)]^{1/2}$	$(S_{12})_m^{(2)} = \sqrt{2}\,[2 - 2\cos(2\pi\vartheta_m) + 2\cos(2\pi\vartheta_m + \phi_T) - \cos(4\pi\vartheta_m + \phi_T) - \cos(\phi_T)]^{1/2}$	$\vartheta_m = 0.5$ $(S_{12})_m = 2$	$\vartheta_m = 0.5$ $\phi_T = \pi$ $(S_{12})_m^{(2)} = 4$

*Dual (identical) Zone operation: identical bed size and bed properties, and identical input temperature functions.

CHAPTER 4

EXPERIMENTAL SYSTEM AND APPARATUS

Activated carbon was chosen as a typical solid adsorbent because is is used in many gas purification processes and exhibits a reasonably large temperature effect on the equilibrium distribution coefficients for many gases. Gaseous mixtures of methane-helium, carbon dioxide-helium, methane-carbon dioxide-helium, and methane-carbon dioxide were selected to evaluate both the purification and enrichment aspects of the cycling zone adsorption process. Although most experiments were limited to dilute concentrations, it is felt that the results are applicable over large concentration ranges.

EXPERIMENTAL SYSTEM

High purity grades (99.9%+) of carbon dioxide, methane, and helium, obtained from the Matheson Company, were used to prepare various gas mixtures. Samples of "BPL" type activated carbon, 12-30 mesh (U.S. Sieve Series), were supplied by the Pittsburgh Activated Carbon Company.

Equilibrium distribution isotherms for "BPL" activated carbon have been reported for methane on 4-10 mesh carbon by Grant and Manes (1962), and for carbon dioxide on 12-30 mesh carbon by Meredith and Plank (1967). It was found that in the low pressure regions at which all experiments in this study were conducted Langmuir behavior adequately described the equilibrium behavior of methane and of carbon dioxide in the presence of helium, a non-adsorbing diluent. The Langmuir constants were determined by a non-linear least squares fitting of the reported isotherm data and are listed in Table 4-1. The predicted loading values, based on these constants, are plotted in Figures 4-1a and 4-1b. The solid line is a smooth line passed through the reported data.

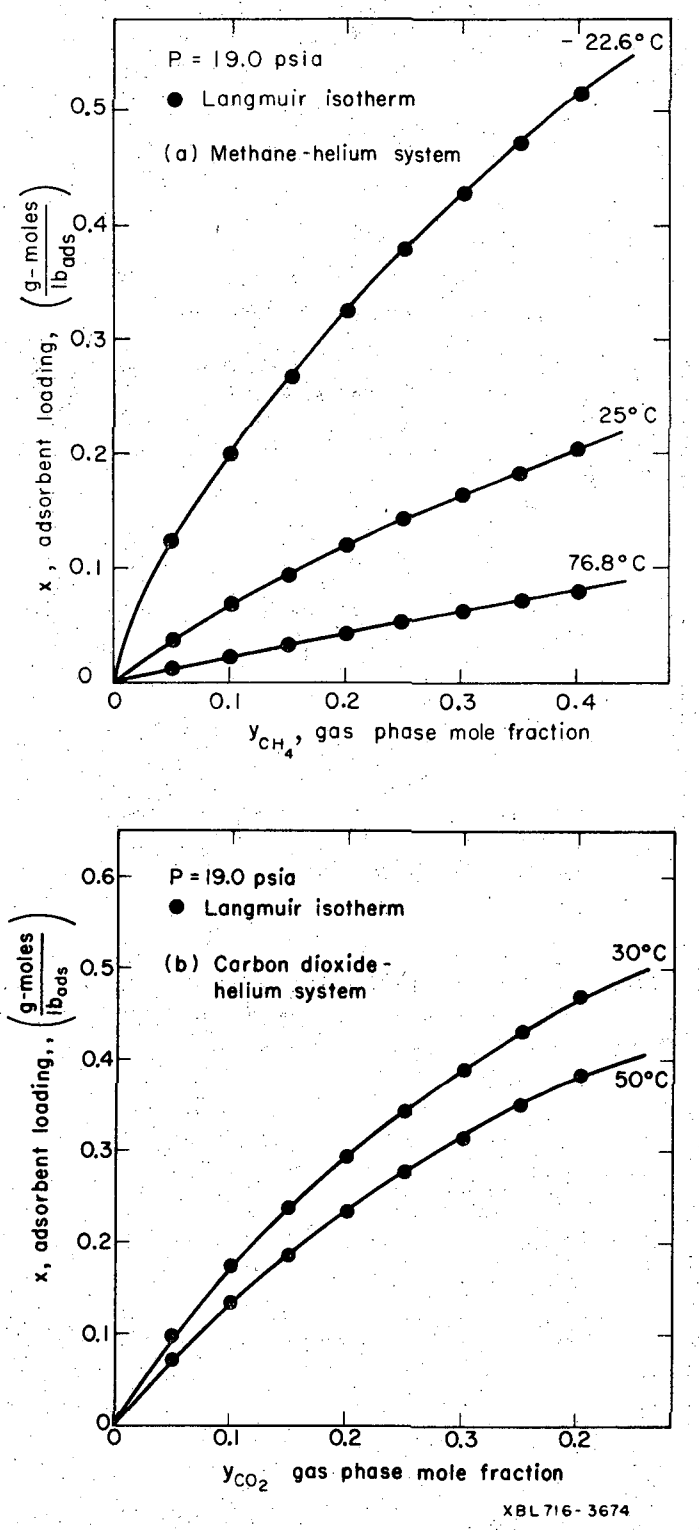

Figure 4-1. Equilibrium Loading Isotherms on Pittsburgh BPL Activated Carbon, Solid lines represent smoothed data of (a) Grant and Manes (1962) and (b) Meredith and Plank (1967).

Table 4-1. Langmuir Isotherm Parameters at 19.0 psia: $x = by/(1 + cy)$

System	Temperature, °C	b	c	$b_o \times 10^4$	$-\Delta H_a/R \times 10^{-3}$
CH_4 - He (4-10 mesh)	- 22.6	1.809	0.960	2.00	2.2
	25.0	0.604	0.447		
	76.8	0.215	0.153		
CO_2 - He (12-30 mesh)	30.0	1.920	1.450	278.0	2.0
	50.0	1.496	1.295		

where b has units of g-moles/lb_{ads}, c is dimensionless, and $\Delta H_a/R$ has units of °K.

The isoteric heat of adsorption is defined as

$$\left(\frac{d\ \ln P}{dT}\right)_x = \frac{\Delta H_a}{RT^2}$$

It can be shown that the Langmuir isotherm results in a constant ΔH_a versus loading, x, and that

$$\left(\frac{d\ \ln b}{dT}\right)_x = \frac{\Delta H_a}{RT^2}$$

This is considered the main weakness of the Langmuir isotherm, and is discussed by Bond (1962). Since b is not a function of x, the above result may be integrated, yielding

$$\ln b = \ln b_o - \Delta H_a/RT$$

The heat of adsorption can then be obtained from the slope of a plot of ln b versus 1/T. Values obtained from the reported isotherms are listed in Table 4-1.

The physical properties of the activated carbon adsorbent are shown in Table 4-2. The interparticle void fraction, ε, which depends

Table 4-2. BPL Activated Carbon Properties*

Property	12-30 Mesh	Units
Structural density, ρ_s'	2.1	gm/cm^3
Particle density, ρ_s	0.8	"
Apparent density, ρ_b	0.5	"
Intraparticle void fraction, χ	0.40	—
Interparticle void fraction, ε[a]	0.36 - 0.45	—
Total surface area, S	1050 - 1150	m^2/gm
Particle diameter, $\langle d_p \rangle$[b]	0.105	cm
Heat Capacity, C_s	0.25	cal/gm-°C

*As supplied by manufacturer.

[a]Depending on particular experiment.

[b]Based upon manufacturer's reported particle size distribution.

on the manner in which the column is packed, was calculated from the expression:

$$\varepsilon = 1 - \frac{W}{\rho_s V_c}$$

where W is the weight of the carbon added to a column whose empty volume is V_c.

EXPERIMENTAL APPARATUS

The experimental apparatus is shown in Figure 4-2 and schematically illustrated in Figure 4-3. The heart of the system is the column section, shown in Figure 4-4.

Column Section

The 1/2-inch O.D. thin-walled stainless steel columns, the details of which are shown in Figure 4-5, were packed with 1-mm glass

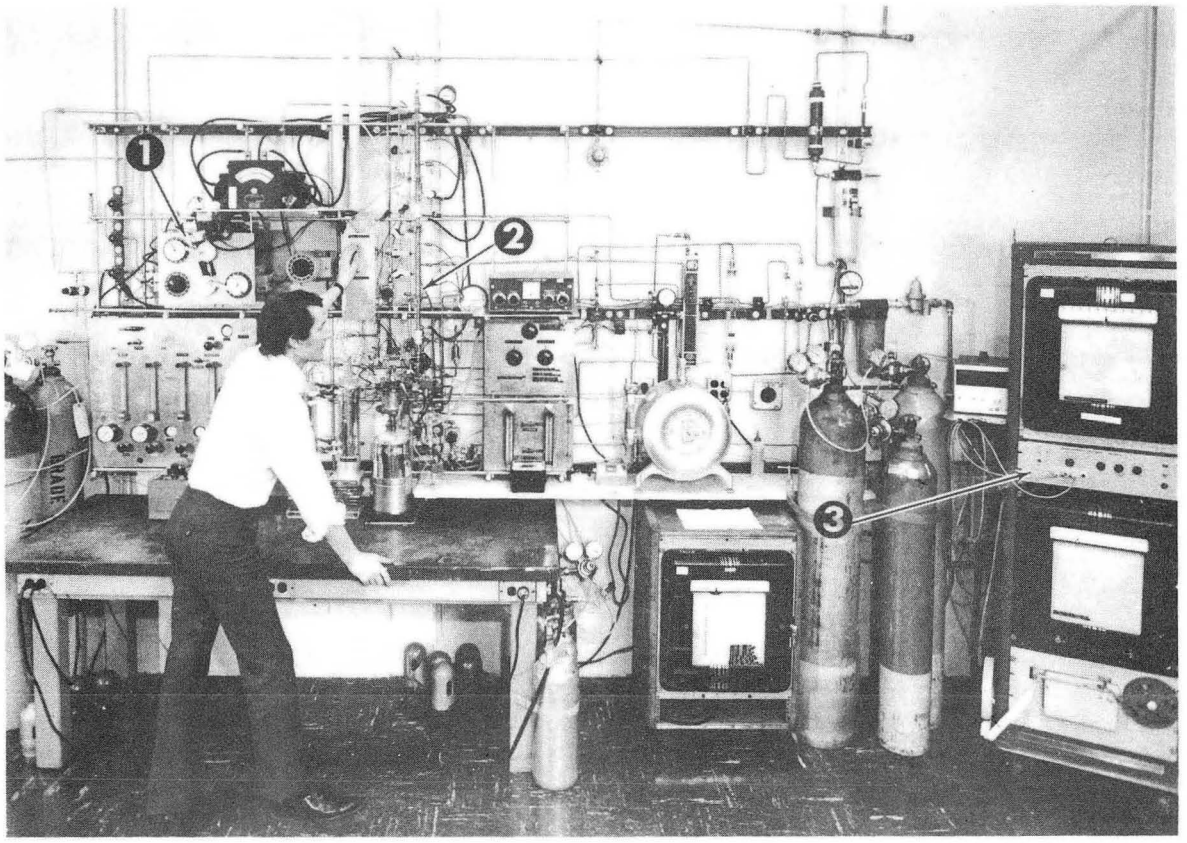

XBB 713-850-A

Figure 4-2. Experimental Apparatus for Cycling Zone Adsorption containing (1) Temperature generation apparatus, (2) Column and analyzer section, and (3) Data digitization equipment.

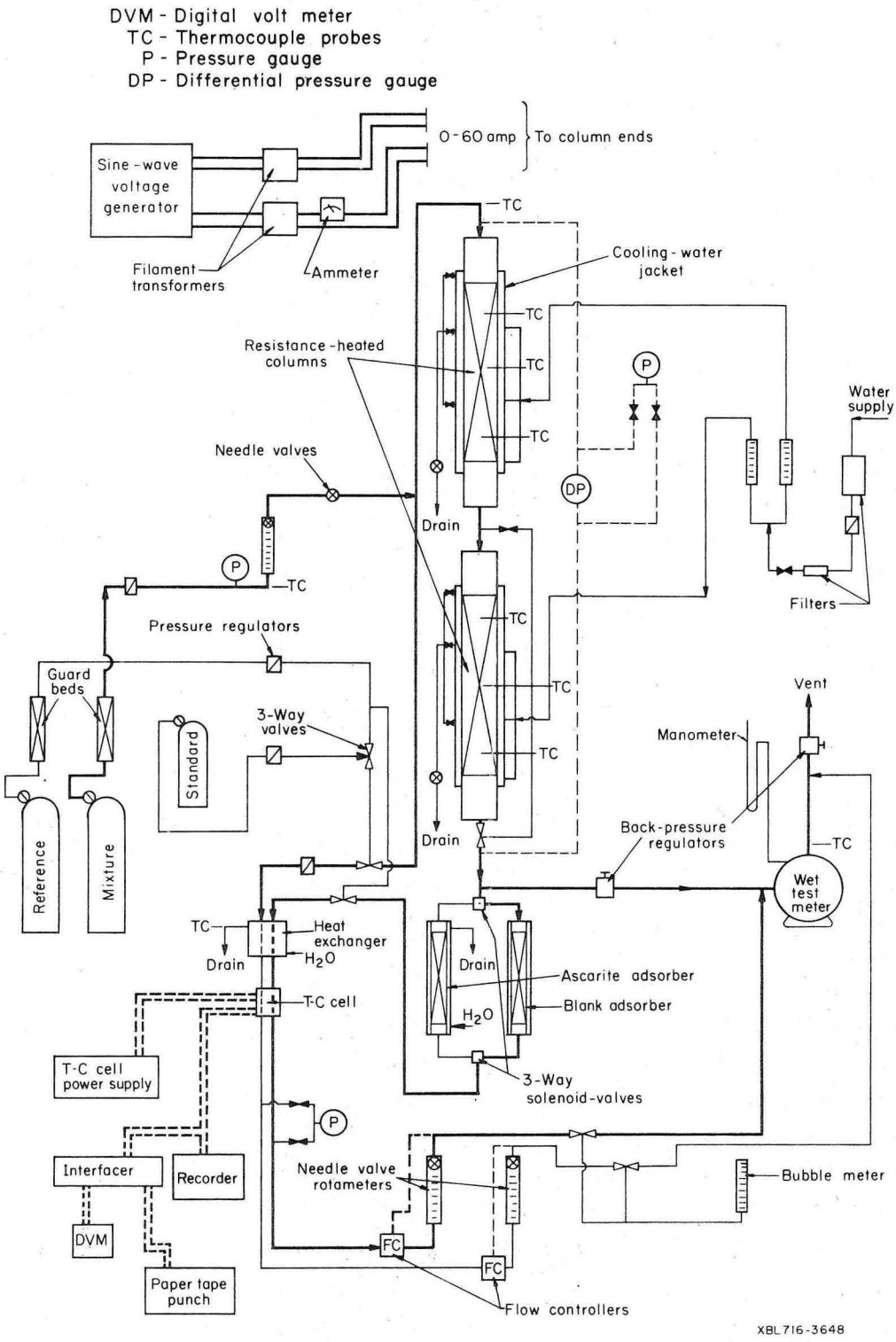

Figure 4-3. Schematic of Experimental Apparatus for Cycling Zone Adsorption.

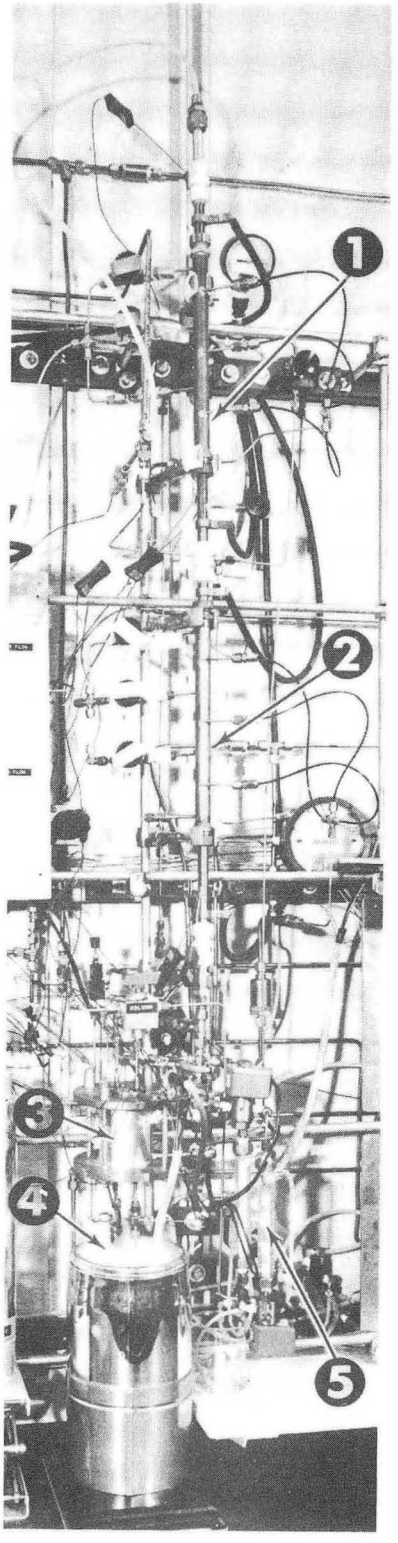

XBB 713-854-A

Figure 4-4. Column and Analyzer Section containing (1) Zone-1, (2) Zone-2, (3) Porous-Bronze plug heat exchanger, (4) T-C cell, and (5) Ascarite bed.

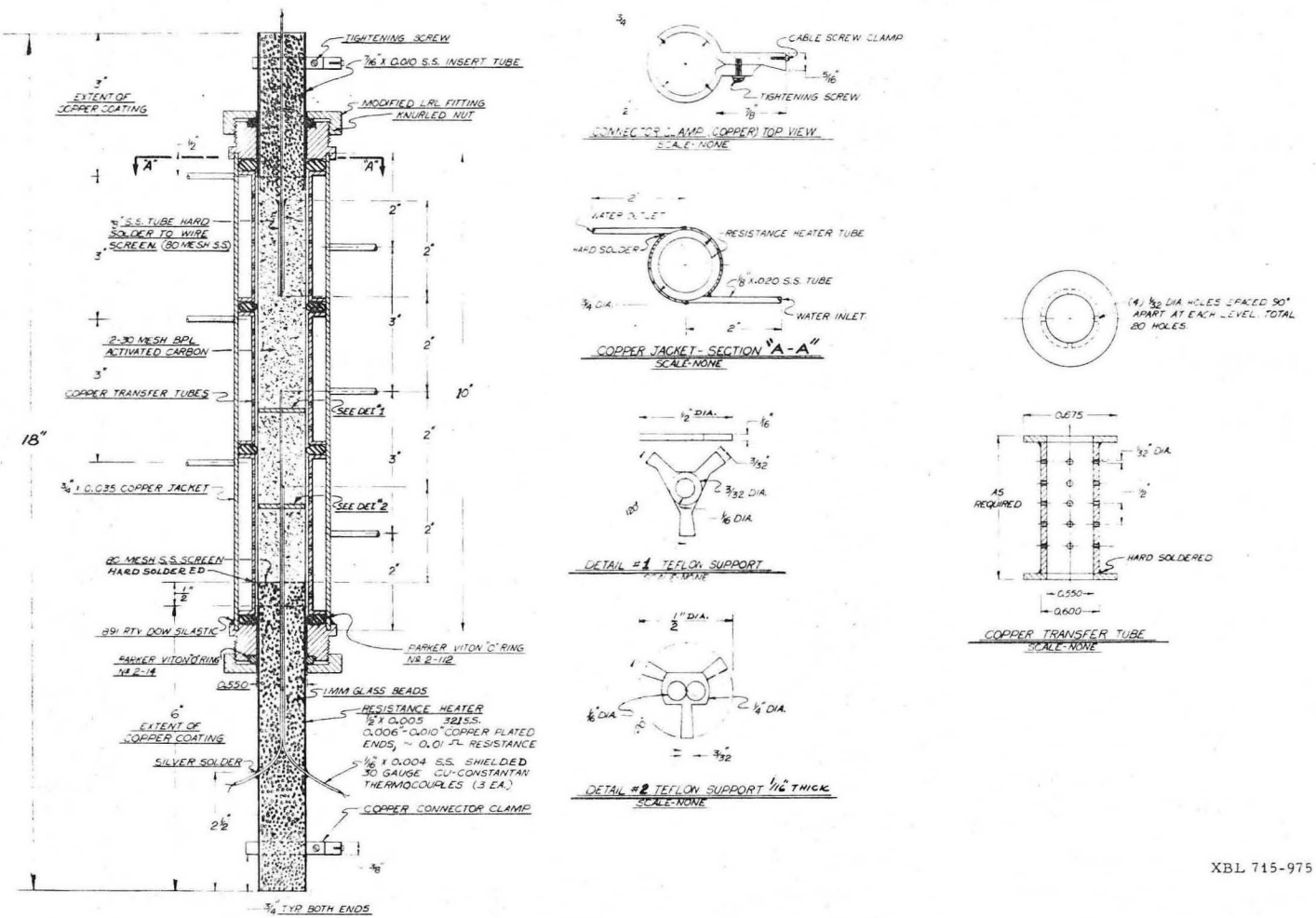

XBL 715-975

Figure 4-5. Detail of Resistance-Heated Cycling Zone Adsorber Column.

spheres at the ends to achieve even flow distribution. Weighed amounts of carbon particles were added to each column, while tapping the column walls to insure uniform packing. The depth of each bed was measured to determine the length of each zone.

The copper jacket surrounding each column was divided into three sections, each provided with inlet and exit cooling water ports. Copper transfer-tubes were inserted between the jacket and the thin-walled column to distribute the heat in each section and allow sealing of the sections.

Three copper-constantan sheathed thermocouples, centrally located in the packing, were used to monitor the adsorbent temperature in each section. The junctions of the thermocouples were coated with Omega's ThermoCoat HT to prevent possible interferences caused by the high current in the tube wall.

Sine-Wave Temperature Generation Apparatus

The thin-walled stainless steel columns, each with a resistance of approximately 0.01 ohm, were heated by passing high current (up to 60 amperes) through them and cooled by passing cooling water thru a copper jacket. The current generation apparatus is shown in Figure 4-6. A mechanical gear system, driven by a variable-speed AC motor, rotated two 115-volt- 10 ampere Powerstats. Adjustable linkage was provided in order to set the output amplitudes of each Powerstat independently and to adjust their phase relationship. The outputs of the Powerstats were fed to two Tranex low-voltage, high-current filament transformers. The output currents were monitored by a Model 155 Weston AC Ammeter. ITT #6 welding cables were used to conduct the current from the transformers to the column end clamps. The sinusoidal Powerstat voltage output produced satisfactory sinusoidal column temperature variations.

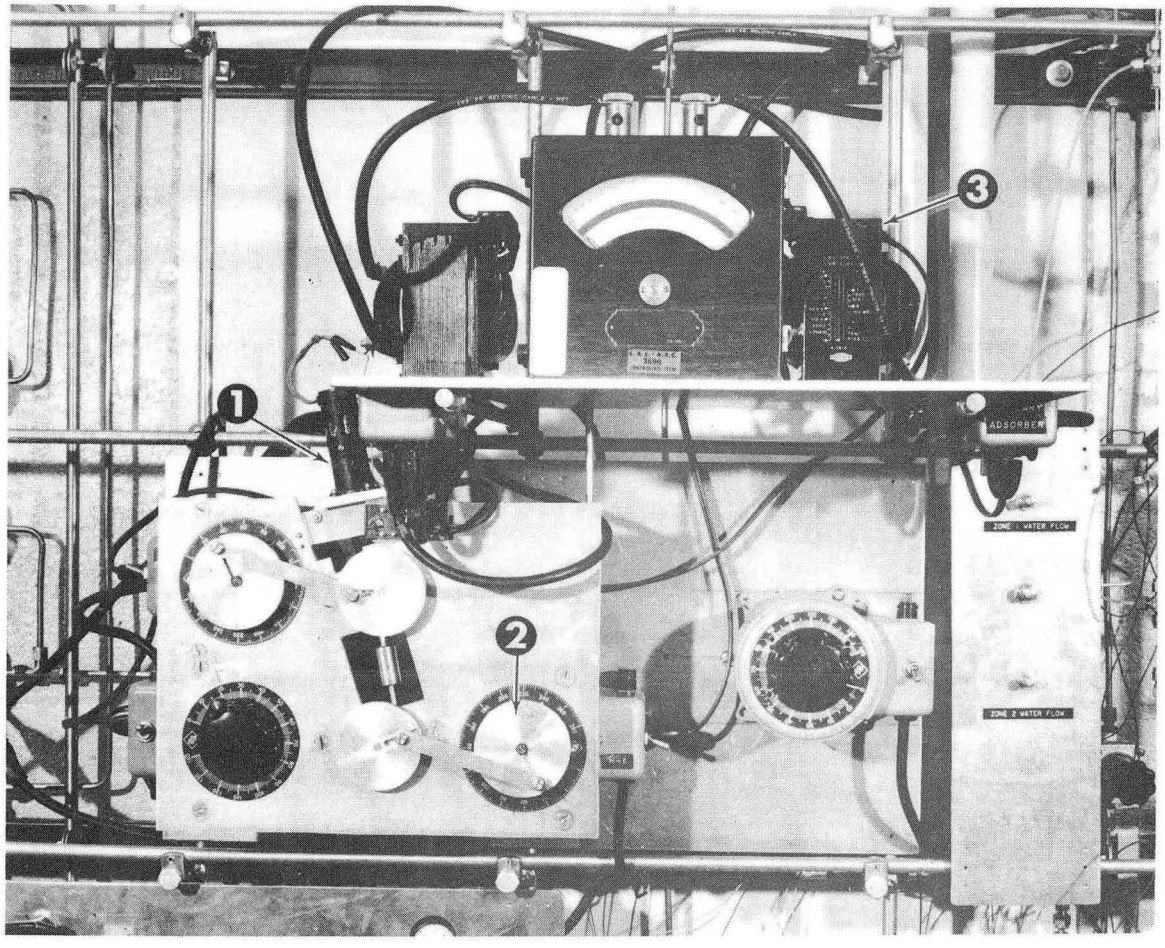

XBB 713-853-A

Figure 4-6. Temperature Generating Apparatus consisting of (1) Variable-speed AC motor, (2) 10-ampere Powerstat, and (3) High-current transformer.

Feed Supply and Effluent Removal

Gaseous mixtures were prepared in standard type-1A gas cylinders. The gas mixture was passed thru a guard bed, containing a mixture of 3-A and 5-A Linde molecular sieves, and then thru a Drierite bed, to remove moisture. It was then fed to a flow metering-rotameter system and split into two streams. One stream was fed the top of the first column; the other was passed thru a porous bronze-plug heat exchanger before entering the reference side of the thermal conductivity (T-C) cell, and finally to vent.

The outlet pressure of the second column, zone-2, was held at 19.0 psia by a Fairchild-Hiller Model 10 back pressure regulator. A bleed from the effluent was passed thru the water cooled heat exchanger and then thru the measurement side of the T-C cell. After passage thru the T-C cell, the bleed stream was recombined with the remaining effluent and fed to a Precision wet test meter, the outlet of which led to vent.

Feed gas mixture flows were controlled by a Nupro "S" fine metering valve. Stream flows thru the T-C cell were controlled and monitored by Moore Model 63BD-L low flow controllers across needle valved Model 1355 Brooks rotameters. Measurement of these flows was made using a soap-bubble meter.

Measurement Systems

Column temperature and concentration (T-C cell) signals were independently recorded dual and single channel Speedomax G strip-chart recorders with chart speed of 60 inches per hour. Other temperature readings were intermittently taken using a Rubicon potentiometer.

Temperature. Copper-constantan thermocouples (30-gauge) were employed for temperature measurements. The thermocouples were embedded in Al_2O_3 and encased by a thin-wall stainless steel sheath of 0.0625 inch outside diameter. The welded hot junctions were coated with a high-temperature cement. Each hot junction had an independent ice junction which was embedded in a 3/16 inch diameter glass tube filled with paraffin wax. Thermocouples were calibrated by comparing their outputs with that predicted from the standard tables at the eutectic point of Na_2SO_4-H_2O (32.384 °C). The Speedomax (0 - 5 mv) recorders were balanced using a potentiometer.

Pressure. The outlet pressure of the column section was monitored by a calibrated Hoke #4044 pressure gauge. The wet test meter exit pressure was measured by using a water-filled manometer, corrected for atmospheric changes.

Concentration. Gas compositions were measured continuously by a Gow-Mac Model 460 flow-thru type thermal conductivity cell, fitted with WX-Rhenium-Tungsten hot wire filaments. The T-C cell was powered by a Gow-Mac Model 40-05C control unit. The details of the analyzer and the low hold-up porous bronze heat exchanger are shown in Figure 4-7. The response time of the cell at stream flows of 50 cm^3/minute was less than 1 sec. A porous bronze-plug heat exchanger was employed to insure that cell streams' temperatures would remain equal and constant. The cell's temperature was allowed to equilibrate by placing it in a Dewer flask filled with glass wool.

Typical T-C cell response curves are shown in Figure 4-8 for standard gas mixtures prepared and analyzed by the Matheson Company. Because of the high degree of linearity, the reference streams used for

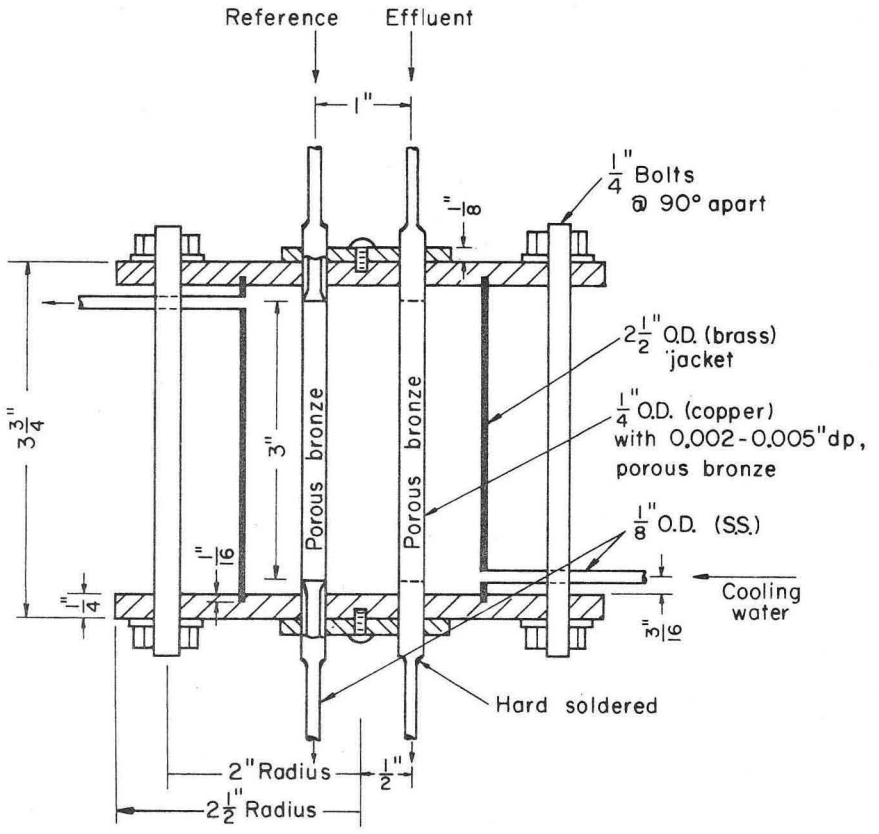

(a) Porous-bronze plug heat exchanger

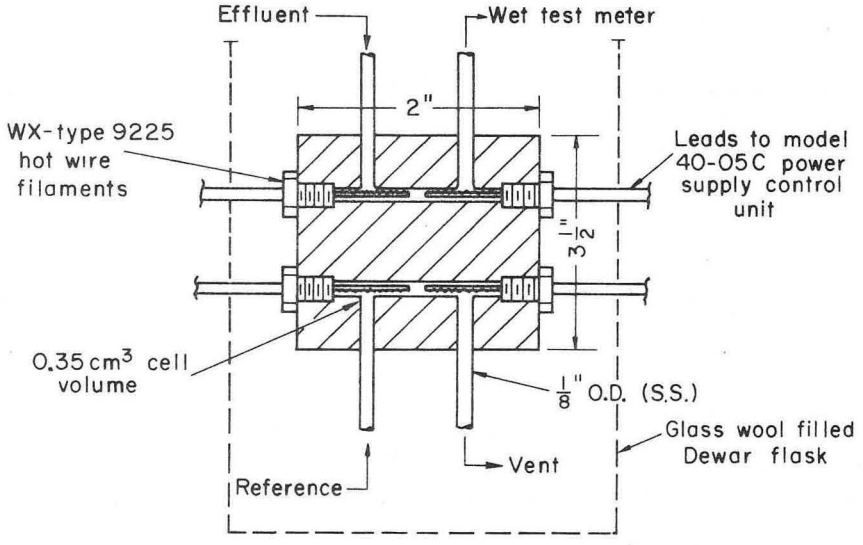

(b) Gow-Mac model 460 flow-through detector

XBL716-3649

Figure 4-7. Details of Porous-Bronze Heat Exchanger and T-C Cell. Hold-up Volumes: (1) From exit of Zone-1 to T-C cell = 25.1 cm^3. (2) From exit of Zone-2 to T-C cell = 20.7 cm^3.

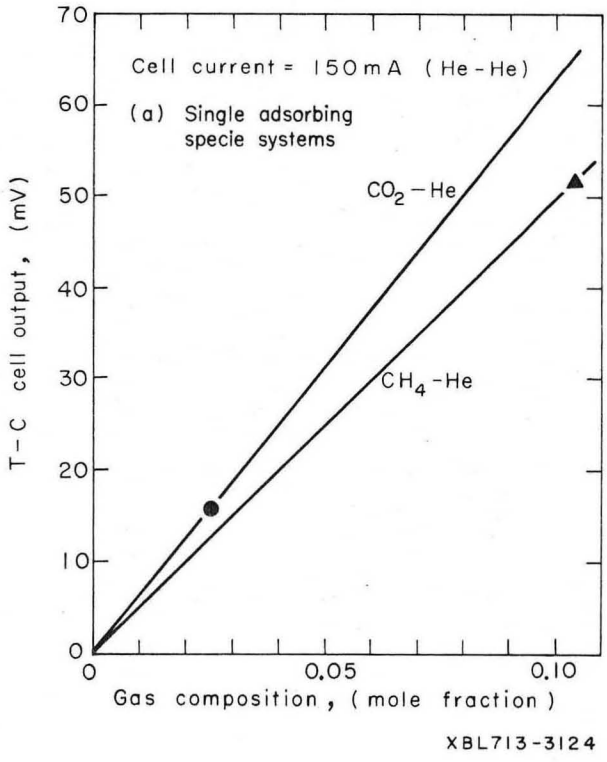

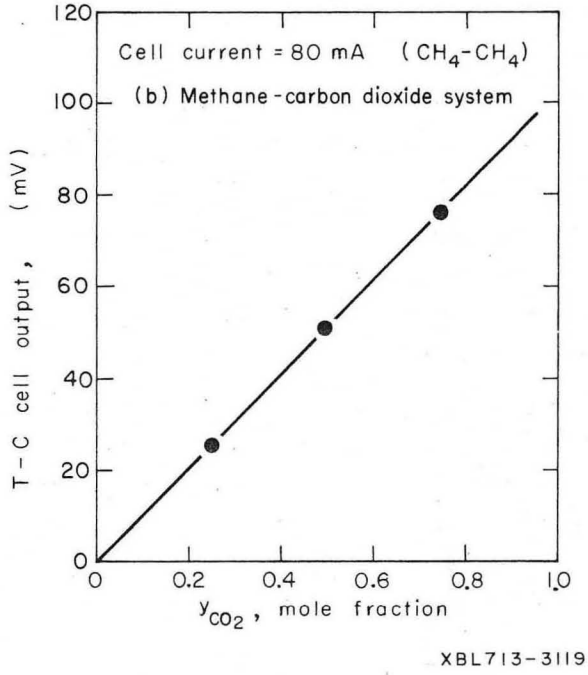

Figure 4-8. Typical T-C Cell Calibrations for stream flows of 50 cm^3/min. and 25 °C cell temperature at 19 psia. Reference gases: (a) Helium, (b) Methane.

calibration could be substituted by the constant composition feed stream, thus the cell output would be proportional to the concentration deviations from the feed.

For the three-component mixtures, the T-C cell was calibrated by measurement of the total response of the standard mixtures (methane-carbon dioxide-helium) referenced to helium. These outputs were fitted to the equation

$$\text{Cell output (mv)} = A_1 y_{CH_4} + A_{11} y_{CH_4}^2 + A_2 y_{CO_2} + A_{22} y_{CO_2}^2 + A_{12} y_{CH_4} \cdot y_{CO_2} \qquad (4\text{-}1)$$

by a non-linear least squares routine, to determine the best set of cell constants (A_1, A_{11}, A_2, A_{22}, A_{12}). A typical set of constants for T-C flows at 50 cm^3/minute and a cell current of 150 ma (current set with helium flows) are given in Table 4-3.

The three-component effluent compositions were determined as follows. The total cell response (all species present) was measured over several cycle times. Starting at the same point in the temperature

Table 4-3. Methane-Carbon Dioxide-Helium T-C Calibration Constants. (millivolts)

A_1	514.52
A_{11}	-66.32
A_2	637.24
A_{22}	405.43
A_{12}	375.95

cycle, the carbon dioxide-free effluent response was also measured over an equal time period. The carbon dioxide was essentially removed by passing the effluent bleed stream through an Ascarite bed, which was water jacketed to remove the heat generated by the CO_2 reacting with the NaOH-impregnated asbestos. In addition to heat removal by a cooling water jacket, 1-mm glass beads were mixed in equal proportions with the Ascarite, to prevent plugging due to reaction with CO_2. The Ascarite adsorber-reactor is shown in Figure 4-9. The total response, C_1, is given by equation (4-1) and the CO_2-free response is

$$C_2 = A_1 \, (y_{CH_4})_{ap} + A_{11} \, (y_{CH_4})_{ap}^2 \tag{4-2}$$

where the apparent concentration of methane is

$$(y_{CH_4})_{ap} = y_{CH_4}/(1 - y_{CO_2}) \tag{4-3}$$

Substituting equation (4-3) into equation (4-2) and solving, we obtain

$$y_{CH_4}/(1 - y_{CO_2}) = \frac{- A_1 + \sqrt{A_1^2 + 4 A_{11} C_2}}{2 A_{11}} = \zeta \tag{4-4}$$

or

$$y_{CH_4} = \zeta(1 - y_{CO_2}) \quad , \quad \zeta \leqslant 1 \tag{4-5}$$

Substituting equation (4-5) into equation (4-1) and solving for y_{CO_2}, yields

$$y_{CO_2} = \frac{- B_1 + \sqrt{B_1^2 - 4 B_2 B_3}}{2 B_2} \tag{4-6}$$

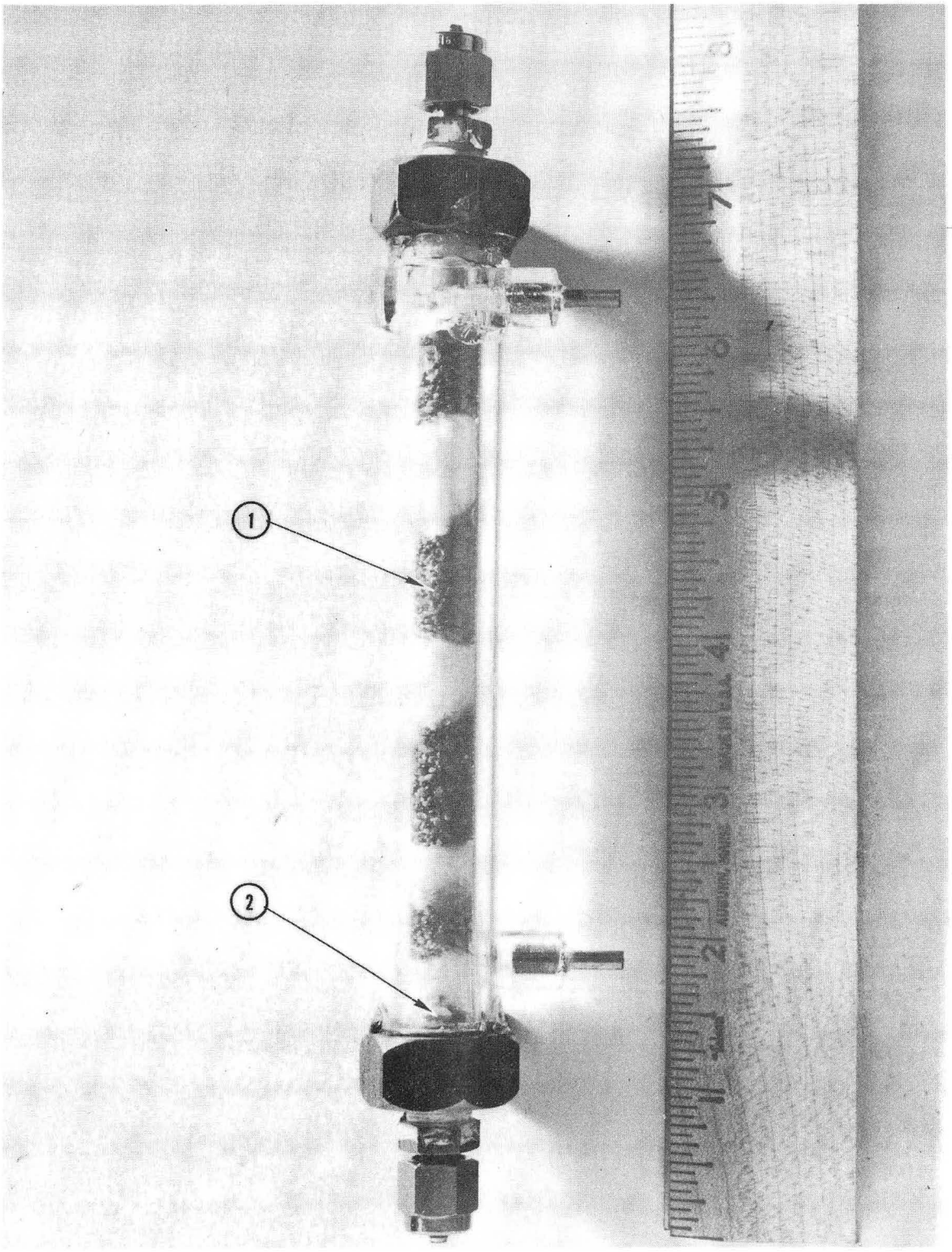

XBB 713-851-A

Figure 4-9. Jacketed Ascarite Adsorber-Reactor containing (1) 20-30 mesh Ascarite mixed with 1-mm glass beads, and (2) Drierite at bed exit. Hold-up Volume $\cong$ 7.3 cm^3.

where

$$B_1 = A_{11}\zeta^2 - A_{12}\zeta + A_{22}$$

$$B_2 = -2\,A_{11}\zeta^2 + \zeta(A_{12} - A_1) + A_2$$

$$B_3 = A_{11}\zeta^2 + A_1\zeta - C_1$$

Thus ζ is determined by CO_2-free response, which in turn allows computation of methane and carbon dioxide compositions from the total response. The above results hold for time-varying effluent compositions when the total and CO_2-free responses are measured at the same point in the periodic cycle.

For the methane-carbon dioxide binary system, the cell output was determined (referenced to pure methane) for various standard mixtures. These are plotted in Figure 4-8b. Methane was used as the reference gas because it yielded better cell stability and sensitivity than carbon dioxide.

The cell output signal was fed both to a (0 - 5 mv) zero-centered Speedomax strip-chart recorder and to a digital interfacing unit, designed by Mr. Tom Merrick of the University of California Department of Chemistry Electronics Lab. In the interfacing unit, shown in Figure 4-10, the signal was amplified, digitized, and punched on paper tape. The interfacing unit allowed for selection of amplifier gain, digitizing time intervals, and total counts per punch run.

Data Reduction

From pressure, temperature, and flow measurements on the column section, the thru-put velocity, bed average temperature, and temperature

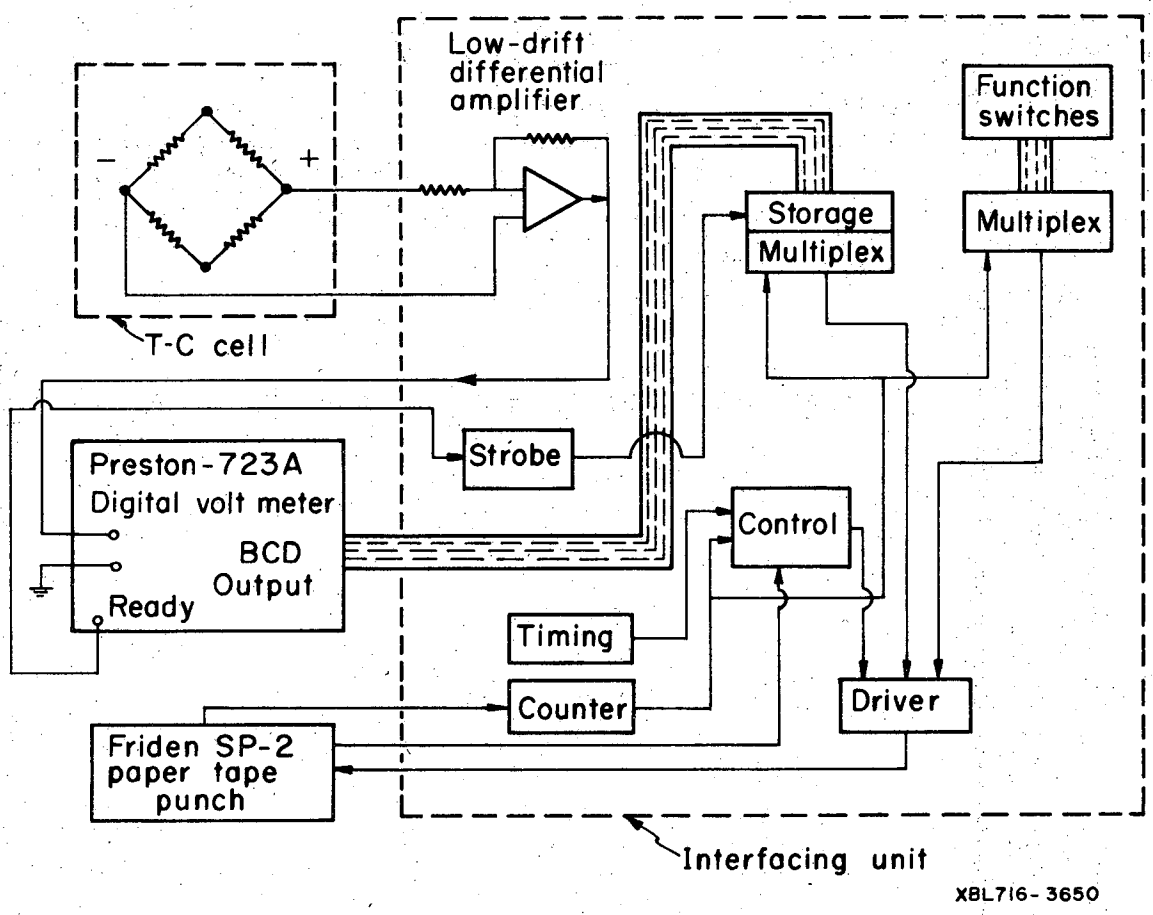

Figure 4-10. Schematic of Digital Interfacing Unit.

input amplitudes were determined. The digitized concentration outputs, referenced to the feed, punched on paper tape, were processed by a Fortran IV computer program which calculated the concentration-time responses, average concentrations of the enriched and depleted portions, and the average separation factors. From the concentration-time responses, upon correction for time delays resulting from the time required for the effluent to reach the detector, the phase relationship between the concentration response wave and the temperature input were determined.

For three-component systems, the phase relationship between the two adsorbing specie concentration waves was determined from their calculated concentration-time responses. In addition these responses were integrated over a half-cycle for various assumed cycle switching locations, β, to determine the best separation factor.

The ranges of the variables encountered in this study are listed in Table 4-4. The original data are in laboratory notebooks on file in Professor R. L. Pigford's office, 125B Lewis Hall, University of California, Berkeley, California 94720.

Table 4-4. Range of Variables Investigated in this Study.

Variable	Range
Average bed temperature, T_o	39 to 61 °C.
Input temperature amplitude, $a_T T_o$	3.8 to 13.8 °C.
Frequency, ω	0.024 to 0.104 rad/sec.
Pressure at column exit, P	19 psia
Length of column, L	19.2 to 20.6 cm.
Weight of carbon packing, W	9.7 to 11.6 gm.
Void fraction, ε	0.450 to 0.360
Interstitial fluid velocity, v	3 to 100 cm/sec.
Temperature inputs' phase, ϕ_T	0.63 to 6.16 radians.
Average shifter bed temperature, T_s	40 to 83 °C.

CHAPTER 5

SINGLE ADSORBING SPECIE EXPERIMENTS

Dilute methane-helium and carbon dioxide-helium gas mixtures were chosen to represent systems containing small amounts of pollutants which present purification problems. The linear equilibrium theory is compared to the experimental results, in order to gage its acceptability as an upper limit predictive method. The ability of the theory to relate important variables of the cycling zone adsorption process is also evaluated.

The experimental apparatus employed for either single or dual zone operation is schematically shown in Figure 4-3. Comparisons of experimental results with the linear equilibrium theory, described in Chapter 3, are presented in graphical form. The solid lines represent the theory based upon a sine wave temperature input and the isotherm parameters, determined by the frequency response technique which is described in Appendix A. The experimental data are presented in Tables at the end of this Chapter.

SINGLE ZONE

Typical experimental input temperature-time and effluent concentration-time curves for a single cycling zone are shown in Figure 5-1a. The input temperature oscillates about the bed average temperature, T_o. The effluent concentration, which oscillates about the feed composition, y_f, may be separated, by appropriate switching valves, into an enriched portion and a depleted portion. The ratio of the average specie concentration in the enriched portion to the average concentration in the depleted portion is defined as the average separation factor, $\langle \alpha \rangle$.

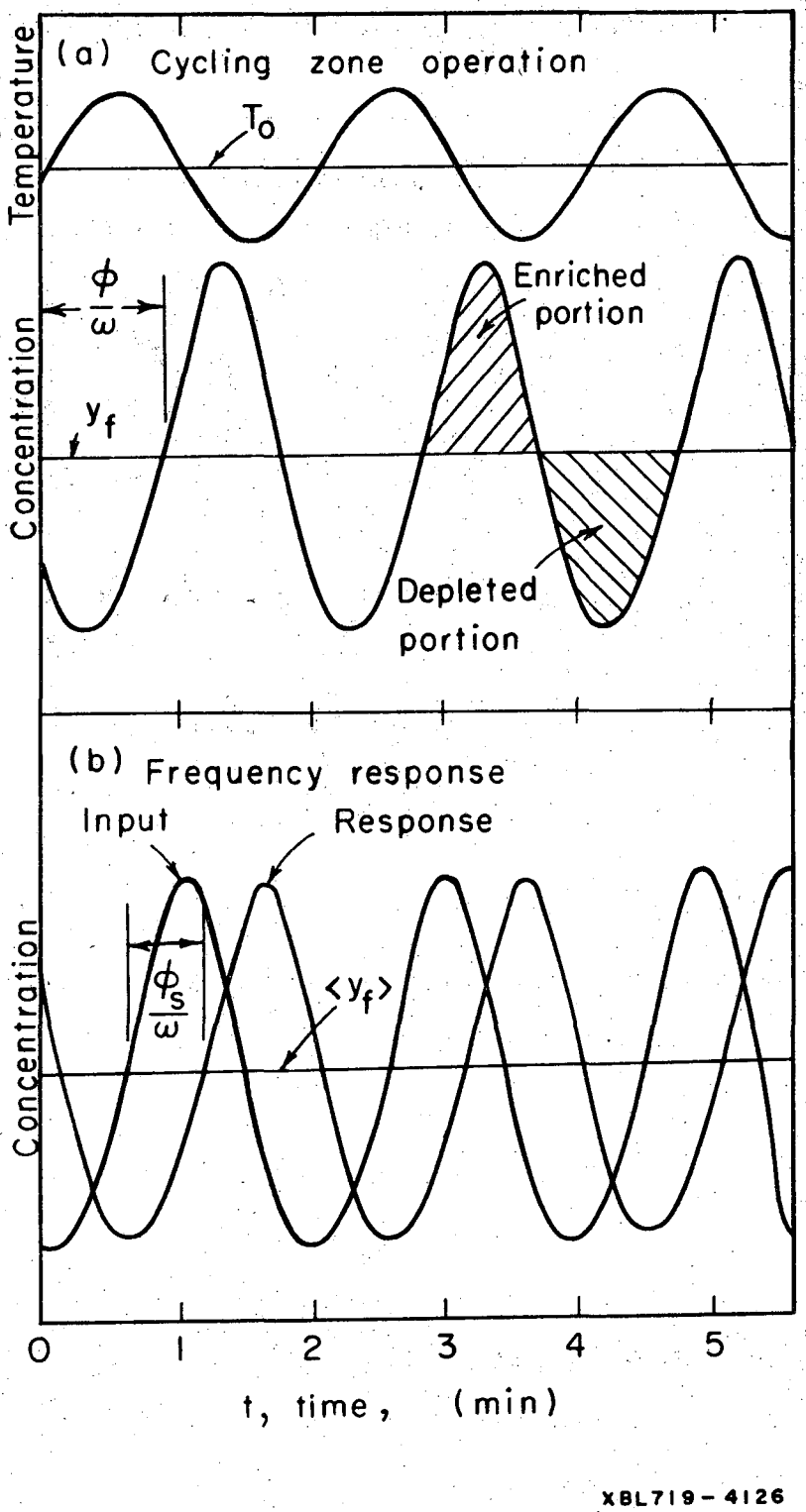

Figure 5-1. Experimental Input Temperature and T-C Cell Response Curves for Single Zone System: Single Solute Feed.

The experimental dimensionless separation factor, $\mathcal{S}$, and the phase lag between the temperature wave and the concentration effluent wave, $\phi/2\pi$, versus the dimensionless frequency factor, $\mathcal{J}$, for the CH_4-He system are presented in Figure 5-2. The CO_2-He results are shown in Figure 5-3. The "trace system" data, plotted on Figure 5-3, were determined from the CO_2 concentration wave response of a single CZA unit being fed a dilute CH_4-CO_2-He mixture. These data indicate that the CO_2 adsorption is essentially independent of the presence of CH_4. This supports the assumption that each specie's concentration response depends only on its respective isotherm in the presence of helium.

The drop off in separation, as compared to the equilibrium theory, with increasing $\mathcal{J}$, in the second loop of Figure 5-3, is expected. Since more than one concentration wave is present within the bed at higher frequencies, implying sharper concentration gradients, dispersion and mass transfer effects would be enhanced. The region at the right corresponds to high frequencies or low velocities, each of which increases mass transfer and diffusion effects, as shown in Figure 3-2.

Both the methane and carbon dioxide systems substantiate the theoretically predicted optimum frequency factor ($\mathcal{J} = 0.5$), giving the maximum separation. This supports the use of the equilibrium theory, since the optimum frequency factor and the separation factor decrease with increasing frequency, as illustrated in Figure 3-2, when mass transfer resistance becomes significant.

An alternate method of investigating the mass transfer aspects of a particular fluid-solid system is to measure the amplitude loss of a concentration wave upon passage through an isothermal adsorbent bed. Typical experimental input and response concentration waves are shown in

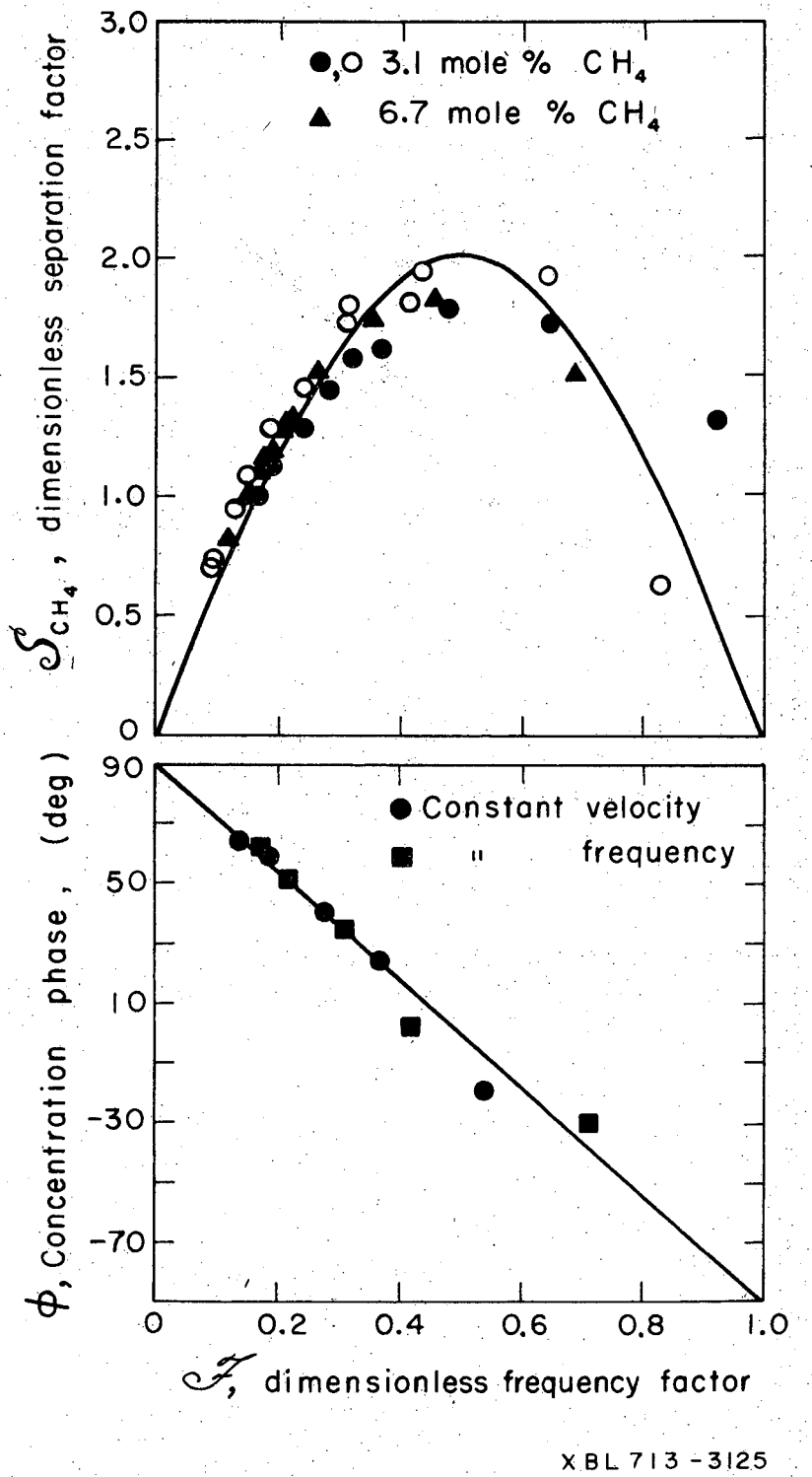

Figure 5-2. Dimensionless Separation Factor and Concentration-Temperature Phase for Single Zone System: Dilute Methane-Helium Feed.

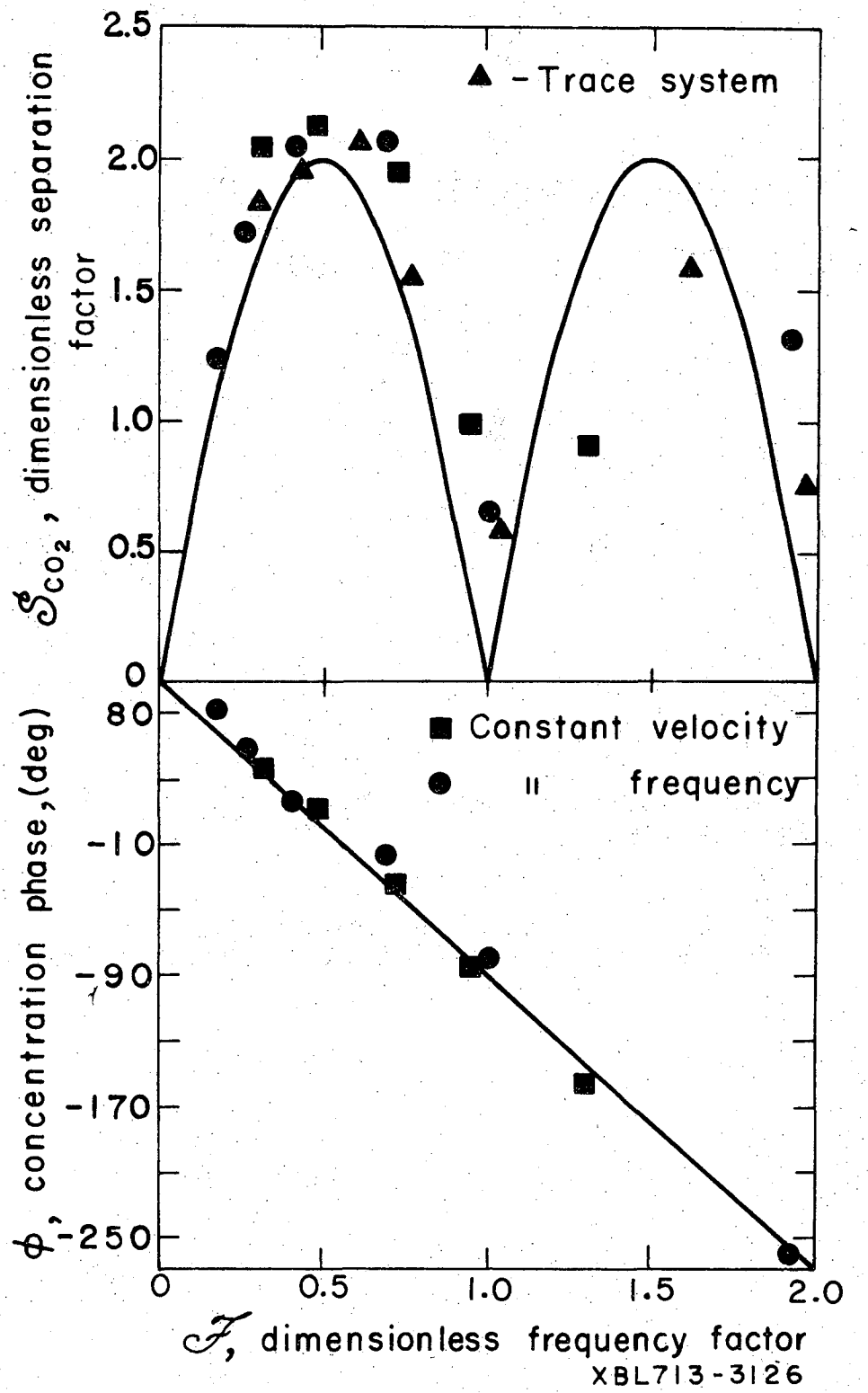

Figure 5-3. Dimensionless Separation Factor and Concentration-Temperature Phase for Single Zone System: Dilute Carbon Dioxide-Helium Feed.

Figure 5-1b. The separation factor ratio (identical to the amplitude ratio for linear systems) versus the fluid velocity, v, for an isothermal bed of activated carbon is shown in Figure 5-4. The upper limit on the velocity, that at which the separation factor ratio decreases upon increasing thru-put, was not achieved because of apparatus design limitations. However, quite large thruputs can be obtained without significant mass transfer losses. Figure 5-4 indicates that at low velocities and high frequencies, the attenuation of the input wave is greater. Thus lower frequencies and higher velocities than those used, in the vicinity of the thru-put velocity limit, are the most desirable regions of operation.

In addition, we find that the attenuation of a concentration wave upon passage thru an isothermal bed is greater for the CO_2-He system than that for the CH_4-He system. Since $(K_o)_{CO_2}$ is greater than $(K_o)_{CH_4}$, the concentration wave velocity, v^*, for CO_2 is less than that for CH_4. Thus, there are more CO_2 concentration waves present within the bed, enhancing mass transfer effects. For a given $\omega(L/v)$ value, $\mathcal{J}_{CO_2}$ is greater than $\mathcal{J}_{CH_4}$, which, according to Figure 3-2, means that mass transfer effects are enhanced more for CO_2 adsorption than for CH_4 adsorption.

DUAL ZONE

In the dual zone operation, the effluent of the first zone was fed to a second zone whose temperature was being oscillated at the same frequency but out of phase with that of the first zone. When the zones are of equal length and diameter the above type of operation is termed "identical zone operation". The effluent of the second zone may be separated, by appropriate switching, into its enriched and depleted

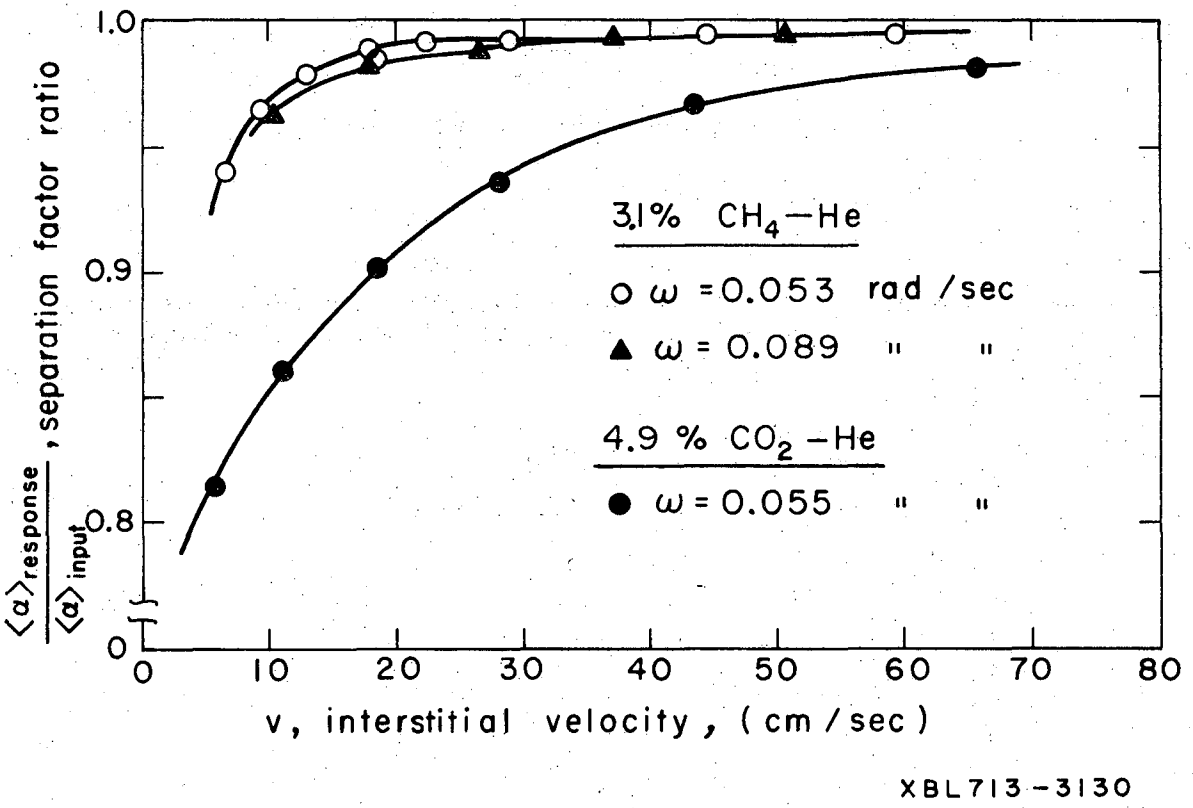

Figure 5-4. Velocity Response of Isothermal Bed: Pittsburgh BPL Activated Carbon at 19 psia. (L = 20.64 cm.)

portions. Based upon the average compositions in the enriched and depleted collections, the dimensionless separation factor may be calculated using the appropriate operating variables and isotherm parameters. The maximum separation achieved, as shown in Figure 5-5, by splitting the second zone's effluent, for the temperature phase, $\phi_T = \pi$, was found to correspond closely to that predicted by the linear theory ($\mathcal{S} = 4$). In Figure 5-6, the dimensionless frequency factor ($\mathcal{J} = \mathcal{J}(\omega, v, T_o)$) was held constant while the temperature phase was changed.

From the above mentioned results, we may conclude that the best operating proceedure for a dual zone system is $\mathcal{J} = 0.5$ and $\phi_T = \pi$. This gives twice the separation that is achieved utilizing a single zone in an optimal manner.

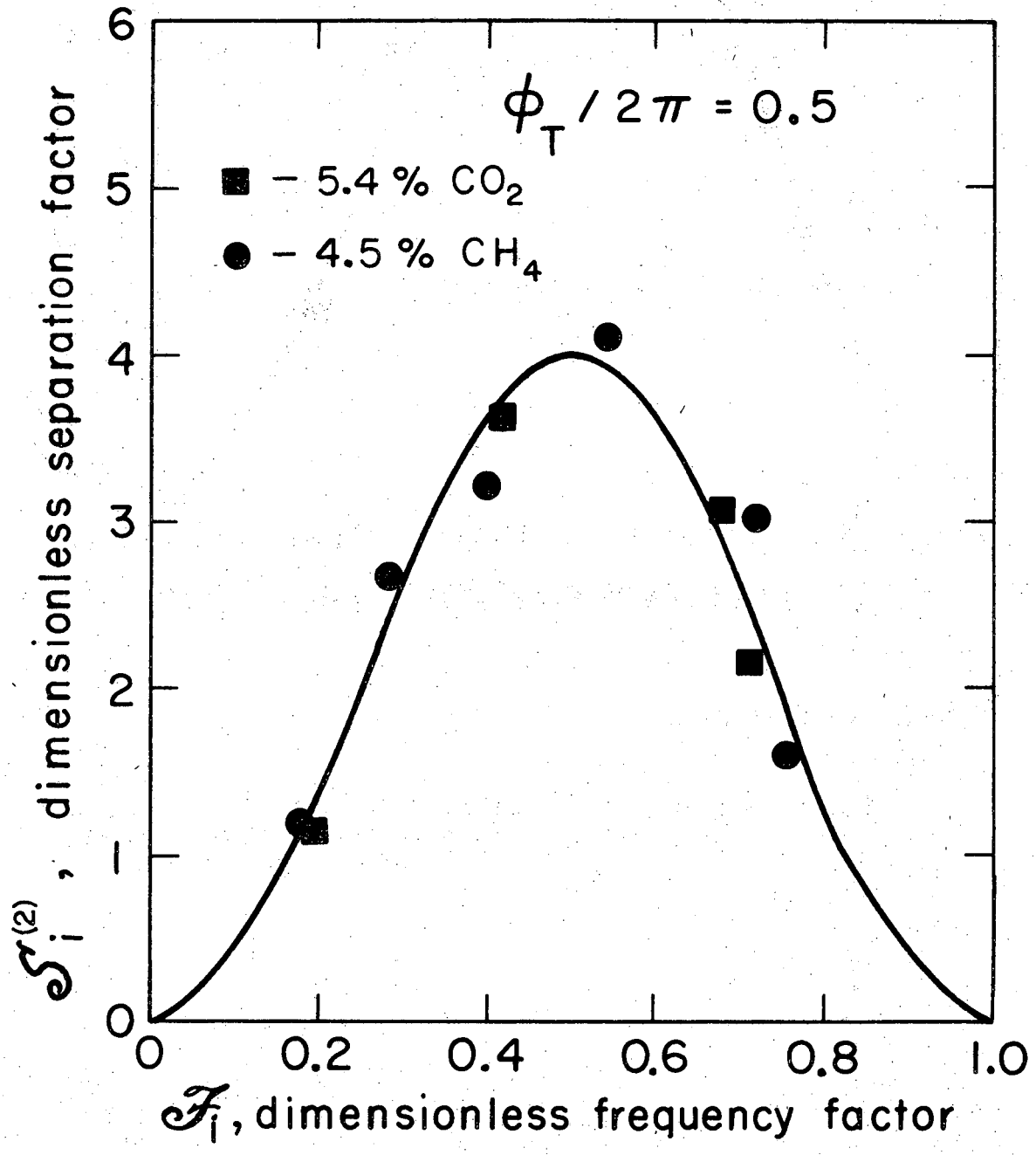

Figure 5-5. Dimensionless Separation Factor, constant Temperature Phase: Dual Zone-Single Adsorbing Specie Feed. (ω = 0.0411 radians/sec.)

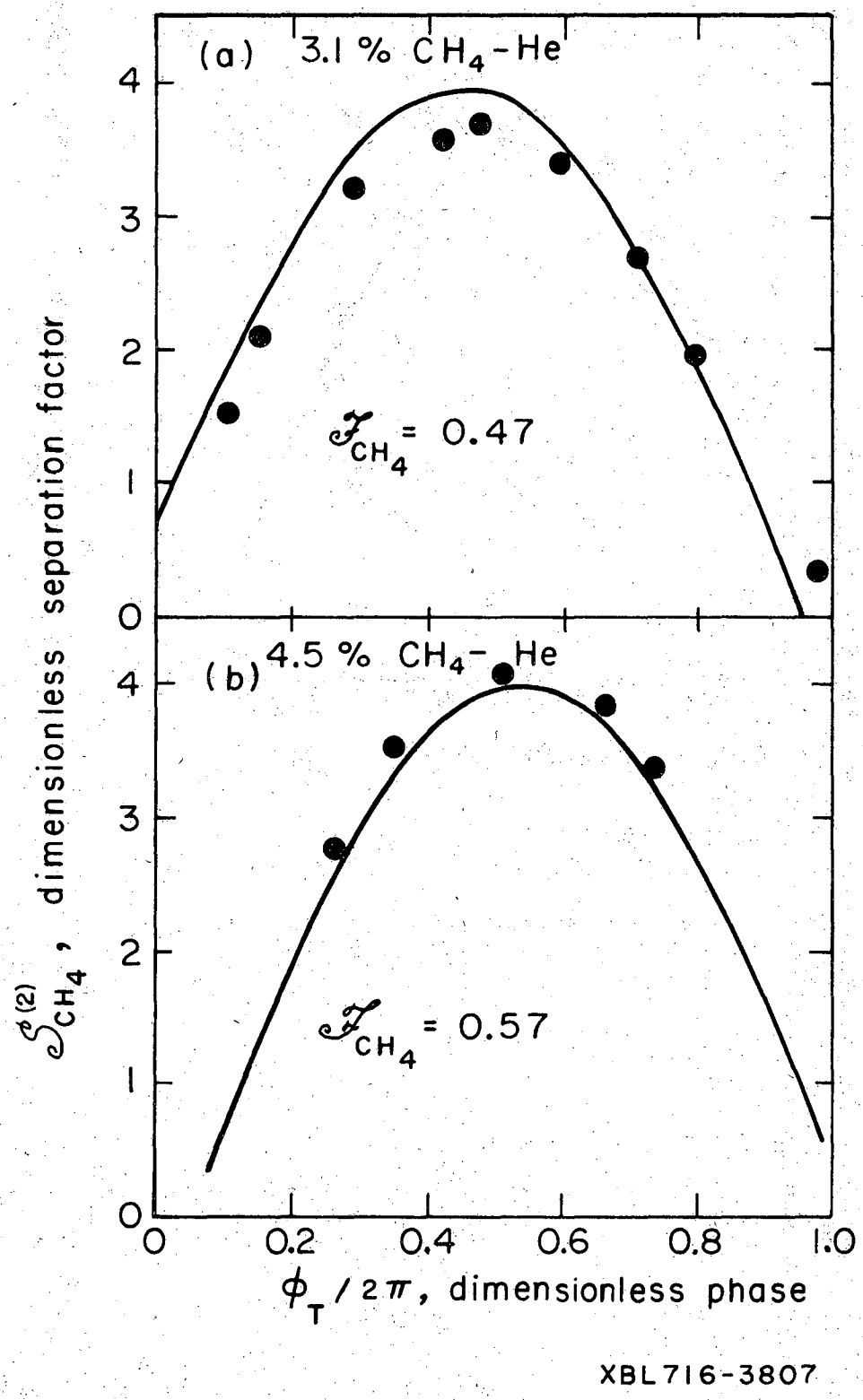

Figure 5-6. Dimensionless Separation Factor, constant Dimensionless Frequency Factor: Dual Zone-Single Adsorbing Specie Feed.

Table 5-1. Single Zone, Single Adsorbing Specie Experimental Data (at 19.0 psia)

System	W, gm.	L, cm.	ω, rad/sec.	L/v, sec.	t_o, °C	K_o, g-moles/lb_{ads}	a_T	$\phi/2\pi$,	$\langle\alpha\rangle$
				7.986					1.639
				5.614					1.868
				4.185					1.900
				3.198					1.791
3.1% CH_4-He	9.73	19.21	0.0334	2.828	41.5	0.590	0.0388		1.773
(ϵ = 0.450)				2.416					1.687
				2.064					1.591
				1.627					1.495
				1.415					1.431
				6.245					1.179
				4.859					1.659
				3.272					1.662
				3.132					1.605
				2.394					1.560
3.1% CH_4-He	9.83	20.32	0.0332	2.339	54.4	0.406	0.0290		1.572
(ϵ = 0.386)				1.799					1.465
				1.385					1.403
				1.119					1.330
				0.961					1.285
				0.739					1.214
				0.692					1.200
				5.176					1.485
				3.406					1.617
				2.672					1.588
				1.975					1.490
				1.636					1.417
6.7% CH_4-He	9.83	20.32	0.0331	1.621	54.4	0.400	0.0290		1.301
(ϵ = 0.386)				1.599					1.329
				1.586					1.385
				1.580					1.408
				1.579					1.366
				1.348					1.353
				1.144					1.302
				0.906					1.239
			0.0259				0.0500	0.181	1.426
			0.0367				0.0379	0.161	1.431
3.1% CH_4-He	11.63	19.38	0.0525	1.010	50.5	0.495	0.0268	0.111	1.396
(ϵ = 0.360)			0.0706				0.0198	0.069	1.332
			0.1039				0.0137	-0.053	1.188
				2.570				-0.054	1.400
				1.781				0.001	1.475
3.1% CH_4-He	11.63	19.38	0.0537	1.325	50.5	0.495	0.0232	0.097	1.422
(ϵ = 0.360)				0.945				0.139	1.330
				0.766				0.172	1.273
				2.991				-0.724	1.331
				1.547				-0.228	1.150
4.9% CO_2-He	11.63	19.38	0.0548	0.929	47.6	1.16	0.0229	-0.047	1.574
(ϵ = 0.360)				0.621				0.070	1.564
				0.402				0.136	1.425
				0.265				0.214	1.292
			0.0238				0.0429	0.095	2.227
			0.0360				0.0324	0.028	1.983
4.9% CO_2-He	11.63	19.38	0.0535	1.105	47.1	1.17	0.0230	-0.089	1.507
(ϵ = 0.360)			0.0711				0.0160	-0.238	1.167
			0.0976				0.0134	-0.428	1.102
				0.777					1.432
			0.0535	1.497	50.4	1.10	0.0218		1.346
Trace System				3.843					1.262
5.4% CO_2-He	11.57	20.64							
4.9% CH_4				0.947					1.627
(ϵ = 0.403)			0.0414	1.404	46.4	1.20	0.0275		1.671
				2.449					1.156
				3.774					1.477

Table 5-2. Velocity Response of a Single Isothermal Zone (at 19.0 psia)

System	ω, rad/sec.	v, cm/sec.	L/v, sec.	t_o, °C	$\phi_s/2\pi$	$\frac{(\alpha)_{response}}{(\alpha)_{input}}$
		17.95	1.150		0.270	0.986
		28.55	0.723		0.172	0.993
		44.68	0.462	49.2	0.118	0.996
		59.33	0.348		0.095	0.997
		100.93	0.205		0.035	0.998
	0.053					
		6.02	3.215		0.765	0.939
		8.96	2.162		0.477	0.965
3.1% CH_4-He		11.93	1.623	49.5	0.424	0.980
(ε = 0.403)		13.20	1.467		0.319	0.982
		16.64	1.164		0.296	0.989
		20.87	0.928		0.236	0.992
		10.34	1.996		0.740	0.963
		18.03	1.145		0.421	0.983
	0.089	26.65	0.774	49.2	0.235	0.988
		36.73	0.562		0.174	0.993
		50.64	0.408		0.126	0.995
		60.53	0.341		0.106	0.996
		5.71	3.616		–	0.814
		11.10	1.860		0.960	0.860
4.9% CO_2-He	0.055	18.52	1.115	49.3	0.581	0.902
(ε = 0.403)		28.17	0.733		0.396	0.938
		43.39	0.476		0.248	0.968
		65.88	0.313		0.169	0.981

L = 20.64 cm., W = 11.57 gm.

Table 5-3. Dual Zone, Single Adsorbing Specie Experimental Data (at 19.0 psia)

System	ω, rad/sec.	L/v, sec.	t_o, °C	K_o, g-moles/lb_{ads}	a_T	$\phi_T/2\pi$	(α)
		0.911					2.440
		1.465					1.953
4.5% CH_4-He	0.0411	2.788	45.5	0.535	0.0275	0.50	2.785
(ε = 0.382)		2.937					2.796
		3.714					2.135
		9.035					1.495
		0.347					1.325
5.4% CO_2-He	0.0411	0.911	45.5	1.210	0.0275	0.50	2.440
(ε = 0.382)		1.465					2.156
		3.714					1.719
						0.103	1.600
						0.160	1.916
						0.292	2.711
						0.425	3.042
3.1% CH_4-He	0.0331	3.474	41.5	0.590	0.0382	0.474	3.179
(ε = 0.415)						0.594	2.895
W = 10.31 gm.						0.709	2.330
L = 19.45 cm.						0.795	1.837
						0.979	1.107
						0.265	1.994
						0.350	2.416
4.5% CH_4-He	0.0411	2.934	45.3	0.540	0.0282	0.513	2.796
(ε = 0.382)						0.662	2.620
						0.734	2.328

For each zone L = 20.00 cm., W = 11.60 gm.

CHAPTER 6

TWO-ADSORBING SPECIE EXPERIMENTS

In the first section of this chapter, the dilute CH_4-CO_2-He gas mixture (4.5% CH_4, 5.4% CO_2), termed a "trace system", was utilized as the feed. Here, the usual chromatographic definition of "trace system" is implied, i.e. the total composition of the adsorbing species is less than 10%. Under "trace conditions", the normal assumption of independent adsorption is very closely approximated, as shown in Figure 5-3, Chapter 5. In this dilute state, each of the adsorbing species may be treated separately, without regard to what is happening to the others. In addition, the presence of another dilute adsorbing component is assumed not to alter the adsorption equilibrium isotherm.

The second section deals with the CH_4-CO_2 binary adsorption system. A mixture of 50.2% CH_4-CO_2 was employed as the feed. This mixture approximates the above "trace system's" composition when the helium carrier gas has been removed. In binary gas adsorption, not only must the influence of each specie on the other's adsorption isotherm be accounted for, but the gas phase material balance must be considered. In the gas phase, a change in one specie's concentration complements a change in the other's, irrespective of what is happening on the solid.

Experimental results were compared graphically to the linear equilibrium theory, described in Chapter 3. The solid theoretical lines are based upon ideal sine temperature inputs and the isotherm parameters, determined by the frequency response method, described in Appendix A. The experimental data are presented in tabular form at the end of each section.

TRACE SYSTEM

A feed of dilute CH_4 and CO_2 in a helium carrier gas was employed, for which it was assumed that each component's adsorption (its gas phase concentration) was independent. The analytical technique utilized to determine effluent concentration behavior of CH_4 and CO_2, described in Chapter 4, involved the measurement of the T-C cell responses for the mixture and for the CO_2-free effluent over identical portions of the temperature cycle. The CO_2 was removed from the effluent by passing it thru an Ascarite bed. It was found that this auxiliary CO_2 adsorber-reactor Ascarite bed was essentially dispersion free. In addition, it effectively removed all the CO_2 from the effluent bleed stream. By employing equations (4-4), (4-5), and (4-6), the separate CH_4 and CO_2 concentration-time responses were calculated.

Typical experimental input temperature-time and effluent concentration-time curves for a dual zone system are shown in Figure 6-1. The location of the enriched and depleted half-cycle portions of the effluent is specified by the switching location parameter, β. The switching location is referred to a sine-wave temperature input and is selected by maximization of the separation factor, $\langle \alpha_{CH_4-CO_2} \rangle$, as defined by equation (3-49), for a given effluent stream. The phase difference between the two adsorbing species effluent composition waves, ϕ_c, and the phase between the two temperature inputs used for two-zone operation, ϕ_T, are also indicated on Figure 6-1.

Single Zone

A constant composition gas mixture containing 4.5% CH_4 and 5.4% CO_2 was fed to a single cycling zone adsorption (CZA) unit. Over the temperature and concentration ranges employed, the isotherm parameters were found to be:

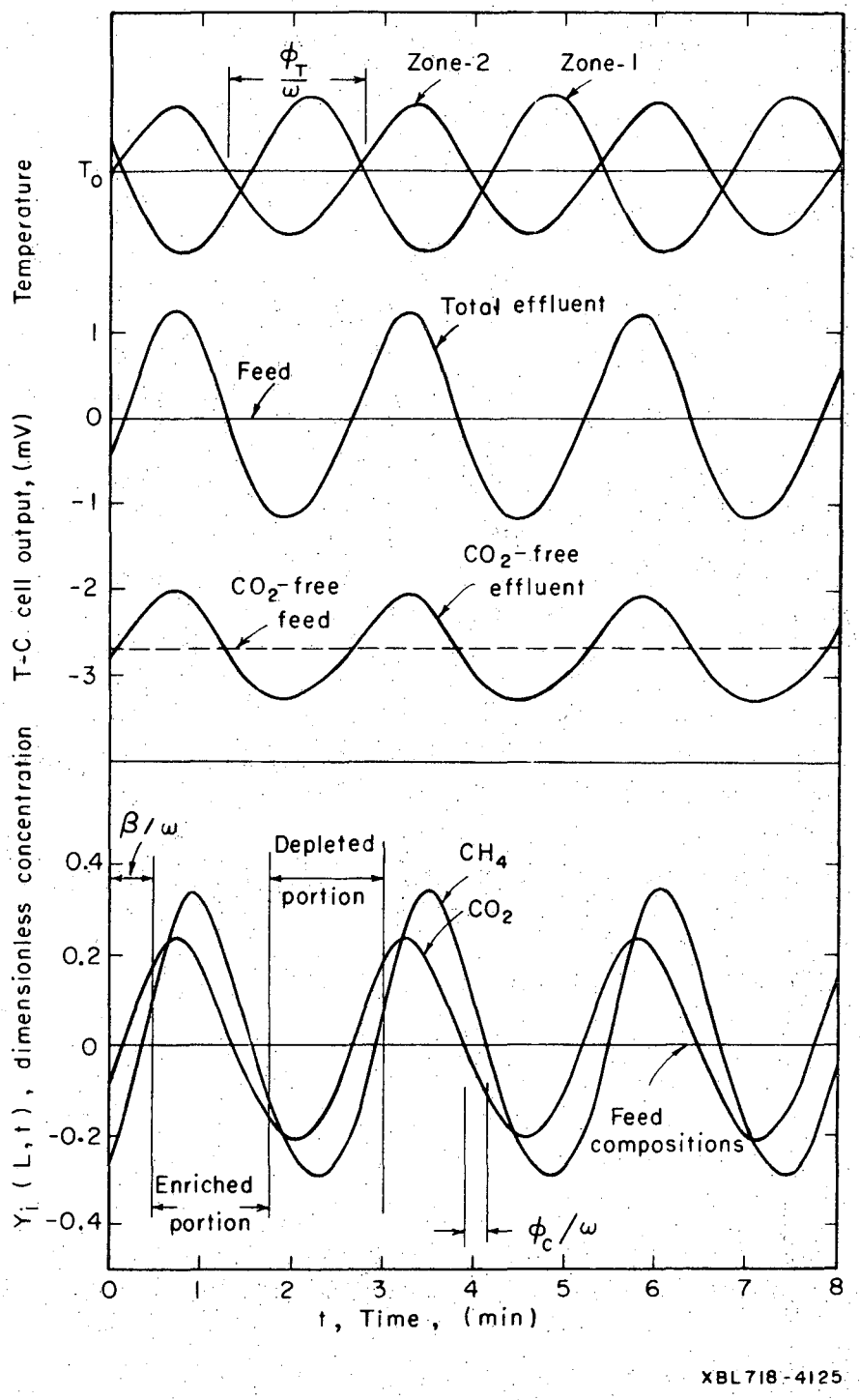

Figure 6-1. Experimental Input Temperatures and T-C Cell Response Curves for Dual (identical) Zone System: Trace Feed.

$$\Lambda = \frac{1 + \frac{\rho_s(1-\varepsilon)}{\rho_f \varepsilon}(K_o)_{CO_2}}{1 + \frac{\rho_s(1-\varepsilon)}{\rho_f \varepsilon}(K_o)_{CH_4}} \cong \frac{(K_o)_{CO_2}}{(K_o)_{CH_4}} \cong 2.2$$

and

$$\gamma = \frac{(-\Delta H_a)_{CO_2}}{(-\Delta H_a)_{CH_4}} \cdot \frac{(K_o)_{CO_2}}{(K_o)_{CH_4}} \cdot \frac{1}{\Lambda} \cong 1.0$$

Since the separation factor for a given pair of concentration waves is a function of the manner in which it is split into enriched and depleted portions, the switching location is arbitrarily selected until the maximum separation factor is achieved. The maximum dimensionless separation factor, $\mathcal{S}_{CH_4\text{-}CO_2}$, and its corresponding switching location, β, versus the methane dimensionless frequency factor, $\mathcal{F}_{CH_4}$, are shown in Figure 6-2. The associated concentration wave phase difference, ϕ_c, is presented in Figure 6-3. The discontinuity in the phase difference occurs at optimum separation. This exists where the amplitude of the CO_2 concentration wave is zero (see Figure 3-3, Chapter 3). In this special case where $\gamma = 1$, the optimum condition for single CZA operation corresponds to a dimensionless frequency factor, $\mathcal{F}_{CH_4}$, such that the second component, CO_2, is not amplified. The CO_2 effluent concentration, at this operating point, remains constant and equal to its feed composition. Therefore, for multi-component separations, a single CZA unit would be designed on the basis of the desired adsorbed species (heavy key) and the next strongly adsorbed species (light key) such that the light key is not amplified.

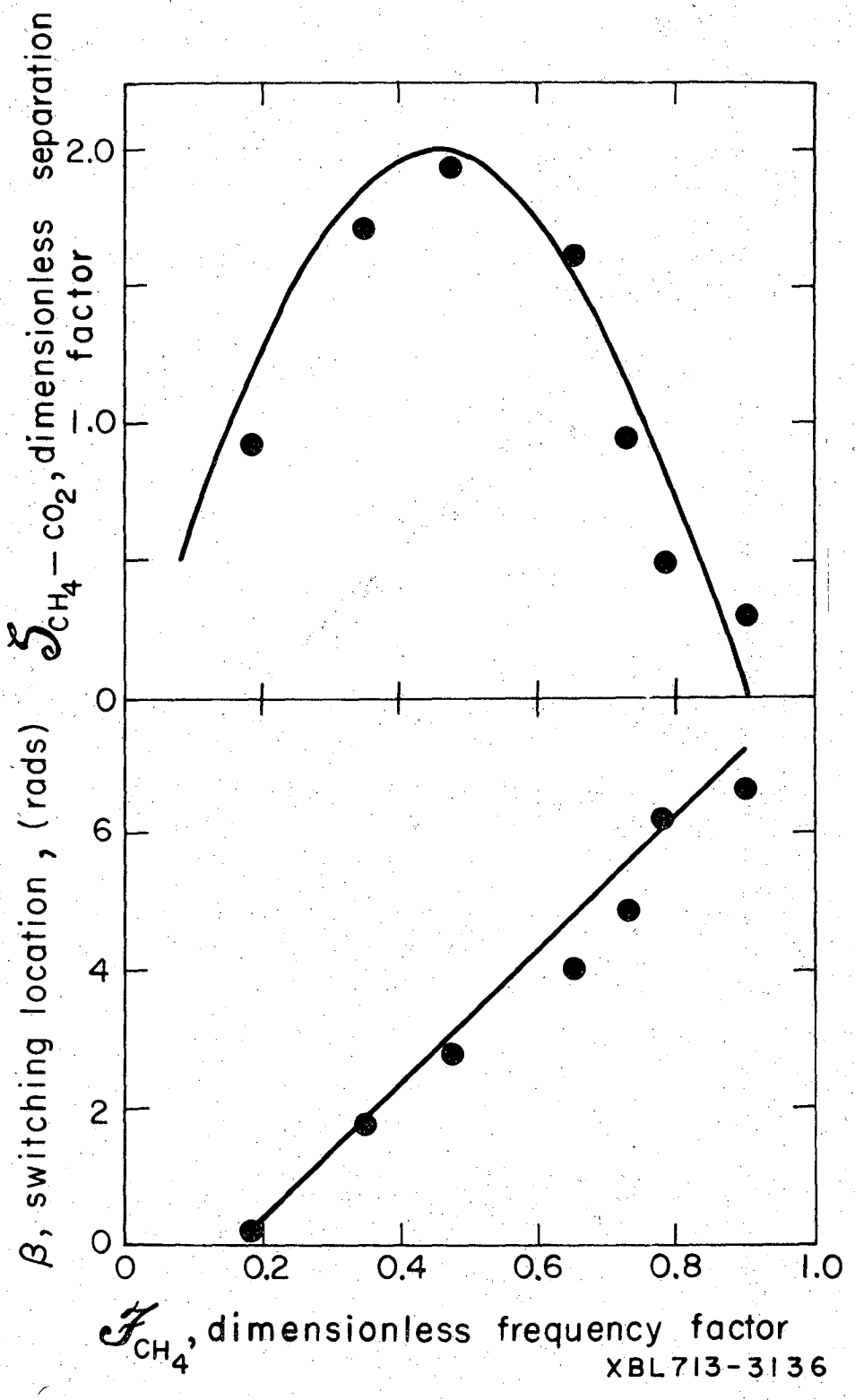

Figure 6-2. Maximum Separation Factor and its corresponding Switching Location: Single Zone-Trace Feed.

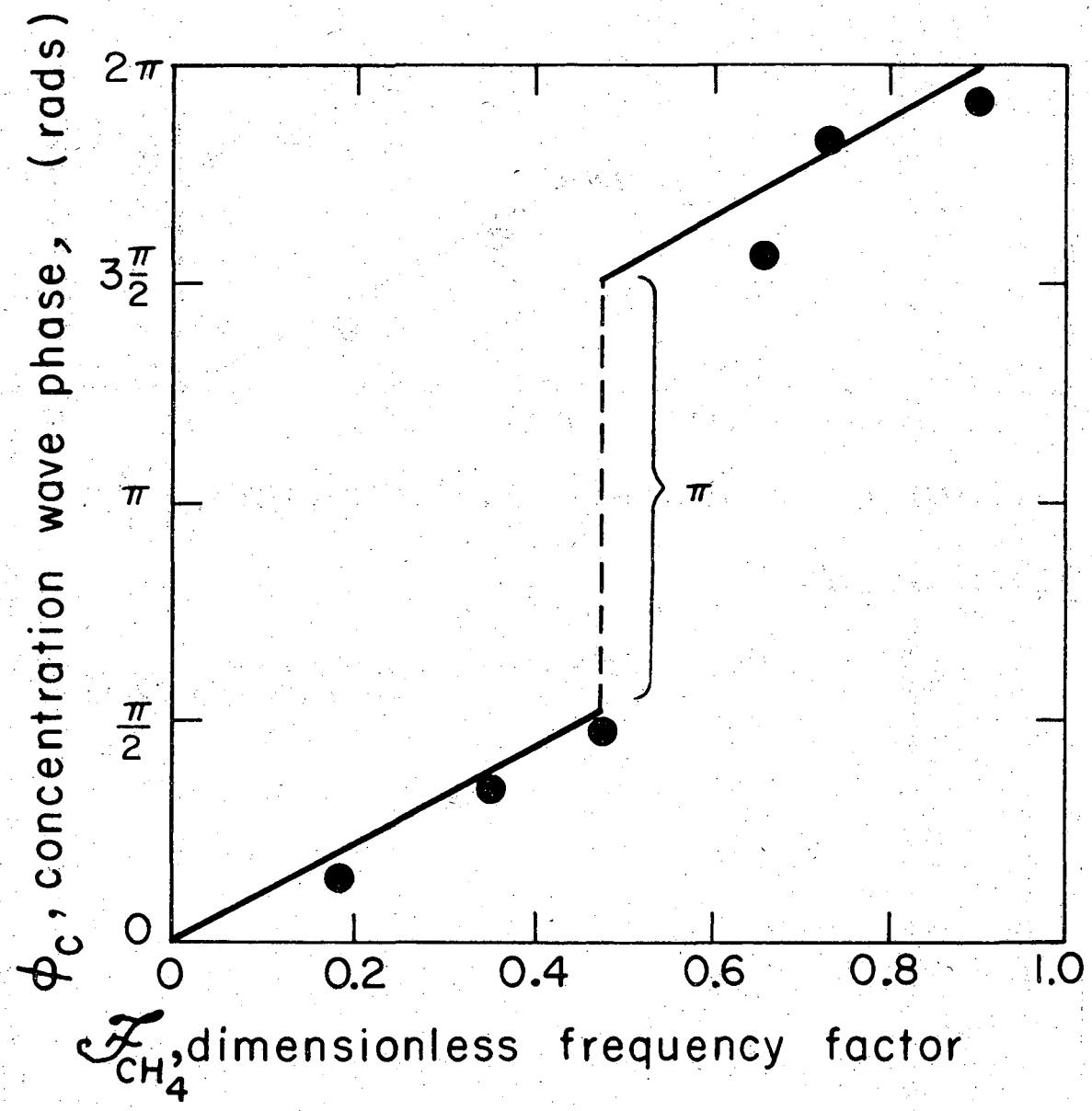

Figure 6-3. Phase Difference between Effluent Concentration Waves: Single Zone-Trace Feed.

Dual Zone

The effluent of the first zone is fed to an identical CZA unit whose temperature is being oxcillated at the same frequency but out of phase with respect to that of the first zone. The dual zone system requires the additional variable, ϕ_T, the phase chosen between the two temperature inputs. The effluent of the second zone is split into enriched and depleted half-cycle portions, initiated at the switching location, β. Holding the temperature phase constant ($\phi_T/2\pi = 0.51$) and scanning the dimensionless frequency factor, $\mathcal{F}_{CH_4}$, the experimental separation factors and their corresponding switching locations are plotted in Figure 6-4. The switching location curve is broken for plotting convenience.

Two important observations can be made: (1) the separation factor versus the dimensionless frequency factor is bi-modal, the first peak being the global maximum; (2) deviations from the linear theory become greater at the higher frequency factors. Fortunately, the global maximum lies in the operating region desired for minimizing mass transfer losses. Around the second peak in the separation factor curve, corresponding to higher frequencies, lower velocities, and longer columns, the effect of mass transfer resistance is enhanced, resulting in reduction of separative power. A very important point is that the maximum separation factor is increased by approximately 2 1/2 times by the addition of the second zone, whereas applying a second zone to the single adsorbing specie system increases the separation by only a factor of 2. This is achieved not only by additional amplification of each species, but by additional shifting of their concentration wave phase difference in the second zone. The associated concentration wave phase differences

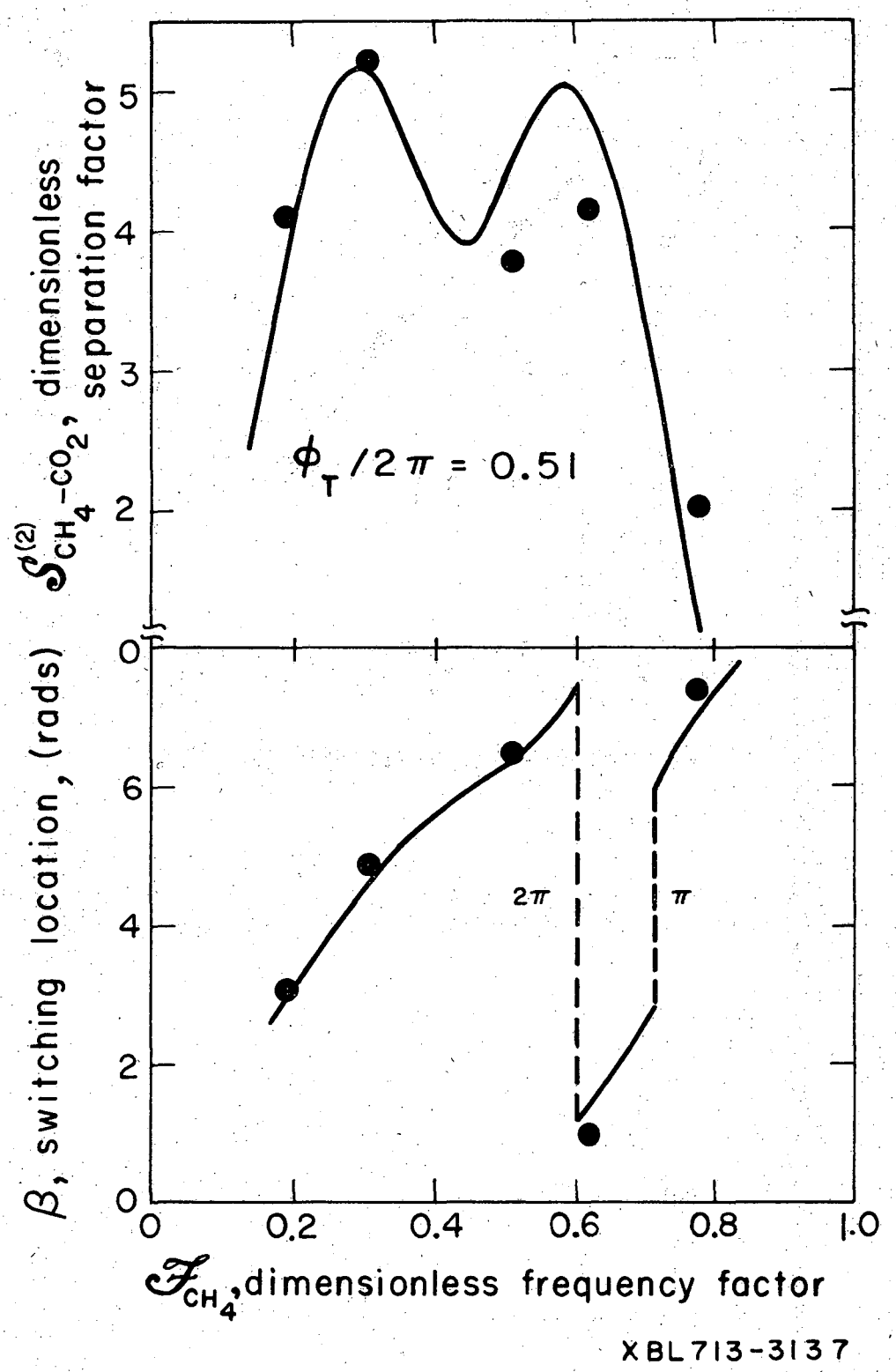

Figure 6-4. Maximum Separation Factor and its corresponding Switching Location, constant Temperature Phase: Dual Zone-Trace Feed.

are shown in Figure 6-5. There is continuity in the phase difference curve, since the point of zero amplification of CO_2 in the second zone occurs near $\phi_c = \pi$. It is apparent that at the optimum separation, $\phi_c = 0.75\pi$, and that further shifting (up to $\phi_c = \pi$) of the two concentration waves would have enhanced the separation still more.

When the dimensionless frequency factor is held constant ($\mathcal{J}_{CH_4} = 0.59$) and the temperature phase is varied, we find that the optimum separation occurs around $\phi_T = \pi$, as shown in Figure 6-6. The large difference between the experimental data and the theory is due to mass transfer resistance, as indicated in Figure 6-4, in the region of $\mathcal{J}_{CH_4} = 0.6$.

Utilization of Isothermal Shifter

When a single adsorbing specie concentration wave is passed thru an isothermal bed packed with an adsorbent, the effluent concentration wave is delayed, resulting in the phase shift, ϕ_s. The dimensionless phase shift versus the shifter dimensionless frequency factor, $\mathcal{J}^*$, is shown in Figure 6-7 for the CH_4-He and CO_2-He systems. The shifter dimensionless frequency factor is defined as:

$$\mathcal{J}^* = \frac{[(1 + \psi_s)\, \omega_{in}(L_s/v_s)]}{2\pi} \qquad (6\text{-}1)$$

where

ω_{in} = input concentration wave frequency, rad/sec.

L_s = length of isothermal shifter bed, cm.

v_s = interstitial velocity within shifter, cm/sec.

ψ_s = solids-fluid capacity ratio at shifter bed average temperature, T_s.

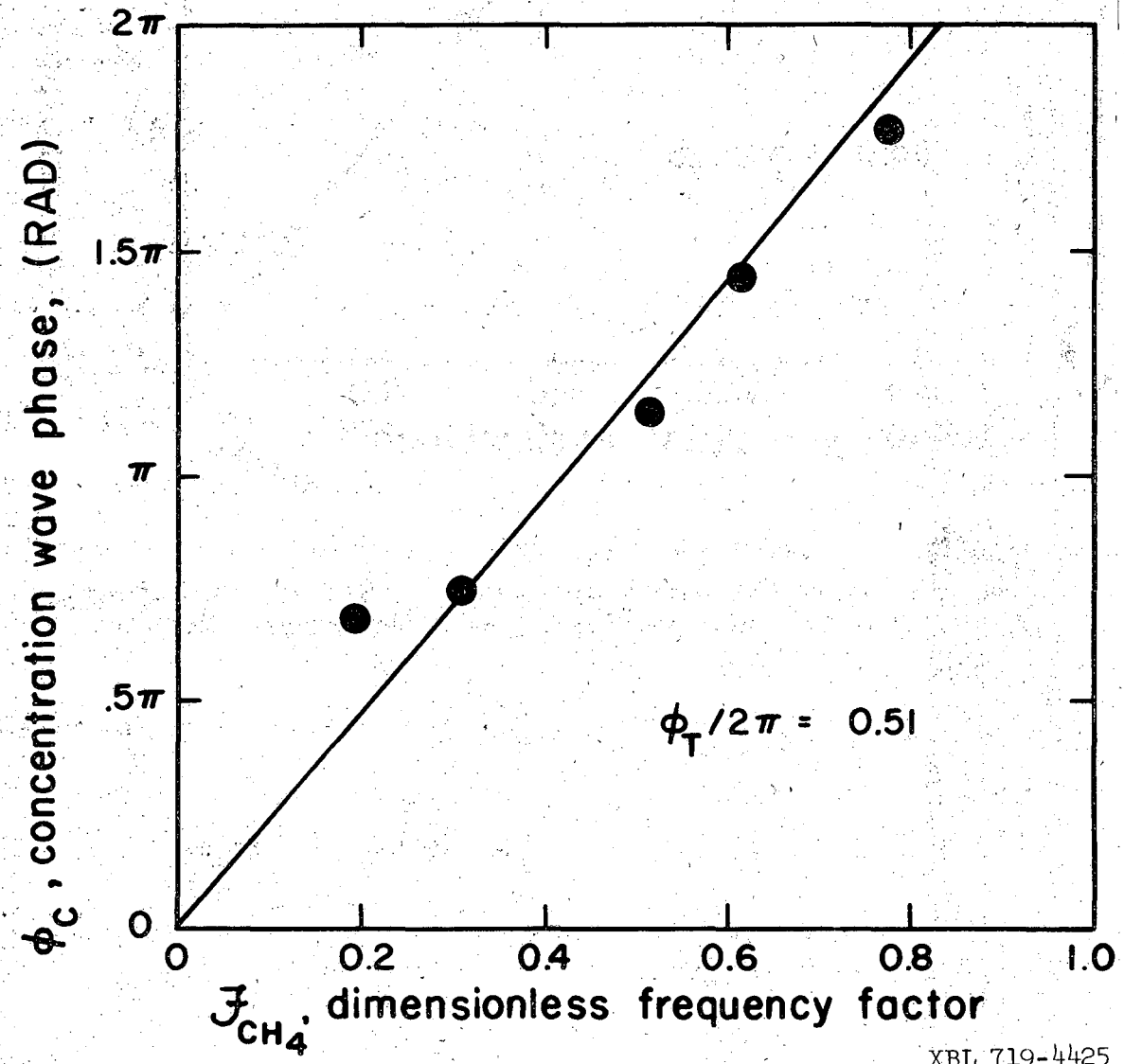

Figure 6-5. Phase Difference between Effluent Concentration Waves, constant Temperature Phase: Dual (identical) Zone-Trace Feed.

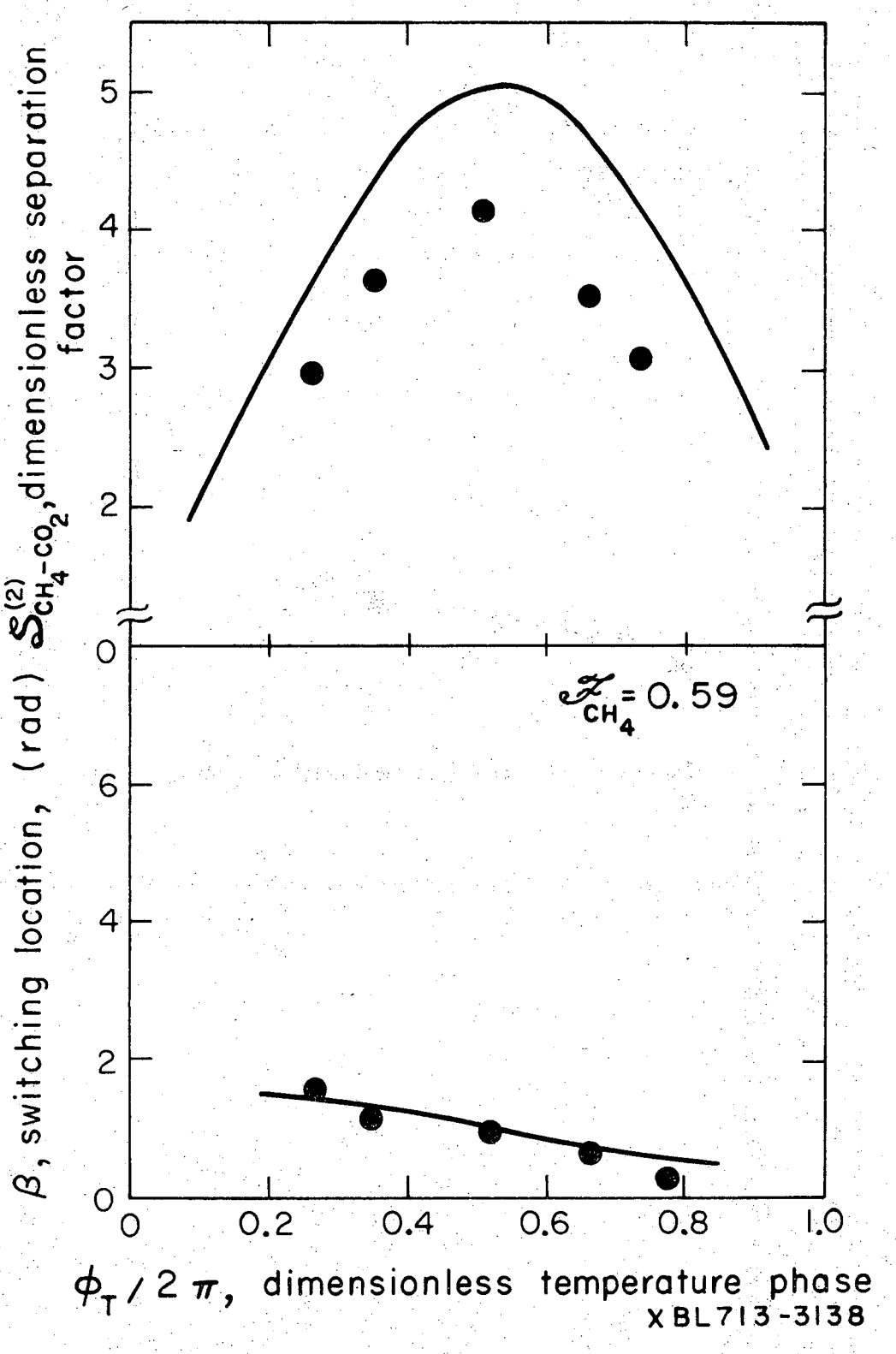

Figure 6-6. Maximum Separation Factor and its corresponding Switching Location, holding Dimensionless Frequency Factor constant; Dual Zone-Trace Feed.

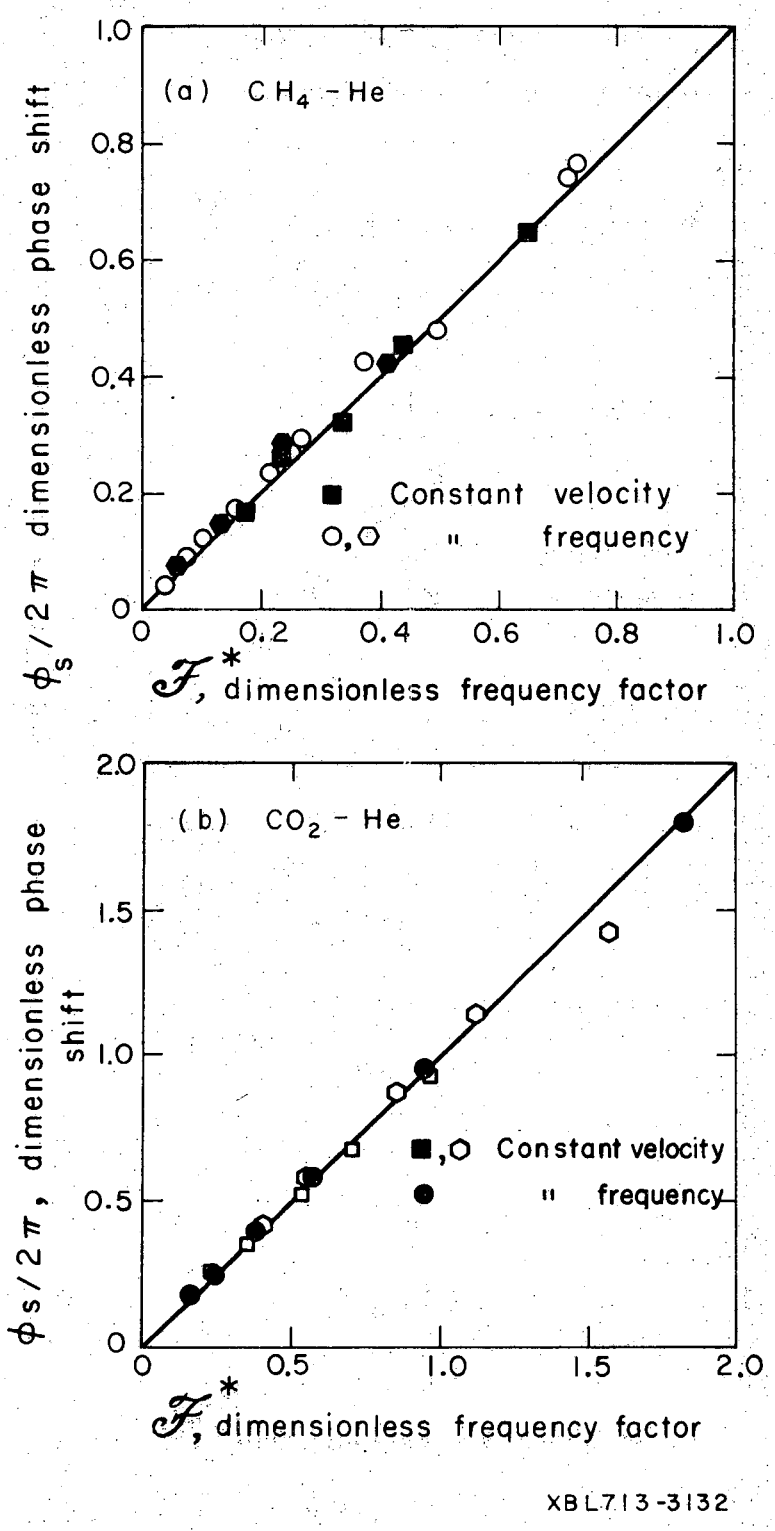

Figure 6-7. Concentration Wave Phase Shift upon passage thru Isothermal Bed: Single Adsorbing Specie Feed.

For two adsorbing species, under "trace conditions", the net additional shift in their concentration wave phase by passage thru an isothermal bed, derived in Chapter 3, is

$$\phi_{net}/2\pi = (\Lambda^* - 1)\mathcal{J}_1^* \qquad (6\text{-}2)$$

where $\mathcal{J}_1^*$ is the dimensionless shifter frequency factor for the main component, 1, and Λ^* is the species concentration wave velocity ratio within the shifter. The net phase shift, ϕ_{net}, can be varied by adjustment of Λ^* and/or $\mathcal{J}_1^*$. Generally, it is more convenient to adjust $\mathcal{J}_1^*$, by changes in either the shifter length or the shifter temperature, T_s, which alters ψ_{1s}.

The best separation of the two species is achieved when their concentration waves are 180° apart before the splitting and collection of the enriched and depleted portions. Thus the output phase difference of the isothermal shifter, $(\phi_c)_{out}$, is equal to π, for the maximum separation. When the input phase is known, the net phase shift required to produce a 180° phase difference in the shifter effluent may be determined:

$$(\phi_c)_{out} = (\phi_c)_{in} + \phi_{net} = \pi \qquad (6\text{-}3)$$

or

$$\phi_{net} = \pi - (\phi_c)_{in}$$

$$= 2\pi(\Lambda^* - 1)\mathcal{J}_1^* \qquad (6\text{-}4)$$

Since $(\phi_c)_{in}$ is a function of $\mathcal{J}_1$, the ratio of frequency factors in the shifter and the preceding thermally driven zone is

$$\mathcal{J}_1^* / \mathcal{J}_1 = \frac{(1 + \psi_{1s})(L_s/v_s)}{(1 + \psi_1)(L/v)} \qquad (6\text{-}5)$$

This gives an estimate of the relative size of the isothermal shifter as compared to that of the cycling zone unit which it follows.

Consider the case of an isothermal shifter following a single CZA unit to which gas mixture containing trace concentrations of CH_4 and CO_2 is fed. The phase between the concentration waves leaving the CZA unit are given in Figure 6-3. From the net shift required to produce 180° phase difference in the shifter effluent, $\mathcal{J}_1^*$ can be determined using equation (6-4). The frequency factor ratio, $\mathcal{J}_1^* / \mathcal{J}_1$, may then be plotted versus $\mathcal{J}_1$, as shown in Figure 6-8. The design of the isothermal shifter is now fixed in terms of $\mathcal{J}_1^*$. Adjustment of either L_s or T_s may be made in order to obtain the required $\mathcal{J}_1^*$. According to Figure 6-2, the optimum separation for the CZA unit lies in the vicinity of $\mathcal{J}_1 = 0.47$.

In the following experiments, the output phase difference in the shifter effluent, for a constant input concentration wave phase, was varied by changing the shifter's temperature. Referring to the experimental apparatus schematic in Figure 4-3, the upper zone was utilized as the CZA unit and the second zone, whose temperature was held constant, served as the isothermal shifter. For the trace system of CH_4-CO_2-He, previously utilized, the improvement in the separation factor, $\langle \alpha_{CH_4\text{-}CO_2} \rangle$, using a shifter, along with the output concentration waves' phase are plotted versus the shifter dimensionless frequency factor in Figures 6-9 and 6-10. The separation factor can be increased from 1.70 to 2.24 and from 1.9 to 2.46 by adding isothermal shifter beds of optimum size. Dispersion and mass transfer effects in the shifter become significant when the thru-put velocity is decreased, as shown in Figure 6-10.

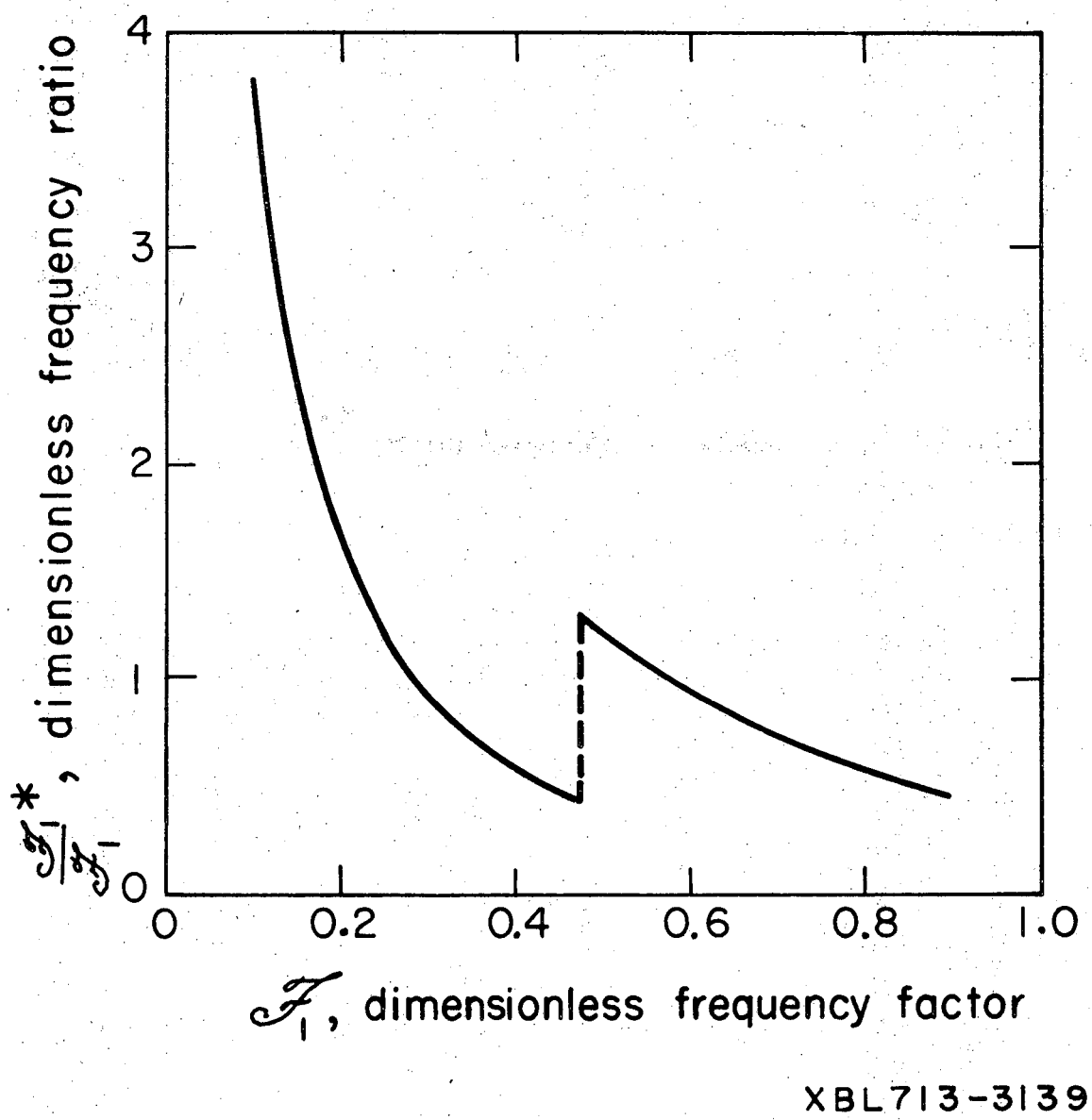

Figure 6-8. Frequency Factor Ratio required to produce Shifter Effluent Concentration Wave Phase difference of 180°: Single Zone + Isothermal Shifter-Trace Feed.

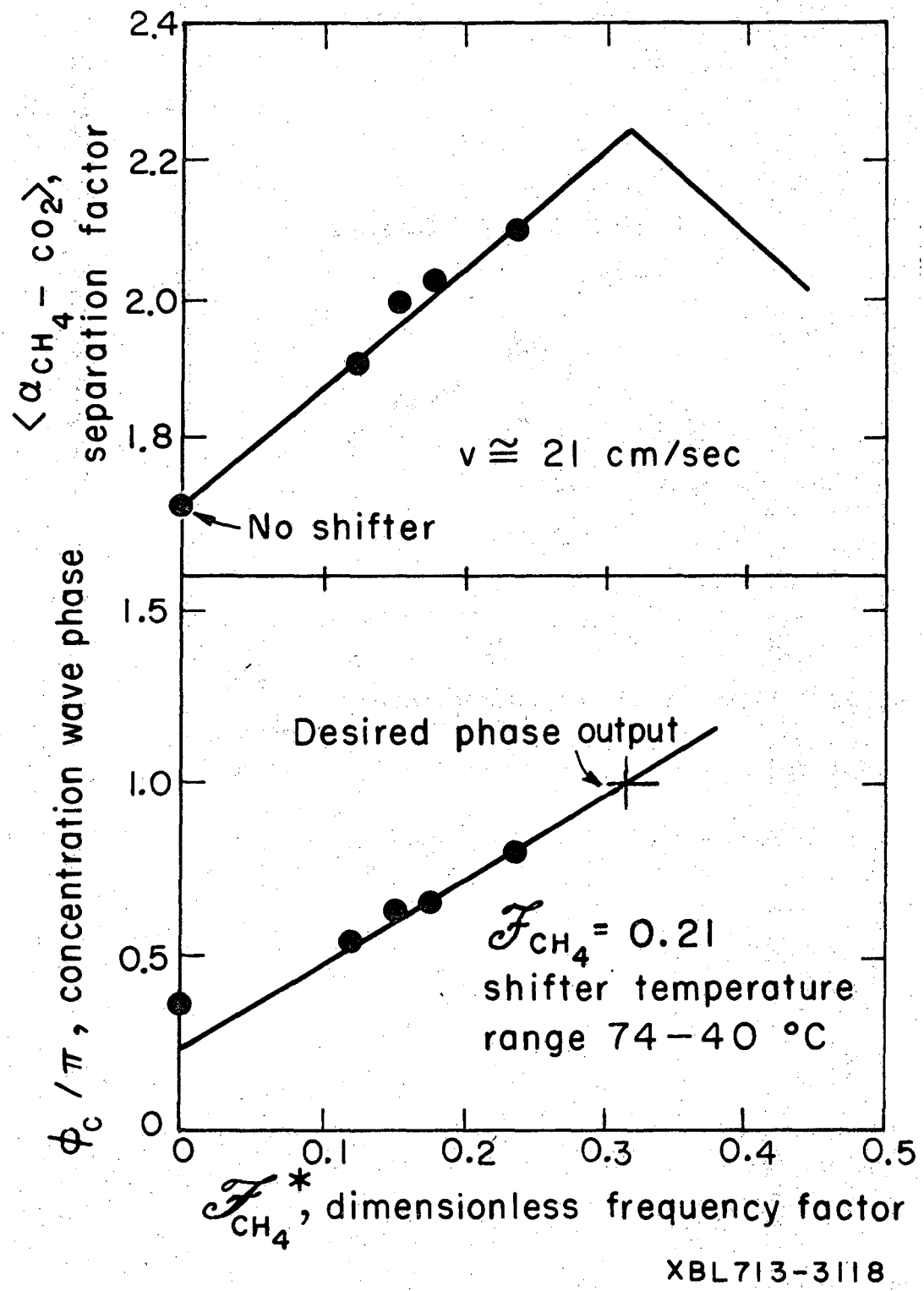

Figure 6-9. Separation Improvement by addition of an Isothermal Bed to an identical Single CZA Unit: Trace Feed.

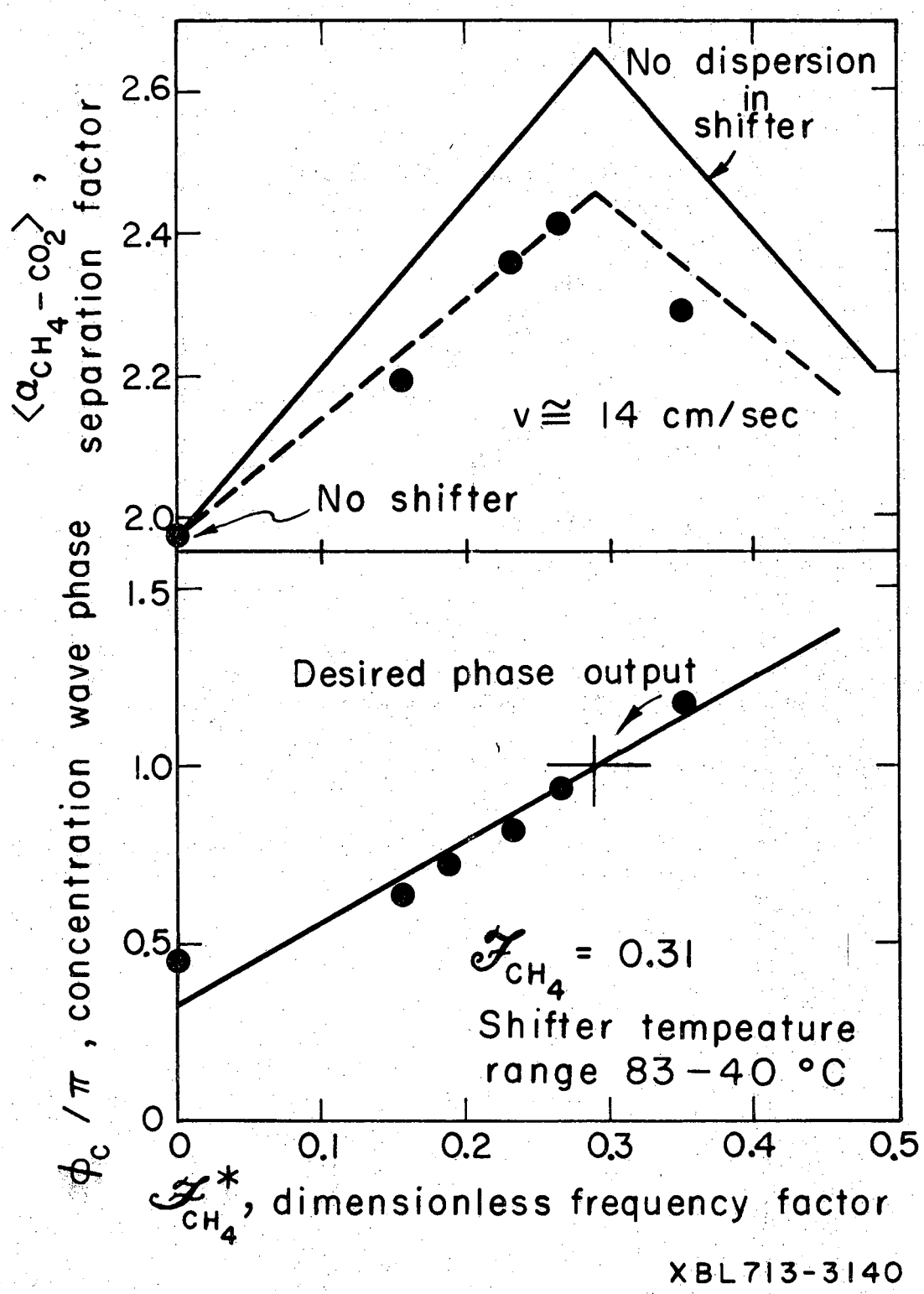

Figure 6-10. Separation Improvement by addition of an Isothermal Bed to an identical Single CZA Unit: Trace Feed.

Table 6-1. Single Zone, Trace System Experimental Data (4.5% CH_4, 5.4% CO_2-He at 19.0 psia)

ω, rad/sec.	L/v, sec.	t_o, °C	K_o, g-moles/lb$_{ads}$ CH_4	K_o, g-moles/lb$_{ads}$ CO_2	a_T	β,* rad.	$\phi_c/2\pi$	$\langle \alpha_{CH_4-CO_2} \rangle$
	3.843					6.65	0.960	1.058
	3.345					6.20	—	1.096
0.0535	2.790	50.4	0.495	1.10	0.0218	4.02	0.781	1.376
	1.497					1.75	0.173	1.354
	0.777					0.20	0.072	1.195
0.0414	3.774	46.4	0.535	1.20	0.0275	4.86	0.910	1.270
	2.449					2.79	0.237	1.620

W = 11.57 gm., L = 20.64 cm., ε = 0.403, Λ = 2.2, $\gamma \cong 1.0$

*Switching location which yields the maximum mean separation factor.

Table 6-2. Dual Zone, Trace System Experimental Data (4.5% CH_4, 5.4% CO_2-He at 19.0 psia)

ω, rad/sec.	L/v, sec.	t_o, °C	K_o, g-moles/lb$_{ads}$ CH_4	K_o, g-moles/lb$_{ads}$ CO_2	a_T	β,* rad.	$\phi_c/2\pi$,	$\phi_T/2\pi$,	$\langle \alpha_{CH_4-CO_2} \rangle$
	9.035					—	—		1.143
	3.714					7.40	0.880		1.631
0.0411	2.788	45.5	0.535	1.21	0.0275	6.49	0.570	0.510	2.520
	1.465					4.74	0.369		3.655
	0.911					3.04	0.342		2.952
						1.51	—	0.265	2.044
						1.17	—	0.350	2.410
0.0411	2.937	45.5	0.535	1.21	0.0275	0.98	0.716	0.513	2.735
						0.69	—	0.662	2.352
						0.30	—	0.734	2.105

For each zone: W = 11.60 gm., L = 20.00 cm., ε = 0.382, Λ = 2.2, $\gamma \cong 1.0$

*Switching location which yields maximum mean separation factor.

Table 6-3. Isothermal Phase Shifter Response, Single Adsorbing Specie Data (at 19.0 psia)

System	ω_{in}, rad/sec.	L_s/v_s, sec.	t_s, °C	K_o, g-moles/lb_{ads}	$\phi_s/2\pi$
		1.150			0.270
		0.723			0.172
		0.462	49.2	0.502	0.118
		0.348			0.095
		0.205			0.035
	0.053				
		3.215			0.765
		2.162			0.477
		1.623			0.424
		1.467	49.5	0.500	0.319
		1.164			0.296
		0.928			0.236
3.1% CH_4-He (ε = 0.403)		1.996			0.740
		1.145			0.421
		0.774			0.235
	0.089	0.562	49.2	0.502	0.174
		0.408			0.126
		0.341			0.106
	0.0259				0.170
	0.0367				0.258
	0.0525	1.467	50.4	0.495	0.319
	0.0706				0.450
	0.1039				0.647
		3.616			1.802
		1.860			0.960
	0.0548	1.115	49.3	1.11	0.581
		0.733			0.396
		0.476			0.248
		0.313			0.169
	0.0238				0.405
	0.0360				0.557
4.9% CO_2-He	0.0535	1.363	38.9	1.42	0.846
(ε = 0.403)	0.0711				1.106
	0.0976				1.430
	0.0238				0.246
	0.0360				0.352
	0.0535	1.265	61.2	0.87	0.518
	0.0711				0.673
	0.0976				0.924

W_s = 11.57 gm., L_s = 20.64 cm.

Table 6-4. Isothermal Phase Shifter following a Single Cycling Zone, Trace System Data
(4.5% CH_4, 5.4% CO_2-He at 19.0 psia)

ω_{in}, rad/sec.	L_s/v_s, sec.	t_s, °C	$(K_o)_{CH_4}$, g-moles/lb$_{ads}$	ϕ_c/π	$\langle \alpha_{CH_4-CO_2} \rangle$
	*(0.860)	(46.1)	(0.540)	(0.362)	(1.701)
	0.937	74.3	0.306	0.543	1.910
0.0429	0.978	60.4	0.396	0.630	1.993
	0.999	53.5	0.460	0.663	2.024
	1.035	40.8	0.616	0.804	2.100
	(1.260)	(46.1)	(0.540)	(0.452)	(1.976)
	1.383	82.7	0.264	0.633	2.191
0.0429	1.418	71.4	0.320	0.721	2.330
	1.462	61.0	0.400	0.814	2.359
	1.482	53.1	0.465	0.929	2.414
	1.552	40.4	0.622	1.162	2.290

*(Without shifter), i.e. Cycling zone data.

Isothermal Shifter: $W_s = 11.57$ gm., $L_s = 20.64$ cm., $\varepsilon_s = 0.403$, $\Lambda^* = 2.2$, $\gamma^* \cong 1.0$

Cycling Zone: $W = 11.63$ gm., $L = 19.38$ cm., $\varepsilon = 0.360$, $\Lambda = 2.2$, $\gamma \cong 1.0$, $\alpha_T = 0.0276$

BINARY ADSORBING SYSTEM

A binary gas adsorbing system is defined as a gas mixture of two components, both of which are significantly adsorbed by the solid adsorbent particles. The equilibrium behavior of each component is described by an equilibrium distribution function which is also a function of the composition of the other component. The gas phase material balance requires that the sum of the mole fractions be equal to unity.

A binary gas mixture, containing 50.2 mole% methane and 49.8 mole% carbon dioxide, was utilized as the feed. The effluent's CO_2 concentration was measured by passing it thru a T-C cell and recording the cell's response. The T-C cell was calibrated using pure methane as the reference gas and known CH_4-CO_2 standard gas mixtures. A typical calibration curve is shown in Figure 4-8b. The methane concentration is then calculated using the gas phase material balance restriction.

Typical experimental input temperature-time and effluent concentration-time curves are shown in Figure 6-11. The phase between the temperature inputs, ϕ_T, and the phase lag between the effluent concentration wave and the input temperature wave, ϕ, are also indicated. Since $y_{CO_2} = 1 - y_{CH_4}$, the phase difference between the adsorbing species' effluent concentration waves, ϕ_c, is always 180°. In the single zone system, the effluent is split into enriched and depleted portions to effect the separation whereas in the dual zone system, the split is performed on the second zone's effluent.

Single Zone

A constant composition gas binary mixture, containing 50.2% CH_4 and 49.8% CO_2, was fed to a single cycling zone adsorption (CZA) unit.

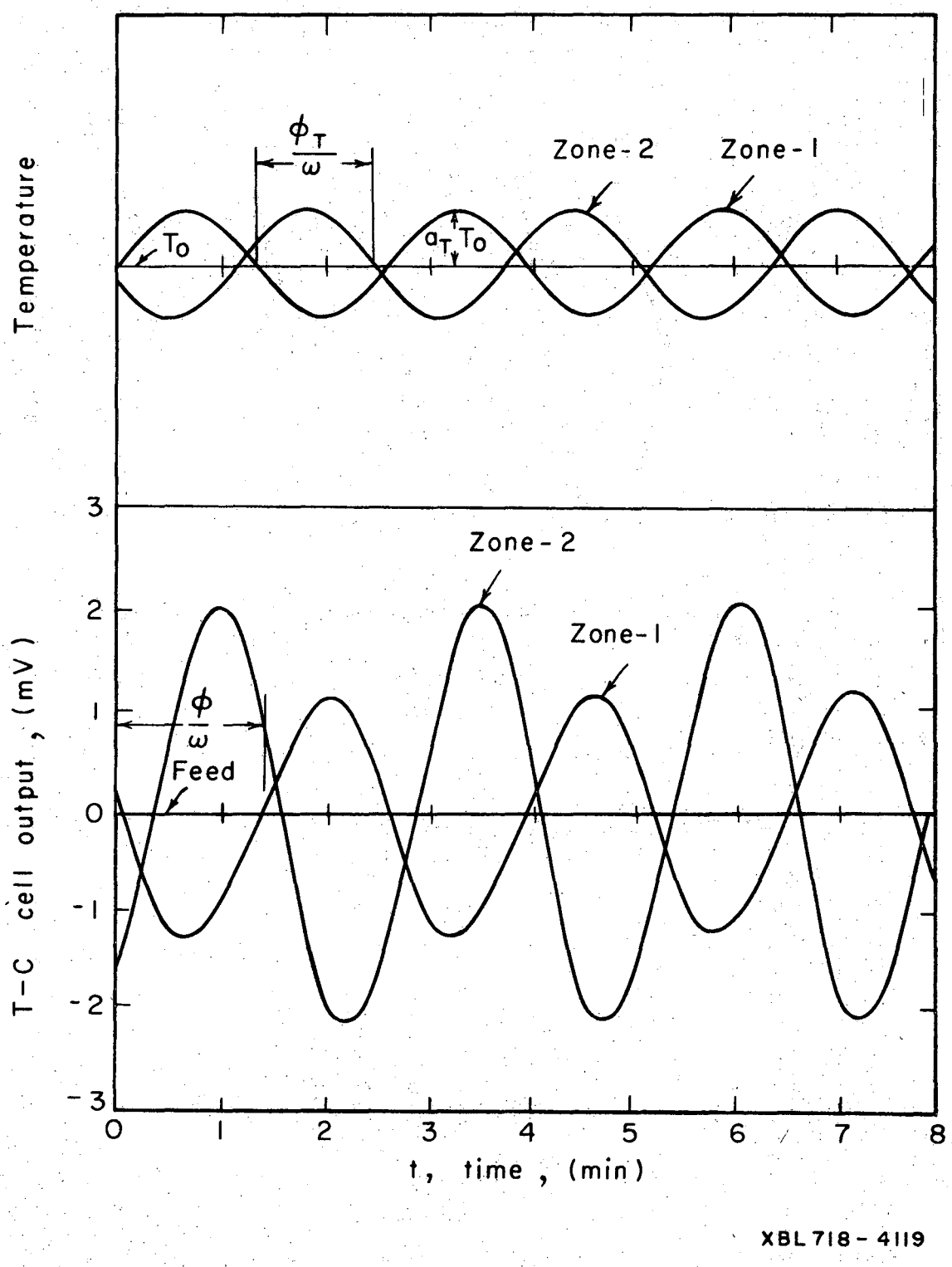

Figure 6-11. Experimental Temperature Inputs and T-C Cell Responses for Dual (identical) Zone System: Binary Feed.

The isotherm parameters, M_o and a_m, may be evaluated from the equilibrium distribution functions employing equations (3-78) and (3-81). Alternatively, the effective distribution coefficient, M_o, may be determined from the binary gas frequency response data as illustrated in Appendix A.

The temperature dependency of M_o can be approximated, in a manner analogous to that for the equilibrium distribution coefficient K_o, over moderate temperature ranges by:

$$M_o = A_m \exp(-\Delta H_m/RT) \tag{6-6}$$

where

ΔH_m = effective heat of adsorption for the binary mixture, cal/g-mole.

and

A_m = constant, g-moles/lb_{ads}.

Equation (6-6) is employed to interpolate various M_o values between those determined by the frequency response technique and are listed in Table 6-5. For small temperature changes, equation (6-6) may be linearized about T_o, yielding:

$$M_o(T) - M_o(T_o) = \frac{dM_o}{dT}\Big|_{T_o} \cdot (T - T_o) = M_o(T_o) \cdot \frac{(\Delta H_m)}{RT_o^2} (T - T_o)$$

or

$$M_o(T) = M_o(T_o) \left[1 + \frac{(\Delta H_m\, a_T)}{RT_o}\, e^{i\omega t}\right] \tag{6-7}$$

Table 6-5. Interpolated Effective Distribution Coefficients (50.2% CH_4, 49.8% CO_2 at 19.0 psia)

Temperature, °C.	M_o, g-moles/$lb_{ads.}$	$A_m \times 10^3$, g-moles/$lb_{ads.}$	$-\Delta_m/R \times 10^{-3}$, °K
*(37.6)	(0.567)		
46.1	0.502		
46.8	0.495	5.88	1.42
49.1	0.480		
*(60.5)	(0.415)		

*From frequency response data, Table A-4.

If equation (6-7) is assumed to be the forcing function being applied to equation (3-74), then it can be shown that the first order terms of the bracketed term in equation (3-74) are

$$y_{2f} X_1 - y_{1f} X_2 \cong M_o(T_o) Y_o + M_o\left(\frac{\Delta H_m a_T}{RT_o}\right) y_{1f} \qquad (6\text{-}8)$$

Hence, it can then be shown that

$$a_m \cong \frac{(\Delta H_m)}{RT_o} a_T \qquad (6\text{-}9)$$

The above approximation for a_m is not required when the equilibrium distribution functions, $F_1(y_1, y_2, T)$ and $F_2(y_1, y_2, T)$, are reasonably known, since a_m may then be calculated using equation (3-81).

The dimensionless separation factor, $(\mathcal{S}_{CH_4\text{-}CO_2})^{(1)}_m$, and its associated concentration-temperature phase lag, ϕ, versus the binary mixture's dimensionless frequency factor, $\mathcal{J}_m$, are plotted in Figure 6-12.

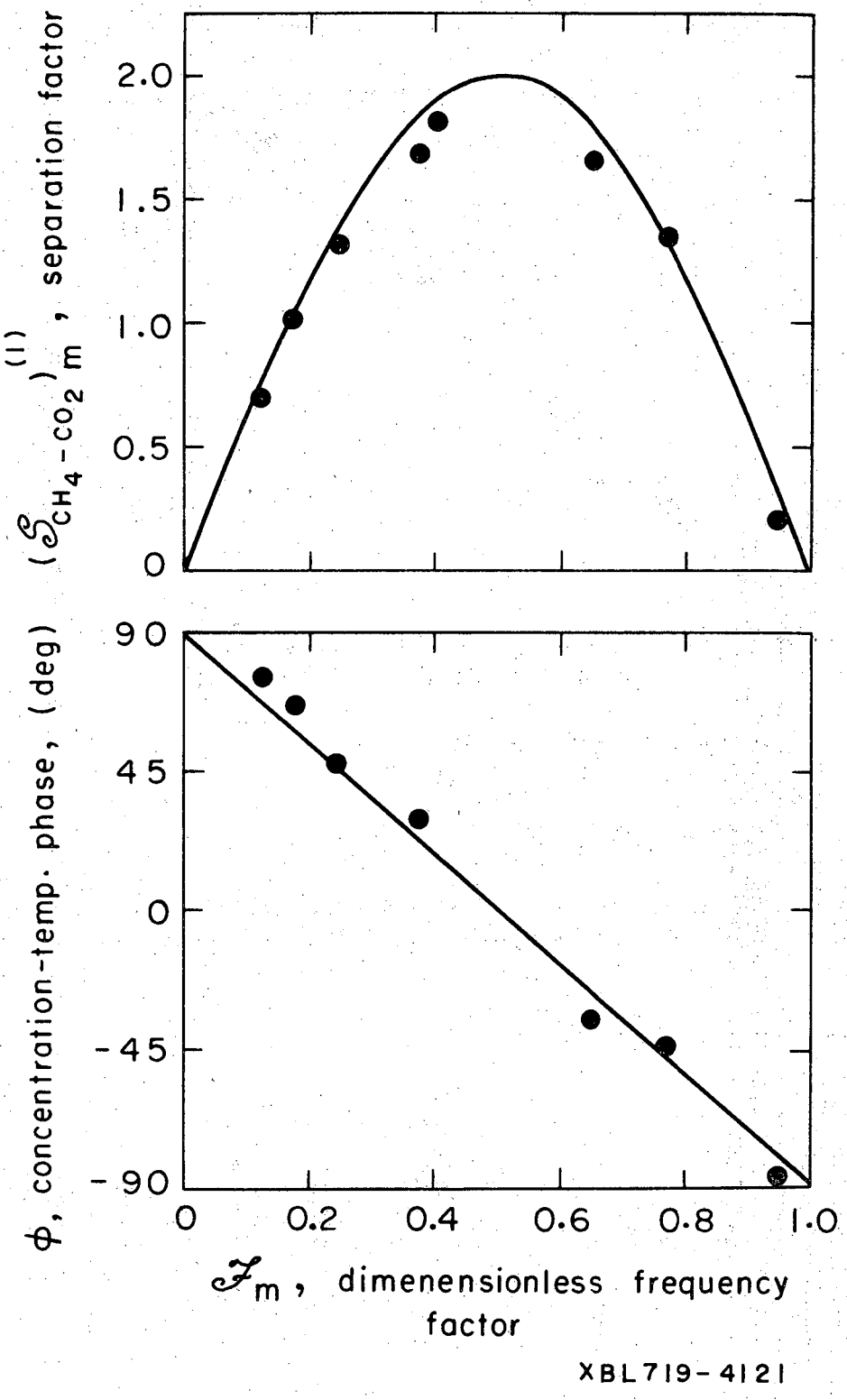

Figure 6-12. Dimensionless Separation Factor and Concentration-Temperature Phase for Single Zone System: Binary Feed.

The maximum separation factor of 2 occurs at $\mathcal{T}_m = 0.5$. At this point, the time of passage of the concentration wave is equal to one-half the cycle time, i.e.

$$L/v^* = (1 + \psi_m)(L/v) = \pi/\omega \qquad (6\text{-}10)$$

Dual Zone

The effluent of the first CZA unit, which is supplied with a constant feed mixture containing 50.2% CH_4 and 49.8% CO_2, is fed to an identical unit whose temperature is being oscillated at the same frequency but whose temperature phase difference is ϕ_T. The effluent of the second zone is split into enriched and depleted half-cycle portions to accomplish the separation.

The experimental dimensionless separation factors for the second zone versus the mixture dimensionless frequency factor, $\mathcal{T}_m$, holding the temperature phase constant ($\phi_T/2\pi = 0.5$), are presented in Figure 6-13. The optimum separation factor of 4 occurs at $\mathcal{T}_m = 0.5$. When the dimensionless frequency factor is held constant ($\mathcal{T}_m = 0.37$) and the temperature phase is varied, we find that the optimum separation occurs around $\phi_T/2\pi = 0.37$, as shown in Figure 6-14. This value is essentially identical to that predicted by equation (3-93).

Effect of Inert Carrier Gas Removal

A graphical comparison of the experimental separation factors for single zone operation for the following cases: (1) a 4.5% CH_4, 5.4% CO_2-He feed mixture, (2) a 4.5% CH_4, 5.4% CO_2-He feed mixture plus an ideal isothermal phase shifter, and (3) a 50.2% CH_4, 49.8% CO_2 binary feed mixture; is presented in Figure 6-15. The third of these may be achieved by removing the He carrier gas from the trace feed utilized in

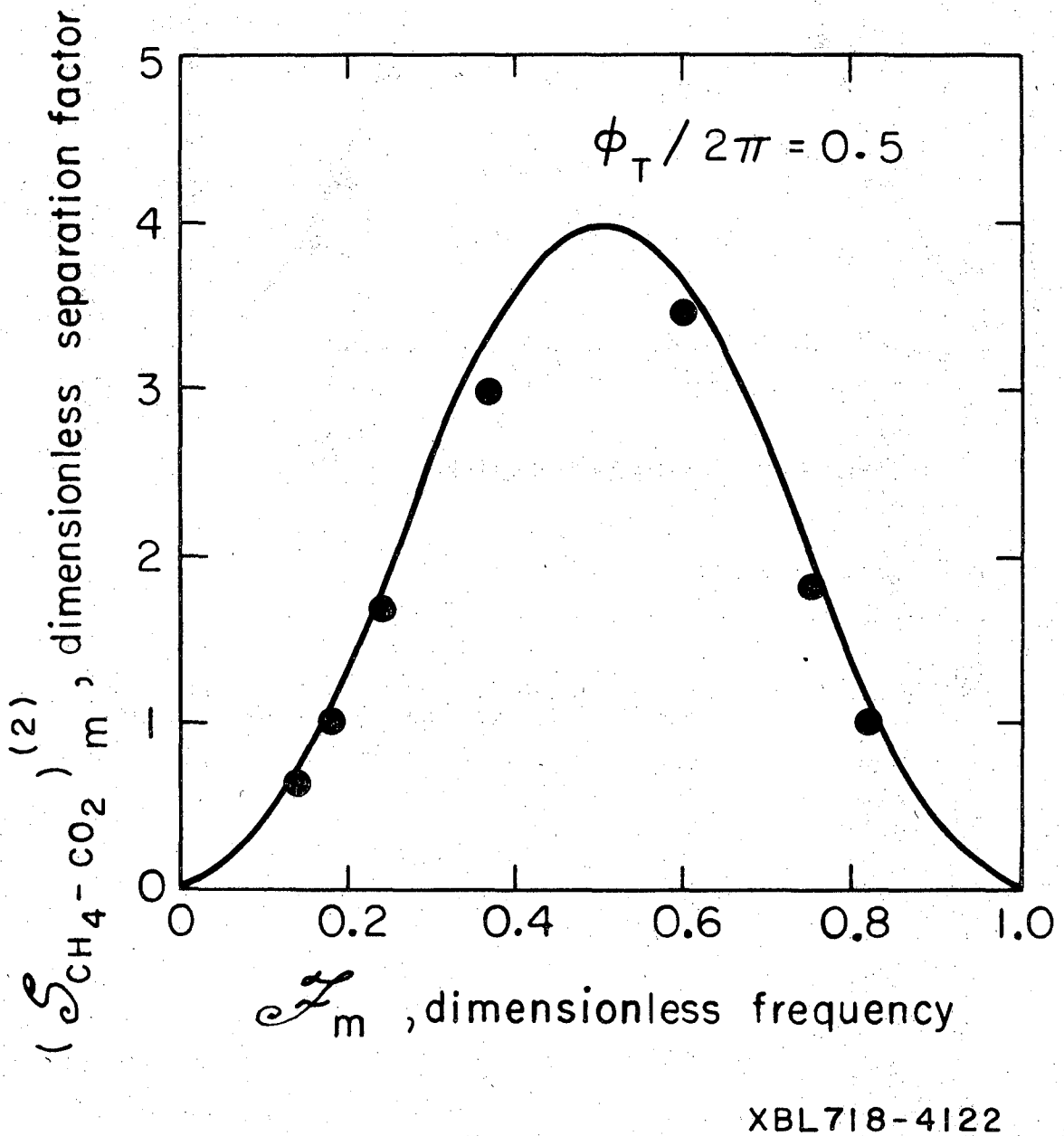

Figure 6-13. Dimensionless Separation Factor, constant Temperature Phase: Dual (identical) Zone-Binary Feed.

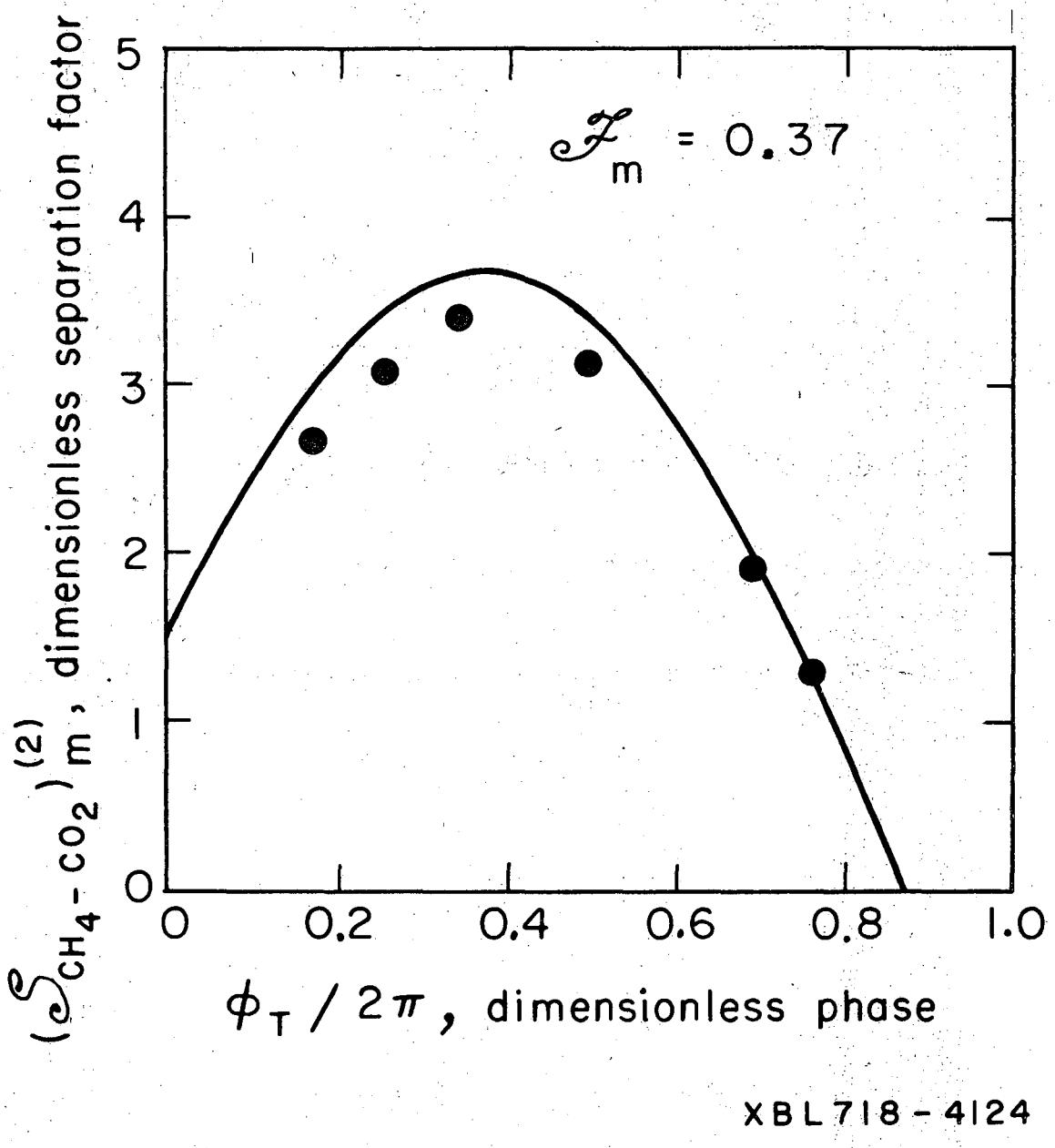

Figure 6-14. Separation Factor, constant Dimensionless Frequency Factor: Dual (identical) Zone-Binary Feed.

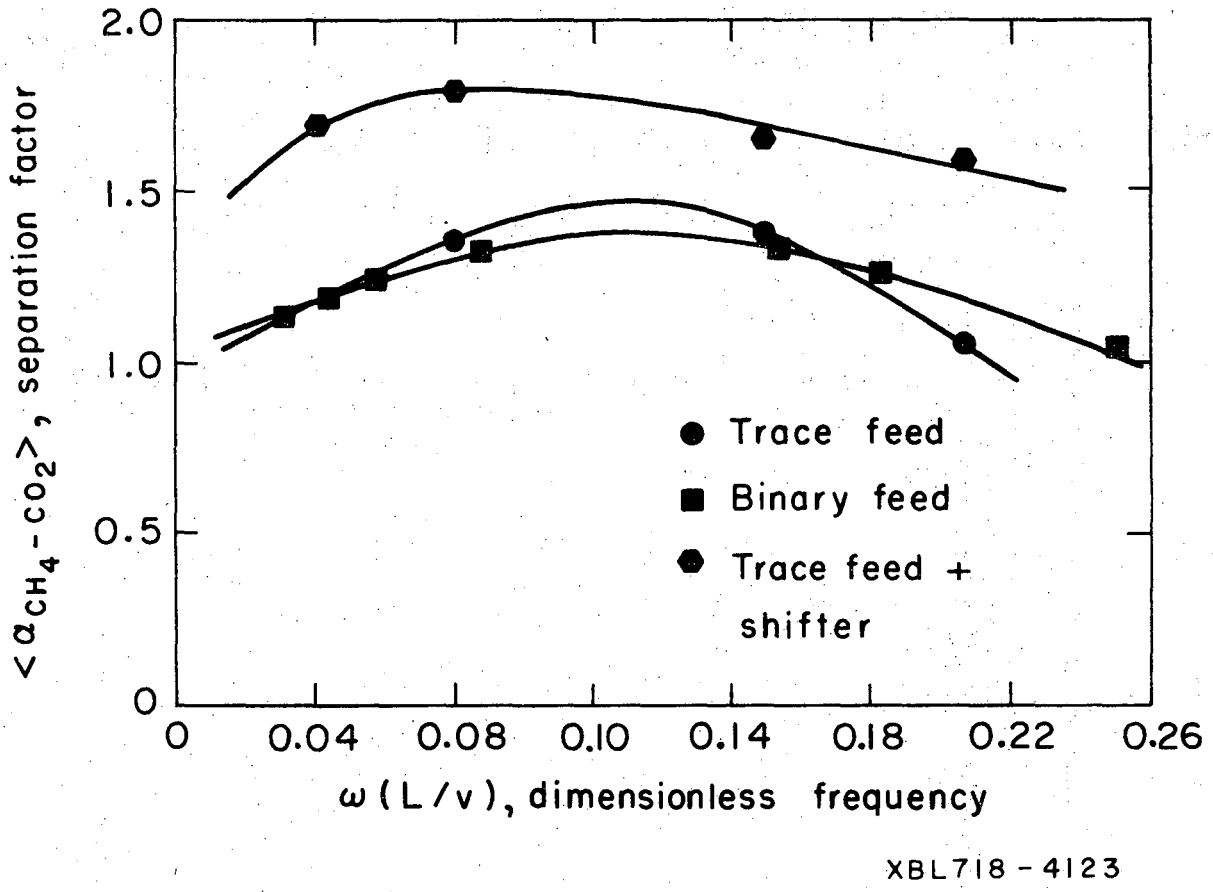

Figure 6-15. Comparison of Separation Factors Obtained from Trace and Binary Feeds: Single Zone.

case 1. It is apparent, for the CH_4-CO_2 - activated carbon system, that removal of the inert carrier gas from the trace feed does not significantly alter the achieved separation factors. In addition, the application of an isothermal shifter to a single CZA unit, supplied with a trace feed, greatly enhances the separation. It must be kept in mind that the above conclusions may not be valid in systems where the binary adsorbates interact significantly. When He is utilized as a feed diluent, it must be removed from the enriched and depleted portions, collected at the exit of a CZA system, and recycled.

Table 6-6. Single Zone, Binary System Experimental Data (50.2% CH_4, 49.8% CO_2 at 19.0 psia).

ω, rad/sec.	L/v. sec.	t_o, °C	M_o, g-moles/lb_{ads}	a_T	a_m	ϕ, degrees	$\langle \alpha_{CH_4-CO_2} \rangle_m^{(1)}$
	5.905					-87	1.037
	4.273					-44	1.256
	3.601					-35	1.320
	2.047					—	1.322
0.0424	2.220	49.1	0.480	0.0168	-0.0737	29	1.360
	1.353					47	1.240
	0.995					66	1.182
	0.708					75	1.129

W = 11.57 gm., L = 20.64 cm., ε = 0.403

Table 6-7. Dual Zone, Binary System Experimental Data (50.2% CH_4, 49.8% CO_2 at 19.0 psia)

ω, rad/sec.	L/v, sec.	t_o, °C	M_o, g-moles/lb_{ads}	a_T	a_m	$\phi_T/2\pi$	$\langle \alpha_{CH_4-CO_2} \rangle_m^{(2)}$
	4.182						1.220
	3.657						1.426
	2.850						1.785
0.0412	1.910	46.8	0.495	0.0189	-0.0835	0.503	1.732
	1.212						1.365
	0.915						1.219
	0.696						1.134
						0.167	1.564
						0.252	1.679
0.0411	1.878	46.1	0.502	0.0180	-0.0798	0.340	1.758
						0.491	1.704
						0.690	1.382
						0.760	1.242

For each zone: W = 11.60 gm., L = 20.00 cm., ε = 0.382

CHAPTER 7

CONCLUSIONS

The separation of gaseous mixtures utilizing the cycling zone adsorption process has been demonstrated theoretically and on a laboratory scale. Significant separations are predicted mathematically, using the linear equilibrium theory. Experimentally significant but not complete separations were obtained using systems which exhibited Langmuir isotherm behavior. The increase in separative power by using multiple zones in series was particularly evident, the temperature change in each zone being out of phase with those in the adjacent zones. The linear theory is obviously defective when the concentration oscillations become large. However, it provides an upper bound on the expected separations.

The main advantages of the cycling zone adsorption process, since it operates without flow reversal and therefore produces enriched and depleted products continuously, are that it requires no regenerative fluid or extreme treatment for regenerating the solid, and that it may not require a sweep fluid which has to be recovered and recycled as for continuously intermittent chromatography. Velocity oscillations, approaching flow reversal conditions, have been shown to neither help nor hinder the separative power.

Several process difficulties are evident. A small shift in the equilibrium isotherm for moderate temperature changes requires that several zones be utilized in series to produce significant separations. This means additional heat requirements. Internal reuse of heat is possible for liquid systems, by utilizing interstage heat regenerators as discussed by Baker (1969). However, the thermal requirements for a

gaseous system consist mainly of heating and cooling the solid adsorbent particles, resulting in reasonable thermal efficiencies (Appendix B).

The experimental results and the linearized predictions (Figure 3-2) indicate that finite mass transfer rates attenuate the separation from that predicted by the linear equilibrium theory. This means that for these intra-particle resistance-controlled systems one must operate at moderate frequencies or with fine particles, both of which restrict the fluid thru-put. The upper frequency limitation decreases significantly when the mass transfer resistances are large.

Axial dispersion (second-derivative, longitudinal diffusion terms) and dispersion caused by non-linear isotherms increase especially in the presence of steep concentration gradients. The encountered concentration gradients increase as one proceeds thru a series, multiple-zone CZA system. In the case of a non-linear isotherm where the concentration wave velocity is a function of the concentration, which produces higher velocity portions of the wave that overtake the slower portions before reaching the end of the bed, the amplitudes of both portions are diminished. A splitting and recycle arrangement may then be required to reduce these attenuations from the linear theory. In such a scheme as shown in Figure 1-7, when amplification of concentration waves by utilizing several zones in series results in significant deviations from the linear theory, the effluent of the multiple-zone system may then be collected in enriched and depleted portions. Each portion is then fed to a subsequent multiple-zone system whose effluent is split into product and recycle portions. The recycle portions are refed to the proper location within the processing system.

For the separation of "trace feeds", dilute concentrations of solutes in a non-adsorbing carrier, the operation of the CZA process is based on the separation of the two key components. A separation can be achieved whenever $\Lambda \neq 1$ for the keys. The optimum separation of the two key components depends upon their concentration wave velocity and distribution coefficient temperature sensitivity ratios. The separation can be significantly improved by addition of an isothermal zone of adsorbent particles at the end of a cycling zone adsorption process. The effect of the isothermal shifter bed, when designed properly, was to shift the two key components' concentration waves into the most favorable splitting position of 180° phase difference. For low mass transfer rates, the waves passing thru the isothermal bed may be significantly attenuated.

Upon removal of the inert carrier fluid from a two-solute trace feed, a binary adsorbing feed results. The separative power then depends upon the mixture's effective distribution coefficient, M_o, which may be determined by the frequency response method discussed in Appendix A. Separations are possible whenever $M_o > 0$. Using activated carbon as an adsorbent, for example, mixtures of CH_4 and CO_2 were separated utilizing a dual zone scheme to yield a separation factor of 1.8 at an interstitial gas velocity of 11 cm/sec. and a heat transfer requirement of approximately 6 kcal/mole of mixture by employing an input temperature amplitude of 6.4 °C. It was found that the separation factors achieved for the CH_4-CO_2 binary feed did not significantly differ from those obtained when the carrier gas, He, was present. Therefore, the sweep fluid may be removed, eliminating the necessity for recycling the carrier gas.

The experimental concentration-time responses contained harmonics, the maxima being more pointed than the minima, resulting from harmonics in the temperature input, isotherm non-linearities, and non-linearity of the distribution coefficient-temperature relationship. However, the harmonics were small since small experimental temperature variations were utilized. Their effects could be essentially removed by employing half-cycle averaged instead of peak concentration measurements for separation factor calculations. In the frequency response experiments, distortions in the input concentration wave are damped upon passage through the isothermal adsorbent bed, as discussed by Kramers and Alberda (1953).

The operation of a cycling zone adsorption process at higher frequencies, ω, causes particle-phase diffusion to have a greater attenuation effect on the separation but permits greater thru-put velocities, v, for the same column bed length (or smaller L for the same v, thus lower investment costs). Since the linearized theory establishes no limit on the thru-put velocity, a practical limit would be imposed by the heat requirements of the process. A reasonable limit would be the velocity at which the heat required for the flowing fluid becomes important relative to that required for heating the solid adsorbent (Appendix B). The velocity at which the flowing fluid heat requirement is 20% of the solid adsorbent heat requirement for the systems investigated was found to be approximately 300 cm/second. The frequency that may be applied at this thru-put, resulting in a 20% attenuation loss due to particle-phase diffusion, was estimated to be about 0.3 radian/second (2.8 cycles/min.). Of course, the transferral of heat throughout the bed at higher frequencies is more difficult and

would impose a physical limit on the employed frequency. Since particle-phase diffusion coefficients are smaller and fluid-phase heat capacities are larger for liquid systems, lower limiting values of frequency and thru-put velocity would be expected.

Most experiments in this study were run at low velocities, approaching the region where fluid-phase molecular diffusion becomes an important transport mechanism. Thus the estimated velocity and frequency limitations have not been experimentally tested although velocities and frequencies as large as 100 cm/sec. and 0.1 radians/sec. respectively were utilized.

In the design of the CZA bed, the pressure drop, radial heat transfer characteristics, fluid-flow distribution, and axial dispersion effects would be considered in the selection of its length and diameter.

In the cyclic frontal adsorption operation of parallel beds with switching feeds, a stripping fluid and heat are required to regenerate the adsorbent in one bed while the other is being saturated with feed. Because the front end of the adsorbent gets saturated and break-thru occurs as the concentration wave in the exit part of the bed begins to emerge, concentration gradients are large within the adsorption zone. That is, the adsorption zone occupies only a small segment of the bed at any fixed time.

Continuously intermittent (pulsed) chromatography requires very long beds and a sweep fluid whose velocity for optimum column efficiency is about 2-5 cm/second. Further velocity increases result in poorer separation efficiencies. Steep concentration gradients occur as peaks (bands) inside the bed, yet separation of trace solutes can be made nearly complete. Non-linear isotherms limit the injection size, which limits the processing capacity. However, no heat transfer is required.

In the CZA process, lower concentration gradients are encountered since the entire bed, which is very short, is utilized. Much greater thru-put velocities are allowable and no carrier fluid is required. The heat requirements are on the order of twice the regenerative heat required for frontal cyclic operation using an equivalent adsorption bed. Separations are not nearly complete and evaluation of a cascade, especially involving recycle, is difficult. However, for a mixture containing one adsorbable constituent, the required recovery not being very great, the CZA process can do a good job with only a series of zones without complicated recycle. Typical examples are the removal of CO_2 from air or N_2 and the desalination of sea water.

Certain other intensive variables which affect the equilibrium distribution coefficient, such as electric fields, magnetic fields, or pressure (for gaseous systems only) may be applied individually or in conjunction with a thermal field, in order to enhance the separative power of a specific system. Previous investigations and this study have been limited to thermally forced variations of the equilibrium distribution coefficient. However, for gaseous systems a reduction in pressure corresponds to lower equilibrium bed capacities since the gas-phase partial pressures are diminished. Both pressure reduction and temperature elevation have been used simultaneously for adsorbent regeneration in cyclic frontal adsorption processes in order to increase desorption rates and reduce pre-saturation levels. Therefore, the simultaneous use of temperature and pressure would result in larger variations in the equilibrium loading capacity of an adsorbent bed than that which would be accessible by each utilized individually.

In its present state, cycling zone adsorption is an attractive process which may be economically employed for intermediate scale separations of pharmaceutical, biological, and isotopic substances which now are separated chromatographically.

Future research on gas-solid systems could include the investigation of the use of synchronous combinations of intensive variables, such as temperature and pressure, to further enhance the separation. Economic comparisons with continuously intermittent chromatographic systems, such as those manufactured by the Abcor Company and discussed by Timmins et al. (1968, 1969), would be most interesting.

NOMENCLATURE

(Dimensionless unless specified)

A_c = cross-sectional area of empty column, cm^2.

A_m = solids-fluid effective equilibrium distribution parameter, g-moles adsorbate/lb adsorbent.

A_o = solids-fluid equilibrium distribution parameter, g-moles adsorbate/lb adsorbent.

A_s = amplitude of output response.

C = heat capacity, cal/g-mole-°K.

$\bar{C}$ = mean heat capacity, cal/g-mole-°K.

D_f = fluid phase molecular diffusivity, cm^2/sec.

D_K = Knudsen (micro-pore) diffusivity, cm^2/sec.

D_M = mass molecular diffusivity, cm^2/sec.

D_p = effective pore diffusion coefficient, cm^2/sec.

D_{pore} = macro-pore diffusion coefficient, cm^2/sec.

D_T = thermal molecular diffusivity, cm^2/sec.

D_z = fluid phase axial dispersion coefficient, cm^2/sec.

E_D = eddy axial dispersion, cm^2/sec.

F = $F(y_i, T)$, equilibrium distribution function, g-mole adsorbate/lb adsorbent.

ΔG = free energy change to accomplish separation, cal/g-mole of feed.

ΔH^o = enthalpy change from solute gas to adsorbed state at 25 °C, cal/g-mole.

ΔH_a = isoteric heat of adsorption, cal/g-mole.

ΔH_{ads} = differential heat of adsorption, cal/g-mole.

HTU = height of a transfer unit, cm.

K = equilibrium distribution coefficient, g-mole adsorbate/lb adsorbent.

K_i = Langmuir constants.

L = length of cycling zone bed, cm.

M_o = effective distribution coefficient for binary mixture, g-mole adsorbate/lb adsorbent.

M_w = molecular weight, gm/g-mole.

N = number of zones in series.

$Pe_f = \frac{\langle d_p \rangle v\varepsilon}{D_f}$, flow Péclet number.

$Pe_z = \frac{\langle d_p \rangle v\varepsilon}{D_z}$, axial dispersion Péclet number.

P = absolute pressure, psia.

Q = heat transfered per half-cycle, cal.

$\dot{Q}$ = heat flow, cal/sec.

Q_T = heat required per mole of feed to accomplish separation, cal/g-mole of feed.

R = gas constant, cal/g-mole-°K.

R' = average particle radius, cm.

S = surface area/unit mass of particles, cm^2/gm.

ΔS = entropy change of mixing, cal/g-mole-°C.

T = absolute temperature, °K.

V_c = volume of empty column, cm^3.

W = weight of solid adsorbent particles contained in the column, gm.

$Y = (y - y_f)/y_f$, dimensionless gas phase concentration.

$\langle Y \rangle$ = dimensionless half-cycle averaged concentration.

$Z = \omega(z/v)$, dimensionless frequency.

a = equilibrium coefficient amplitude response parameter.

a' = surface area/bed volume ratio, cm^{-1}.

a_T = temperature input amplitude parameter.

b = Langmuir isotherm parameter, g-moles adsorbate/lb adsorbent.

b' = velocity input amplitude parameter.

c = Langmuir isotherm parameter.

$\langle d_p \rangle$ = mean adsorbent particle diameter, cm.

h = enthalpy, cal/g-mole.

h' = heat transfer coefficient, cal/cm^2-sec-°K.

k_m = mass transfer coefficient, cm/sec.

k_p = overall particle phase mass transfer coefficient, cm^2/sec.

m = Langmuir equilibrium adsorbate loading capacity, g-moles adsorbate/lb adsorbent.

r = radial distance from center of particle, cm.

t = time, sec.

v = interstitial fluid velocity, cm/sec.

v^* = $v/(1 + \psi)$, concentration wave velocity, cm/sec.

x = solid-phase loading, g-moles adsorbate/lb adsorbent.

x^* = equilibrium solid-phase loading, g-moles adsorbate/lb adsorbent.

y = gas-phase concentration, mole fraction.

y^* = equilibrium gas-phase concentration, mole fraction.

$\langle y \rangle$ = half-cycle averaged concentration, mole fraction.

z = axial distance from column entrance, cm.

$\mathcal{A}$ = $\dfrac{Y_{max.}}{a\,\psi/(1 + \psi)}$, dimensionless response amplitude.

$\mathcal{F}$ = $\dfrac{(1 + \psi)\omega(L/v)}{2\pi}$, dimensionless frequency factor.

ℓ = molecular mean free path, Å.

ℓ_p = average pore diameter, Å.

$\mathcal{S}$ = $\dfrac{\ln \langle \alpha \rangle \ (\pi/4)}{a\,\psi/(1 + \psi)}$, dimensionless mean separation factor.

$\langle \alpha \rangle$ $= \langle y \rangle_R / \langle y \rangle_L$, mean separation factor.

β = switching location: lag between initial switching point where collection of the enriched half-cycle begins and the temperature input wave, radians.

β' = Freundlich isotherm parameter.

Γ $= \dfrac{\omega / k'_p a'_p}{1 + \psi}$, dimensionless mass transfer-capacity ratio.

γ $= \dfrac{(K_o \Delta H_a)_2}{\Lambda (K_o \Delta H_a)_1}$, equilibrium isotherm parameter for the two adsorbing specie (trace) system.

ε = interparticle void fraction.

ζ $= y_1/(1 - y_2)$, concentration ratio of component 1 to the component 2-free mixture.

θ = ωt, dimensionless time.

Λ $= \dfrac{1 + \psi_2}{1 + \psi_1} = \dfrac{v^*_1}{v^*_2}$, concentration wave velocity ratio.

ρ_s = adsorbent density, lb adsorbent/ft^3 of adsorbent.

ρ_f = fluid molar density, g-moles/ft^3 of fluid.

σ_c = molecular collision diameter, Å.

τ = tortuosity of adsorbent particle.

ϕ = phase angle, radians.

ϕ_c = phase difference between component effluent waves, radians.

ϕ_s = phase shift of concentration wave upon passage thru an isothermal shifter bed, radians.

ϕ_T = phase between temperature inputs for dual zone operation, radians.

ψ $= \dfrac{\rho_s (1 - \varepsilon) K_o}{\rho_f \varepsilon}$, solids-fluid equilibrium capacity ratio.

Ω $= \omega / k'_p a'_p$, dimensionless mass transfer resistance factor.

ω = frequency, radians/sec.

$\underline{\omega}$ = $\omega(L/v)$, dimensionless frequency.

χ = intraparticle void fraction.

Subscripts

a = solute (adsorbing specie).

ads = adsorbent or adsorption.

ap = apparent.

C = cold.

E = enriched half-cycle portion.

f = feed condition or fluid.

H = hot.

I = input.

i = component i.

L = lean half-cycle portion.

m = binary mixture.

n = inert carrier fluid.

o = average value or initial condition.

opt = optimum.

p = particle.

R = enriched half-cycle portion.

Rp = response.

s = solids or isothermal shifter.

w = wall.

1 = component 1.

2 = component 2.

12 = component 1 relative to component 2.

Superscripts

(N) = zone-N.

(1) = zone-1.

(2) = zone-2.

* = isothermal shifter bed or adsorbed state.

REFERENCES

Acrivos, A., Ind. Engr. Chem., 48, 703 (1956).

Adamson, A. W., Physical Chemistry of Surfaces, 398 (Interscience, New York, 1967).

Alexis, R. W., Chem. Engr. Progr., 63, No. 5, 69 (1967).

Amundson, N. R. and Aris, R., Proc. Roy. Soc. (London), A286, 129 (1965).

Aris, R., Ind. Engr. Chem. Fundamentals, 8, 603 (1969).

Baddour, R. F., U. S. Patent #3,250,058 (1966).

Baker, B. III, Ph.D. Dissertation, Univ. of Calif., Berkeley (1969).

Baker, B. III and Pigford, R. L., Ind. Engr. Chem. Fundamentals, 10, 285 (1971).

Bohrer, B. B., U. S. Patent #3,233,748 (1965).

Bond, G. C., Catalysis by Metals, 71 (Academic Press, New York, 1962).

Deisler, P. F. and Wilhelm, R. H., Ind. Engr. Chem., 45, 1219 (1953).

DeVault, D., J. Am. Chem. Soc., 65, 532 (1943).

Fuller, E. N., Schettler, P. D. and Giddings, J. C., Ind. Engr. Chem., 58, 19 (1966).

Glueckauf, E., Trans. Faraday Soc., 51, 34 (1955).

----------, Ibid., 60, 729 (1964).

Grant, R. J., Manes, M. and Smith, S. B., AIChE Journal, 8, 403 (1962).

Hall, K. R., Eagleton, L. C., Acrivos, A. and Vermeulen, T., Ind. Engr. Chem. Fundamentals, 5, 212 (1966).

Himmelblau, D. M. and Bischoff, K. B., Process Analysis and Simulation, 28 (John Wiley & Sons, New York, 1968).

Hirschfelder, J. O., Bird, R. B. and Spotz, E. L., Chem. Rev., 44, 205 (1949).

Holsen, J. N. and Strunk, M. R., Ind. Engr. Chem. Fundamentals, 2, 143 (1964).

Horn, F. J. and Lin, C. H., J. Phys. Chem. (German), 73, 575 (1969).

Hyun-Kee, R. and Amundson, N. R., Ind. Engr. Chem. Fundamentals, 9, 303 (1970).

Jencewski, T. J. and Myers, A. L., AIChE Journal, 14, 509 (1968).

Kramers, H. and Alberda, G., Chem. Engr. Sci., 2, 173 (1953).

Kehde, H., Chem. Engr. Progr., 44, 575 (1948).

Lapidus, L. and Amundson, N. R., J. Phys. Chem., 56, 984 (1952).

Lawson, A. E. and Miller, J. M., J. Gas Chromatography, 4, 273 (1966).

McNair, H. M. and Bonelli, E. J., Basic Gas Chromatography, 35 (Consolidated Printers, California, 1968).

Meredith, J. M. and Plank, C. A., J. Chem. & Engr. Data, 12, 259 (1967).

Meyer, O. A., Ph.D. Dissertation, State University of New York, Buffalo, 82 (1966).

Myers, A. L., Ind. Engr. Chem., 60, 45 (1968).

Petersen, E. E., Chemical Reaction Analysis, 116 (Prentice-Hall, New Jersey, 1965).

Pigford, R. L., Baker, B. III and Blum, D. E., Ind. Engr. Chem. Fundamentals, 8, 144 (1969a).

----------, Ibid., 604 (1969b).

----------, Ibid., 848 (1969c).

Pigford, R. L., Baker, B. III and Blum, D. E., Cycling Zone Adsorption Process, U. S. Patent #3,542,525 (Nov. 1970).

Rolke, R. W. and Wilhelm, R. H., Ind. Engr. Chem. Fundamentals, 8, 235 (1969).

Ryan, J. M., Timmins, R. S. and O'Donnell, J. F., Chem. Engr. Progr., 64, 53 (1968).

Skarstrom, C. W., Ann. New York Academy of Sciences, 72, 760 (1959).

Sweed, N. H. and Wilhelm, R. H., Ind. Engr. Chem. Fundamentals, 8, 221 (1969).

Timmins, R. S., Mir, L. and Ryan, J. M., Chem. Engr., 170 (1969).

Van Ness, H. C., Ind. Engr. Chem. Fundamentals, 8, 464 (1969).

Vermeulen, T., Adsorption and Ion Exchange, 4th Ed. Perry's Chemical Engineering Handbook, 16-15 (McGraw-Hill, New York, 1963).

Vermeulen, T., Private Communication (1970).

Weiss, D. E., Royal Australian Chem. Inst. Procd., 32, 287 (1965).

Weiss, P. B., Z. Physik. Chem. (German), 11, 1 (1957).

Wilhelm, R. H., Rice, A. W. and Bendelius, A. R., Ind. Engr. Chem. Fundamentals, 5, 141 (1966).

Wilhelm, R. H. and Sweed, N. H., Science, 159, 522 (1968a).

Wilhelm, R. H., Rice, A. W., Rolke, R. W. and Sweed, N. H., Ind. Engr. Chem. Fundamentals, 7, 337 (1968b).

Wunder, J. W. J., Oil and Gas Journal, 137 (1962).

APPENDIX A

DETERMINATION OF EQUILIBRIUM DISTRIBUTION COEFFICIENTS BY FREQUENCY RESPONSE TECHNIQUES

By applying a sinusoidal concentration disturbance in the inlet feed to an adsorbent bed, the measurement of the amplitude attenuation and the phase shift between input and output signals yield information about the distribution coefficients and mass transfer parameters for a given fluid-solid system. For small input amplitudes, a linear system response is approached where the dynamic behavior is independent of the input amplitude, as discussed by Kramers and Alberda (1953).

The following assumptions are made in the following analysis:

1) Linear system dynamics
2) No radial concentration or velocity gradients
3) Constancy of temperature and pressure
4) Dispersive effects owing to longitudinal mixing or diffusion are unimportant

SINGLE ADSORBING SPECIE

A single adsorbing specie within a non-adsorbing carrier gas is termed a single adsorbing specie system. Its equilibrium adsorption is governed by its gas phase concentration.

Local Equilibrium

First we assume that axial diffusion and pore diffusion are unimportant, and that the fluid and solid are in equilibrium.

Conservation of matter within a differential segment of the packed bed at some distance, z, from the entrance of the bed yields:

$$\frac{\partial y}{\partial t} + v \frac{\partial y}{\partial z} + \frac{\rho_s (1 - \varepsilon)}{\rho_f \varepsilon} - \frac{\partial x}{\partial t} = 0 \qquad \text{(A-1)}$$

The solid-fluid equilibrium relationship is

$$x = F(y)$$

For a sinusoidal concentration input at the entrance of the bed:

$$y(0,t) = y_f(1 + a\, e^{i\omega t}) \tag{A-2}$$

For small changes in y:

$$x - x_f = \frac{dF}{dy}\Big|_{y_f} \cdot (y - y_f) \tag{A-3}$$

For linear system dynamics, the responses may be written in the form:

$$y(z,t) = y_f + Y_1(z)\, a e^{i\omega t} \tag{A-4}$$

$$x(z,t) = x_f + X_1(z)\, a e^{i\omega t} \tag{A-5}$$

Substitution of the above equations into equation (A-3) leads to the definition of the equilibrium distribution coefficient:

$$K_o = \frac{X_1(z)}{Y_1(z)} = \frac{dF}{dy}\Big|_{y_f} \tag{A-6}$$

Substitution of the equations (A-4), (A-5), and (A-6) into equation (A-1) gives

$$\left[1 + \frac{\rho_s(1 - \varepsilon)}{\rho_f\, \varepsilon}\, K_o\right] Y_1 + \frac{v}{i\omega}\, \frac{dY_1}{dz} = 0 \tag{A-7}$$

The solids-fluid capacity ratio is defined as:

$$\psi = \frac{\rho_s(1 - \varepsilon)}{\rho_f\, \varepsilon}\, K_o$$

The inlet condition requires that:

$$Y_1(0) = y_f$$

The solution of equation (A-7), obtained by applying an integration factor, is

$$Y_1(z) = y_f \exp[-(1 + \psi)\frac{i\omega z}{v}]$$

The response then has the form:

$$Y(z,t) = y(z,t) - y_f = y_f \exp[-(1 + \psi)\frac{i\omega z}{v}]\ a\ e^{i\omega t}$$

$$= A\ e^{-i\phi}\ e^{i\omega t} \qquad \text{(A-8)}$$

where

$$A = y_f a, \text{ the input amplitude}$$

$$\phi = (1 + \psi)\ \omega(z/v), \text{ the phase lag} \qquad \text{(A-9)}$$

Therefore a plot of ϕ versus ω gives a straight line passing thru the origin with a slope of $(1 + \psi)(z/v)$. From the slope, the equilibrium distribution coefficient may be determined:

$$K_o = \frac{[\text{slope}/(z/v)] - 1}{\frac{\rho_s(1 - \varepsilon)}{\rho_f\ \varepsilon}} \qquad \text{(A-10)}$$

We note that there is no amplitude attenuation for the local equilibrium situation.

Local Equilibrium with Pore Diffusion

Wilhelm and Deisler (1953) investigated the non-adsorbing, frequency-response situation including both axial diffusion and pore diffusion. They showed that pore diffusion produces a significantly stronger effect on the phase lag than that of axial diffusion. On this basis, we include the pore diffusion effect in the differential material balance, which gives:

$$\frac{\partial y}{\partial t} + \frac{(1 - \varepsilon)}{\varepsilon} \left[\chi \frac{\partial \langle y_p \rangle}{\partial t} + \frac{\rho_s}{\rho_f \varepsilon} \frac{\partial \langle x \rangle}{\partial t} \right] + v \frac{\partial y}{\partial z} = 0 \qquad \text{(A-11)}$$

where:

$\langle y_p \rangle$ = average concentration in the fluid inside the particle, mole fraction.

$\langle x \rangle$ = average loading on solid surface, g-moles/lb_{ads}.

χ = intraparticle void fraction

Thus

$$\langle y_p \rangle = \frac{3}{R'^3} \int_0^{R'} y_p(r,z,t)\, r^2\, dr \qquad \text{(A-12)}$$

and

$$\langle x \rangle = \frac{3}{R'^3} \int_0^{R'} x(r,z,t)\, r^2\, dr \qquad \text{(A-13)}$$

where

R' = average particle radius.

From the equilibrium relationship,

$$x = F(y_p)$$

small changes in y give:

$$\langle x \rangle - \langle x_f \rangle = \frac{dF}{dy}\Big|_{y_f} \cdot (\langle y_p \rangle - y_f) \qquad \text{(A-14)}$$

The assumed solution responses for linear dynamics are

$$y(z,t) = y_f + Y_1(z)\, a e^{i\omega t}$$

$$\langle y_p(z,t) \rangle = y_f + \langle Y_1(z) \rangle\, a e^{i\omega t} \qquad \text{(A-15)}$$

$$\langle x \rangle = x_f + \langle X_1(z) \rangle\, a e^{i\omega t}$$

The equilibrium distribution coefficient is then defined as:

$$K_o = \frac{dF}{dy}\Big|_{y_f} = \frac{\langle X_1(z) \rangle}{\langle Y_1(z) \rangle} \qquad \text{(A-16)}$$

Substitution of equations (A-15) and (A-16) into equation (A-11) gives:

$$Y_1 + \frac{(1-\varepsilon)}{\varepsilon}\left[\chi + \frac{\rho_s}{\rho_f \varepsilon} K_o\right] \langle Y_1 \rangle + \frac{v}{i\omega} \frac{dY_1}{dz} = 0 \qquad \text{(A-17)}$$

with the boundary condition:

$$y(0,t) = y_f(1 + a\, e^{i\omega t})$$

The material balance on the solid particle of radius R' is

$$D_p \frac{\chi}{r^2} \frac{\partial}{\partial r}\left(r^2 \frac{\partial y_p}{\partial r}\right) = \frac{\partial}{\partial t}\left[\chi\, y_p + \frac{\rho_s}{\rho_f} x\right] \qquad \text{(A-18)}$$

where

D_p = pore diffusion coefficient, $cm^2/sec.$

Since the assumption of local equilibrium at each point along a pore implies that $x(r) = K_o\, y_p(r)$, rearrangement of equation (A-18) gives

$$\frac{1}{1 + \frac{\rho_s}{\chi\, \rho_f} K_o} \frac{D_p}{r^2} \frac{\partial}{\partial r}\left(r^2 \frac{\partial y_p}{\partial r}\right) = \frac{\partial y_p}{\partial t} \qquad \text{(A-19)}$$

with the boundary conditions on y_p:

$$y_p(R',t) = y(z,t)$$

$$\frac{\partial y_p(0,t)}{\partial r} = 0$$

For the assumed solution forms:

$$y(z,t) = y_f + Y_1(z)\, ae^{i\omega t}$$

$$y_p(r,z,t) = y_f + Z_1(r,z)\, ae^{i\omega t} \qquad \text{(A-20)}$$

the boundary conditions become

$$Y_1(0) = y_f$$

$$Z_1(R',z) = Y_1(z)$$

$$\frac{\partial Z_1(0,z)}{\partial r} = 0$$

Substitution of the assumed solution forms, equation (A-20), into equation (A-19) gives

$$D_p^* \frac{1}{r^2} \frac{d}{dr}\left(r^2 \frac{dZ_1}{dr}\right) = i\omega Z_1 \qquad \text{(A-21)}$$

where

$$D_p^* = \frac{D_p}{1 + \frac{\rho_s}{\chi \rho_f} K_o}$$

The solution of equation (A-21) is obtained by setting $Z_1 = W(r)/r$, which puts it into the form:

$$\frac{d^2W}{dr^2} = \frac{i\omega}{D_p^*} W$$

the solution of which, is

$$Z_1(r,z) = \frac{A \sinh(r\sqrt{i\omega/D_p^*})}{r}$$

When A is evaluated from the boundary condition at $r = R'$, we obtain

$$Z_1(r,z) = Y_1(z)\ \frac{R'}{r}\ \frac{\sinh(r\sqrt{i\omega/D_p^*})}{\sinh(R'\sqrt{i\omega/D_p^*})} \qquad \text{(A-22)}$$

Averaging over the particle, yields:

$$\langle Z_1(r,z) \rangle = 3\ Y_1(z) \int_0^1 \xi\ \frac{\sinh(\xi\sqrt{i\omega R'^2/D_p^*})}{\sinh(\sqrt{i\omega R'^2/D_p^*})}\ d\xi$$

$$= Y_1(z)\ G(\omega R'^2/D_p^*) \qquad \text{(A-23)}$$

where

$$\xi = R'/a$$

and

$$G(\omega R'^2/D_p^*) = \frac{3\ D_p^*}{i\omega\ R'^2} \left\{ \frac{\sqrt{i\omega R'^2/D_p^*}\ \cosh\sqrt{i\omega R'^2/D_p^*} - \sinh\sqrt{i\omega R'^2/D_p^*}}{\sinh\sqrt{i\omega R'^2/D_p^*}} \right\} \qquad \text{(A-24)}$$

Substitution of equation (A-23) into equation (A-17) gives

$$Y_1 + \frac{(1-\varepsilon)}{\varepsilon}\left[\chi + \frac{\rho_s}{\rho_f} K_o\right] Y_1 \cdot G(\omega R'^2/D_p^*) + \frac{v}{i\omega}\ \frac{dY_1}{dz} = 0$$

the solution of which is

$$Y_1(z) = B \exp\left\{ -\left[1 + \frac{(1-\varepsilon)}{\varepsilon}\left[\chi + \frac{\rho_s}{\rho_f} K_o\right]\ G(\omega R'^2/D_p^*)\right]\ \frac{i\omega z}{v} \right\} \qquad \text{(A-25)}$$

From the boundary condition at $z = 0$, $Y_1(0) = B = y_f$. Splitting $G(\omega R^2/D_p^*)$ into its real, G_{Re}, and imaginary, G_{Im}, parts, the response is of the form:

$$Y_1(z) = A(\omega) \exp[-i\phi(\omega)]$$

where the output amplitude is

$$A(\omega) = y_f \exp\left(\left[1 + \left\{ \frac{(1-\varepsilon)\chi}{\varepsilon} + \psi \right\} G_{Im} \right] \frac{\omega z}{v} \right) \qquad \text{(A-26)}$$

and the phase lag is

$$\phi(\omega) = \left\{ 1 + \left[\frac{(1-\varepsilon)\chi}{\varepsilon} + \psi \right] G_{Re} \right\} \left(\frac{\omega z}{v} \right) \qquad \text{(A-27)}$$

After considerable algebraic manulipulation, we obtain the following approximations, valid for small values of $\omega R'^2/D_p^*$:

$$G_{Re} \cong 1 - \frac{2}{315} \left(\frac{\omega R'^2}{D_p} \right)^2 (1+\psi)^2$$

$$G_{Im} \cong \frac{-6 \left(\frac{\omega R'^2}{D_p} (1+\psi) \right)}{\left[\frac{\omega R'^2}{D_p} (1+\psi) \right]^2 + 90}$$

Therefore, the phase shift is

$$\frac{\phi(\omega)}{\omega(z/v)} - 1 = \left[\frac{(1-\varepsilon)\chi}{\varepsilon} + \psi \right] \cdot \left[1 - \frac{2}{315} (1+\psi)^2 \left(\frac{\omega R'^2}{D_p} \right)^2 \right] \qquad \text{(A-27a)}$$

Thus, plotting $\phi(\omega)/\omega(z/v) - 1$ versus ω^2 should give a straight line with

$$\text{intercept: } \frac{(1-\varepsilon)\chi}{\varepsilon} + \psi \quad , \quad \text{at } \omega^2 = 0$$

and

$$\text{slope} = -\frac{2}{315}\,(\text{intercept})\,(1+\psi)^2\,(R'^2/D_p)^2$$

The equilibrium distribution coefficient, K_o, may then be determined from the intercept:

$$K_o = \frac{\text{intercept} - \dfrac{(1-\varepsilon)\chi}{\varepsilon}}{\dfrac{\rho_s(1-\varepsilon)}{\rho_f\,\varepsilon}} \qquad \text{(A-28)}$$

and the effective pore diffusion coefficient, D_p, from the slope:

$$D_p = \sqrt{\frac{-\dfrac{2}{315}\,(\text{intercept})\,(1+\psi)^2\,R'^4}{\text{slope}}} \qquad \text{(A-29)}$$

The amplitude ratio is:

$$\frac{\mathcal{A}_{\text{out}}}{\mathcal{A}_{\text{in}}} = \exp\left\{\left(\frac{(1-\varepsilon)}{\varepsilon}\chi + \psi\right)\left[\frac{-6(\omega R'^2/D_p^*)}{\left(\dfrac{\omega R'^2}{D_p^*}\right)^2 + 90}\right]\left(\frac{\omega z}{v}\right)\right\} \qquad \text{(A-30)}$$

Experimental Results

A constant-composition feed is fed to the top zone, as shown in the schematic diagram of the experimental apparatus, Figure 4-3. The temperature of the zone is oscillated sinusoidally. The first zone then serves as the concentration wave generator. The sinusoidal oscillating composition effluent of the cycling zone is fed to the second zone, which is held at constant temperature and pressure. Each zone contained 12-30 mesh Pittsburgh BPL activated carbon. The phase shift of the

second zone's output concentration wave and its average separation factor, $\langle \alpha \rangle$, are measured. For linear behavior the ratio of output separation factor to input separation factor is unity.

The flow velocity was held constant, while the input frequency was varied over the approximate range of 0.02 to 0.10 radians per second. The experimental frequency data are tabulated in Table A-3.

Methane-Helium System. A 3.1 mole % CH_4-He yielded the results shown in Figure A-1. In Figure A-1a, the phase shift and amplitude ratio values are plotted. It was found that the amplitude loss was less than 10% over the investigated frequency range and that the phase shift was proportional to frequency. This indicates that mass transfer effects were small and, in addition, that the effect of pore diffusion on the phase shift, represented by the squared factor in equation (A-27a), is small. The least squares determined slope of the phase shift, using equation (A-10), yielded $K_o = 0.483$ g-moles/lb_{ads}. Taking into account the pore diffusion effect following equations (A-28) and (A-29), the values obtained were: $K_o = 0.490$ g-moles/lb_{ads} and $D_p = 3.2 \times 10^{-3}$ cm^2/sec. The correction for the pore diffusion effect amounted to only 2%. Figure A-1b indicates that at low frequencies, the pore diffusion correction will be significantly smaller. This suggests that correction can be neglected for data taken in the lower frequency range.

An alternative procedure is to determine the phase shift by holding the frequency constant at a value less than 6×10^{-2} radians/sec., and varying the fluid velocity, v. A plot of ϕ versus L/v should be linear, with a slope, derived from equation (A-9), of

$$\text{slope} = (1 + \psi)\,\omega \qquad \text{(A-31)}$$

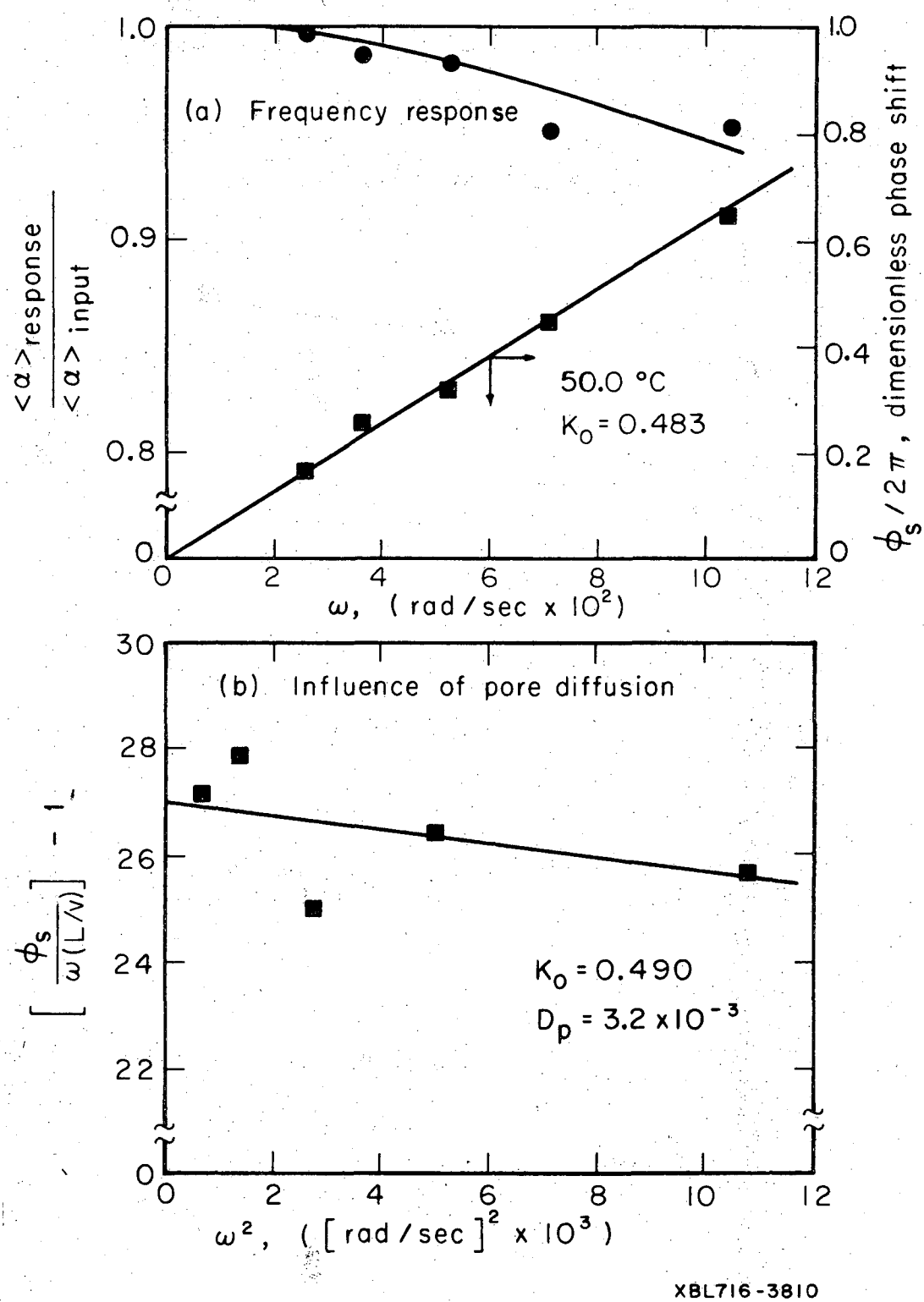

Figure A-1. Frequency Response: 3.1% CH_4-He on Pittsburgh BPL Activated Carbon at 19 psia.

Utilizing a 3.1 mole % CH_4-He mixture, the response of an isothermal bed, whose input frequency was 0.053 radians/sec., was determined over the velocity range of 6.5 to 103 cm/sec. The phase shift results plotted in Figure A-2, yield K_o = 0.502 g-moles/lb_{ads}. This compares very favorably with those previously determined.

A comparison with the distribution coefficient interpolated from the data of Grant and Manes (1962) is listed in Table A-1. Grant and Manes' data were fitted to the Langmuir form as discussed in Chapter 4. The distribution coefficient is then:

$$K_o = \frac{dx}{dy}\Big|_{y_f} = \frac{1}{(1 + c\, y_f)^2} \qquad \text{(A-32)}$$

Grant and Manes used a 4-10 mesh BPL Activated carbon, which is now obsolete. It had lower surface area and higher ash content than the carbon used in this study. It would be expected that the two carbons should have similar heats of adsorption, and that their difference is essentially in their adsorptive capacities. Therefore, the slope, $-\Delta H_a/R$, of the CH_4-He system's distribution coefficient function, shown in Figure A-5, was set equal to 2200 $°K^{-1}$, the value obtained from Grant and Manes' data.

Table A-1. Equilibrium Distribution Coefficients at 50 °C (3.1% CH_4-He)

	K_o, g-moles/lb_{ads}
Grant & Manes (1962)	0.43
This study*	0.49 ± 0.01

*Used to interpret CZA data.

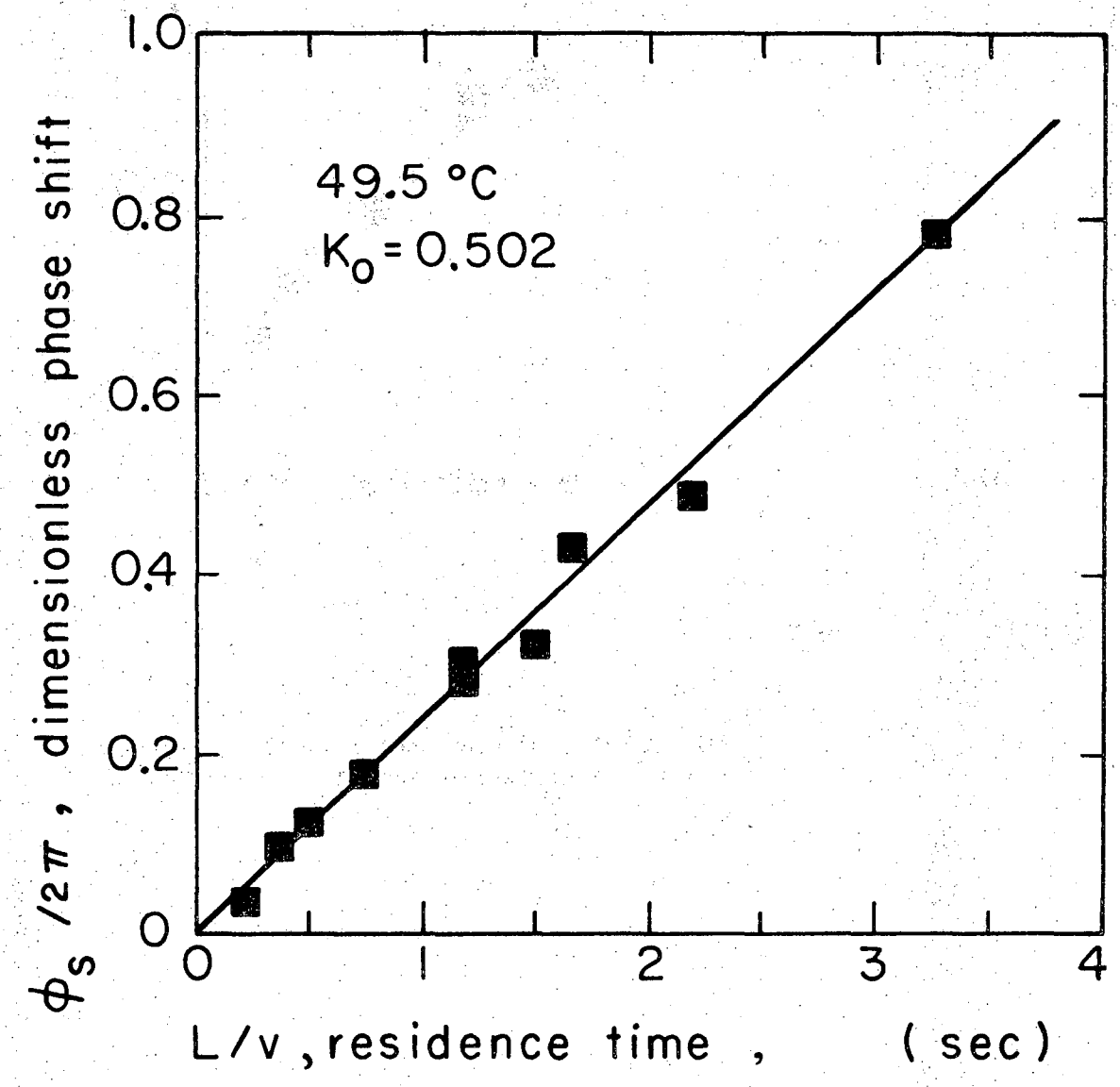

Figure A-2. Velocity Response (ω = 0.053 rad/sec.): 3.1% CH_4-He on Pittsburgh BPL Activated Carbon at 19 psia.

Carbon Dioxide-Helium System. A 4.9 mole% CO_2-He mixture was used for frequency response experiments. The results are shown in Figure A-3a. The pore diffusion effect, as shown in Figure A-3b, required a correction of the distribution coefficient of about 9%. Results from the alternative method, shown in Figure A-4, were taken at:

$$\omega = 0.055 \text{ radians/sec.}$$

$$5.7 \leq v \leq 69 \quad , \quad \text{cm/sec.}$$

The distribution coefficients, corrected for pore diffusion effect, are plotted versus 1/T in Figure A-5. The slope of which gives a $-\Delta H_a/R$ value of 2.3×10^3 $^\circ K^{-1}$. A comparison to those values obtained by interpolation of data reported by Meredith and Plank (1967) is listed in Table A-2. The distribution coefficients determined in this study were at low adsorbate partial pressures (0.5 - 1.0 psia), a region in which it is difficult to obtain accurate determination of adsorbate loading by the static balance method employed by Meredith and Plank (1967).

Table A-2. Equilibrium Distribution Coefficients (4.9% CO_2-He)

	K_o, g-moles/lb_{ads}			$-\Delta H_a/R \times 10^{-3}$, $^\circ K^{-1}$
Temperature, °C	38.9	49.5	61.2	
Meredith & Plank (1967)	1.48	1.16	0.95	2.0
This study*	1.42	1.11	0.87	2.3

*Used to interpret CZA data.

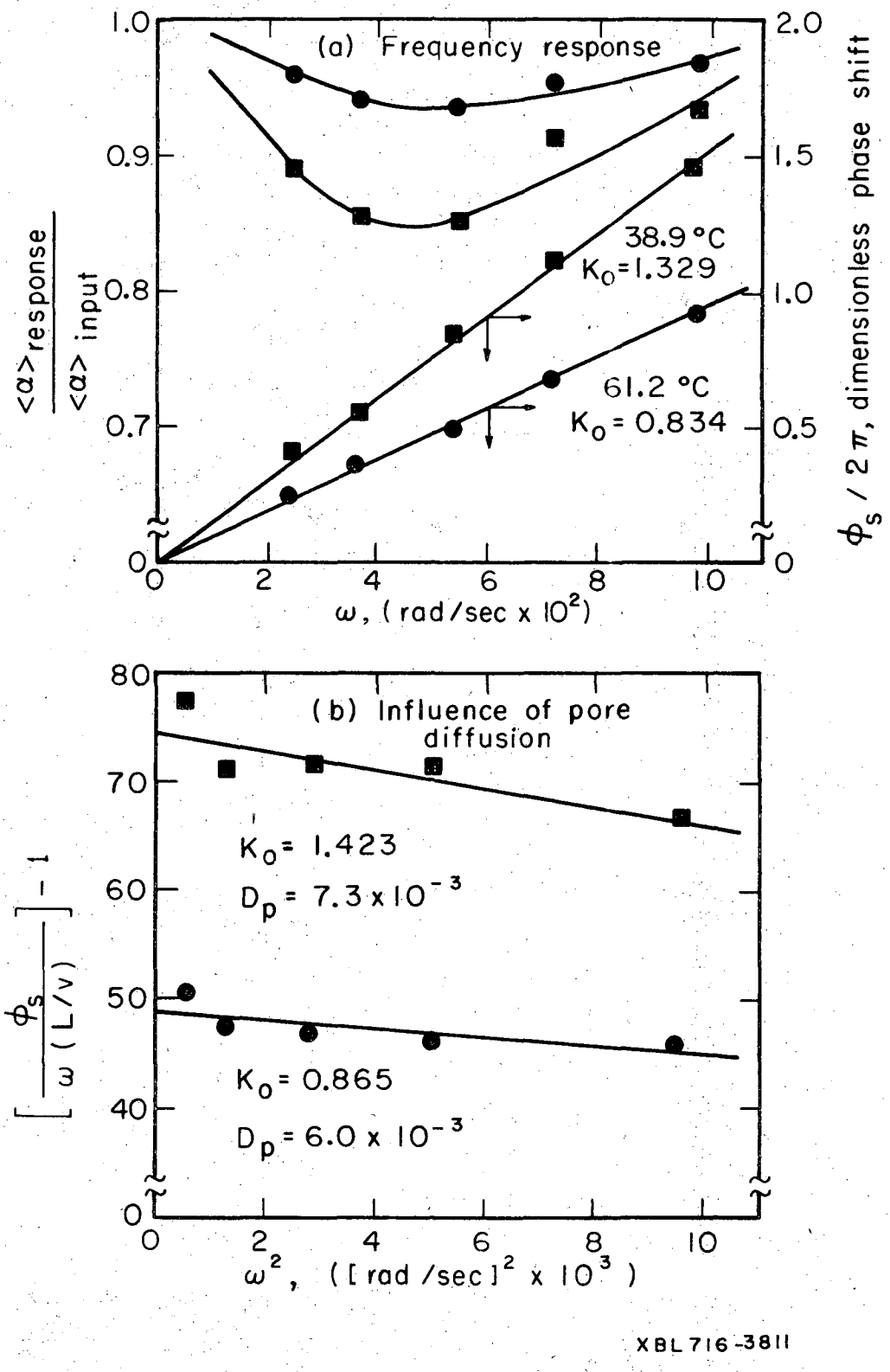

Figure A-3. Frequency Response: 4.9% CO_2-He on Pittsburgh BPL Activated Carbon at 19 psia.

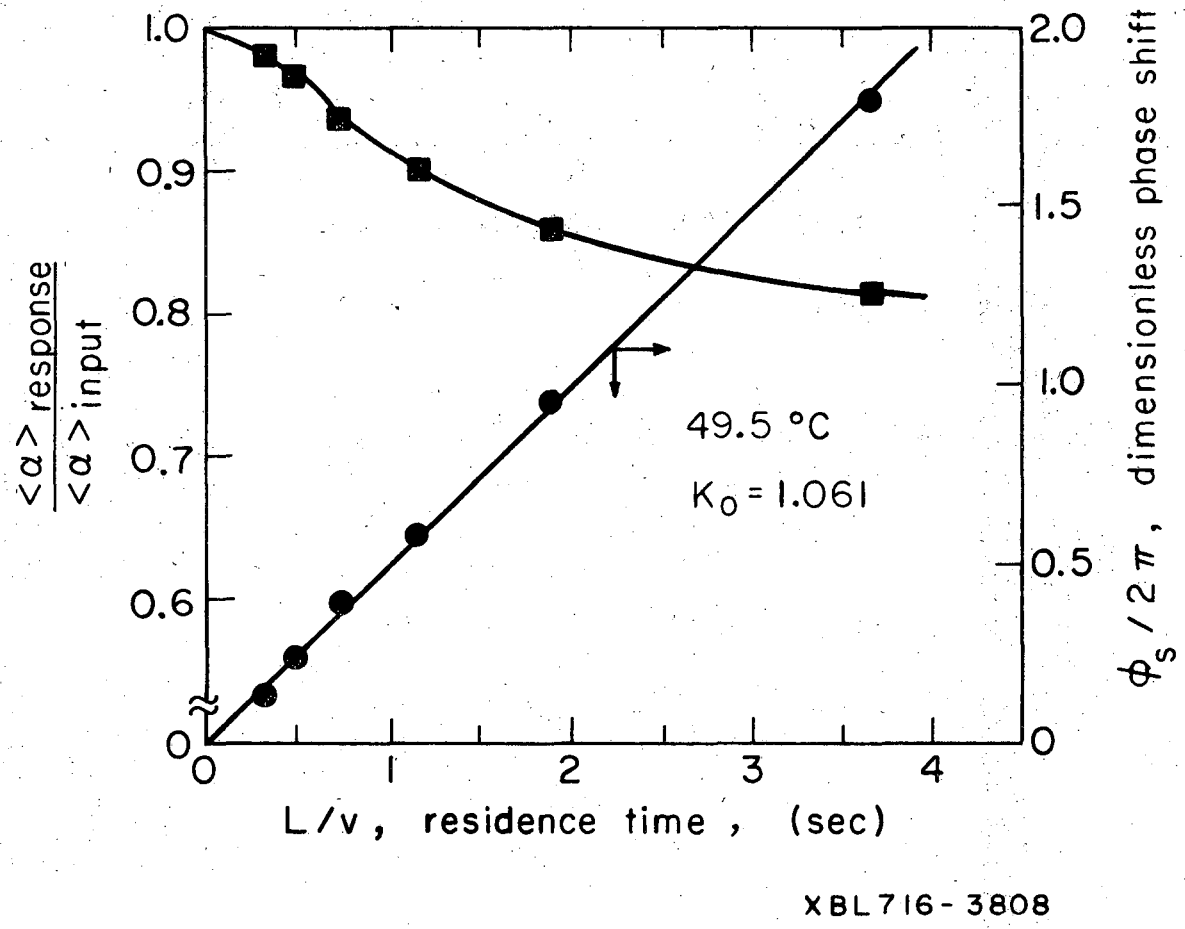

Figure A-4. Velocity Response (ω = 0.055 rad/sec.): 4.9% CO_2-He on Pittsburgh BPL Activated Carbon at 19 psia.

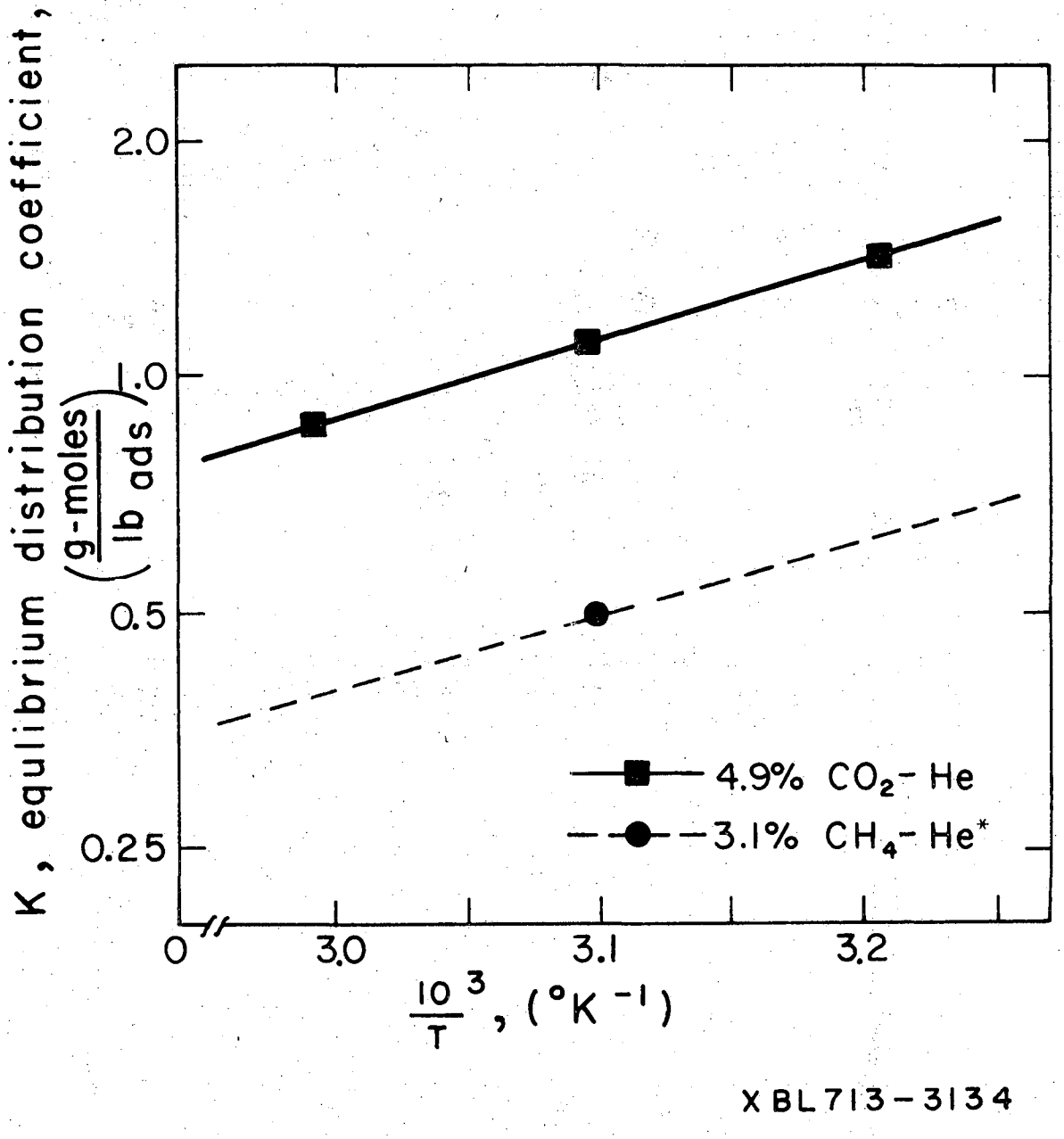

Figure A-5. Equilibrium Distribution Coefficients: Pittsburgh BPL Activated Carbon. (*Slope determined from data of Grant and Manes, 1962)

Table A-3. Frequency Response Data: Single Adsorbing Specie Systems (at 19.0 psia)

System	ω, rad/sec.	L/v, sec.	t_o, °C	$\rho_s(1-\varepsilon)/\rho_f\varepsilon$, lb_s/g-mole	$\phi_s/2\pi$	$\frac{\langle\alpha\rangle_{response}}{\langle\alpha\rangle_{input}}$
	0.0259				0.170	0.996
	0.0367				0.258	0.985
	0.0525	1.470	50.0	53.81	0.319	0.983
	0.0706				0.447	0.976
	0.1039				0.647	0.975
3.1% CH_4-He						
		3.215			0.765	0.939
		2.162			0.477	0.965
		1.623			0.424	0.980
		1.467			0.319	0.982
	0.053	1.164	49.5	53.66	0.296	0.989
		0.928			0.236	0.992
		0.723			0.172	0.993
		0.462			0.118	0.996
		0.348			0.095	0.997
	0.0238				0.246	0.959
	0.0360				0.352	0.941
	0.0535	1.265	61.2	55.61	0.518	0.938
	0.0711				0.673	0.956
	0.0976				0.924	0.967
	0.0238				0.405	0.892
	0.0360				0.557	0.855
4.9% CO_2-He	0.0535	1.363	38.9	51.89	0.846	0.853
	0.0711				1.106	0.915
	0.0976				1.430	0.936
		3.616			—	0.814
		1.860			0.960	0.860
	0.055	1.115	49.3	53.62	0.581	0.902
		0.733			0.396	0.938
		0.476			0.248	0.968
		0.313			0.169	0.981

W = 11.57 gm., L = 20.64 cm., ε = 0.403, χ = 0.40

BINARY ADSORBING SYSTEM

In mixed-gas adsorption, it is a tremendous saving of experimental effort to avoid the measurement of the adsorbate composition. Such measurements are so difficult that mixed-gas adsorption data are rare. A summary of mixed-gas adsorption thermodynamic theories is presented by Myers (1968).

A thermodynamic procedure for interpreting data which avoids the measurement of the adsorbate composition was proposed by Van Ness (1969). His method requires that adsorption isotherms be measured at constant gas composition while varying the pressure. Herein lies the main advantage of the frequency response method, in which a sinusoidal concentration disturbance about a fixed composition level is fed to an isothermal packed adsorbent bed, operated at various pressures. The measured phase shift versus frequency at each pressure can be used to calculate the distribution coefficient variance with respect to pressure at a constant average composition level. Experiments of this type were not conducted during the present study because it was not considered to be necessary to find the true composition of the adsorbate phase using thermodynamically exact computations. Instead, in order to reduce the work required, measurements were taken at one pressure. Interpretation was made by assuming a form for the equilibrium isotherm.

In this study, the methane-carbon dioxide binary system was investigated at constant pressure. The pore diffusion effect on the phase shift was neglected in order to simplify the computations.

Local Equilibrium

For two adsorbing species, the component material balances over a small section of the adsorbtive section are

$$\frac{\partial y_1}{\partial t} + \frac{(1 - \varepsilon)}{\varepsilon} \left[\chi \frac{\partial y_1}{\partial t} + \frac{\rho_s}{\rho_f} \frac{\partial x_1}{\partial t} \right] + \frac{\partial}{\partial z} (v\, y_1) = 0 \qquad \text{(A-33)}$$

$$\frac{\partial y_2}{\partial t} + \frac{(1 - \varepsilon)}{\varepsilon} \left[\chi \frac{\partial y_2}{\partial t} + \frac{\rho_s}{\rho_f} \frac{\partial x_2}{\partial t} \right] + \frac{\partial}{\partial z} (v\, y_2) = 0 \qquad \text{(A-34)}$$

For a binary system, the gas-phase material balance requires that $y_1 + y_2 = 1$. Adding equations (A-33) and (A-34) gives

$$\frac{\rho_s(1 - \varepsilon)}{\rho_f\, \varepsilon} \frac{\partial}{\partial t} (x_1 + x_2) = - \frac{\partial v}{\partial z} \qquad \text{(A-35)}$$

Substitution of equation (A-35) into equation (A-33) yields:

$$\left[1 + \frac{(1 - \varepsilon)\chi}{\varepsilon} \right] \frac{\partial y_1}{\partial t} + \frac{\rho_s(1 - \varepsilon)}{\rho_f\, \varepsilon} \left[y_2 \frac{\partial x_1}{\partial t} - y_1 \frac{\partial x_2}{\partial t} \right] + v \frac{\partial y_1}{\partial z} = 0 \qquad \text{(A-36)}$$

The equilibrium relationships may be written in the form:

$$x_1 = F_1(y_1, y_2)$$

$$x_2 = F_2(y_1, y_2)$$

For the input concentration disturbance of

$$y_1(0,t) = y_{1f}(1 + a\, e^{i\omega t})$$

the assumed solution forms are

$$y_1(z,t) = y_{1f} + Y(z)\, a e^{i\omega t}, \qquad |Y| \ll y_{1f} \qquad \text{(A-37)}$$

$$x_1(z,t) = x_{1f} + X_1(z)\, a e^{i\omega t},$$

$$x_2(z,t) = x_{2f} + X_2(z)\, a e^{i\omega t}. \qquad |X_i| \ll x_{if} \qquad \text{(A-38)}$$

Since $y_1 + y_2 = 1$,

$$y_2(z,t) = y_{2f} - Y(z)\, a e^{i\omega t} \qquad \text{(A-39)}$$

Substitution of equations (A-37), (A-38), and (A-39) into equation (A-36), retaining the first order terms only, gives:

$$\left[1 + \frac{(1-\varepsilon)\chi}{\varepsilon}\right] Y + \frac{\rho_s(1-\varepsilon)}{\rho_f\, \varepsilon}\left[y_{2f}\, X_1 - y_{1f}\, X_2\right] + \frac{v}{i\omega}\,\frac{dY}{dz} = 0 \qquad \text{(A-39)}$$

Linearization of the equilibrium expressions about the feed composition gives:

$$x_1 - x_{1f} = \frac{\partial F_1}{\partial y_1}\Big|_{y_f} (y_1 - y_{1f}) + \frac{\partial F_1}{\partial y_2}\Big|_{y_f} (y_2 - y_{2f})$$

$$x_2 - x_{2f} = \frac{\partial F_2}{\partial y_1}\Big|_{y_f} (y_1 - y_{1f}) + \frac{\partial F_2}{\partial y_2}\Big|_{y_f} (y_2 - y_{2f})$$

Substitution of equations (A-37), (A-38), and (A-39) into the linearized equilibrium relationships, we obtain

$$X_1(z) = (A_{11} - A_{12})\, Y(z) \qquad \text{(A-40)}$$

$$X_2(z) = (A_{21} - A_{22})\, Y(z) \qquad \text{(A-41)}$$

where

$$A_{11} = (\partial F_1/\partial y_1)_{y_{1f},y_{2f}}$$

$$A_{12} = (\partial F_1/\partial y_2)_{y_{1f},y_{2f}}$$

$$A_{21} = (\partial F_2/\partial y_1)_{y_{1f},y_{2f}}$$

$$A_{22} = (\partial F_2/\partial y_2)_{y_{1f},y_{2f}}$$

Therefore:

$$y_{2f} X_1 - y_{1f} X_2 = [y_{2f}(A_{11} - A_{12}) + y_{1f}(A_{22} - A_{21})] Y$$

$$= M_o Y$$

Substituting the above result into equation (A-39) yields the ordinary differential equation:

$$\left[1 + \frac{(1 - \varepsilon)\chi}{\varepsilon} + \frac{\rho_s(1 - \varepsilon)}{\rho_f \varepsilon} M_o\right] Y + \frac{v}{i\omega} \frac{dY}{dz} = 0 \qquad \text{(A-42)}$$

The solution to equation (A-42) with the boundary condition, $Y(0) = y_{1f}$, is

$$Y(z) = y_{1f} \exp\left[\frac{-i\omega z}{v}\left(1 + \frac{(1 - \varepsilon)\chi}{\varepsilon} + \psi\right)\right]$$

$$= y_{1f} \exp(-i\phi)$$

where the solids-fluid capacity ratio is

$$\psi = \frac{\rho_s(1 - \varepsilon)}{\rho_f \varepsilon} M_o$$

The phase shift is therefore:

$$\phi = \omega(z/v) \left[1 + \frac{(1 - \varepsilon)\chi}{\varepsilon} + \psi\right] \qquad \text{(A-43)}$$

A plot of ϕ versus $\omega(L/v)$ yields a straight line with a slope of $1 + \frac{(1 - \varepsilon)\chi}{\varepsilon} + \psi$. From the slope, M_o may be determined by

$$M_o = \frac{\text{slope} - 1 - (1 - \varepsilon)\chi/\varepsilon}{\frac{\rho_s(1 - \varepsilon)}{\rho_f \varepsilon}} \qquad \text{(A-44)}$$

where M_o is related to the average feed compositions and the derivatives of the equilibrium isotherms:

$$M_o = y_{2f}(A_{11} - A_{12}) + y_{1f}(A_{22} - A_{21}) \qquad \text{(A-45)}$$

Langmuir Behavior

Consider the special case where both species exhibit Langmuir behavior, then the loading functions of the components in the mixture are

$$x_1 = \frac{m_1 K_1 y_1}{1 + K_1 y_1 + K_2 y_2}$$

$$x_2 = \frac{m_2 K_2 y_2}{1 + K_1 y_1 + K_2 y_2} \qquad \text{(A-46)}$$

where

m_i = adsorbate loading capacity, g-moles/lb_{ads}

K_i = Langmuir constants, dimensionless

Evaluating the partial derivatives of equations (A-46) and substituting into equation (A-45), the expression for M_o is found to be:

$$M_o = \frac{y_{1f}[m_2K_2(1 + K_1)] + y_{2f}[m_1K_1(1 + K_2)]}{(1 + K_1y_{1f} + K_2y_{2f})^2} \qquad (A-47)$$

The end points of equation (A-47) are

$$M_o = \frac{m_2 K_2}{1 + K_1} \quad \text{at} \quad y_{1f} = 1$$

$$M_o = \frac{m_1 K_1}{1 + K_2} \quad \text{at} \quad y_{1f} = 0 \qquad (A-48)$$

Rearrangement of equation (A-47) gives the linear relationship:

$$M_o[1 + K_2 + y_{1f}(K_1 - K_2)]^2 = y_{1f}[m_2K_2(1 + K_1) - m_1K_1(1 + K_2)]$$

$$+ m_1K_1(1 + K_2)$$

$$= M^* \qquad (A-49)$$

When each component, individually in the presence of a non-adsorbing carrier gas such as helium, exhibits Langmuir behavior, the loading functions may be written as:

$$x_1 = \frac{m_1 K_1 y_1}{1 + K_1 y_1} \qquad (A-50)$$

and

$$x_2 = \frac{m_2 K_2 y_2}{1 + K_2 y_2} \tag{A-51}$$

The distribution coefficients, as previously defined, are then:

$$K_{o1} = \frac{dx_1}{dy_1}\Big|_{y_{1f}} = \frac{m_1 K_1}{(1 + K_1 y_{1f})^2} \tag{A-52}$$

$$K_{o2} = \frac{dx_2}{dy_2}\Big|_{y_{2f}} = \frac{m_2 K_2}{(1 + K_2 y_{2f})^2} \tag{A-53}$$

Experimental Results

The frequency response results for 25, 50, and 75 mole% CH_4-CO_2 mixtures at 19.0 psia and temperatures of 37.6 and 60.5 °C, are shown in Figure A-6. The experimental data are listed in Table A-6. The amplitude ratios remained fairly constant. Thus, the drop from unity is probably due to harmonics in the input concentration signal. This, of course, could be ascertained by a Fourier analysis on the input and output signals, which was not performed in this study because the phase shift, on which calculations were based, is less sensitive to diffusional effects than the amplitude. A method suggested by Deisler and Wilhelm (1953) employing a packed bed to filter the concentration disturbance before entering the test zone, was not utilized in this investigation since the experimental apparatus was originally designed for cycling zone experiments.

The distribution coefficients, determined by the frequency response method, for the binary CH_4-CO_2, CH_4-He, and CO_2-He mixtures are

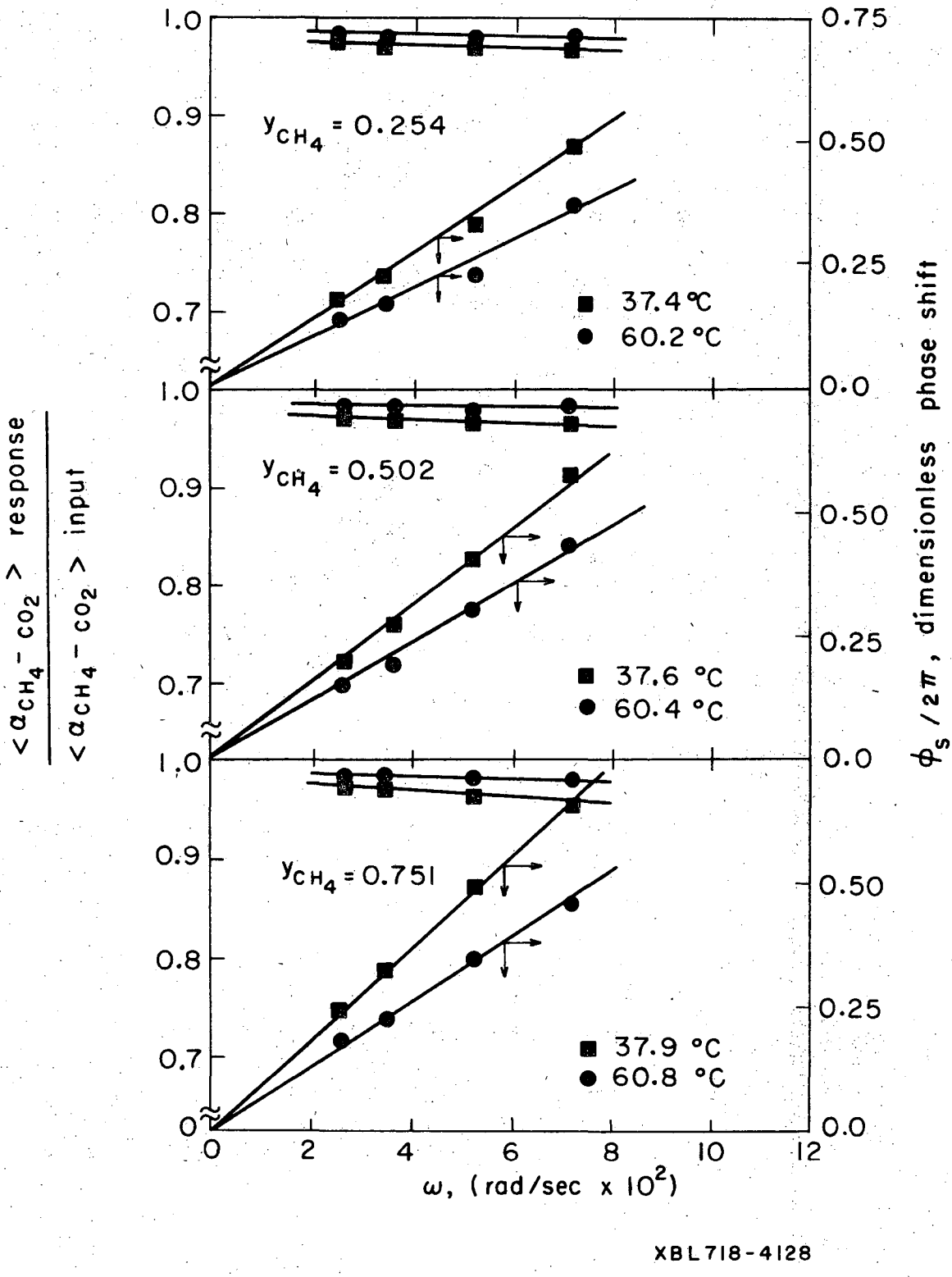

Figure A-6. Frequency Response: Binary Mixtures of CH_4-CO_2 on Pittsburgh BPL Activated Carbon at 19 psia.

listed in Table A-4. The binary adsorbing system's distribution coefficients, M_o, are presented in Figure A-7a. The solid lines represent the predicted function M for the best set of m_1K_1, m_2K_2, K_1, K_2 values consistent with the data listed in Table A-4. The best-fit values of the Langmuir parameters are listed in Table A-5. The temperature dependency of the parameters are of the form, $A_o\exp(-\Delta H_a/RT)$. A plot of the natural log of the parameter versus 1/T has a slope equal to $-\Delta H_a/R$.

Table A-4. Experimental Distribution Coefficients at 19.0 psia.

System	Temperature, °C	37.6	60.5	Composition, m.f.
		Distribution Coeff., g-moles/lb$_{ads}$		
CH_4-He*	K_{o1} =	0.66	0.39	y_1 = 0.031
CO_2-He*	K_{o2} =	1.47	0.89	y_2 = 0.049
CH_4-CO_2	M_o =	0.465	0.355	y_1 = 0.254
		0.567	0.415	= 0.502
		0.746	0.513	= 0.751

*Interpolated values from Figure A-5.

Table A-5. Langmuir Parameters at 19.0 psia.

Parameters	Temperature, °C 37.6	60.5	$-\Delta H_a/R \times 10^{-3}$, $^\circ K^{-1}$
K_1	0.790	0.620	0.97
m_1K_1, g-mole/lb$_s$	0.690	0.405	2.15
K_2	1.040	0.560	2.48
m_2K_2, g-mole/lb$_s$	1.615	0.939	2.16

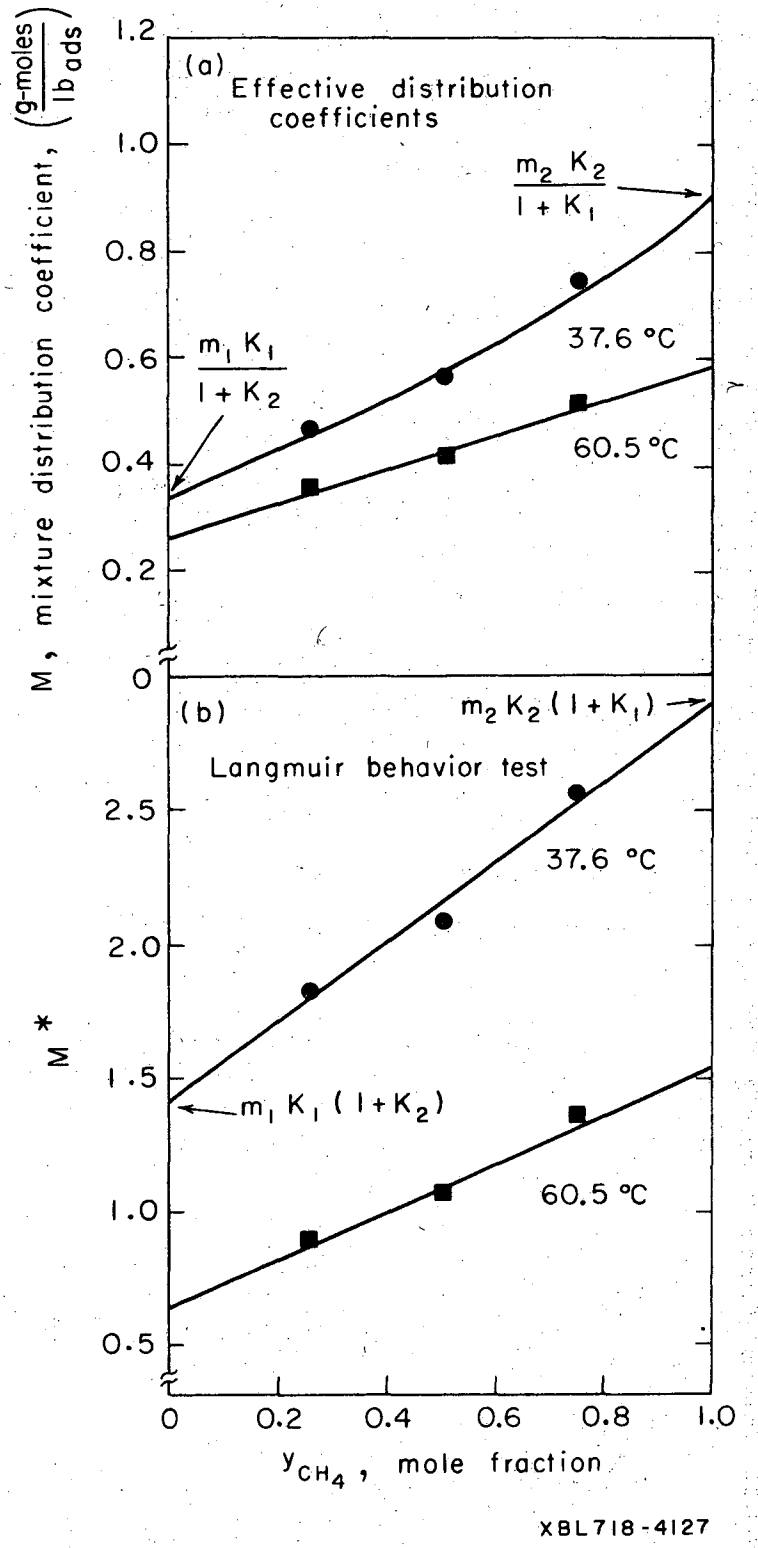

Figure A-7. Effective Equilibrium Distribution Coefficients of CH_4-CO_2 Binary Mixtures.

A test of the data, in order to evaluate the "goodness" of the assumed Langmuir behavior, may be made by application of equation (A-49), employing the calculated parameters listed in Table A-5. For true Langmuir behavior a plot of M^* versus y_1 should be linear. The response data for the system investigated, plotted in Figure A-7b, indicate that the behavior exhibited by the CH_4-CO_2 system is nearly that assumed. More experiments would be necessary to determine the isotherm forms with greater precision. The results obtained above, however, are of sufficient accuracy to be used to evaluate the isotherm parameters required in the cycling zone analyses.

Table A-6. Frequency Response Data: CH_4-CO_2 Binary Adsorbing System (at 19.0 psia)

$(y_{CH_4})_f$, mole fraction	ω, rad/sec.	L/v, sec.	t_o, °C	$\rho_s(1-\varepsilon)/\rho_f\varepsilon$, lb_s/g-mole	$\phi_s/2\pi$	$\frac{\langle\alpha\rangle_{response}}{\langle\alpha\rangle_{input}}$
	0.0249				0.176	0.976
	0.0347	1.634	37.4	51.64	0.222	0.969
	0.0524				0.333	0.971
	0.0720				0.491	0.970
0.254						
	0.0249				0.134	0.983
	0.0347	1.500	60.2	55.44	0.167	0.980
	0.0524				0.229	0.981
	0.0720				0.415	0.982
	0.0261				0.195	0.972
	0.0361	1.570	37.6	51.68	0.270	0.969
	0.0517				0.403	0.967
	0.0712				0.579	0.965
0.502						
	0.0261				0.150	0.982
	0.0361	1.464	60.4	55.46	0.190	0.983
	0.0517				0.301	0.980
	0.0712				0.439	0.983
	0.0254				0.244	0.976
	0.0346	1.474	37.9	51.73	0.320	0.973
	0.0522				0.495	0.965
	0.0721				0.660	0.961
0.751						
	0.0254				0.183	0.985
	0.0346	1.384	60.8	55.55	0.222	0.987
	0.0522				0.349	0.982
	0.0721				0.448	0.980

W = 11.57 gm., L = 20.64 cm., ε = 0.403, χ = 0.40

APPENDIX B

TRANSPORT PROPERTIES FOR THE CZA PROCESS

TRANSPORT PARAMETERS

Various transport properties for the cycling zone adsorption processes investigated in this study are estimated in order to give a general insight into the physical limitations imposed upon its operation. The general correlation of transport properties for fixed-bed systems, proposed by Vermeulen (1963)*, is used to determine the controlling mode of mass transfer and to estimate the heights of transfer units, HTU.

Molecular Diffusion-Limiting Velocity

From Vermeulen's correlation chart, the lower limit on the interstitial velocity, v, for which transport by longitudinal molecular diffusion in the fluid stream becomes significant compared to the bulk flow transport, occurs aroung Péclet numbers of 0.7 to 1.5. The Péclet number is defined by:

$$Pe_f = \frac{\langle d_p \rangle v\varepsilon}{D_f} \qquad \text{(B-1)}$$

where

$\langle d_p \rangle$ = average particle diameter, cm.

v = interstitial velocity, cm/sec.

ε = void fraction

D_f = fluid phase molecular diffusivity, cm^2/sec.

---

* Corrected by Vermeulen (1970) (to be published in 5th Edition of Perry's Chemical Engineering Handbook, McGraw-Hill, New York).

The approximate limiting velocity range for which molecular diffusion becomes important is determined by rearrangement of equation (B-1) as:

$$v_{limiting} = \frac{D_f (Pe_f)_{limiting}}{\langle d_p \rangle \varepsilon} \qquad (B-2)$$

The molecular diffusivities and limiting velocity ranges for the systems investigated in this study are listed in Table B-1.

Table B-1. Molecular Diffusivities and Limiting Velocities

System	D_f, $cm^2/sec.$		$^*v_{limiting}$, cm/sec.
	0°C & 1 atm	50°C & 19 psia	50°C & 19 psia
CH_4-He	0.590 (a)	0.595	9.9 to 21.2
CO_2-He	0.522 (b)	0.530	8.7 to 12.6
CH_4-CO_2	0.153 (c)	0.155	2.6 to 5.5

(a) Fuller (1966)
(b) Holsen (1964)
(c) Hirschfelder (1949)

*Based on $\langle d_p \rangle$ = 0.105 cm., ε = 0.400

Axial Dispersion

Taylor-type dispersion results from deviations in the velocity distribution from the idealized plug-flow profile. The deviations within fixed beds usually result from flow channeling near the walls, which can be minimized by setting $L/d_p > 180$, as proposed by Himmelblau (1968). In this study, the L/d_p ratio was around 185.

It is common practice to lump Taylor dispersion and other longitudinal dispersive effects into an axial dispersion coefficient. The

limiting value of the dispersive Péclet number, Pe_z, may be used to evaluate the upper limit on the axial dispersion coefficient. For gaseous systems, the limiting Pe_z has been shown by Meyer (1966) to be approximately:

$$(Pe_z)_{limiting} = \frac{\langle d_p \rangle v\varepsilon}{D_z} \cong 2 \qquad \text{(B-3)}$$

where D_z is the axial dispersion coefficient in cm^2/sec. Thus

$$\left(\frac{D_z}{v}\right)_{limiting} = \frac{\langle d_p \rangle \varepsilon}{2} \qquad \text{(B-4)}$$

An order of magnitude comparison of the dispersive and bulk flow terms in the material balance equations, shows that axial dispersion becomes negligible if:

$$\left| D_z \frac{\partial^2 y}{\partial z^2} / v \frac{\partial y}{\partial z} \right| \ll 1$$

or

$$\left(\frac{D_z}{v}\right) \left| \frac{\partial^2 y}{\partial z^2} / \frac{\partial y}{\partial z} \right| \ll 1 \qquad \text{(B-5)}$$

The linear equilibrium theory results indicate that the concentration derivatives are of the order L^{-1}. Therefore, for $D_z/vL \ll 1$, the axial dispersive effects may be ignored. In this study, $(D_z/v)_{limiting}$ evaluated from equation (B-4) was approximately equal to 0.02 cm. Thus D_z/vL was found to be on the order of 10^{-3}, which was assumed to be negligible.

Solid Phase Diffusion

The effective intraparticle diffusivity, D_p, incorporates the three particle-phase mass transfer mechanisms: (1) gaseous diffusion in the macro pores, (2) Knudsen diffusion in the tortuous micro pores, and (3) surface migration (diffusion) in the adsorbed state. The magnitude of the effective intraparticle diffusivity can be estimated from the gaseous molecular diffusivity, the molecular mean free path, and the average pore diameter of the adsorbent, using the equations given by Weiss (1957):

$$D_p \cong \frac{\ell_p}{\ell} D_f \qquad \text{(B-6)}$$

and

$$\ell = \frac{454\ T}{P\ \sigma_c^2} \qquad \text{(B-7)}$$

where

ℓ_p = average pore diameter, Å

ℓ = molecular mean free path, Å

σ_c = molecular diameter, Å

P = absolute pressure, psia

T = absolute temperature, °K

Vermeulen (1970) proposed a more restrictive equation for the estimation of the diffusivity in the macro pores, D_{pore}, in the form of:

$$D_{pore} = \frac{\chi}{\tau} \left[\frac{3}{4\ \ell_p} \left(\frac{\pi\ M_w}{2RT} \right)^{1/2} + \frac{1}{D_f} \right]^{-1} \qquad \text{(B-8)}$$

where

τ = tortuosity (2-6 for gases)

M_w = molecular weight

The Knudsen diffusivity, D_K, may be estimated by employing the result given by Petersen (1965):

$$D_K = \frac{8\chi}{3S\rho_b}\sqrt{\frac{2RT}{\pi M_w}} \qquad \text{(B-9)}$$

where

S = surface area/unit mass, cm^2/gm.

ρ_b = apparent particle density, gm/cm^3.

The estimated values of the above mentioned diffusivities and the experimental effective diffusivities, determined by the frequency response technique, are listed in Table B-2. The lower and upper bounds on the effective diffusivity are the Knudsen and molecular diffusivities, respectively. For the systems investigated, macro pore diffusion and surface diffusion appear to be the important transport mechanisms, where surface migration is of greater significance for CO_2 adsorption.

Table B-2. Solid Phase Diffusivities (at 19.0 psia)

System	Temperature °C	D_{pore}, $cm^2/sec.$ Eqn (B-8)	D_K, $cm^2/sec.$ Eqn (B-9)	D_p, $cm^2/sec.$ Eqn (B-6)	D_p, $cm^2/sec.$ Exp.
3.1% CH_4-He	50	2.2×10^{-3}	11.2×10^{-7}	1.6×10^{-2}	3.2×10^{-3}
4.9% CO_2-He	39	—	—	—	7.3×10^{-3}
	50	1.3×10^{-3}	6.7×10^{-7}	1.7×10^{-2}	—
	61	—	—	—	6.0×10^{-3}
50% CH_4-CO_2	50	1.5×10^{-3}	8.1×10^{-7}	4.5×10^{-3}	—

($S = 1100\ m^2/gm.$, $\chi = 0.400$, $\ell_p = 15$ Å, $\tau = 4$; supplied by manufacturer)
$(\sigma_c)_{CH_4} = 3.76$ Å, $(\sigma_c)_{CO_2} = 3.94$ Å, $(\sigma_c)_{CH_4\text{-}CO_2} = 3.85$ Å.

Height of Transfer Unit (HTU)

Again employing Vermeulen's correlation chart, the height of a transfer unit for these solid-phase diffusion controlled processes was estimated. These values are listed in Table B-3. The height of a transfer unit is a characteristic length which reflects the ratio of

Table B-3. Height of Transfer Unit (at 50°C and 19 psia)

System	Pe_f	$0.6D_{pore}/D_f$	HTU, cm.
CH_4-He	1.4	0.0022	0.9
CO_2-He	1.6	0.0015	1.2
CH_4-CO_2	5.4	0.0058	1.4

$v = 20$ cm/sec., $L = 20$ cm.

the mass transfer resistance to the equilibrium driving potential. These small values indicate reasonable approach to equilibrium operation, as also suggested by the experimental results reported in Chapters 5 and 6. Typically, very good chromatographic systems, described by McNair and Bonelli (1968), exhibit HTUs in the range of 1 to 3 mm.

PROCESS HEAT REQUIREMENTS

The heat duty per mole of feed gas, containing a single adsorbing specie, for the full cycle operation of a single cycling zone is estimated by utilizing the material and energy balances for a linear system. The standard enthalpy states (h = 0) are the normal states at 25°C. The heat duty is compared with the minimum free energy, assuming ideal gases, required to accomplish the desired separation.

Material Balances

The material balances for the inert and solute species for the system shown in Figure B-1 are

$$\text{solute:}\quad \varepsilon v\, \rho_f y_o = v_{out}\, \rho_f y_L + \frac{d}{dt}\left\{ \varepsilon\, \rho_f \int_o^L y\, dz + (1-\varepsilon)\rho_s \int_o^L x\, dz \right\} \tag{B-10}$$

$$\text{inert:}\quad \varepsilon v\, \rho_f (1-y_o) = v_{out}\, \rho_f (1-y_L) + \frac{d}{dt}\left\{ \varepsilon\, \rho_f \int_o^L (1-y)\, dz \right\} \tag{B-11}$$

where

ρ_f = gas molar density, g-moles/cm^3

ρ_s = adsorbent density, lb/cm^3.

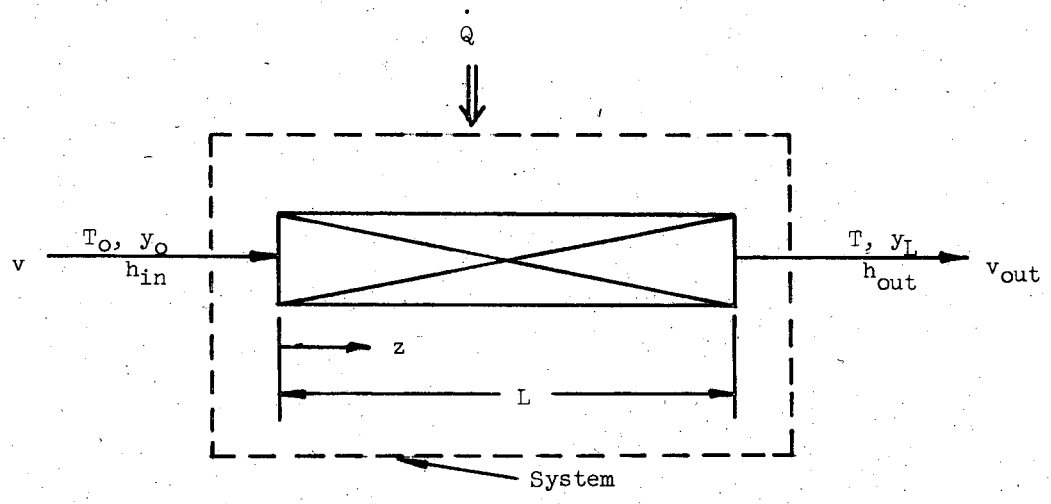

Figure B-1. Material and Energy Balances-
Single CZA Unit.

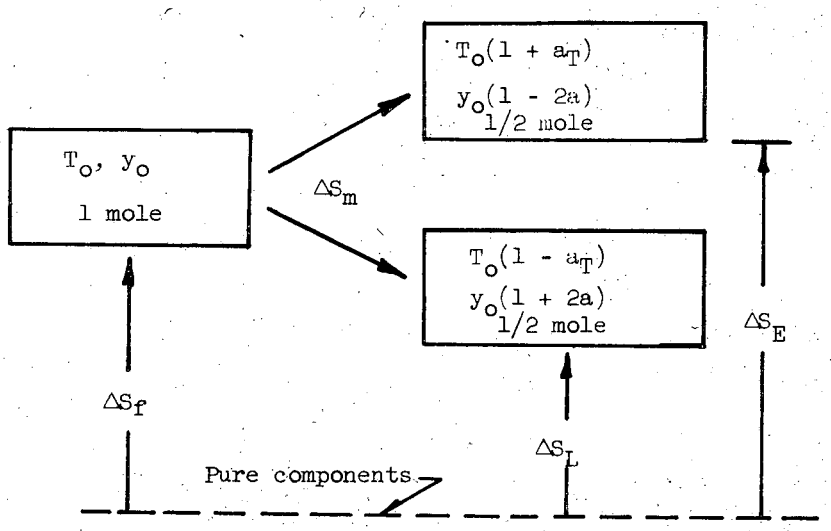

Figure B-2. Minimum Free Energy Change per
Mole of Feed Mixture.

XBL 719-4426

Combining equations (B-10) and (B-11), we have:

$$v_{out} = v - \frac{\rho_s(1 - \varepsilon)}{\rho_f \varepsilon} \frac{d}{dt} \int_o^L x \, dz \qquad \text{(B-12)}$$

The elimination of v_{out} from equation (B-10) yields:

$$v(y_o - y_L) = \int_o^L \left[\frac{\partial y}{\partial t} + \frac{\rho_s(1 - \varepsilon)}{\rho_f \varepsilon} (1 - y_L) \frac{\partial x}{\partial t}\right] dz$$

or

$$\frac{\partial y}{\partial t} + \frac{\rho_s(1 - \varepsilon)}{\rho_f \varepsilon} (1 - y) \frac{\partial x}{\partial t} + v \frac{\partial y}{\partial z} = 0 \qquad \text{(B-13)}$$

Enthalpy Balance

The enthalpy balance for the system is

$\dot{Q}$ = flow enthalpy out - flow enthalpy in
+ time-rate of change of system enthalpy

where

$\dot{Q}$ = heat flow, cal/sec.

For standard states at 25°C, the heat flow is

$$\dot{Q}/(\varepsilon \rho_f v A_c) = \left\{v - \frac{\rho_s(1 - \varepsilon)}{\rho_f \varepsilon} \frac{d}{dt} \int_o^L x \, dz\right\} [(1 - y_L)C_n + y_L C_a] \cdot \frac{(T - 298)}{v}$$

$$- [(1 - y_o)C_n + y_o C_a] (T_o - 298)$$

$$+ \frac{d}{dt} \left\{ \int_o^L [(1 - y)C_n + yC_a] \frac{(T - 298)}{v} \, dz \right.$$

$$\left. + \frac{\rho_s(1 - \varepsilon)}{\rho_f \varepsilon v} \int_o^L C_s'(T - 298) \, dz + \frac{\rho_s(1 - \varepsilon)}{\rho_f \varepsilon v} \int_o^L x[C_a^*(T - 298) - \Delta H^\circ] \, dz \right\} \qquad \text{(B-14)}$$

where:

C_i = molar heat capacities, cal/g-mole-°K.
n = inert, a = solute, s = solids, * = adsorbed solute.

$\Delta H^\circ = (h_a^\circ)_{gas} - (h_a^\circ)_{adsorbate} = -\Delta H_a^\circ$, heat of adsorption at 25°C, cal/g-mole.

A_c = cross-sectional area of empty bed, cm^2.

After considerable algebraic manipulation, employing equation (B-13) and the linear approximation $x = K_o y$, equation (B-14) becomes

$$\dot{Q} = \varepsilon \rho_f v A_c \left[\underbrace{\overline{C}_o(T - T_o)}_{\text{sensible heat gain of feed stream}} + \underbrace{(L/v) \dot{T} \overline{C}_g}_{\text{gas hold-up}} - \underbrace{\Delta H_a(y_L - y_o)}_{\text{solute desorption removed from bed}} - \underbrace{\frac{\Delta H_a}{v} \int_o^L \frac{\partial y}{\partial t} \, dz}_{\text{solute desorption remaining in bed}} \right.$$

$$\left. + \underbrace{\frac{\rho_s(1 - \varepsilon)}{\rho_f \varepsilon} (L/v) \dot{T} \overline{C}_s}_{\text{adsorbent particles}} \right] \qquad \text{(B-15)}$$

where the mean heat capacities are defined by:

$\bar{C}_o = C_n(1 - y_o) + C_a y_o$, average heat capacity of inlet fluid.

$$\bar{C}_g = \frac{1}{L} \int_o^L [C_n(1 - y) + C_a y]\, dz,$$ average heat capacity of fluid hold-up.

$$\bar{C}_s = \frac{1}{L} \int_o^L [454 \cdot C_s + C_a^* K_o y]\, dz,$$ ave. heat capacity of solid + adsorbate on the bed.

and

$$\dot{T} = \frac{dT}{dt}$$

$$-\Delta H^\circ = -\Delta H + (C_a - C_a^*)(T - 298)$$

The estimated values of the heat capacities of the species encountered in this study are listed in Table B-4.

Table B-4. Heat Capacities at 50°C (cal/g-mole-°K)

C_n	C_a		C_a^*		C_s, cal/gm-°K
He	CH_4	CO_2	CH_4	CO_2	Activated Carbon
5.0	8.8	9.1	10.3	10.9	0.25

Hougen, O. A. and Watson, K. M., Chemical Process Principles, 258, (1947). Pittsburgh Activated Carbon Company.

Heat Requirements for Single CZA Unit

The heat required per mole of feed gas for a full heating half-cycle of operation is

$$Q_T = \frac{\int_{\text{half-cycle}} \dot{Q}\, dt}{\int_{\text{half-cycle}} \varepsilon\, \rho_f v A_c\, dt} = \frac{\omega}{\pi\, \varepsilon\, \rho_f v A_c} \int_{\text{half-cycle}} \dot{Q}\, dt \qquad \text{(B-16)}$$

For the input temperature forcing of

$$T = T_o(1 + a_T \sin \omega t)$$

it has been shown that:

$$y_L = y_o \left\{1 - \frac{a\,\psi}{1 + \psi} \left[\sin(\omega t) - \sin(\omega t - \omega L/v^*)\right]\right\}$$

where

$$a = \left(\frac{\Delta H_a}{RT_o}\right) a_T \qquad \text{and} \qquad v^* = v/(1 + \psi)$$

For the maximum amplification of the adsorbing specie, $\omega L/v^* = \pi$, the heat flow may be written in the form:

$$\dot{Q} = \varepsilon\, \rho_f v A_c (A \sin \omega t + B \cos \omega t)$$

$$= \varepsilon\, \rho_f v A_c \left[\sqrt{A^2 + B^2}\, \sin(\omega t - \phi)\right] \qquad \text{(B-17)}$$

where

$$\phi = \tan^{-1}(B/A)$$

$$A = a_T T_o \left[\overline{C}_o + \frac{2\Delta H_a^2}{RT_o^2}\, y_o \left(\frac{\psi}{1 + \psi}\right)^2\right] \qquad \text{(B-18)}$$

$$B = a_T T_o \left(\frac{\pi}{1+\psi}\right)\left[\left(\overline{C}_g + \frac{\rho_s(1-\varepsilon)}{\rho_f\,\varepsilon}\,\overline{C}_s\right) + \frac{\Delta H_a^2}{RT_o^2}\,y_o\left(\frac{\psi}{1+\psi}\right)\right] \tag{B-19}$$

The total heat required per mole of feed, equation (B-16), upon integration from ϕ to $\phi + \pi/\omega$, may be written as:

$$Q_T = \frac{2}{\pi}\left(A^2 + B^2\right)^{1/2} \tag{B-20}$$

From equation (B-19), it is evident that for gaseous systems having components with identical properties, excepting the equilibrium solids-fluid capacity ratio, ψ, the heat requirements to process one mole of feed, at the maximum amplification condition, decreases with increasing ψ. In other words, the larger the solute bed capacity, the greater the processing rate per heat cycle will be.

For the dilute CH_4-He and CO_2-He systems under the conditions listed in Table B-5, the heat requirement, minimum free energy, and the

Table B-5. Single Zone Operating Conditions and Parameters at 19.0 psia for $\langle\alpha\rangle = 1.8$, $\omega(L/v^*) = \pi$.

System	ψ,	$\overline{C}_o$, cal/g-mole	$\overline{C}_g$, cal/g-mole	$\overline{C}_s$, cal/lb_s.	ω, rad/sec.
3.1% CH_4-He	25	5.1	5.1	110.7	0.121
4.9% CO_2-He	55	5.2	5.2	110.9	0.056

$\varepsilon = 0.400$, $v = 20$ cm/sec., $L = 20$ cm., $T_o = 323°K$ (50°C), $a_T = 0.020$, $a = -0.143$, $(\Delta H_a)_{CH_4} \cong (\Delta H_a)_{CO_2} \cong -4600$ cal/g-mole, $\dfrac{\rho_s(1-\varepsilon)}{\rho_f\,\varepsilon} = 50$ lb_s/g-mole

thermal efficiency were determined for a separation corresponding to $\langle \alpha \rangle = 1.8$, and are listed in Table B-6. It is evident that the greatest expenditure of energy for the cycling zone adsorption process goes into the heating and cooling the adsorbent particles.

For ideal gases, the minimum free energy change to effect the separation, assuming $\psi \gg 1$, shown in Figure B-2, is:

$$\Delta G = - T_o \Delta S_m \tag{B-21}$$

where

$$\Delta S_m = \Delta S_E + \Delta S_L - \Delta S_f$$

and

ΔS_E = entropy change from pure components to the enriched half-cycle.

ΔS_L = entropy change from pure components to the depleted (lean) half-cycle.

ΔS_m = entropy change from pure components to the feed mixture.

Therefore, equation (B-21) becomes:

$$\Delta G = \underbrace{a_T T_o \overline{C}_o}_{\text{temperature effect}} - RT_o\Big[y_o \ln y_o + (1 - y_o)\ln(1 - y_o) - \tfrac{1}{2}\{y_o(1 - 2a)\cdot \ln[y_o(1 - 2a)] + y_o(1 + 2a)\ln[y_o(1 + 2a)] + [1 - y_o(1 - 2a)]\ln[1 - y_o(1 - 2a)] + [1 - y_o(1 + 2a)]\cdot \ln[1 - y_o(1 + 2a)]\}\Big] \tag{B-22}$$

$$\underbrace{\qquad\qquad\qquad\qquad\qquad\qquad\qquad\qquad\qquad\qquad}_{\text{composition effect}}$$

Table B-6. Heat Requirements per mole of Feed to Produce the Separation of $\langle \alpha \rangle$ = 1.8 at 19.0 psia.

System	Heat Requirements Based on Solid Phase Heat=100				Q_T, cal/g-mole	ΔG, cal/g-mole		*Thermal Efficiency, %
	Solid Phase	Flowing Fluid	Desorption Expelled	Desorption Retained		Temp. Effect	Comp. Effect	
3.1% CH_4-He	100	0.75	0.96	0.06	2,840	33.3	1.2	2.1
4.9% CO_2-He	100	1.63	3.34	0.10	1,300	33.7	1.1	4.2

*Based on Q_{min} required to produce the composition effect free energy change.

The minimum heat required to produce the minimum free energy change for a perfect reversible process is

$$Q_{min} = \Delta G[T_o/(T_H - T_o)] \qquad \text{(B-23)}$$

or

$$Q_{min} = \Delta G/a_T \qquad \text{(B-24)}$$

Velocity Limitation

The equilibrium theory puts no limit on the thru-put velocity since $\omega L/v^* = \pi$ is the only criterion for maximum amplification. Also, no velocity limit is imposed by the intraparticle diffusion resistance attenuation, given in equation (A-30). However, a practical limit would be the fluid velocity for which the heat requirement for the flowing fluid becomes approximately 20% of that required for the solid adsorbent particles. This velocity may be estimated, using the appropriate terms, from equation (B-15) which gives

$$v \cong 0.20 \frac{\overline{C}_s}{\overline{C}_o} \frac{\rho_s(1 - \varepsilon)}{\rho_f \varepsilon} (\omega L) \qquad \text{(B-25)}$$

For the systems investigated in this study, listed in Table B-5, we find that the limiting velocity is approximately 300 cm/sec.

Frequency Limitation

The intraparticle diffusional resistance imposes a limitation on the frequency that can be applied to a CZA process. Assume that the velocity limit estimated in the previous section is reasonable from a heat transfer requirement viewpoint. The frequency that can be applied

at this velocity may be estimated from equation (A-30) for a 20% attenuation. For the following conditions of

$L = 20$ cm.	$D_p = 0.01$ cm^2/sec.
$v = 300$ cm/sec.	$R = 0.05$ cm.
$\psi = 50$	$\mathcal{A}_{out}/\mathcal{A}_{in} = 0.80$

the corresponding frequency was found to be approximately 0.3 radians/sec. ($\sim$ 2.8 cycles/min.). Obviously the process of transferring heat to the adsorbent particles becomes more difficult at higher frequencies.

APPENDIX C

SAMPLE CALCULATIONS

Average bed temperatures, T_o, and input temperature amplitudes, $a_T T_o$, were determined from the averaged responses of the three calibrated thermocouples, located within the adsorbent bed, over several cycles. The frequency, ω, of the input temperature oscillation was calculated from several measured cycle times. The phase between input temperatures, ϕ_T, for dual zone operation was measured directly from the thermocouple response curves.

Effluent concentration waves were calculated from the T-C cell response curves using the T-C cell calibrations and procedures described in Chapter 4. The phase difference between the effluent concentration waves, ϕ_c, for the adsorbing trace components was measured directly from their calculated response curves. The phase lag between the effluent concentration wave and the temperature input, ϕ, was also measured. The concentration waves were integrated over a half-cycle starting at the switching location, β, to determine the average concentrations, $\langle y \rangle$, for both the enriched and depleted portions of the effluent. Using these half-cycle averaged compositions and the appropriate expression for the particular feed-type utilized, the average separation factor, $\langle \alpha \rangle$, was computed.

Interstitial fluid velocities, v, were calculated from the measured volumetric flows corrected to average column conditions. The pressure drops across the 12-30 mesh Pittsburgh BPL activated carbon adsorbent beds were small.

The equilibrium distribution coefficients, either K_o or M_o, determined by the frequency response method presented in Appendix A,

specify the solids-fluid capacity ratio, ψ. From the heat of adsorption, ΔH_a, and the input temperature amplitude, the perturbation parameter, a, was calculated. The dimensionless frequency factor, $\mathcal{F}$, and the dimensionless separation factor, $\mathcal{S}$, were then computed.

Sample calculations are presented for each of the feed-types employed in this study.

SINGLE SOLUTE FEED

A 3.1 mole% CH_4-He gas mixture was fed to a single CZA unit packed with 11.63 gm. of activated carbon. The volume of the packed bed was 22.71 cm^3 and its length was 19.38 cm, resulting in a void fraction of

$$\varepsilon = 1 - \frac{W}{\rho_s V_c} = 1 - \frac{11.63 \text{ gm}}{(0.8 \text{ gm/cc})(22.71 \text{ cm}^3)}$$

$$= 0.360$$

The input temperature whose frequency was 0.0706 radian/second and amplitude was 6.4°C, oscillated about an average temperature of 50.5°C.

The phase lag between the effluent concentration wave and the temperature input, ϕ, was found to be 24.9°. The average methane mole fractions of the enriched and depleted half-cycle portions were 0.0348 and 0.0262, respectively. The average separation factor is

$$\langle \alpha_{CH_4} \rangle = \langle y \rangle_R / \langle y \rangle_L$$

$$= 0.0348/0.0262 = 1.332$$

The measured volumetric flow, Q_s, was 585.2 cm^3/min at 25°C and 1 atm. The actual flow within the column is

$$Q_f = Q_s \frac{14.7}{19.0} \times \frac{323.7}{298.2}$$

$$= 490.3 \text{ cm}^3/\text{min.}$$

Therefore, the interstitial fluid velocity is

$$v = \frac{Q_f L}{\varepsilon V_c (60)} = \frac{(490.3)(19.38)}{(0.360)(22.71)(60)}$$

$$= 19.3 \text{ cm/sec.}$$

From Figure A-5, at $T_o = 323.7°K$, K_o was interpolated to be 0.495 g-moles/lb_{ads}. For this dilute system, $-\Delta H_a/R$ was about $2200°K^{-1}$. The solids-fluid capacity ratio is

$$\psi = \frac{\rho_s(1 - \varepsilon)}{\rho_f \varepsilon} K_o = \frac{\rho_s(1 - \varepsilon) K_o}{(P/RT_o) \varepsilon}$$

$$= \frac{(49.9 \text{ lb}_{ads}/\text{ft}^3)(1 - 0.360)(0.495 \text{ g-moles/lb}_{ads})}{(0.360)\left(\frac{19.0 \text{ atm}}{14.7}\right)(28.32 \text{ lit/ft}^3)/\left[\left(\frac{0.08205 \text{ ℓ-atm}}{\text{g-mole-°K}}\right)(323.7°K)\right]}$$

$$= 31.4$$

and the perturbation parameter is

$$a = a_T T_o \left(\frac{\Delta H_a}{RT_o^2}\right) = \frac{(6.4)(2200)}{(323.7)(323.7)}$$

$$= 0.135$$

Therefore, using the above results, the dimensionless frequency factor is

$$\mathcal{I}_{CH_4} = \frac{(1 + \psi)\omega(L/v)}{2\pi} = \frac{(1 + 31.4)(0.0706)(1.10)}{2\pi}$$

$$= 0.367$$

and the dimensionless separation factor is

$$\mathcal{S}_{CH_4} = \frac{\ln \langle \alpha_{CH_4} \rangle \ (\pi/4)}{a\ \psi/(1 + \psi)} = \frac{(0.280)(0.786)}{(0.135)(0.970)}$$

$$= 1.66$$

TWO ADSORBING SPECIES-TRACE FEED

A dilute mixture of 4.5 mole% CH_4 and 5.4 mole% CO_2 in helium was fed to a single CZA unit packed with 11.57 gm. activated carbon. The volume of the bed was 24.25 cm^3 and its length was 20.64 cm., resulting in an ε of 0.403. The input temperature, frequency equal to 0.0535 radian/second and amplitude equal to 7.0°C, oscillated about the average temperature of 50.4°C.

The phase difference between the methane and carbon dioxide output concentration waves, ϕ_c, was found to be 1.08 radians. The switching location which yielded the maximum separation was β = 1.75 radians. The mole fractions of CH_4 and CO_2 in the enriched and depleted half-cycle portions located by the switching location were calculated to be

$$\langle y_{CH_4} \rangle_R = 0.0486 \qquad \langle y_{CO_2} \rangle_R = 0.0490$$

$$\langle y_{CH_4} \rangle_L = 0.0425 \qquad \langle y_{CO_2} \rangle_L = 0.0580$$

Therefore, the average separation factor is

$$\langle \alpha_{CH_4\text{-}CO_2} \rangle = \frac{\langle y_{CH_4} \rangle_R}{\langle y_{CH_4} \rangle_L} \cdot \frac{\langle y_{CO_2} \rangle_L}{\langle y_{CO_2} \rangle_R}$$

$$= \frac{(0.0486)(0.0580)}{(0.0425)(0.0490)} = 1.354$$

From Figure A-5, at $T_o = 323.6°K$, $(K_o)_{CH_4} = 0.495$ and $(K_o)_{CO_2} = 1.10$ g-moles/lb_{ads} were read. The solids-fluid capacity ratios for the adsorbing components are:

$$\psi_1 = \psi_{CH_4} = \frac{\rho_s(1 - \varepsilon)\ (K_o)_{CH_4}}{\rho_f\ \varepsilon} = (53.8)(0.495)$$

$$= 26.6$$

$$\psi_{CO_2} = \frac{\rho_s(1 - \varepsilon)\ (K_o)_{CO_2}}{\rho_f\ \varepsilon} = (53.8)(1.10)$$

$$= 59.1$$

Therefore, the concentration wave velocity ratio is

$$\Lambda = \frac{1 + \psi_{CO_2}}{1 + \psi_{CH_4}} \cong \psi_{CO_2}/\psi_{CH_4} \cong 2.2$$

Since $(\Delta H_a)_{CH_4} \cong (\Delta H_a)_{CO_2}$, the isotherm parameter is approximately

$$\gamma = (1/\Lambda) \cdot \frac{(K_o)_{CO_2}}{(K_o)_{CH_4}} \cong 1.0$$

The perturbation parameter for the methane is

$$a_1 = a_T \frac{(\Delta H_a)_{CH_4}}{RT_o} = \frac{(0.0218)(2200)}{(323.6)} = 0.149$$

For the determined interstitial velocity of 13.8 cm/sec, the dimensionless frequency factor for methane was

$$\mathcal{J}_{CH_4} = \frac{(1 + \psi_{CH_4})\omega(L/v)}{2\pi} = \frac{(27.6)(0.0535)(1.497)}{2\pi}$$

$$= 0.352$$

and the dimensionless separation factor was

$$\mathcal{S}_{CH_4\text{-}CO_2} = \frac{\ln \langle \alpha_{CH_4\text{-}CO_2} \rangle (\pi/4)}{a_1 \psi_1/(1 + \psi_1)}$$

$$= \frac{(0.303)(0.786)}{(0.149)(0.970)} = 1.65$$

BINARY ADSORBING FEED

A binary gas mixture containing 50.2 mole% CH_4 and 49.8 mole% CO_2 was fed to a single CZA unit packed with 11.57 gm activated carbon. The volume of the bed was 24.25 cm^3 and its length was 20.64 cm, resulting in a void fraction of 0.403. The input temperature, frequency of 0.0424 radian/second and amplitude of 5.4°C, oscillated about the mean temperature of 49.1°C.

The phase lag between the effluent concentration wave and the input temperature, ϕ, was found to be 29°. The average mole fractions

of CH_4 and CO_2 of the enriched and depleted half-cycle portions were calculated to be

$$\langle y_{CH_4} \rangle_R = 0.541 \qquad \langle y_{CH_4} \rangle_L = 0.465$$

$$\langle y_{CO_2} \rangle_L = 0.535 \qquad \langle y_{CO_2} \rangle_R = 0.459$$

Therefore, the average separation for the binary mixture is

$$\langle \alpha_{CH_4\text{-}CO_2} \rangle_m = (0.541)(0.535)/(0.465)(0.459)$$

$$= 1.360$$

From Figure A-7, interpolating between the temperatures investigated using the method described in Chapter 6 with results listed in Table 6-5, the effective distribution coefficient for the mixture, M_o, at $T_o = 322.3°K$ was found to be 0.480 g-moles/lb_{ads} with $-\Delta H_m/R$ equal to $1420°K^{-1}$. Therefore, the solids-fluid capacity ratio for the mixed system is

$$\psi_m = \frac{\rho_s(1 - \varepsilon)\, M_o}{\rho_f\, \varepsilon} = (53.60)(0.480)$$

$$= 25.7$$

The perturbation parameter for the mixture is

$$a_m = a_T(\Delta H_m/RT_o) = (0.0168)(1420/322.3)$$

$$= 0.0737$$

Using the determined interstitial fluid velocity of 9.3 cm/sec, the dimensionless frequency factor is calculated to be

$$\mathcal{J}_m = \frac{(1 + \psi_m)\omega(L/v)}{2\pi} = \frac{(26.7)(0.0424)(2.220)}{2\pi}$$

$$= 0.400$$

The dimensionless separation factor for the process, using the definition given in equation (3-87), is

$$(\mathcal{S}_{CH_4\text{-}CO_2})_m = \frac{(1 - y_{CH_{4f}}) \ln \langle \alpha_{CH_4\text{-}CO_2} \rangle_m \cdot (\pi/4)}{a_m \psi_m/(1 + \psi_m)}$$

$$= \frac{(0.498)(0.307)(0.786)}{(0.0737)(0.963)}$$

$$= 1.75$$

ACKNOWLEDGEMENTS

The author wishes to express his sincere appreciation to Professor Robert L. Pigford for his intuitive insight during the course of this research.

The many suggestions and excellent work of G. G. Young and especially R. H. Escobales of the Lawrence Berkeley Laboratory during construction of the experimental apparatus was appreciated.

Thanks are due to the Pittsburgh Activated Carbon Company for the donation of the activated carbon adsorbent used in this study.

Financial assistance provided by the Atomic Energy Commission through AEC contract W-7405-eng-48 is gratefully acknowledged.

TECHNICAL INFORMATION DIVISION
LAWRENCE BERKELEY LABORATORY
UNIVERSITY OF CALIFORNIA
BERKELEY, CALIFORNIA 94720